



# Seismic Assessment and Retrofit of an Existing Reinforced Concrete School Building in Italy

A Dissertation Submitted in Partial Fulfilment of the Requirements  
for the Master Degree in

Earthquake Engineering

By

Wilson Wladimir Carofilis Gallo

Supervisors: Dr. Gerard O'Reilly

Prof. Andre Filiatrault

Dr. Daniele Perrone

Prof. Ricardo Monteiro

February, 28, 2018

Istituto Universitario di Studi Superiori di Pavia

The dissertation entitled "Seismic Assessment and Retrofit of an Existing Reinforced Concrete (RC) School Building in Italy", by Wilson Wladimir Carofilis Gallo, has been approved in partial fulfilment of the requirements for the Master Degree in Earthquake Engineering.

Dr. Gerard O'Reilly



Prof. Andre Filiatralut



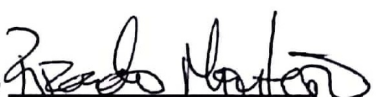
Andre  
Filiatralut

Digitaly signed by Andre  
Filiatralut  
Date: 2011-06-02 16:41:10  
Location: 10.0.0.104  
Country: Canada

Dr. Daniele Perrone



Prof. Ricardo Monteiro



## ABSTRACT

Poor performance of old reinforced concrete (RC) frame buildings in Italy has highlighted their vulnerability to seismic events. For instance, after the Emilia-Romagna earthquake in 2012, not only were substantial structural damage and collapses reported, but also considerable economic losses, especially for old RC buildings built before the introduction of modern seismic design provisions. This study conducts a seismic assessment of an existing RC school building in Italy so that its performance can be determined and therefore upgraded through a retrofit aimed to not only improve its seismic behaviour but also reduce its potential economic losses. This building is representative of the RC school buildings in Italy built before the 1970s, which were typically designed to withstand only gravity loads and lack seismic design provision and requirements. A numerical model was developed in OpenSees to consider all possible issues related to gravity load designed RC frames with masonry infills. The seismic assessment of this structure was based on the procedure outlined by FEMA P58 and also incorporates requirements specified by the Italian building code, NTC 2008. The first part of this thesis focuses on determining its structural performance, evaluating it through the requirements of NTC 2008. The second part refers to analysis comprising loss estimation and collapse assessment, utilising the PEER PBEE methodology.

Based on the results of the assessment, some retrofit alternatives were proposed and evaluated so that a better overall performance could be achieved. These retrofit schemes were primarily aimed at improving the structural behaviour of the original structure in addition to the improved performance of the non-structural elements. This was achieved by increasing the lateral resistance and deformation capacity of the building, reducing the damage undergone by the structural elements and guaranteeing an appropriate strength hierarchy in structural elements. Therefore, several schemes were trialled, including the combination of FRP material, a perimeter gap isolating the masonry infill from the surrounding frame and the provision of additional steel bracing. By conducting the performance assessment for the retrofit alternatives, it was found that the perimeter gap was not a practical solution since no overall improvement was obtained. The FRP enhanced the structural capacity but did not mitigate non-ductile mechanisms. Overall, the most desirable was the steel braces, which achieved the best structural performance. Moreover, the structural response was taken as independent of the non-structural

## Abstract

elements and therefore, the retrofit of non-structural elements was assessed separately without modifying the numerical models. This improvement was included in the loss estimation through improved fragility functions since it is known that retrofitted non-structural elements influence considerably the monetary losses.

In summary, a better overall performance could be provided to the existing RC school building when improving not only the structural behaviour but also by considering the non-structural elements.

*Keywords:* structural; assessment performance; retrofit; loss estimation; non-structural elements; collapse.

## ACKNOWLEDGEMENTS

I have learned the farther one goes, the more complete one becomes. That feeling of fulfillment and self-growth are connected to the experiences one acquires, and also to the people one meets along the journey.

My words cannot express how grateful I am for the people I have met, who have taught me a different perspective of this world. Amazing human beings who gave me a hand in one way or another.

I want to start by expressing my eternal gratefulness to the most valuable people in my life: my family. Without them these two years would have not been possible. Even though some miles separate us, their supportive words made me preserve and flourish.

Secondly, I will always be thankful for the outstanding people I met in Patras. The first place where my adventure started, the city where I met my beloved friends. Thank you for sharing countless joyful moments and stories that we will always laugh about.

Furthermore, I am very pleased with the fellows in Pavia, where my path has ended. I appreciate all of you as I consider you as my foreign family. Thank you for being part of this ERASMUS experience that has enriched my life.

Likewise, this acknowledgment is also meant for my Ecuadorian friends. I would like them to know that even if distance and time have played a role in my forgetful mind, I never take for granted the fact that our friendship has grown unbroken and more fulfilled than always. Thank you for your supportive words and the trust you put on me.

I cannot conclude without thanking to my supervisors for their work and dedication; especially all the knowledge they have shared and patience they put on me to succeed in this study. Thank you very much for being such remarkable mentors.

Many people believe that destiny is meant to be, but as I once heard, “Things happen randomly for no reason at all, but they create opportunities. You learn from those opportunities even the missed ones. The question is, can you recognize the next opportunity when it matters the most?”

## TABLE OF CONTENTS

	Page
ABSTRACT .....	i
ACKNOWLEDGEMENTS.....	iii
TABLE OF CONTENTS .....	iv
LIST OF FIGURES .....	vii
LIST OF TABLES.....	xiii
LIST OF SYMBOLS.....	xvi
1 INTRODUCTION .....	1
1.1 Review of Past Damage to School Buildings .....	3
1.2 Scope and Layout of Thesis.....	5
2 LITERATURE REVIEW .....	7
2.1 Introduction.....	7
2.2 Existing Guidelines on Assessment and Retrofitting of RC Buildings.....	7
2.3 Assessment Methods.....	12
2.3.1 SLaMA Method .....	13
2.3.2 Static Pushover Analysis.....	13
2.3.3 N2 Method .....	14
2.3.4 Strength Hierarchy Assessment.....	16
2.4 Past Studies on Loss Estimation .....	18
2.5 Retrofitting Techniques .....	19
2.5.1 Structural Retrofitting .....	20
2.5.2 FRP Retrofitting.....	21
2.5.3 Brace Retrofitting.....	23

2.5.4 Infill Walls Retrofitting.....	24
2.5.5 Non-structural Retrofitting.....	25
2.6 Summary and Discussions .....	26
3 ASSESSMENT OF AN EXISTING SCHOOL BUILDING .....	27
3.1 Introduction.....	27
3.2 Overview of the School Building.....	27
3.3 Building Survey Information .....	28
3.4 Structural Layout .....	30
3.5 Numerical Modelling.....	30
3.6 Static Pushover Analysis.....	32
3.7 Evaluation of Structural Performance.....	35
3.7.1 Selection of Elastic Response Spectra .....	35
3.7.2 Application of the N2 Method .....	38
3.7.3 Assessment of Limits States .....	40
3.7.4 N2 Method Application Results.....	40
3.7.5 Hierarchy Assessment.....	44
3.8 N2 Analysis on the Bare Frame .....	47
3.9 Summary and Discussions .....	51
4 IDENTIFICATION OF POTENTIAL RETROFITTING SOLUTIONS.....	53
4.1 Introduction.....	53
4.2 Structural Retrofitting .....	53
4.2.1 Retrofit Alternative A: Gap .....	54
4.2.2 Retrofit Alternative B: FRP .....	56
4.2.3 Retrofit Alternative C: FRP + Braces .....	66
4.2.4 Retrofit Alternative D: FRP + Gap .....	71
4.3 Non-Structural Retrofitting .....	71
4.3.1 Drift-Sensitive Components.....	71
4.3.2 Acceleration-Sensitive Components .....	72
4.3.3 Velocity-Sensitive Components.....	72
4.3.4 Improved Fragility Functions .....	72
4.4 Evaluation of Retrofitting Solutions .....	74
4.4.1 Modal Properties.....	74
4.4.2 Pushover Analyses .....	75
4.4.3 Limit States Assessment .....	77
4.5 Summary and Discussions .....	81
5 ASSESSMENT OF RETROFITTING SCHEMES.....	83

5.1	Introduction.....	83
5.2	Site Hazard and Ground Motion Selection .....	83
5.3	Non-linear Response History Analysis (NRHA) .....	85
5.4	Evaluation of Retrofitting Techniques.....	93
5.4.1	Collapse Assessment.....	93
5.4.2	Loss Estimation.....	98
5.5	Summary and Discussions .....	106
6	SUMMARY, CONCLUSIONS AND FUTURE STUDIES .....	107
6.1	Summary .....	107
6.2	Conclusions.....	108
6.3	Future Studies .....	111
7	REFERENCES .....	112
	APPENDIX A (PERFORMANCE ASSESSMENT) .....	A1
	APPENDIX B (NON-STRUCTURAL ELEMENTS RETROFIT) .....	B1
	APPENDIX C (STRUCTURAL ELEMENTS) .....	C1

## LIST OF FIGURES

	Page
Figure 2.1. Overview of PEER PBEE assessment framework outlined by Cornell and Krawinkler [2000].....	12
Figure 2.2. Non-linear pushover analysis and acceleration-displacement response spectrum (ADRS), [after NZSEE, 2016].....	13
Figure 2.3. SPO application and evaluation, (a) Static Pushover, (b) Identification of limit-States, (c) Establish Performance Criterion, [after O'Reilly, 2016].....	14
Figure 2.4. Idealization of force–displacement relationship, (a) Infill reinforced concrete frame [after Dolšek and Fajfar, 2005], (b) frame structures [after EN 1998-3:2005]. .....	15
Figure 2.5. Determination of the target displacement for the equivalent SDOF, (a) Short period range, (b) Medium and long period range, [after EN 1998:2005].....	16
Figure 2.6. Sequence of N2 Method.....	16
Figure 2.7. Step involving the evaluation of the strength hierarchy, [after Tasligedik <i>et al.</i> , 2016].....	17
Figure 2.8. Strength hierarchy evaluation.....	17
Figure 2.9. Inputs involving a strength hierarchy evaluation.....	18
Figure 2.10. Different structural retrofitting interventions, [after Inashai and Pinho, 1998]....	19
Figure 2.11. Typical uniaxial tension stress-strain diagrams for different fibres and comparison with steel, [after Triantafillou, 2018].....	21
Figure 2.12. Comparison of strength capacity increase using FRP, [after Triantafillou, 2018]. .....	23
Figure 2.13. Different configuration of FRP, (a) bars, (b) strips and/or sheets.....	23
Figure 2.14. Infill wall with separation gaps between infill and columns and beam, [after Charleson, 2008].....	24

Figure 3.2. Typical floor layout of school, where the beams and columns are dimensioned along with the spanning of the slabs, [after O'Reilly, 2016].....	28
Figure 3.1. Front and rear elevation of case study school building, [after O'Reilly, 2016]. ....	28
Figure 3.3. Modelling of joints, includes proposed beam-column joint model and hysteretic material model for beam-column joints, [after O'Reilly, 2016].....	31
Figure 3.4. Modelling of beam-column elements, includes proposed beam-column element model and proposed moment-curvature relationship for beam-column plastic hinge zone, [after O'Reilly and Sullivan, 2018a].....	31
Figure 3.5. (a) Proposed modelling for infill walls elements [after O'Reilly and Sullivan, 2018a], (b) Numerical model of school building in OpenSees.....	32
Figure 3.6. Shape mode of the first four periods of the school building. ....	33
Figure 3.7. SPO curve for both directions of the school building. ....	34
Figure 3.8. Weak-Storeys mechanism after performing SPO, (a) mechanism in the second floor in Y, (b) mechanism in the first floor in X.....	35
Figure 3.9. Scheme of the software REASSESS V 2.0 for obtaining a UHS.....	36
Figure 3.10. Determination of parameter for fitting the elastic response spectrum for $T_r = 1463$ years, (a) initial fitting, (b) defining periods according to the different ranges. ....	37
Figure 3.11. Idealised Elastic Response Spectrum for $T_r = 1463$ years. ....	37
Figure 3.12. Idealised elastic response spectrum for Cassino, soil type C. ....	38
Figure 3.13. Idealised strength capacity of the school building, (a) SPO in longitudinal-X direction, (b) SPO in transverse-Y direction.....	39
Figure 3.14. Determination of target displacement for SDOF for the $T_r = 1463$ years in both directions.....	39
Figure 3.15. Maximum storey drift of the school building for the serviceability limit states. .	41
Figure 3.16. Maximum storey drift of the school building for the ultimate limit states.....	41
Figure 3.17. Criteria for defining the failure of an element, after a drop of 20% of its maximum capacity.....	42
Figure 3.18. Failure of elements for the target displacement of $T_r = 1463$ years, (a) Column fails at shear, (b) Column fails at flexure, (c) Joint fails at flexure, (d) Beam fails at flexure. ....	43
Figure 3.19. Damage presented in structural elements due to SPO for $T_r = 1463$ yrs.....	44
Figure 3.20. Beam-column joints evaluated according to the strength hierarchy procedure. ..	44
Figure 3.21. Strength hierarchy evaluation of some beam-column joints. ....	45

Figure 3.22. Combined flexural and shear response for columns, (b) shear strength-displacement ductility relationship, [after Galal and Ghobarah, 2004]. .....	46
Figure 3.23. Combined shear strength and flexural strength to evaluate whether a ductile or shear failure mode controls the behaviour in a column, (a) moderate-ductile behaviour, (b) ductile behaviour.....	47
Figure 3.24. Idealised strength capacity of the bare frame, (a) SPO in longitudinal-X direction, (b) SPO in transverse-Y direction.....	48
Figure 3.25. Shape mode of the first four periods for the bare frame.....	49
Figure 3.26. Maximum storey drift of the bare frame for the serviceability limit state. ....	49
Figure 3.27. Maximum storey drift of the bare frame for the ultimate limit state.....	50
Figure 3.28. Weak-Stories mechanism after performing SPO for the bare frame, (a) mechanism in the second floor in Y, (b) mechanism in the first floor in X. .....	50
Figure 3.29. Damage presented in structural elements due to SPO for $T_r = 1463$ years, bare frame. .....	51
Figure 4.1. Gap retrofitting, (a) cellular material between the infill and frame, (b) structural response of a single bay for different gap width.....	54
Figure 4.2. Comparison of the structural response of the school building for different gap width, (a) SPO in the longitudinal-X direction, (b) SPO in the transverse-Y direction. ..	55
Figure 4.3. Gap modelling, (a) numerical model of gap and infills, (b) model of the stress-strain behaviour of the gap material, [after Tsantilis and Triantafillou, 2018].....	56
Figure 4.4. Strength hierarchy improvement for columns and joints, showing the capacity of the beam, column and joint as a function of the axial load.....	57
Figure 4.5. CFRP U-jackets configuration, (a) Scheme for beams connecting internal joints, (b) CFRP scheme for beam ends, [after Triantafillou, 2018]. .....	58
Figure 4.6. (a) FRP anchorage scheme for beams, (b) FRP wrapping scheme at the end of columns, [after Triantafillou, 2018].....	59
Figure 4.7. FRP strips assumptions for design, [after Del Vecchio <i>et al.</i> , 2015]. .....	59
Figure 4.8. Flange strips scheme for retrofitting internal joints, [after Yu <i>et al.</i> , 2015] and [after Maher <i>et al.</i> , 2012]. .....	60
Figure 4.9. Modelling of retrofitted beam-column joint with FRP.....	61
Figure 4.10. Interaction diagram for a RC column retrofitted with FRP, [after Triantafillou, 2018]. .....	62
Figure 4.11. . Modelling of retrofitted beam-column elements with FRP.....	63

Figure 4.12. Combined shear strength and flexural strength after wrapping columns with FRP, (a) previous moderate-ductile behaviour, post-retrofit ductile behaviour, (b) ductile behaviour.....	63
Figure 4.13. FRP scheme for retrofitting columns, [after Triantafillou, 2018].....	64
Figure 4.14. Strength hierarchy evaluation after retrofitting the elements with FRP with their failure mechanisms. ....	65
Figure 4.15. Modelling of steel braces.....	67
Figure 4.16. Target stiffness of each storey.....	67
Figure 4.17. Distribution of lateral load along the height of the building. ....	70
Figure 4.18. Braces configuration along the height of the building, (a) The longitudinal-X direction, (b) The transverse-Y direction.....	70
Figure 4.19. Illustration of a fragility function for a suspended ceiling, C3032.001b: PACT library.....	71
Figure 4.20. Translational period comparison among models.....	75
Figure 4.21. Comparison of capacities in for the different models, (a) SPO in longitudinal direction, (b) SPO in transverse direction.....	76
Figure 4.22. Comparison of maximum drifts for the different alternatives for the serviceability limit state.....	78
Figure 4.23. Comparison of maximum drifts for the different alternatives for the ultimate limit state. ....	79
Figure 4.24. Comparison of structural damage due to flexural failure.....	80
Figure 4.25. Comparison of structural damage due to shear failure.....	81
Figure 5.1. Illustration of the hazard curve for the site Cassino. ....	85
Figure 5.2. Median of the maximum values over the height for peak storey drift in X (longitudinal) direction, conditioned on no collapse. ....	86
Figure 5.3. Median of the maximum values over the height for peak storey drift in Y (transverse) direction, conditioned on no collapse. ....	86
Figure 5.4. Median of the maximum values over the height for peak floor acceleration in X (longitudinal) direction, conditioned on no collapse. ....	88
Figure 5.5. Median of the maximum values over the height for peak floor acceleration in Y (transversal) direction, conditioned on no collapse. ....	88

Figure 5.6. Time history response of joint 9272 in terms of Moment-rotational capacity, (a) Hysteresis behaviour conditioned to $T^*=0.5$ sec., (b) Hysteresis behaviour conditioned to $T^*=1.0$ sec.....	90
Figure 5.7. Time history response of beam 7274 in terms of Moment-rotational capacity, (a) Hysteresis behaviour conditioned to $T^*=0.5$ sec., (b) Hysteresis behaviour conditioned to $T^*=1.0$ sec.....	91
Figure 5.8. Time history response of column 5271 in terms of Moment-rotational capacity, (a) Hysteresis behaviour conditioned to $T^*=0.5$ sec., (b) Hysteresis behaviour conditioned to $T^*=1.0$ sec.....	92
Figure 5.9. Fitting of the collapse fragility function for different conditioning periods, (a) Fragility curve conditioned to $T^*=0.5$ sec., (b) Fragility curve conditioned to $T^*=1.0$ sec.....	94
Figure 5.10. Evaluation of collapse criteria for each model, (a) Fragility curve conditioned to $T^*=0.5$ sec., (b) Fragility curve conditioned to $T^*=1.0$ sec.....	97
Figure 5.11. Mean annual frequency of collapse.....	98
Figure 5.12. Vulnerability curves comparison.....	100
Figure 5.13. EAL ratio of the replacement cost.....	103
 Figure A. 1. Determination of target displacement for SDOF in both directions, original building.....	A2
Figure A. 2. Determination of target displacement for SDOF in both directions, bare frame.....	A3
Figure A. 3. Strength hierarchy evaluation of some beam-column joints .....	A4
Figure A. 4. Strength hierarchy evaluation after retrofitting the elements with FRP .....	A5
 Figure B. 1. Gap scheme, [FEMA 3-74, 2012].....	B1
Figure B. 2. Illustration on how to prevent out-of-plane failure in infill walls, [after FEMA 3-74, 2012].....	B1
Figure B. 3. Fragility functions for infill walls.....	B2
Figure B. 4. Fragility functions for doors.....	B3
Figure B. 5. Fragility functions for desks.....	B4
Figure B. 6. Fragility functions for chairs.....	B4
Figure B. 7. Retrofitting schemes for ceiling systems, [after FEMA 3-74, 2012].....	B5

Figure B. 8. Fragility functions for ceiling systems.....	B6
Figure B. 9. Fragility functions for fancoils. ....	B7
Figure B. 10. Retrofitting schemes for light systems, [after FEMA 3-74, 2012]. .....	B8
Figure B. 11. Fragility functions for lights. ....	B8
Figure B. 12. Retrofitting schemes for piping systems, [after FEMA 3-74, 2012]. .....	B9
Figure B. 13. Fragility functions for piping-water distribution. ....	B9
Figure B. 14. Retrofitting schemes for bookshelves, [after FEMA 3-74, 2012]. .....	B10
Figure B. 15. Fragility functions for bookcases, (a) Original, (b) Retrofitted. ....	B11
Figure B. 16. Retrofitting schemes mobile boards, [after FEMA 3-74, 2012]. .....	B12
Figure B. 17. Fragility functions for mobile blackboards. ....	B12
Figure B. 18. Retrofitting schemes electronic blackboards, [after FEMA 3-74, 2012].....	B13
Figure B. 19. Fragility functions for electronic blackboards. ....	B13
Figure B. 20. Retrofitting schemes computers and printers, [after FEMA 3-74, 2012]. .....	B14
Figure B. 21. Fragility functions for computers and printers. ....	B14
Figure B. 22. Fragility functions for projectors. ....	B15
Figure B. 23. Retrofitting schemes for switchboards, [after FEMA 3-74, 2012]. .....	B16
Figure B. 24. Fragility functions for switchboards. ....	B16
 Figure C. 1. Fragility functions for exterior beam-column joints, Cardone [2016], PACT library.....	C1
Figure C. 2. Fragility functions for interior beam-column joints, Cardone [2016], PACT library.....	C2
Figure C. 3. Fragility functions for ductile columns, Cardone [2016], PACT library. ....	C3
Figure C. 4. Fragility functions for exterior masonry infills, Cardone and Perrone [2015], PACT library.....	C4
Figure C. 5. Fragility functions for stairs, PACT library, (a) Original, (b) Retrofitted. ....	C5

## LIST OF TABLES

	Page
Table 1-1. Damage report of some school and university building around the world, U.S. Department of Commerce National Oceanic and Atmospheric Administration .....	3
Table 2-1. Reference return period and ground motion scaling factors for 100%NBS for – Basic Performance Objective Equivalent to New building Standards defined in ASCE 4- 13 (2014) for use with that document – Table C1.1 NZSEE-C1 2016.....	8
Table 2-2. Assessment outcomes (potential building status), Table A3.1 NZSEE 2016 .....	8
Table 2-3. Return period and the probability of exceedance in 50 years for each limit state for ordinary new buildings, [EN 1998-3:2005, 2005].....	9
Table 2-4. Description structural performance objectives based on the limit state for concrete frame, [FEMA 356].....	10
Table 2-5. NTC 2008 return period for each limit state of a school building with nominal life of 50-years, which has a Class III usage.....	11
Table 2-6. Typical properties of fibres (from Feldman [1989] and Kim [1995]).....	22
Table 3-1. List and quantities of damageable elements in each school building. Quantities in the longitudinal direction of the school building are listed with the transverse direction listed adjacent in parentheses [O'Reilly and Perrone, 2016].....	29
Table 3-2. Periods of the school building.....	32
Table 3-3. Target displacements for the seismic assesment of the school building.....	40
Table 3-4. Compliance criteria defined in NTC 2008 for the protection of drift sensitive non- structural elements.....	40
Table 3-5. Dynamic properties of the bare frame structure (school building modelled without infills).....	48
Table 3-6. Target displacements for the seismic assesment of the bare frame.....	48

Table 4-1. Definition of material model for the isolation joints [Tsantilis and Triantafillou, 2018]. .....	56
Table 4-2. Distribution of shear strength and stiffness in the longitudinal direction in the linear range (T <sub>r</sub> = 1463 yrs.). .....	68
Table 4-3. Distribution of shear strength and stiffness in the longitudinal direction in the non-linear range (T <sub>r</sub> = 1463 yrs.). .....	68
Table 4-4. Distribution of shear strength and stiffness in the transverse direction in the linear range (T <sub>r</sub> = 1463 yrs.). .....	69
Table 4-5. Distribution of shear strength and stiffness in the transverse direction in the non-linear range (T <sub>r</sub> = 1463 yrs.). .....	69
Table 4-6. Table of improved fragility function for non-structural elements.....	73
Table 4-7. Comparison of dynamic properties among all the retrofitting alternatives.....	74
Table 5-1. Conditional periods for different structural models. ....	84
Table 5-2. Median collapse intensity and dispersion for each model.....	93
Table 5-3. Collapse margin ratio to evaluate the collapse safety. ....	96
Table 5-4. List of the element fragility curves used for the loss estimation of the school building. ....	101
Table 5-5. Inputs values for performing the loss estimation assessment.....	104
Table 5-6. Loss estimation results and expected repair cost.....	105
Table B-1. Description of damage states for infill walls. ....	B2
Table B-2. Description of damage states for Doors.....	B3
Table B-3. Description of damage states for desks.....	B4
Table B-4. Description of damage states for chairs.....	B5
Table B-5. Description of damage states for ceiling systems.....	B6
Table B-6. Description of damage states for fancoils.....	B7
Table B-7. Description of damage states for lights.....	B8
Table B-8. Description of damage states for piping-water distribution.....	B10
Table B-9. Description of damage states for bookcases .....	B11
Table B-10. Description of damage states for mobile blackboard.....	B12
Table B-11. Description of damage states for electronic blackboard.....	B13
Table B-12. Description of damage states for computer and printers .....	B14
Table B-13. Description of damage states for projectors. ....	B15

Table B-14. Description of damage states for switchboards .....	B16
Table C-1. Description of damage states for exterior beam-column joints .....	C1
Table C-2. Description of damage states for interior beam-column joints.....	C2
Table C-3. Description of damage states for columns.....	C3
Table C-4. Description of damage states for exterior masonry infills.....	C4
Table C-5. Description of damage states for stairs.....	C5

## LIST OF SYMBOLS

$A_b$	= Area of steel braces
$a_g$	= Design ground acceleration on type A ground
$a_{\max}$	= Maximum spectral acceleration, constant branch
$A_{f,tot}$	= Total area of FRP
$A_{s,tot}$	= Total area of steel reinforcement
$b_f$	= Width of FRP strip (mm)
$b_w$	= Member width
$d^*$	= Displacement
$d$	= Section depth
$D$	= Location site of assessment
$D_e$	= Displacement in the elastic range
$d^*_{et}$	= Target displacement SDOF for T*
$d_f$	= Height of FRP crossed by the shear crack (mm)
$D_{F\max}$	= Displacement at maximum strength
$D_{F\min}$	= Displacement at the minimum strength
$d^*_{m}$	= Displacement at maximum strength
$DM$	= Damage level
$D_s$	= Displacement at the start of strength degradation
$d^*_{t}$	= Target displacement SDOF
$DV$	= Decision variable
$d^*_{y}$	= Displacement at yielding
$D_y$	= Displacement at yielding
$EAL$	= Expected annual loss
$E_c$	= Modulus of elasticity of concrete
$EDP$	= Engineering demand parameter
$E_f$	= Elastic modulus of FRP (MPa)
$E^*m$	= Deformation energy
$E_s$	= Modulus of elasticity of steel
$F^*$	= Strength

$f_c$	= Mean compressive strength of concrete
$f_{cd}$	= Compression strength of concrete
$f_{ccd}$	= Strength of confined concrete
$f_{ctm}$	= Mean tensile strength of concrete (MPa)
$F_e$	= Strength in the elastic range
$f_{fu,W}(R)$	= Tensile strength of closed jackets
$F_i$	= Equivalent static force at floor level i
$F_{jt}$	= Floor equivalent static force acting on a joint
$F_{min}$	= Minimum strength
$F_y^*$	= Ultimate strength
$F_y$	= Maximum strength
$F_{yst}$	= Yielding strength of steel
$H$	= Storey height
$h_b$	= Beam height
$h_c$	= Column height
$K_{eff}$	= Equivalent stiffness
$K_i$	= Initial stiffness
$K_{vi}$	= Lateral Stiffness at storey i
$K_T$	= Total lateral stiffness
$L_p$	= Plastic hinge length
$m^*$	= Mass of equivalent SDOF
$M$	= Bending moment
$M_1$	= Bending moment at end 1
$M_2$	= Bending moment at end 2
$M_c$	= Capping moment
$M_{crack}$	= Crack joint moment
$M_{Ed}$	= Total bending moment
$M_{peak}$	= Peak joint moment
$M_u$	= Ultimate moment
$M_{ult}$	= Ultimate joint moment
$M_y$	= Yielding moment
$N$	= Axial load
$N_{Ed}$	= Total axial force
$N_i$	= Variation of axial load caused by lateral seismic actions
$N_b$	= Axial force in the brace
$N_G$	= Gravity load in column
$n_l$	= Number of FRP layers
$n_s$	= Number of joint panels sides strengthened in shear with FRP systems in the plane of the load
$P_c$	= Compression axial load at joint
$P_t$	= Tension axial load at joint

$p_{t,c}$	= Concrete contribution of joint panel principal tensile stress
$R$	= Radius at the corner of the cross section
$S$	= Soil factor
$S_d$	= Spectral displacement
$S_e$	= Spectral acceleration
$S_e(T^*)$	= Spectral acceleration for $T^*$
$S_v$	= Spectral Velocity
$T^*$	= Equivalent period SDOF
$T_B$	= Period of the initial part of the constant acceleration branch
$T_C$	= Period of the final part of the constant acceleration
$T_D$	= Period of the initial part of the constant displacement
$t_{\text{inf}}$	= Thickness of the infill equivalent strut model
$t_{\text{joint}}$	= Thickness of the gap
$t_f$	= FRP strip thickness (mm).
$T_r$	= Return period
$u_i$	= Lateral displacement at storey i.
$V$	= Shear force
$V_1$	= Shear force at end 1
$V_2$	= Shear force at end 2
$V_f$	= Additional strength due to strengthening
$V_i$	= Shear load in column
$V_{\max}$	= Maximum capacity of the building
$V_{si}$	= Total shear at storey i.
$V_y$	= Yielding strength of the building
$w_{\text{inf}}$	= Width of the infill equivalent strut model
$\alpha$	= Angle of FRP strips
$\beta$	= Angle of strips
$\beta_{D,a}$	= Total dispersion in peak floor acceleration demand
$\beta_{DR,a}$	= Record-to-record variability in peak floor acceleration demand
$\beta_{DU,a}$	= Modelling uncertainty in peak floor acceleration demand
$\beta_{D,\theta}$	= Total dispersion in peak storey drift demand
$\beta_{DR,\theta}$	= Record-to-record variability in peak storey drift demand
$\beta_{DU,\theta}$	= Modelling uncertainty in peak storey drift demand
$\gamma$	= Shear deformation
$\gamma_{\text{crack}}$	= Crack shear joint deformation
$\gamma_{\text{peak}}$	= Peak shear joint deformation
$\gamma_{\text{ult}}$	= Ultimate shear joint deformation
$\Delta_{d, \text{target}}$	= Target displacement.
$\Delta_{\text{roof}}$	= Displacement at the roof or top of the structure.
$\Delta_u$	= Ultimate displacement
$\Delta_y$	= Yielding displacement

$\varepsilon$	= Strain of foamed material
$\varepsilon_{cu}$	= Ultimate compression strain
$\varepsilon_{ccu}$	= Ultimate confined strain
$\theta_i$	= Angle of the infill equivalent strut model
$\theta$	= Angle of shear cracks
$\theta_{crit}$	= Critical storey drift
$\lambda$	= Mean annual frequency of exceedance (MAFE)
$\sigma$	= Compression stress of foamed material
$\sigma_{fed}$	= Design value of mean stress in the FRP crossing the shear crack
$\sigma_{lud}$	= Confining stress
$\phi$	= Moment curvature
$\phi_c$	= Capping curvature
$\phi_y$	= Yielding curvature
$\phi_u$	= Ultimate curvature

## 1 INTRODUCTION

Extensive damage in different structures has been observed during past earthquakes in Italy. In fact, Wilson and Boehler [2016] reported that over the last century, Italy has suffered a series of deadly earthquakes leading to casualties as a result of building collapses. Even though Italy is a country with a high seismic hazard, many of its structures are not prepared to withstand these events. The poor performance of reinforced concrete (RC) frames during seismic events is addressed by the study of O'Reilly [2016], which identifies soft-storey mechanisms, brittle shear failure in columns, poor beam-column joint behaviour, among other factors. These type of structural problems, which are common in structures built before the 1970s, are the main contributors to this poor performance. As a result, extensive damage and/or collapse in structures has been reported [Borzi *et al.*, 2013; O'Reilly, 2016; Gara *et al.*, 2017]. Special attention has to be given to school buildings as they represent a high priority for seismic risk evaluation due to their public use, especially since they may serve as emergency shelters after earthquakes. However, many of these school buildings in Italy are not built to meet requirement of modern seismic design codes. This was illustrated through the catastrophic collapse of the school at San Giuliano during the October 2002 earthquake in Italy, which took the life of thirty people, of which twenty-seven were young students and one of their teachers [Borzi *et al.*, 2013].

As Madhab Mathema, former senior of Human Settlements (HABITAT), expressed “*When an earthquake destroys schools, it takes away the children's future—and with it, the future of the country itself*” [GEOHAZARDS INTERNATIONAL]. It is clear that collapses are a really high risk, but not only that, the structure itself represented a hazard for its occupants. Non-structural elements such as infill walls, partitions, equipment and any other building content may not compromise a building's stability but may place people and the contents of the building at risk. De Angelis and Pecce [2015] have mentioned the importance of non-structural elements in Italian school buildings, after the death of a student and the injury of another caused by the collapse of a classroom ceiling on November 22, 2008, at Darwin High School in Rivoli, Italy. This tragic event highlights that the lack of seismic provisions for non-structural elements increases their seismic vulnerability. As mentioned before, schools may be used as emergency shelters or bases for the civil protection services after a seismic event. Therefore, they must maintain operational functionality immediately after an earthquake. If the seismic performance of the non-structural elements is not met, then this target cannot be achieved. In fact, the damage observed in some school buildings in Italy from past earthquakes reported recently by Calvi *et*

*al.* [2016] supports that non-structural elements can lower the performance level of the entire building system when they are not design to withstand seismic actions.

In addition to casualties, economic losses is another important consequence produced by earthquakes that also affects society. For example, Taghavi and Miranda [2003] noted that the damage of non-structural elements yields the largest economic losses due to earthquakes. In fact, non-structural elements can represent from 60% to 90% of the total cost for buildings with the intended use of office/schools, hotels, and hospitals. For instance, after the Emilia Romagna earthquake, little structural damage was reported, but widespread losses for non-structural elements was observed [Jones, 2016]. Between the years 1990 and 2014, Italy faced over 44% of economic losses as consequence of natural hazards [Prevention Web, 2017] highlighting the severe economic impact of these natural events. However, not only the economic impact of earthquakes is important, but also the interruption of services and daily life have been demonstrated to be a very critical aspect. For instance, Jones [2016] mentioned this as a critical issue in the ongoing recovery of the city of L'Aquila following the 2009 event.

Consequently, the Italian laws [OPCM 20.03.2003 n3274, 2003; DM 14.01.2008, 2008] have stated that the public administrations have an obligation to perform the vulnerability assessment of the strategic buildings of their property, attracting the attention of practitioners toward procedures for the seismic safety assessment of existing structures. What's more, the safety level has to be checked according to the present Italian National Code [NTC, 2008]. Seismic vulnerability has materialised the necessity for seismic assessment as a tool to quantify risk and propose alternatives to diminish that risk. Traditionally, seismic assessment is focused on improving the structural behaviour for a specified intensity level and structural limit state. For example, Fiore *et al.* [2012] implemented the HAZUS methodology for assessing school buildings located in the province of Foggia, Italy. This methodology compares the “seismic demand”, expressed in terms of the dimensionless displacement response spectrum, and the “structural capacity”, expressed by an equivalent force-displacement curve obtained from a non-linear analysis. As mentioned by Verderame *et al.* [2010], the application of this semi-quantitative approach is conditioned by the great amount of basic data and relevant computational effort. Another more common method, as presented by FEMA 365 and NTC 2008 or Eurocode 8, part 3, provides guidelines to develop a performance assessment so that different limit states can be enhanced. Cardone and Perrone [2016] and O'Reilly [2016] examined the application of the methodology outlined in FEMA P58 [FEMA P58-1, 2012; FEMA P58-2, 2012] throughout the assessment of several RC frame buildings designed without any modern seismic design code provisions. As explained by Gara *et al.* [2017], following the after-shock sequence of the 2016 Central Italy earthquake, retrofitting of a school with two dissipative towers was undertaken and improved the seismic behaviour of the building. Therefore, the structure was able to withstand a subsequent seismic event with almost no damage in neither structural nor non-structural elements.

Likewise, the seismic vulnerability of non-structural elements is important for ensuring the life safety of occupants and cost limitation since the damage of non-structural elements is typically associated with more frequent, medium-to-low intensity compared to structural damage that typically is induced during higher intensity events. As reported by Taghavi and Miranda [2003]

the structure typically represents about 20% of the cost of the whole building, whereas the rest typically consist of non-structural elements and contents. As stated by Sousa and Monteiro [2016], the damage of non-structural elements presents a substantial economic loss for residential buildings as results of past earthquakes [Calvi *et al.*, 2016], and by retrofitting these elements; for instance, infills and partitions walls, can result in a reduction of seismic losses, as well as the threat to an occupant's life. FEMA 74 [FEMA E-74, 2012] provides several simple measures for retrofitting several non-structural elements based on a combination of common sense and additional protective measures such as seismic anchorage and bracing which can be enough to improve their seismic behaviour. Therefore, retrofitting interventions on these elements based on a seismic vulnerability assessment define a priority that can be used for better management and reduction on the seismic risk and improvement of the safety of users [De Angelis and Pecce, 2015].

### 1.1 Review of Past Damage to School Buildings

The U.S. Department of Commerce National Oceanic and Atmospheric Administration presented a brief review of the damage sustained by school and university building around the world as a result of major earthquakes. This report discusses 17 destructive earthquakes that occurred in nine countries over the period of more than a century from 1886 to 1985. Some of these events are described in the Table 1-1.

**Table 1-1. Damage report of some school and university building around the world, U.S. Department of Commerce National Oceanic and Atmospheric Administration.**

Place	Date	Damage description
Long Beach, California, USA	March 10, 1993	Total damage \$40 million, collapse of John Muir School on Pacific Avenue.
Helena, Montana, USA	October 31, 1995	Total damage \$4 million, collapsed of - the west wing of Helena High Scholl despite being completed only two month prior the earthquake, cost \$500,000.
Lima, Peru	October 3, 1974	Over 2000 people were injured, column failure caused the roof to sag on a one-story classroom at Agricultural University.
Lice, Turkey	September 6, 1975	Total damage \$17 million, all lateral resisting elements were shattered in the west wall of the high school building.
Tanshan, People's Republic of China	July 27, 1976	Total damage \$5,600 million, collapse of a classroom and laboratory building at the College Minin Institute, more than 2000 students were killed.

One of the parameters used during the initial steps of a seismic assessment is the age of the building, since it provides an idea of construction procedures and design criteria implemented

at the time of its conception. Furthermore, other aspects such as school layout, construction material, and practices used reveal inadequate material quality and insufficient anchoring and overlapping lengths of steel bars in case of RC buildings. Moreover, non-structural hazards, such as falling objects like loose ceiling tiles and hanging light fixtures, all contribute to the seismic vulnerability of schools [Calvi *et al.*, 2016]. Additionally, two special structural features are found to be important: short columns and soft stories [O'Reilly, 2016].

The relatively recent introduction of a more refined method for seismic design incorporated into the Italian code also has influenced the poor response of many structures built before these requirements were introduced in the 1970s. The story of the Italian rules concerning RC buildings as stated by Sollazzo and Sgobbo [2011], can be divided into two generations. The first one from 1925 to 1938, with the Regio Decreto no. 229 of 16/11/1939 [Regio Decreto, 1939] being the main reference ruled as the standard for the design and the execution of RC structures during this period. The second generation corresponds to all the modern building codes developed from 1970s up until the present day. In 1972, the law D.M. 30/05/1972 [D.M. LL. PP., 1972] introduced several innovations, including the concept of "characteristic strength", which paved the way for the probabilistic approach in structural safety. Then in 1980, the semi-probabilistic limit state design is introduced, and a vast operation of seismic zoning of the territory was completed, but only after 1980s methods of seismic analysis were introduced, such as equivalent static analysis and modal analysis, which subsequently found widespread applications.

Fiore *et al.* [2012] highlighted the main aspects causing the collapse of old RC structures generally built prior to the 1970s. Among these factors are the number of floors and the regularity in plan and in elevation, being the influence of the geometric configuration on the structural response of the building recognised worldwide. Material quality has also been considered: in the case of concrete there is a high strength variability [Fiore *et al.*, 2012], and in the case of steel, reinforcement bars are non-corrugate with values of admissible tensile strength comprised between 140 and 200 MPa. Similarly, O'Reilly [2016] illustrated several issues concerning old RC frame buildings in Italy prior to 1970 through a set of case study buildings. O'Reilly [2016] discussed the potential shear failure on columns as a result of the interaction with masonry infills. Moreover, as these RC frames were designed using just gravity load, they exhibited non-ductile modes on columns, column-sway mechanisms, and beam-column joint mechanisms, among others, during seismic events. The lack of transverse reinforcement is also related to the shear failure of columns. Salvatore *et al.* [2009] provide a summary of observed damage to six different school structures as a result of the L'Aquila earthquake. In the Scuola Media G. Carducci in L'Aquila during the 2009 event, some shear cracking of column members was presented, in addition to the shear failure, buckling of longitudinal reinforcement was also observed, indicating that the spacing between stirrups was sufficiently large to allow bars to buckle, and also suggesting that lack of transversal reinforcement. During the Emilia-Romagna earthquake in 2012, further shear failures were observed, with some of the shear failures associated to the effect of short columns. This type of failure occurs when the length of the column is reduced by a non-structural element, generally an infill wall, in consequence, the column is subjected to higher shear force but with a constant flexural capacity. Salvatore *et al.* [2009] noted that the ground floor columns at the Istituto

Tecnico Commerciale L. Rendina in L'Aquila showed signs of shear cracking corresponding to the points at which the staircases were attached, which was again noted at the Scuola Media G. Carducci. This type of behaviour is clearly highlighted in the reconnaissance report by Verderame *et al.* [2009]. Also, considerable damage has been noted due to the flexural response of column members due to a lack of capacity design considerations resulting in an unfavourable strong beam-weak column strength hierarchy in many buildings. In the case of beam-column joints, which are typically considered as rigid zones with no special consideration during design, lack of transverse shear reinforcement also plays an important role in their ductile behaviour, causing concrete cracking and crushing, forming diagonal cracks and producing buckling of longitudinal reinforcement leading to a loss of axial load carrying capacity. Masonry infills, although typically considered as non-structural elements, have led to damage and failure of the surrounding structural elements since they modify the seismic response of the structure through their interaction. The presence of masonry infills reduces the fundamental period of the structure and the additional forces can be problematic, causing both in-plane and out-of-the plane failure.

## 1.2 Scope and Layout of Thesis

The main objective of this study is to assess the seismic vulnerability of an existing RC school building and propose a number of retrofitting schemes. These retrofitting techniques will be both structural and non-structural and will demonstrate their relative performance through advanced seismic assessment methods.

The initial part of the study will aim to assess the performance of the structure, which has been carried out to a good extent as part of the existing project entitled “Progetto Scuole” at the European Centre for Training and Research in Earthquake Engineering (EUCENTRE) that aimed to assess existing school buildings in Italy. Further work presented herein aim to accurately quantify the different limit states of the building using the Italian National Code [NTC, 2008]. From the initial analysis, the vulnerable structural elements will be identified and modified based on maintaining the structural integrity of the building. From the list of vulnerable elements, a number of retrofitting schemes will be proposed. These will be based on the list of vulnerable components and also in consultation with an engineering firm in Italy. Methods to implement these structural retrofits will be determined along with the cost and the updated component fragilities. Information from the repairs carried out following the 2009 L'Aquila earthquake will be incorporated and the retrofitting will be carried out to match some target objectives. Considering non-structural retrofit and four structural retrofits, an analysis matrix of the different cases will be created. The non-linear analysis of the retrofitted buildings will be carried out again and the loss estimation also repeated. Relative improvements in the performance, defined in terms of annualised economic losses and collapse risk, will be identified and discussed. Furthermore, these are carried out within the performance and requirements of the Italian National code [NTC, 2008] so as to provide an indication of how these requirements improve the seismic performance when evaluated using new extensive methodologies.

The above scheme is consistent with the recent study outlined by O'Reilly *et al.* [2017], featuring a number of extensions regarding the consideration of alternative retrofitting

solutions. Among these are the use of an existing school building that is representative of the existing RC school building stock in Italy. A number of retrofitting techniques will be explored for both structural and non-structural elements. Attention to detail will be paid to the sizing and layout of the retrofits with respect to design codes and also with input from practitioners. Following this framework, the thesis has been organised as follows:

Chapter 2 presents a literature review on the existing guidelines for assessing and retrofitting RC buildings. An extensive literature review will be carried out so that the most convenient assessment method can be implemented during the case study application. Additionally, different retrofitting techniques will also be presented for both structural and non-structural elements in order to highlight the importance of retrofitting both elements.

Chapter 3 explains the considerations made to develop the numerical model as well as presents the assessment of the original building from a structural point of view by following the procedures stated in Chapter 2. Results of the performance analysis are shown not only for the original building but also for the bare frame (i.e. original building without infill walls) in order to point out its influence on the overall structural response by incorporating the infills into the numerical model.

Chapter 4 explores each of the retrofitting alternatives defined in Chapter 2 by explaining how each retrofitting was performed and/or idealised. Here these alternatives are only evaluated from a structural point of view, comparing the different improved aspect achieved such as strength capacity, displacement capacity, and element damage control with the requirement imposed by the local code [NTC, 2008] regarding different limit states.

Chapter 5 further examines the assessment of the retrofitting alternatives by considering more detailed aspects such as non-linear history analyses response of structural elements, collapse risk, and loss estimation. This section is considered a special topic since it compares each of the retrofitting schemes from the loss estimation point of view, as well as demonstrates the influence of retrofitting the non-structural elements as a way of reducing the expected annual loss. In the end, the most effective retrofitting proposal in terms of reduction in both the expected annual loss and collapse risk is identified.

In general, this work is aimed to be a guide for practitioners, students and other engineers working in the seismic assessment field. This is to explore the different assessment techniques that can be implemented as well as to select the most beneficial retrofit intervention, not only considering the structural performance, but also the performance of the non-structural elements via loss estimation.

## 2 LITERATURE REVIEW

### 2.1 Introduction

Seismic assessment aims to verify whether an existing building satisfies or not a defined set of performance goals for a given level of seismic hazard. This is typically done through a set of tools to determine the existing vulnerability of a structure by quantifying its performance in terms of strength and deformation capacity. The results indicate if the building needs structural intervention; in case of structural intervention, the inputs values for designing a retrofitting scheme can be derived from the results of the assessment. Despite these being the traditional criteria, performance can now be described also in terms of monetary losses, loss of life and downtime in what can be described as the “3Ds” referring to deaths, dollars, and downtime previously outlined in Porter [2003]. With this in mind, an effective retrofitting intervention seeks to improve the overall structural behaviour so that damage in both structural and non-structural elements can be minimised and also the expected annual loss (i.e. integral of vulnerability curve of the structure with the hazard curve for the site under consideration) reduced. Regarding the non-structural elements, it has been demonstrated [Taghavi and Miranda, 2003; O'Reilly *et al.*, 2018a] that they also contribute considerably to the EAL. Therefore, retrofitting these elements can result in a better overall performance defined in terms of expected annual loss (EAL). What is more, EAL and collapse risk are related since by improving the structural behaviour, the collapse risk decreases, although O'Reilly and Sullivan [2018a] have demonstrated that improved structural behaviour does not necessarily translate in improved EAL. Consequently, the overall effectiveness of a retrofitting intervention could be evaluated in terms of EAL rather than on code-defined performance limits aimed to ensure damage limitation and life-safety.

### 2.2 Existing Guidelines on Assessment and Retrofitting of RC Buildings

Assessment approaches are described by different international building codes, which provide guidelines on seismic assessment. For instance, the New Zealand building code [NZSEE, 2016], presents elastic (force-based procedure) and non-linear (non-linear static pushover, non-linear time history), and displacement-based analysis methods to evaluate a building's life safety performance. The procedure is based on the seismic rating of the building, expressed as a percentage of new building standard (%NBS), which meets the requirement of the current code and is described by Equation (2.1):

$$\%NBS = \frac{\text{Ultimate capacity (seismic) of the building}}{\text{Ultimate Limits Stated (ULS) seismic demand}} \times 100\% \quad (2.1)$$

Table 2-1 indicates the scaling factor to be used in a performance assessment as a function of the return period for each importance level. These values are based on the provision specified by ASCE 4-13 [2014]. Likewise, Table 2-2 presents limits to classify the performance of the building in term of the risk level through the seismic rating of the building (%NBS). These guidelines are quite similar to the requirement presented by the Italian national code [NTC, 2008] detailed in Table 2-5.

**Table 2-1. Reference return period and ground motion scaling factors for 100%NBS for – Basic Performance Objective Equivalent to New building Standards defined in ASCE 4-13 (2014) for use with that document – Table C1.1 NZSEE-C1 2016.**

Importance Level (IL)	Building performance level	
	Life safety (return period)	Collapse prevention (scale factor)
IL 1	100	1.8
IL 2	500	1.8
IL 3	1000	1.8
IL 4	2500	1.8

For the assessment of a school building, the importance level is given as IL 3 according to AS/NZS1170.0:2002 for the intended used of a structure, then the response spectra and peak ground acceleration, are obtained for a return period of 1000 years, to ensure life safety a scale factor of 1.8 is intended to be applied to the ground motion so that collapse prevention can be evaluated.

**Table 2-2. Assessment outcomes (potential building status), Table A3.1 NZSEE 2016.**

Percentage of New Building Standard (%NBS)	Alpha rating	Approx. risk relative to a new building
>100	A+	Less than or comparable to
80-100	A	1 – 2 times greater
67-79	B	2 – 5 times greater
35-66	C	5 – 10 times greater
20-34	D	10 – 25 times greater
<20	E	25 times greater

The performance criteria of NZSEE [2016] specifies three points for risk level of existing buildings meanwhile new building presents no risk as long as the building is designed according

to the seismic design provision specified in the code. The performance criteria are described as follows:

- New buildings: the building shall be shown to attain its ultimate state (ULS) when subjected to no less than 100% of the design earthquake shaking based on the importance level at the site.
- Existing buildings – low risk: The building shall be shown to attain ULS when subjected to no less than 67% of the design earthquake shaking at the site.
- Existing buildings – moderate risk: The building shall be shown to attain ULS when subjected to no less than 33% of design earthquake at the site.
- Existing building - high risk: A high risk existing building is one that attains ULS when subjected to less than 33% of the design earthquake at the site.

In the same way, Eurocode 8 [EN 1998-3:2005, 2005], provides criteria for evaluating the seismic assessment performance of individual buildings, as well as a set of possible retrofitting approaches. Among the analyses described are the elastic methods (lateral force analysis, modal response spectrum analysis), non-linear (static pushover analysis, time history dynamic analysis) and lateral force method (q-factor approach). Three limits states (LS) are defined in this code, namely near collapse (NC), significant damage (SD), and damage limitation (DL). Table 2-3 describes the return periods related to each LS as well as the probability of exceedance in 50 years limit to evaluate a building's performance.

**Table 2-3. Return period and the probability of exceedance in 50 years for each limit state for ordinary new buildings, [EN 1998-3:2005, 2005].**

Limits State (LS)	Building performance level	
	Return Period (years)	Probability of exceedance in 50 yrs.
DL	225	20%
SD	475	10%
NC	2475	2%

On the other hand, ASCE [2017] describes rehabilitation objectives (basic safety objective, enhanced rehabilitation objectives, limited rehabilitation objectives), target building performance levels (structural performance levels and ranges, non-structural performance levels, designation of target building performance levels), and analysis procedures (linear static procedure, linear dynamics procedure, nonlinear static procedure, nonlinear dynamics procedure). For example, Table 2-4 details a description of performance levels for a concrete frame.

In addition to international codes, the available Italian national code [NTC, 2008] provides four types of analysis (linear analysis or non-linear, static analysis or dynamic, non-linear analysis or static, non-linear static analysis or dynamics) and four LSs, which are described as follows:

- Stato Limite di Operatività – “Operational” (SLO): following the earthquake the building’s structural and non-structural elements maintain their function and do not suffer any damage or significant interruption of their usage.
- Stato Limite di Danno – “Damage Control” (SLD): following the earthquake the buildings structural and non-structural elements suffer damage that does not put the occupants at risk and does not significantly compromise the overall capacity and stiffness of the structure to maintain the vertical and horizontal actions.
- Stato Limite di Salvaguardia della Vita – “Life Safety” (SLV): following the earthquake the building suffers damage and collapse to the non-structural elements and damage to the structural elements that result in a significant loss of lateral stiffness, but still maintains gravity load carrying capacity and a margin of safety against collapse.
- Stato Limite di Prevenzione del Collasco – “Collapse Prevention” (SLC): following the earthquake the structure suffers heavy damage to both structural and non-structural elements, the structure maintains gravity load carrying capacity and has a slender margin of safety against collapse.

**Table 2-4. Description structural performance objectives based on the limit state for concrete frame, [FEMA 356].**

Type	Structural Performance Levels		
	Collapse Prevention S-5	Life Safety S-3	Immediate Occupancy S-1
Primary	Extensive cracking and hinge formation in ductile elements. Limited cracking and/or splice failure in some non-ductile columns. Severe damage in short columns	Extensive damage in beams. Spalling of cover and shear cracking ( $<1/8$ " width) for ductile columns. Minor spalling in non-ductile columns. Joint cracks $<1/8$ " wide.	Minos hairline cracking. Limited yielding possible at a few locations. No crushing (strain below 0.003).
Secondary	Extensive spalling in columns (limited shortening) and beams. Severe joint damage. Some reinforcement buckled.	Extensive cracking and hinge formation in ductile elements. Limited cracking and/or splice failure in some non-ductile columns. Severe damage in short columns	Minor spalling in few places in ductile columns and beams. Flexural cracking in beams and columns. Shear cracking in joints $< 1/16$ " width.
Drift	4% transient or permanent	2% transient; 1% permanent	1% transient; Negligible permanent

The first two limit states, SLO and SLD, were defined arbitrarily in a 2009 addendum to the NTC 2008 guidelines in Italy as fixed values, while the last two were based on the occurrence of the ultimate chord rotation in the frame members using the expression given in Equation A.3 of Eurocode 8 – Part 3. These four limit states correspond to structures of usage Class II, but for the case of school buildings, which is deemed Class III, the time period is amplified by a factor of 1.5. The following values presented in Table 2-5 have been taken and modified from

the Table 2.4.II of NTC 2008 for the assessment of school buildings to illustrate the return period of ground motion shaking that school buildings are to be assessed with.

**Table 2-5. NTC 2008 return period for each limit state of a school building with nominal life of 50-years, which has a Class III usage.**

Limits State		Probability of Exceedance	Return Period [years]
Serviceability limit State (SLE)	SLO	83%	45
Ultimate Limit State (SLU)	SLD	63%	75
	SLV	10%	712
	SLV	5%	1463

All the aforementioned methods describe traditional performance assessments based on limit state definitions for strength and deformation capacity. However, the PEER (Pacific Center for Earthquake Engineering Research) Centre methodology, performance-based earthquake engineering (PBEE) proposed in the early 2000's [Cornell and Krawinkler, 2000], quantifies the performance of buildings in a more useful way for decisions making. This framework has been extensively developed. FEMA has published the P-58 guidelines to aid practitioners in implementing the method. FEMA P-58 [FEMA P58-1, 2012; FEMA P58-2, 2012, FEMA P58-3, 2012] addresses this performance methodology in terms of the probability of incurring casualties, repair, and replacement cost, repair time, and unsafe placarding. The performance can be assessed for a particular earthquake scenario or considering all earthquakes that may occur, and the likelihood of each, over a specified period. In this case, the performance is described as the expected losses due to induced damage in the building instead of speaking of the maximum storey drift at specified limit state, for example. The foundation of PEER PBEE assessment methodology was settled by Cornell and Krawinkler [2000]; and it can be generally described by Equation (2.2):

$$\lambda[DV|D] = \iiint P[DV|DM, D] P[DM|EDP, D] P[EDP|IM, D] \lambda[IM|D] dIM dEDP dDM \quad (2.2)$$

Where  $P[A|B]$  is the conditional probability of A given B,  $\lambda$  represents the mean annual frequency of exceedance (MAFE) for the decision variable (DV), which can be defined in terms of the aforementioned performance measures, such as monetary losses, for a given structure located at site D. The variable DM represents a given damage level and IM ground motion intensity. The performance is computed by evaluating the triple integral in Equation (2.2), computing the exceedance of the decision variable DV for a given structure and site location. This damage is determined as a function of the demand on the structure defined by its engineering demand parameter (EDP) that can be determined from analysis of a representative numerical model of its behaviour. This structural response is then computed for a range of IM, which are then, in turn, linked back to the MAFE using the site's hazard curve determined from probabilistic seismic hazard analysis (PSHA). Figure 2.1 outlines this procedure from beginning to end. Figure 2.1 illustrates the components of PEER PBEE assessment methodology and also described each one of the variables used in the assessment.

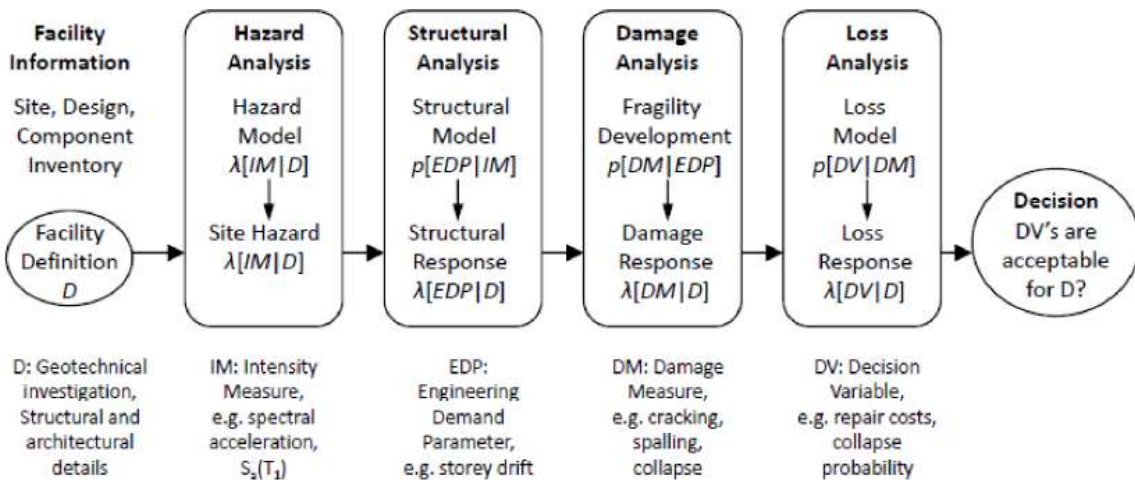


Figure 2.1. Overview of PEER PBEE assessment framework outlined by Cornell and Krawinkler [2000].

The EAL of a building can be computed by integrating the expected losses expressed as a function of intensity over the site hazard curve obtained from PSHA as shown in Equation (2.3).

$$EAL = \int E[L_T|IM] \left| \frac{d\lambda_{IM}}{dIM} \right| dIM \quad (2.3)$$

Where  $E[L_T|IM]$  represents the total expected losses for a given intensity measure (IM) level of shaking and site D, as described above. In this study, a performance assessment in terms of NTC 2008 limit state requirements and an overall loss assessment of the building was conducted to examine not just the life safety performance of the building, but also its economic vulnerability due to damage induced in the structural and non-structural elements. Even more, with these results, several retrofitting techniques were proposed aimed at improving the structural performance and reducing the EAL and collapse risk. These points are explained in the coming Chapters.

### 2.3 Assessment Methods

Once the numerical representation of a building is completed, an initial assessment can be developed, this may consist of modal and static pushover (SPO) analyses that determine properties and capacity of the structure. Likewise, it examines the fundamental aspect of its structural behaviour such as the presence of any soft or weak-storey mechanisms, type of failure in elements, among other factors. Generally, these simplified non-linear analyses can provide more detailed assessment results as local vs global failure modes, strength hierarchy of elements and failure sequence. Then, more elaborated methods can be used to obtain the properties of the subjected structure to dynamics actions, which may consist of incremental dynamic analysis (IDA) or multiple strip analysis (MSA) [Baker, 2015], which are procedures used to characterise the structural response with respect to increasing intensity that are then used in collapse assessment and loss estimation analysis. Based on either of these methods, a selection of retrofit strategies, their design and implementation can be presented.

### 2.3.1 SLaMA Method

The simple lateral mechanism analysis, or SLaMA, determines the strength to deformation (pushover) relationship for the building as a whole. The New Zealand code [NZSEE, 2016], recommends this method as a starting point for any detailed seismic assessment, which provides information about the probable inelastic deformation mechanism and the lateral strength and displacement capacity through load path, the hierarchy of strength, and the available ductility. In other words, this method determines the global nonlinear pushover capacity. Figure 2.2 illustrates this procedure. This method is well developed for ductile reinforced concrete structures [Priestley, 1996; Park, 1996; Priestley and Calvi, 1991], and some recent advancement have been made by Sullivan *et al.* [2009]. The main weakness is that the sequence of development of inelastic action between different members of the structure may not be identified. For this study, some of the approaches presented for the SLaMa method were employed, but the capacity and failure mechanisms were obtained from conventional non-linear analysis, using the SPO and N2 methods.

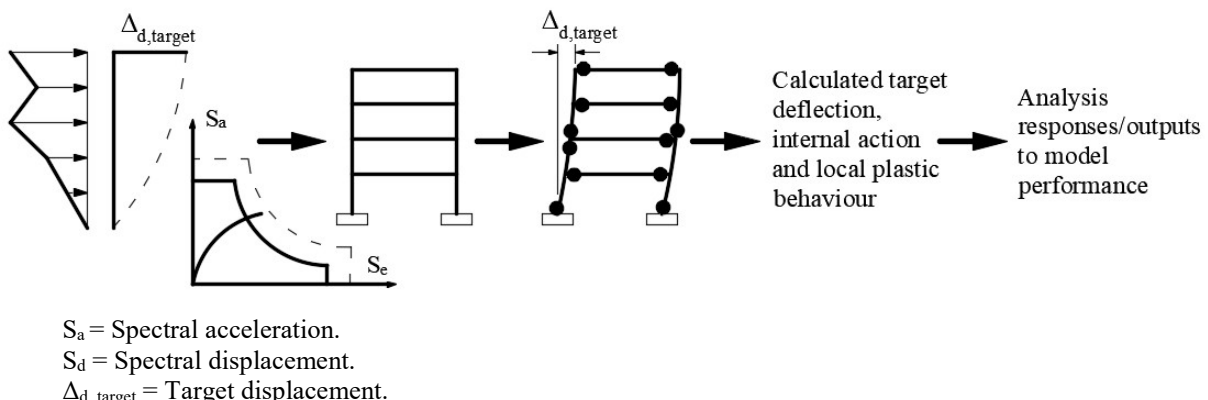


Figure 2.2. Non-linear pushover analysis and acceleration-displacement response spectrum (ADRS), [after NZSEE, 2016].

### 2.3.2 Static Pushover Analysis

The SPO analysis determines the capacity of the structure under increasing horizontal loads and also tracks the progression of damage in the structures. The lateral loads are applied in proportion to the product of the mass and elevation at each level until a control node of the numerical model reaches a specified target displacement. As the structure deforms laterally, the exceedance of a number of limit states may be identified, as illustrated in Figure 2.3.

Performance levels cited in PBEE documents such as the Vision 2000 document [SEAOC, 1995] or the Italian National Code (NTC 2008) [NTC, 2008], are based on the limit states obtained from SPO analysis. Cornell and Krawinkler [2000] explained that limit states may be defined as a function of the SPO curves as:

- SLO – 0.25% peak storey drift based on the median values of the first damage state for typical gypsum partitions and other drift sensitive non-structural elements.

- SLD – the minimum value between 0.5% and the structural yield point on the SPO curve, which is in keeping both with the non-structural drift requirements of NTC 2008 and not to significantly compromise the overall capacity and stiffness of the structure.
- SLV – the point of maximum lateral capacity of the structure, as this corresponds to a significant loss of lateral stiffness, but still maintains gravity load carrying capacity and a margin of safety against collapse.
- SLC – this is defined as the point of a 20% drop in lateral capacity of the structure, as this maintains gravity load carrying capacity and has a slender margin of safety against collapse.

The displaced shape profile can be used to identify the critical storey drift in the structure of that particular limit state.

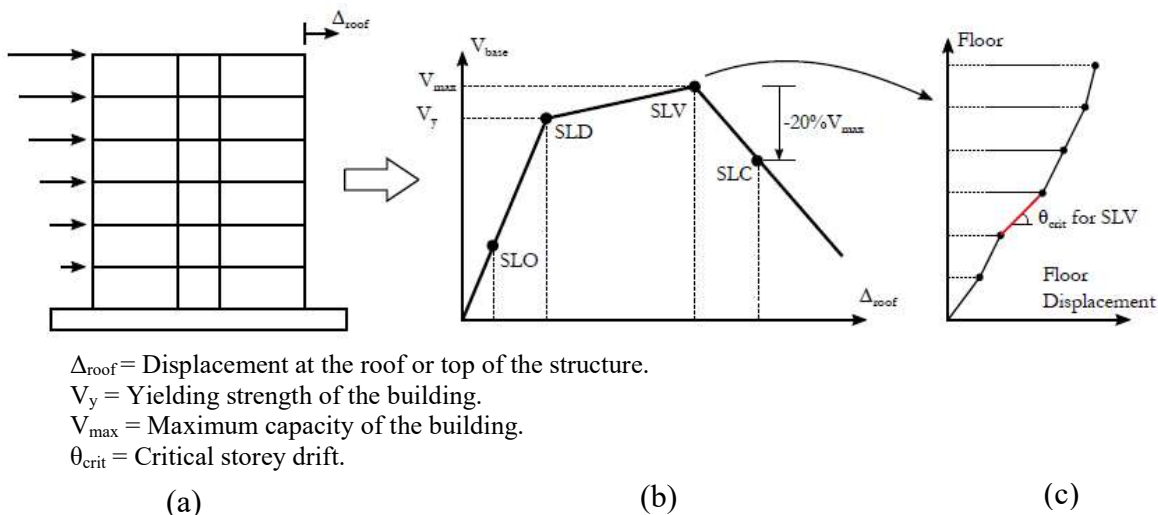


**Figure 2.3. SPO application and evaluation, (a) Static Pushover, (b) Identification of limit-States, (c) Establish Performance Criterion, [after O'Reilly, 2016].**

### 2.3.3 N2 Method

The N2 method [Fajfar, 2000] is described in Annex B of the Eurocode 8 [EN 1998-3:2005] as a non-linear static analysis method which combines the pushover analysis of a multi-degree-of-freedom system (MDOF) with the response spectrum analysis of an equivalent single-degree-of-freedom (SDOF) system to identify the exceedance of predefined limit states for a given level of seismic hazard. This relatively simple method provides a good estimate of the structure performance in terms of capacity, displacement, drift, failure mechanism, among other parameters, this N2 method is nothing more than a capacity spectrum method for which the capacity curve must be compared to the demand spectrum corresponding to the equivalent viscous damping of the structure at the target displacement, being the equivalent damping equal to 5%. The procedure can be summarised by the following steps:

- First, the elastic response spectrum for the return period of the limit state to be assessed is determined. This spectrum is idealised based on the equations proposed by the

Eurocode 8 [EN 1998-3:2005] on the part of design response spectrum for a 5% of equivalent damping ratio, which is discussed further in Chapter 3.

- An equivalent SDOF capacity curve is computed by using the guidelines of Fajfar [2000], in the case of considering the contribution of infills walls within the analysis, the procedure described by Dolšek and Fajfar [2004, 2005] ought to be followed. Figure 2.4 displays both cases of SDOF capacity curves.
- The equivalent SDOF capacity curve and response capacity spectrum are plotted together illustrating whether the equivalent period is lower or higher than the upper limit of the period of the constant spectral acceleration branch, this difference influence the computation of the target displacement as shown in Figure 2.5. Dolšek and Fajfar [2004] and Dolšek and Fajfar [2005] explain how to compute the equivalent period ( $T$ ), ductility( $\mu_s$ ), reduction factor ( $R(\mu_s)$ ) and target displacement for the SDOF.
- Finally, the target displacement of the equivalent SDOF is transformed into the target displacement of the MDOF (original structure) for a specified level of seismic hazard. Figure 2.6 summarises the whole procedure described above.

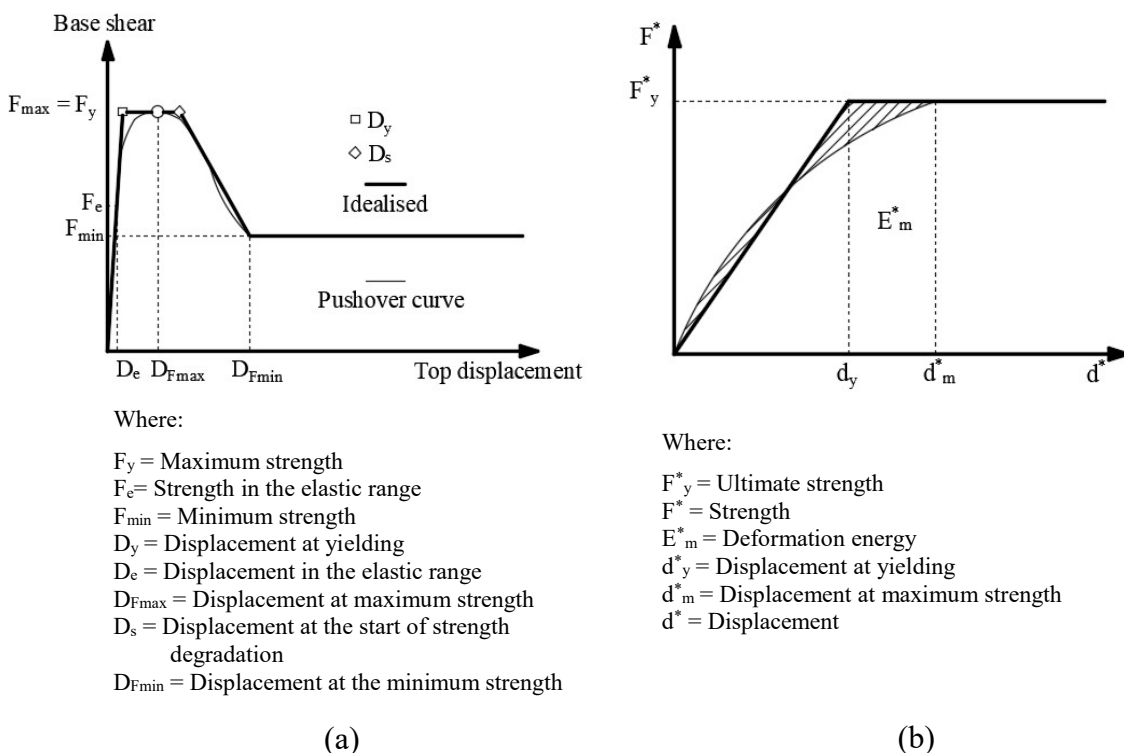


**Figure 2.4. Idealization of force–displacement relationship, (a) Infill reinforced concrete frame [after Dolšek and Fajfar, 2005], (b) frame structures [after EN 1998-3:2005].**

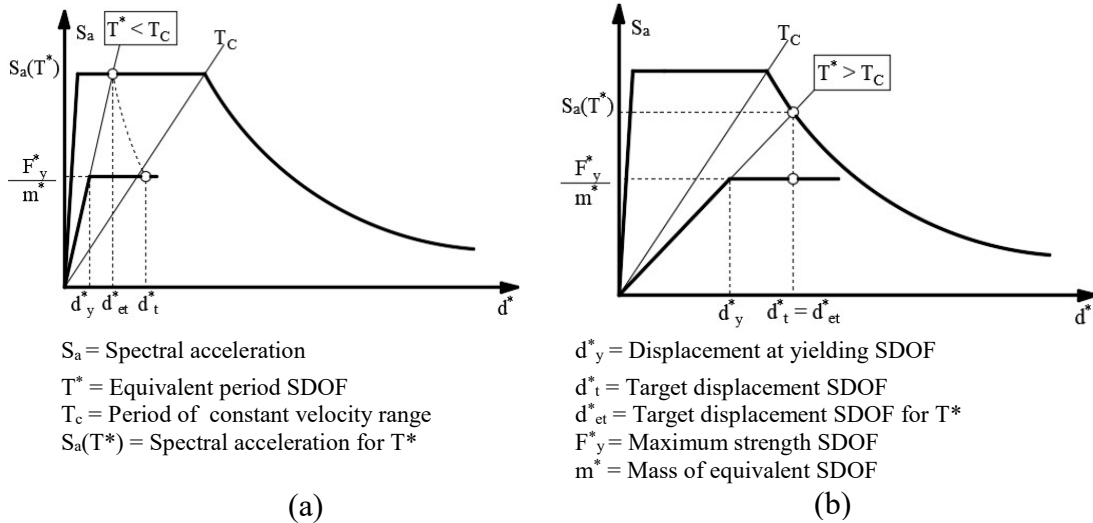


**Figure 2.5. Determination of the target displacement for the equivalent SDOF, (a) Short period range, (b) Medium and long period range, [after EN 1998:2005].**

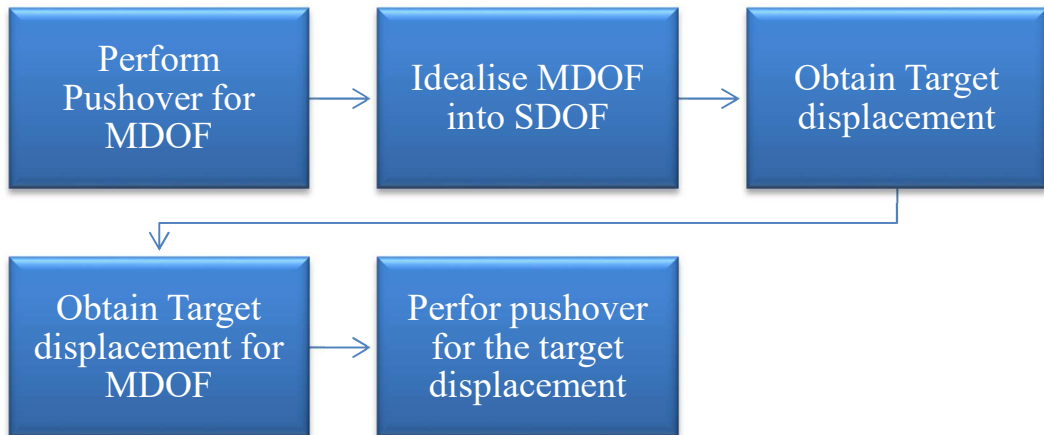


**Figure 2.6. Sequence of N2 Method.**

#### 2.3.4 Strength Hierarchy Assessment.

This method identifies the weakest structural element in a reinforced concrete (RC) beam-column joint [Tasligedik *et al.*, 2016]. Notably, this technique is quite useful since it allows engineers to prevent undesirable failure mechanisms by determining which element must be strengthened in order to ensure ductile behaviour. This is defined as beam hinging in which the first elements to undergo inelastic damage are the beams, which are then followed by the column and lastly the joint.

This procedure is well described by Tasligedik *et al.* [2016], and consists in performing a linear static analysis by applying a lateral load as a function of the capacity of the building. From this analysis is determined the path of loads for each element. Furthermore, the moment capacity of each element within a joint is computed as function of the axial load as shown in Figure 2.7(a), this includes the ultimate moment capacity of the beam, which is constant for any axial load, the joint moment capacity obtained as function of its shear capacity, the interaction diagram of the column and the shear capacity of the column as in terms of moment capacity. Finally, these

capacities and the variation of the axial load in the column due to the non-linear analysis are plotted all together.

The variation of axial load corresponds to the two inclined displayed in Figure 2.7(c) since seismic loads are reversible but the non-linear analysis is just performed in just one direction. Therefore, this variation takes the cyclic loading nature of earthquakes into account. The failure sequence is determined as the variation of axial load intersects each of the capacity curves of the elements in sequential order as shown in the Figure 2.7(c). Since the capacity of the structure and load paths can be already obtained after performing a SPO, it is not necessary to apply the SLAMA method, instead, the values from the SPO can be employed. As shown in Figure 2.8, however, an idealisation of the axial load through a linear variation (shown by a red dotted line) needs to be carried out considering either the maximum axial load or moment within a column.

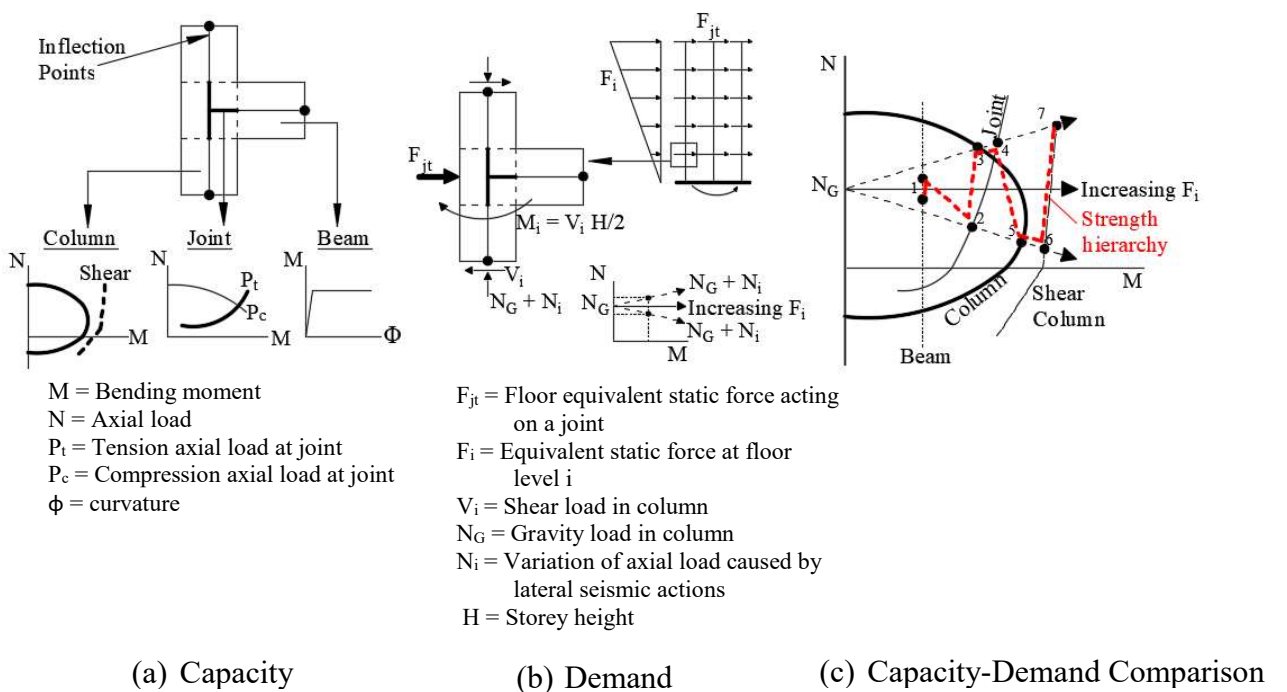


**Figure 2.7.** Step involving the evaluation of the strength hierarchy, [after Tasligedik *et al.*, 2016].

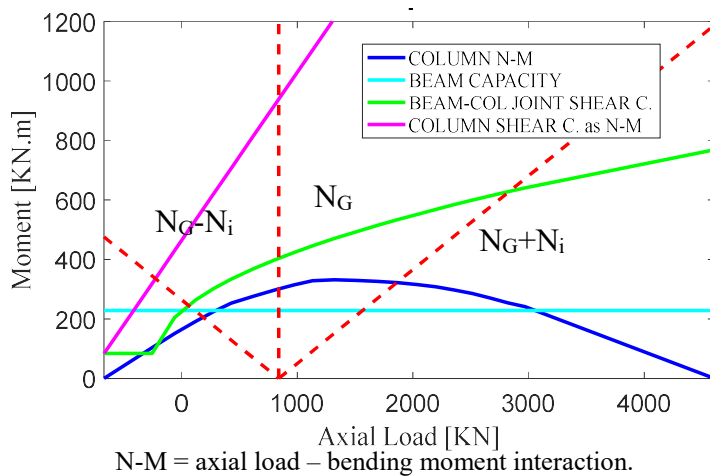


**Figure 2.8. Strength hierarchy evaluation.**

To summarise the strength hierarchy assessment, Figure 2.9 highlights the important parameters and inputs needed to perform this analysis.

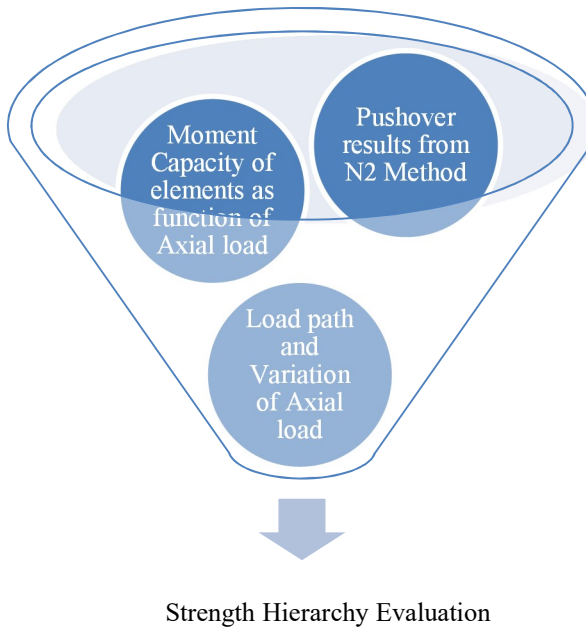


**Figure 2.9. Inputs involving a strength hierarchy evaluation.**

## 2.4 Past Studies on Loss Estimation

Economic losses in a building with increasing seismic intensity is commonly referred to as vulnerability function, representing the direct losses associated with repairing that building as fraction of its replacement cost. In recent years, seismic assessment based on loss estimation has gained popularity since it quantifies the performance of a structure in terms of its EAL. This is obtained by integrating the expected losses as result of the repair costs of all the damaged structural and non-structural elements of a building for every level of ground-motion intensity of interest. In other words, the area underneath the expected monetary loss vs. mean annual frequency of exceedance curves. Many studies on seismic performance classification of RC buildings based on EAL have been developed [Calvi *et al.*, 2014; Liel and Deierlein, 2013; Cardone *et al.*, 2017; O'Reilly *et al.*, 2018a]. For example, Liel and Deierlein, [2013] found that the EAL for non-ductile RC frame buildings evaluated in California ranges from 0.8% to 1.3% of their replacement cost, whereas O'Reilly *et al.* [ 2018a] and Cardone *et al.*, [2017] reported that for RC frame buildings in Italy EAL is about 0.3% and 0.75% respectively. Likewise, this procedure determines from which level of intensity, expressed in terms of return periods, results in complete losses as illustrated by O'Reilly *et al.* [2018a]. Furthermore, EAL assessment can be used to evaluate retrofitting strategies, which are likely to be more realistic and cost effective choices for seismic mitigation. For instance, Cardone *et al.* [2017] selected EAL as a main parameter to determine the most cost-effective seismic rehabilitation strategy for a stock of RC frame buildings, comparing the performance of each alternative in terms of the initial cost of intervention and reduction of repair cost due to earthquake damage. Similarly, Liel and Deierlein [2013] used the break-even point, number of years needed to fully amortize

the cost of the intervention, for evaluating some retrofitting alternatives, indicating what replacement costs are not justified by the benefits when their cost-benefit ratios exceeds the break-even point. It is important to notice that not only structural elements contribute to the expected annual loss, therefore, retrofitting intervention should not be only limited to structural elements but also to non-structural ones, Calvi *et al.*, [2014] illustrated this point by only limiting non-structural interventions, EAL could be significantly reduced. In the same way, Liel and Deierlein [2013] and Cardone *et al.* [2017] came out to the same conclusion. The main reason for this conclusion is that non-structural damage occurs at much lower seismic intensities associated with much higher probability of exceedance than ground motions causing significant structural damage. Therefore, EAL is often mainly controlled by the replacement of expensive non-structural elements under moderate seismic intensities.

## 2.5 Retrofitting Techniques

Traditionally the most common techniques have been related to the design response parameters namely, stiffness, strength and ductility. Elnashai and Pinho, [1998] stated that these parameters can be the starting point for repairing and retrofitting earthquake-damaged structures, along with new requirements of local deformations, performance design and other design criteria imposed by current building codes. Figure 2.10 illustrates how different types of interventions can improve the behaviour of a structure in terms of strength, stiffness and deformation. Where  $F_y$  refers to the maximum strength capacity,  $K_i$  is the initial stiffness,  $K_{eff}$  represents the equivalent stiffness,  $\Delta_y$  and  $\Delta_u$  refers to the yielding and ultimate displacement respectively. Once the aforementioned retrofitting are implemented the new capacities previously described are represented by an apostrophe ( $F'_y$ ,  $F'_i$ ,  $K'_{eff}$ ,  $\Delta'_y$ ,  $\Delta'_u$ ).

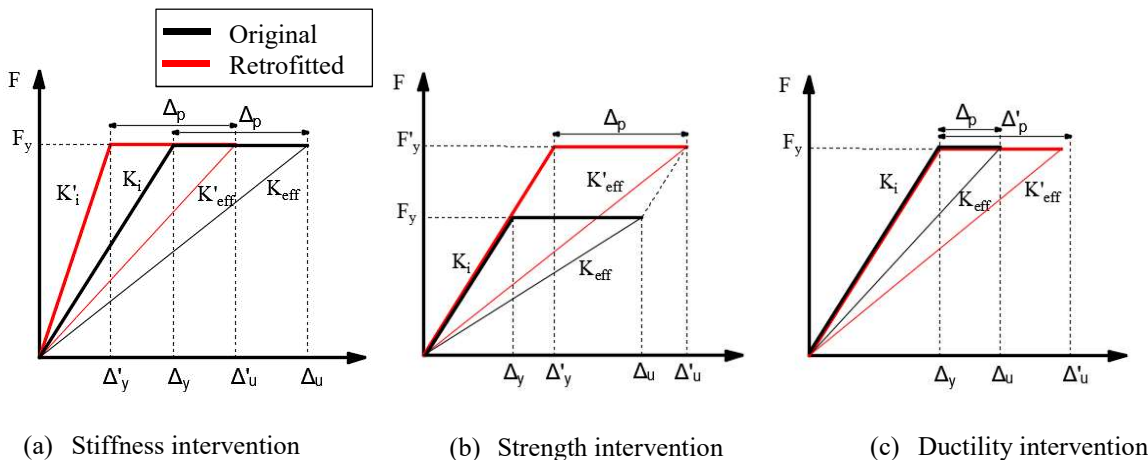


**Figure 2.10. Different structural retrofitting interventions, [after Inashai and Pinho, 1998].**

In a stiffness intervention, illustrated in Figure 2.10(a), the global displacement decreases since the period of the structure has been shortened, but this can lead to an increase on the acceleration demand in the case of small intensities which may be detrimental not only for some structural elements but also for non-structural elements. In the case of strength intervention, illustrated in Figure 2.10(b), the strengthening is done in strategically located members, generally the ones that failed or compromise the overall capacity of the structure or its stability. Additionally, increasing strength would give rise to higher floor accelerations, which would be detrimental

to non-structural elements. In the ductility intervention, illustrated in Figure 2.10(c), the structure is able to undergo higher deformations without significant loss in strength avoiding collapse.

Moreover, Oliveto and Marletta [2005] describe some innovative approaches for seismic retrofitting, which are summarized below:

- Stiffness reduction: this consists of period elongation to decrease the seismic action. Despite being a minor reduction, this may lead to large displacements, and story drifts, which could cause damage to displacement-sensitive non-structural elements and compromising the building's functionality as well. Base isolation can be considered as a special case of stiffness reduction.
- Ductility increase: this is carried through flexural and compressed local confinement, the most common technique being Fibre Reinforced Polymers (FRP), which increases the strength and deformability capacity of structural elements and also reduces damage.
- Damage controlled structures: this is relatively new concept that introduces additional stiffness and energy dissipation by placing a parallel system, called auxiliary structure, so that the primary structure behaves elastically under most severe earthquakes while the auxiliary one responds to the seismic actions. This type of retrofitting has been implemented by Gara *et al.* [2017] in the retrofit of a school building in Central Italy through two steel truss towers placed externally.
- Composite materials: this technique is popular in applications for retrofitting old construction, especially masonry buildings. It confers strong traction resistance in the panel where they are applied, limiting crack extension and width and favouring its closure,
- Active control: this is performed by means of a monitoring and control systems that activate servo-actuated devices capable of applying opposites forces to the seismic actions.
- Hybrid - any suitable combination of the above methods.

All the techniques and methods described above should be applied according to the conditions within a particular project so that the most practical and beneficial retrofit can be achieved. As described by Pampanin [2017], the goal in a retrofitting strategy lies in a balance among the technique effectiveness, its simplicity, and its cost. The retrofitting intervention is effective as long as undesirable mechanisms, such as collapse can be avoided or if the level of damage in the structure is reduced. It is simple when it can be applied with limited engineering, in other words, its application and implementation is not complicated. Finally, it is cost effective when the cost of the whole intervention is reasonable in relation to the value of the old building to the socio-economic reality of the area.

### ***2.5.1 Structural Retrofitting***

The present study is focused on presenting a less invasive retrofitting alternative that can improve the lack of strength in some elements and besides slightly modifies the dynamic properties of the structure. Therefore, for this work, the most convenient retrofitting technique and implementation that can meet this requirement is the use of FRP.

### 2.5.2 FRP Retrofitting

Fibre reinforced polymer (FRP), also denominated as composites, are comprised of two materials; fibres and the matrix. Composites are available as thin unidirectional strips, which work only in one direction, and flexible sheets or fabrics, which act in one or at least two different directions. Fibres are the primary load-carrying elements, their diameter ranges from 5 to 25 $\mu\text{m}$ . Their main characteristics are their high tensile strength and linear elastic behaviour to failure. The matrix, typically a polymer of thermoplastic type, has the main functions of protecting the fibres against abrasion or environment corrosion, to bind the fibres together and to distribute the load. Therefore, it is assumed that only fibres carry stresses.

The applicability of any FRP configuration is related to systems that have been tested extensively on reinforced concrete or masonry structures. For instance, wet lay-up, prefabricated elements and special systems meet this requirement [Triantafillou, 2018] as well as strips and bars.

FRPs are available in the market as Carbon (CFRP), Glass (GFRP), Aramid (AFRP), and hybrid and Table 2-6 displays some properties of these composites. Figure 2.11 displays the stress-strain behaviour of these different fabrics compared to steel.

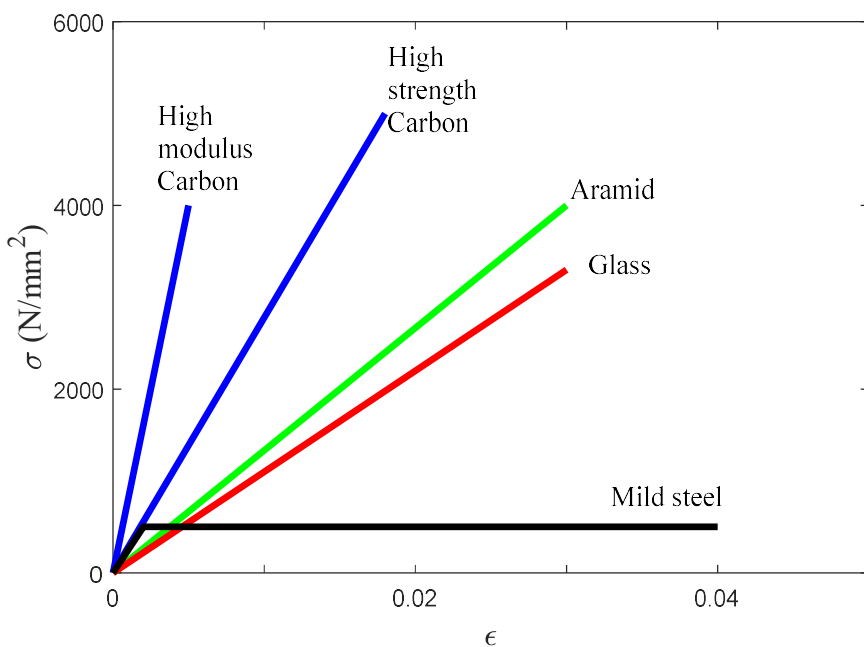


**Figure 2.11. Typical uniaxial tension stress-strain diagrams for different fibres and comparison with steel, [after Triantafillou, 2018].**

**Table 2-6. Typical properties of fibres (from Feldman [1989] and Kim [1995]).**

Material	Elastic modulus (KN/mm <sup>2</sup> )	Tensile strength (N/mm <sup>2</sup> )	Ultimate tensile strain (%)
Carbon			
High strength	215-235	3500-4800	1.4-2.0
Ultra high strength	215-235	3500-6000	1.5-2.3
High modulus	350-500	2500-3100	0.5-0.9
Ultra high modulus	500-700	2100-2400	0.2-0.4
Glass			
E	70-75	1900-3000	3.0-4.5
AR	70-75	1900-3000	3.0-4.5
S	85-90	3500-4800	4.5-5.5
Aramid			
Low modulus	70-80	3500-4100	4.3-5.0
High modulus	115-130	3500-400	2.5-3.5

**(a) Benefits of FRP**

The implementation of FRP for retrofitting represents some benefits in term of its application since it is fast and relatively simple with a low invasive intervention that reduces labour cost and time. In the same way, FRP is light-weight and does not add any additional mass to the structure and does not change the cross sections of the elements. Therefore, there is no stiffness change since generally the amount of FRP is small compared with the gross section of the elements. Furthermore, it is less vulnerable to corrosion in comparison with other materials. In structural terms, the very high tensile strength of FRP provides not only strength improvement, but also a better deformation capacity to structural members. This behaviour is seen in Figure 2.12. FRP is known to improve the flexural behaviour of columns, slabs, and especially beams; it also increases the shear capacity of beams, columns, walls, and joints. Great improvement of axial strength, member ductility, delay of longitudinal rebar buckling and lap splice clamping in a confined axially loaded member.

**(b) Problems Dealing with FRP**

FRP can have some issues related to its high material cost, and vulnerability to high temperatures, especially since fire may cause premature degradation and collapse. From a structural point of view, as fibres behave in an elastoplastic manner up to failure, they are not considered ductile, therefore, sustaining long-term stresses can cause the fibres to fail suddenly. Special attention needs to be paid to anchorages, which controls the design in most of the cases. Flexural strengthening of columns can be difficult to achieve, as it needs a high ratio of FRP cross-sectional area to increase the strength capacity, and there is no possible stiffness improvement of elements since the sections of FRP are relative low.

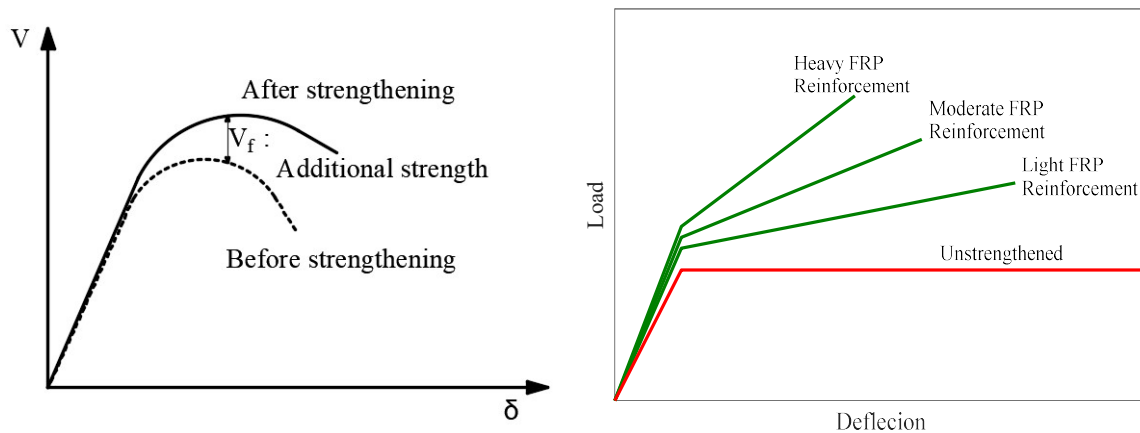


**Figure 2.12. Comparison of strength capacity increase using FRP, [after Triantafillou, 2018].**

Figure 2.13 displays the most common commercial configuration of FRP, bars and strips, [Triantafillou, 2018].

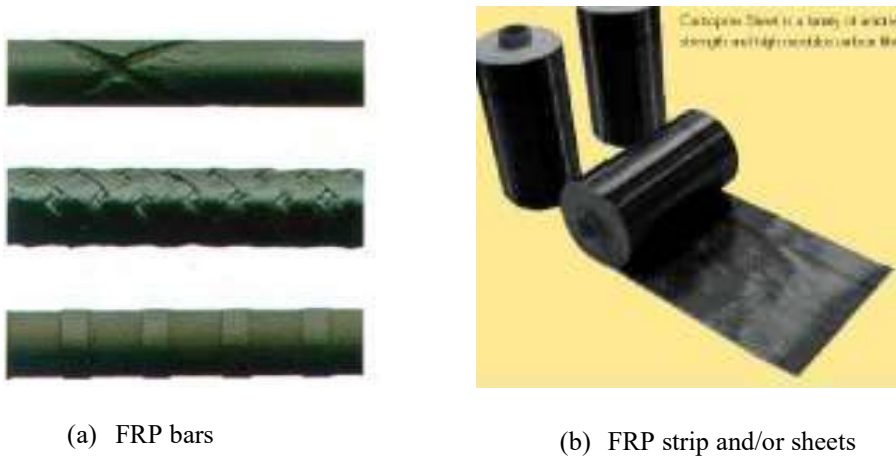


**Figure 2.13. Different configuration of FRP, (a) bars, (b) strips and/or sheets.**

### 2.5.3 Brace Retrofitting

Steel braces can be considered as an efficient solution for seismic performance upgrading of RC frame structures. In fact, as stated by Kadid and Yahiaoui [2011], steel bracing can work either for rehabilitation of structures damaged by an earthquake or for strengthening of an undamaged structure made necessary by revisions in structural design or building codes of practice. In the same way, Massumi and Tasnimi [2008] illustrate that adding cross bracing to a RC frame of low ductility significantly increases the frame stiffness and modifies its behaviour.

#### (a) Benefits of Braces

This technique is simple, cheap and efficient for strengthening RC frames against lateral load induced by earthquakes. The additional stiffness increases the lateral capacity of the system and this also reduces storey drifts, which may prevent any soft-storey. Likewise, considering the ease of construction and the relatively low cost, steel bracing appears to be attractive compared to other conventional upgrading techniques such as adding concrete or masonry shear walls or base isolation systems.

### (b) Problems Dealing with Braces

Since additional stiffness is incorporated to the structural system, the period of the structure reduces leading to a higher demand and therefore high floor acceleration in the case of dynamic loading. This is detrimental for non-structural elements vulnerable to accelerations. Modelling of steel braces can be troublesome since the more complicated effect of brace buckling needs to be incorporated.

#### 2.5.4 Infill Walls Retrofitting

Infill walls are constructed from unreinforced masonry which is generally too weak to resist high lateral load unlike RC frames. Therefore, this may lead to loss of integrity, a soft storey on the first floor, local high shear forces in short columns, among other issues. Fortunately, one solution available to lessen the problem associated with infills is achieved by incorporating separation gaps, which allow the frame to deflect freely without being restricted by the wall as seen in Figure 2.14. Even though infill walls are considered as non-structural elements, the gap retrofitting modifies also the structural response of the structure. For this reason, this technique is presented in this section, but a wider explanation of the procedure is detailed in Section 2.5.5.

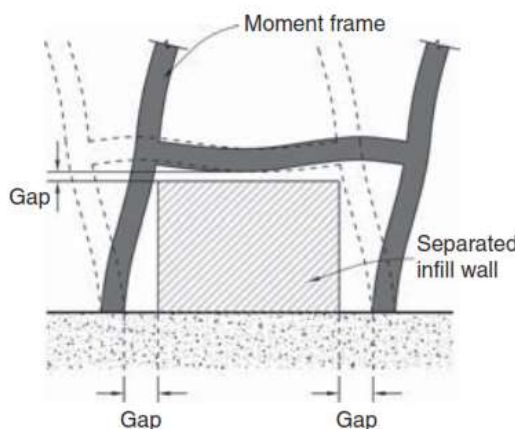


**Figure 2.14. Infill wall with separation gaps between infill and columns and beam, [after Charleson, 2008].**

#### (a) Benefits of Gap Separation

The concept of isolating infill walls preserves the integrity of infill panels at moderate storey drifts during moderate earthquakes, and increases the shear strength and lateral stiffness of the frames at higher deformations. The gap also reduces the high potential of infill-frame interactions delaying its damage.

#### (b) Problems Dealing with Gap Separation

Wall becomes vulnerable to out-of-plane forces leading to failure in this plane; in other words, one solution creates another. Consequently, brackets have to be provided on the top of the wall and connected to the slab or beam above so that the infill is stabilised for out-of-plane failure. However, the preferred option is to design the infill to resist out-of-plane forces with also a careful structural detailing at the top of the infill to provide sufficient strength. Additionally, the lateral stiffness of the structure is reduced tending to the behaviour of a lateral system without infills. FEMA E74 [FEMA E-74, 2012]

document provides standard details for this although engineering calculations are required.

### **2.5.5 Non-structural Retrofitting**

The non-structural retrofit unlike structural retrofit is a bit more challenging since various typologies of non-structural elements can be presented in a building requiring different non-structural retrofit procedures [FEMA E-74, 2012]. However, the approach followed for retrofitting non-structural elements considered in this study was less elaborated than the structural retrofitting. The structural response is taken as independent of the non-structural elements and therefore, their improvement can be assessed separately without the need of modifications to the numerical models. The retrofit is obtained by following the recommendation of FEMA E-74, which provides descriptions of tasks to undertake for each non-structural element in order to reduce the risks damage during earthquakes. The improvement of these elements can be reflected in the loss estimation analysis by simply changing the already defined fragility functions by the improved fragility functions taken from FEMA P58-3 [2012] database.

Other retrofitting alternatives with more engineering application for the case of masonry infills walls or partitions are described by Sousa and Monteiro [2016]. The retrofitting of infills includes two possible approaches: disconnect the infill from the structural system or consider it into the overall response of the structure. In the case of the first approach, many countries such as Japan, the United States or New Zealand have opted for isolating the infill walls. As a result, for the case of small earthquakes, no damage is presented and for larger events, the primary structural response is not affected, indeed, the use of unreinforced masonry walls as seismic force-resisting system in high seismic zones of the United States is prohibited by the International Building Code. Nevertheless, a very common way of disconnecting the wall is by providing a vertical gap between 18mm and 80mm wide and a horizontal one of 25mm. Restraints must be placed on top and bottom of the wall since with this intervention the infill is prone to out-of-the plain failure [Charleston, 2008]. The use of sliding joint connections is another approach for disconnecting the infills, this procedure subdivides the infill panels into multiple vertical or horizontal subsections while introducing connections that allow the in-plane sliding between these panels [Preti *et al.*, 2016]. Moreover, using fuses for partial disconnection of walls is achieved by detaching them vertically, once the gap material activates, which means it deforms energy dissipation is produced. However, this retrofit may lead to out-of-the plane instability. Therefore, to ensure out-of-the plane stability is necessary to place some brackets and guides on the top of walls. Furthermore, in the case of the second approach, a very popular technique is the use of FRP, which provides a significant increase in strength and ductility, delaying infill crack and failure. Engineered cementitious composites are other technique similar to FRP to enhance the ductility and delayed strength degradation. Likewise, reinforced mesh (RM) also achieve the same as FRP and cementous composites, and is applied by wire mesh needing of adequate anchored in the concrete frames [Calvi and Bolognini, 2001].

Previous studies on loss estimation of RC frames [Cardone *et al.*, 2017] have demonstrated that CFRP strips placed diagonally on infill walls, RM, and horizontal sliding joints are inapplicable from an economic point of view as a retrofitting alternative for infill walls in the case of

undamaged structures. However, they can be implemented to improve the seismic performance of infill walls previously damaged by earthquakes. It was also highlighted by Cardone *et al.* [2017] that intervention with RM or CFRP strips require a much longer breakeven time (above 30 years).

## 2.6 Summary and Discussions

As the structure under consideration in this study corresponds to a school building located in Italy, the limits and guidelines specified by the local code, NTC 2008, in terms of limits state and seismic assessment were discussed.

Moreover, the non-structural elements were not directly enhanced here. In other words, no specific design was conducted for these components but instead, this study presents the procedures and what actions should be addressed to retrofit these elements, (guidelines of FEMA E-74), and therefore, the improvement is only shown in the loss estimation assessment.

The retrofitting technique selected was FRP, given that, even though it presents some disadvantages over other materials, it also has many benefits like being a less invasive technique and increasing the strength of structural elements. For these reasons, different retrofitting alternatives with this material were evaluated and determined whether this approach is effective or not for the case study. All the criteria stated here are used for the coming Chapters involving the part of the assessment of the original building and assessment of the retrofitting alternatives. In particular Chapter 3 will cover a detailed description of the performance assessment of the school building.

## 3 ASSESSMENT OF AN EXISTING SCHOOL BUILDING

### 3.1 Introduction

Progetto Scuole arose from concern regarding the poor performance of Italian school buildings during past seismic events. This led the European Centre for Training and Research in Earthquake Engineering (EUCENTRE) to carry out research aimed at assessing school buildings of different typologies and configurations so that their performance under seismic hazards were evaluated. O'Reilly *et al.* [2018a] describes school buildings typologies which represent all the existing school building stock in Italy (reinforced concrete frame, unreinforced masonry buildings, and precast concrete). However, the present work focused only on the assessment and retrofitting of one reinforced concrete (RC) frame school building. This section provides an overview of its structural behaviour, performance, and properties using the assessment procedure detailed in Chapter 2.

### 3.2 Overview of the School Building

The school building considered in this study is a RC frame structure, built in the 1960's in Central Italy, with three storeys including an underground level. Each level has an area of  $689.10\text{ m}^2$  and inter-storey height of 3.83m for the underground level and first storey, and 3.77m for the second storey. The longest side of the school is 57m long and the shortest 15m. A scheme of the longest side of the building is displayed in Figure 3.2 and a typical floor plan layout is shown in Figure 3.1. Externally, the upper part of each bay has large openings for the windows while the lower part includes thick masonry infill walls.

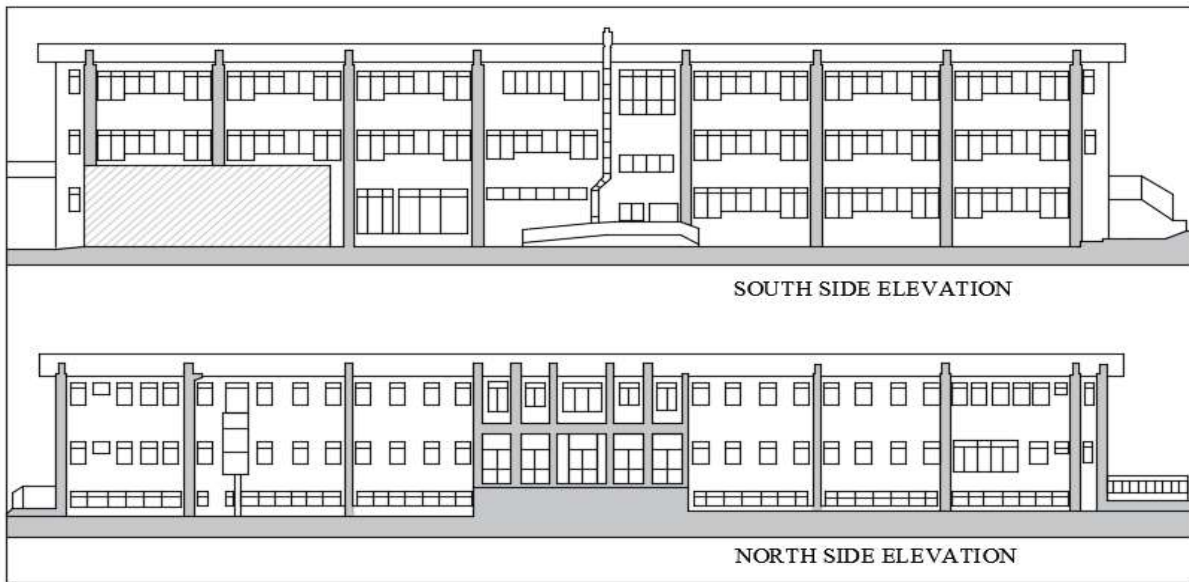


**Figure 3.2.** Front and rear elevation of case study school building, [after O'Reilly, 2016].

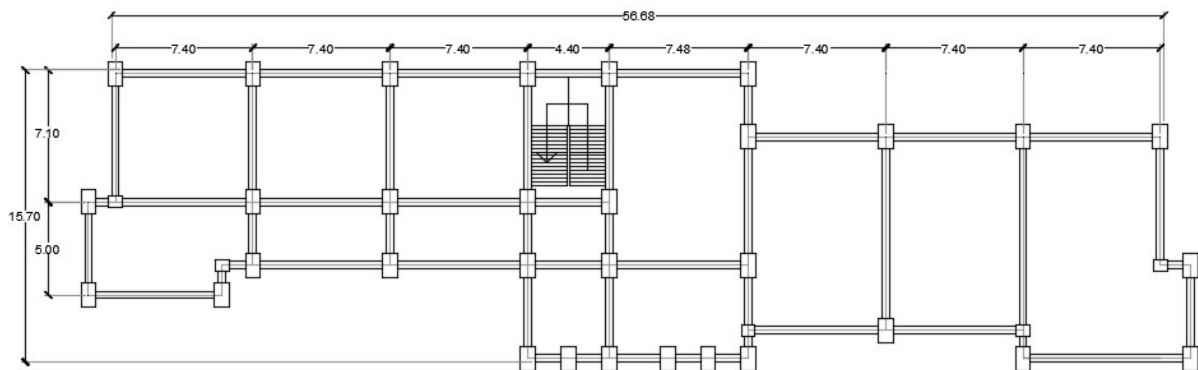


**Figure 3.1.** Typical floor layout of school, where the beams and columns are dimensioned along with the spanning of the slabs, [after O'Reilly, 2016].

### 3.3 Building Survey Information

As a preliminary step for the building initial assessment, an inventory of damageable structural and non-structural elements was compiled based on the information gathered during in-situ surveys. Using both the surveys and available architectural drawings, as presented in Figure 3.1, the geometry of the building as well as its structural layout could be verified. The possible degradation or cracking of structural elements was also checked and included in the reports and surveys [O'Reilly and Perrone, 2016]. Later on, the dynamic properties of the building were tested through a structural monitoring system for verifying its shape modes [O'Reilly *et al.*, 2017b; O'Reilly *et al.*, 2018a]. Additionally, specific forms were developed to inventory all non-structural elements. These forms allowed these elements, for which the forms were divided into six sections, to be quantified systematically. The first section has a general description of the non-structural elements with a photo to provide an overview of connections and supports. In the second section, the location and the quantity are described and different units are used to quantify them. The third section is a preliminary evaluation of the seismic risk for the non-structural elements. In the fourth section, some retrofitting strategies are defined, which are

proposed by published codes and some guidelines [FEMA E-74, 2012; Dipartimento Protezione Civile, 2009]. Finally, the last two sections provide all information required for the loss assessment. More detailed information can be found in O'Reilly *et al.* [2018a] and O'Reilly [2016]. Table 3-1 displays the inventory carried out in which the demand parameter corresponds to the parameter that each element is sensitive to, or at which its monetary loss is related, where PFA denotes peak floor acceleration, PFV for peak floor velocity and PSD for peak storey drift.

**Table 3-1. List and quantities of damageable elements in each school building. Quantities in the longitudinal direction of the school building are listed with the transverse direction listed adjacent in parentheses [O'Reilly and Perrone, 2016].**

Element	Demand Parameter	Fragility Function Source	Repair Costing Source	Unit	Quantities		
					RC		
					Ground	1 <sup>st</sup> Storey	2 <sup>nd</sup> Storey
<b>Structural Elements</b>							
Exterior Beam-Column Joints	Drift [%]	Cardone [2016]	Cardone and Perrone [2015]	each	20(26)	20(26)	20(26)
Interior Beam-Column Joints	Drift [%]			each	23(15)	23(15)	22(14)
Non-Ductile Columns	Drift [%]			each	44	44	44
Exterior Masonry Infill	Drift [%]	FEMA P58-3 [2012]	m <sup>2</sup>	454.4(2.0)	454.4 (127.8)	447.3 (125.8)	
Staircase	Drift [%]		each	1	1	1	
<b>Non-Structural Elements</b>							
Internal Partitions	Drift [%]	Sassun <i>et al.</i> [2015]	Expert Opinion	m <sup>2</sup>	317.8 (335.3)	291.9 (243.6)	268.1 (231)
Infill Walls	Drift [%]			m <sup>2</sup>	198.9 (65.9)	198.9 (65.9)	195.7 (64.8)
Doors	Drift [%]			each	18(15)	13(10)	15(10)
Windows	Drift [%]			each	23(17)	50(9)	53(9)
Desks	Drift [%]			each	110	145	182
Chairs	Drift [%]			each	140	182	182
Ceiling System	PFA [g]	FEMA P58-3 [2012]		m <sup>2</sup>	560	588	566
Fancoils	PFA [g]			each	28	30	30
Lighting	PFA [g]			each	66	48	48
Piping – Water Distribution	PFA [g]			m	452	452	452
Piping – Heating Distribution	PFA [g]			m	476	476	476
Bookcases	PFV [m/s]			each	16	22	14
Mobile Blackboards	PFA [g]			each	3	3	4
Electronic Blackboards	PFA [g]			each	0	3	3
Computers and Printers	PFA [g]			each	6	20	0
Projectors	PFA [g]			each	0	3	3
Switchboards	PFA [g]			each	1	3	3

### 3.4 Structural Layout

From the provided documentation and the surveys, dimensions of beams and columns were determined. On one hand, the column reinforcement ratio was estimated based on the information provided by Salvatore *et al.* [2009]. Meanwhile, the beam reinforcement was set at a reasonable level for all members based on limited information available for a portion of the member. In the case of the reinforcing steel material, the longitudinal and transverse rebar strength was defined as 381.3MPa, the mean value observed in the test results provided in an existing in-situ test report document compiled previously and also reported the ultimate strength to be 1.43 times the yielding strength and Young's modulus as 200GPa. Regarding the diameter of steel bars, the diameter of longitudinal bars in columns was assumed to be 20mm while the longitudinal reinforcement in beams to be 16mm, and the transverse reinforcement (stirrups) assumed to be 6mm. The cover was assumed to be 20mm based on engineering judgment and implicit information provided in previous in-situ test reports. Furthermore, in the case of concrete, three different values of  $f'_c$  were defined for the structure. These values are based on core samples extracted at the different levels of the building (underground floor, first and second storey) and by using BS 1881[BS 1881, 1996], these  $f'_c$  values correspond to 14.4 MPa, 10.8 MPa, and 8.8 MPa for each floor respectively. The elastic modulus of the concrete was computed through Equation (3.1).

$$E_c = 3320\sqrt{f'_c} + 6900 \text{ [MPa]}, \text{ where } f'_c \text{ [MPa]} \quad (3.1)$$

$f'_c$  = mean compressive strength

### 3.5 Numerical Modelling

It is important to highlight that the school building was completed in 1960, which implies poor construction quality since common practice back then was to build using low-quality materials and no modern seismic design provisions to ensure adequate ductile behaviour, when compared to modern standards. For instance, low concrete strength with smooth steel bars but more importantly, the lack of efficient seismic design was a main issue since it led to poor structural behaviour and seismic performance. Therefore, the numerical model developed had to consider all these factors and recreate the structural behaviour of RC frame members built in Italy before 1970s [O'Reilly *et al.*, 2018a]. The numerical model was performed with the software OpenSees [McKenna *et al.*, 2000], using force-based beam-column elements<sup>1</sup> with lumped plasticity for beams and columns as shown in Figure 3.4, and zero-length spring<sup>2</sup> coupled with a rotational hinge at the joint centreline to capture the nonlinear behaviour of joints, as displayed in Figure 3.3. It was assumed that the beam-column joints contain end-hook bars with no joint reinforcement since this was common at that time in Italy. For this reason, the hysteresis modelling approach proposed in O'Reilly *et al.* [2015] for beam-columns and joints was adopted here along with the calibrated parameters outlined in that study as well.

---

<sup>1</sup> [http://opensees.berkeley.edu/wiki/index.php/Force-Based\\_Beam-Column\\_Element](http://opensees.berkeley.edu/wiki/index.php/Force-Based_Beam-Column_Element)

<sup>2</sup> [http://opensees.berkeley.edu/wiki/index.php/ZeroLength\\_Element](http://opensees.berkeley.edu/wiki/index.php/ZeroLength_Element)

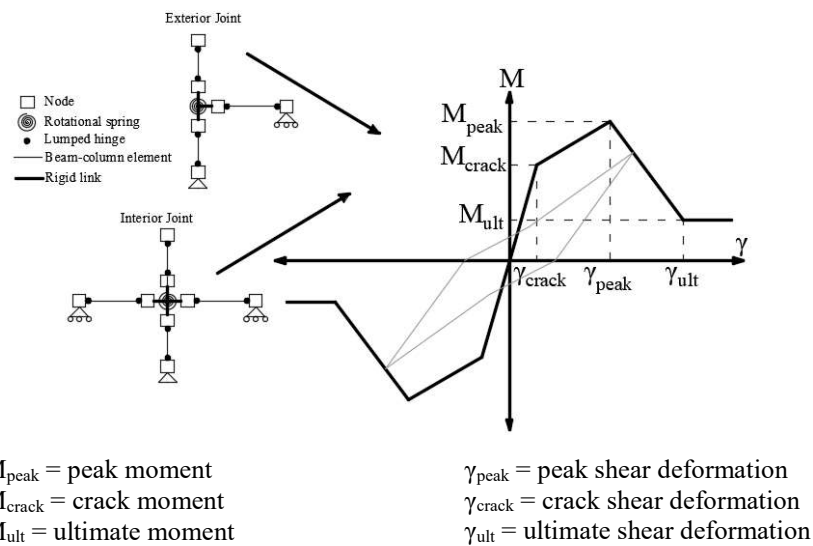


**Figure 3.3. Modelling of joints, includes proposed beam-column joint model and hysteretic material model for beam-column joints, [after O'Reilly and Sullivan, 2018b].**

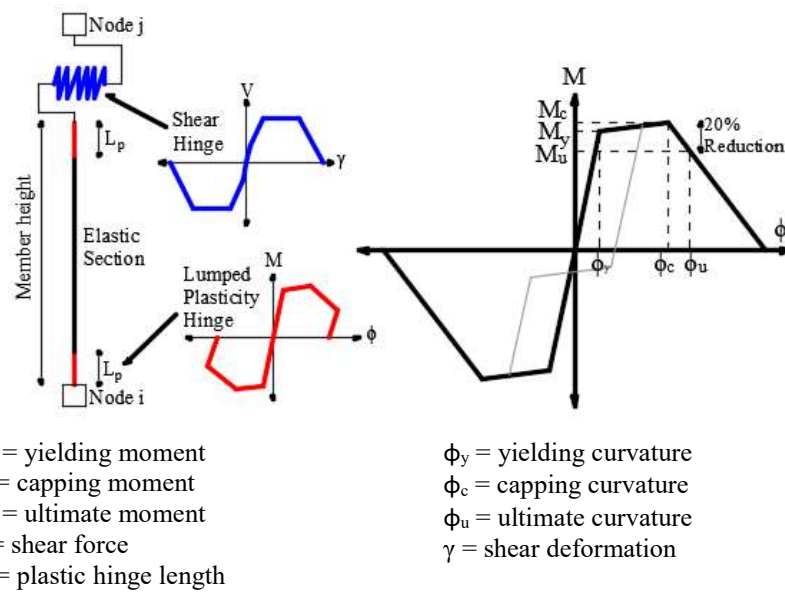


**Figure 3.4. Modelling of beam-column elements, includes proposed beam-column element model and proposed moment-curvature relationship for beam-column plastic hinge zone, [after O'Reilly and Sullivan, 2018b].**

Masonry infills were idealised as macroelements through a diagonal strut model [Crisafulli *et al.*, 2000], as illustrated in Figure 3.5(a). All these models had been validated and calibrated with statistical data presented by O'Reilly *et al.* [2018a] and O'Reilly [2016]. Moreover, the exterior masonry infill was determined to consist of double leaf hollow clay brick masonry, but with medium strength material properties provided in Hak *et al.* [2012]. The effects of modelling openings such as windows or doors were not considered as part of this study. It is important to mention that infills were modelled only for in-plane failure so out-of-the plane

(OOP) failure was not considered, this was adopted for model simplicity. Moreover, Kohrangi *et al.* [2016] concluded that considering OOP collapse of the masonry infill during the damage assessment has a relatively small effect on the expected annual loss (EAL) of the buildings examined, with no significant or obvious trend noted. Therefore, this simplifying assumptions is not anticipated to have a significant effect on the general conclusion of the study presented herein.

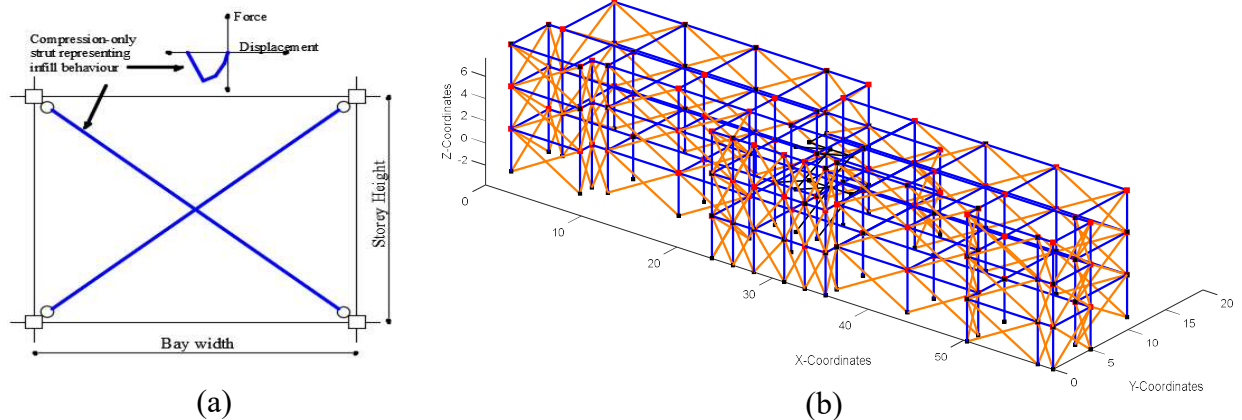


**Figure 3.5. (a) Proposed modelling for infill walls elements [after O'Reilly and Sullivan, 2018b], (b) Numerical model of school building in OpenSees.**

In the case of the staircase, it was modelled with elastic elements so that increased stiffness was captured and therefore potential shear failure of surrounding columns. The model also included a rigid floor slab and second-order geometry effects (P- $\Delta$ ) effects, the later incorporated by nodal loads of the tributary contribution of each floor. Additionally, a 5% tangent stiffness proportional Rayleigh damping model to the first and third modes periods was adopted. The decision of assuming a rigid floor slab was taken in light of the examination of the actual “laterizio” floor system in place [O'Reilly and Perrone, 2016]. From engineering judgment, the system did not represent a flexible floor configuration. Some additional considerations in the joint model were the axial stiffness and infinitely rigid behaviour in the rest of the directions. In the case of beams and columns, properties in other directions were considered elastic, assuming failure mechanisms were governed by plastic hinges.

### 3.6 Static Pushover Analysis

By using the numerical representation of the school building, illustrated in Figure 3.5(b), some initial analyses were conducted such as modal and static pushover (SPO) analysis to examine the fundamental aspects of the structural behaviour. The first four fundamental periods of the buildings are listed in the Table 3-2.

**Table 3-2. Periods of the school building.**

Mode	Period [s]	Motion	Participation Mass
1	0.61	Translational Y	41.7%
2	0.44	Torsional	0.1%
3	0.36	Translational X	42.4%
4	0.23	Translational Y	6.0%

Figure 3.6 displays the results of the modal analysis in terms of the first four shape modes. Table 3-2 indicates that the controlling translational mode corresponds to the first mode for the shortest or transversal direction (translation in Y). The third shape mode corresponds to the longitudinal direction (translation in X). Despite the second mode relates to a torsional case, its participation mass is very small, having no effect on the translational response. This data was useful for performing the nonlinear time history analysis in which a conditional period for the selection of ground motion is needed, as described in Chapter 5. Regarding the SPO, this was performed by applying a lateral force proportional to the modal shape for the two principal directions of the structure, this load was incremented gradually until a control node reaches a target displacement. In this case, the control node is located in the roof at the centre of mass. The plots of the pushovers analyses in the two principal directions are shown in Figure 3.7 along with points indicating yielding and cracking of different structural elements. These points aim to show how the linearity of the pushover curves change as the structural elements start yielding due to flexural yielding and/or cracking due to shear forces. These points were obtained by tracking the forces in each element as the gradual load of the SPO increases. When an element exceeded its capacity at either yielding or cracking, it was noted and the first exceedance for each element was plotted on the SPO curve.

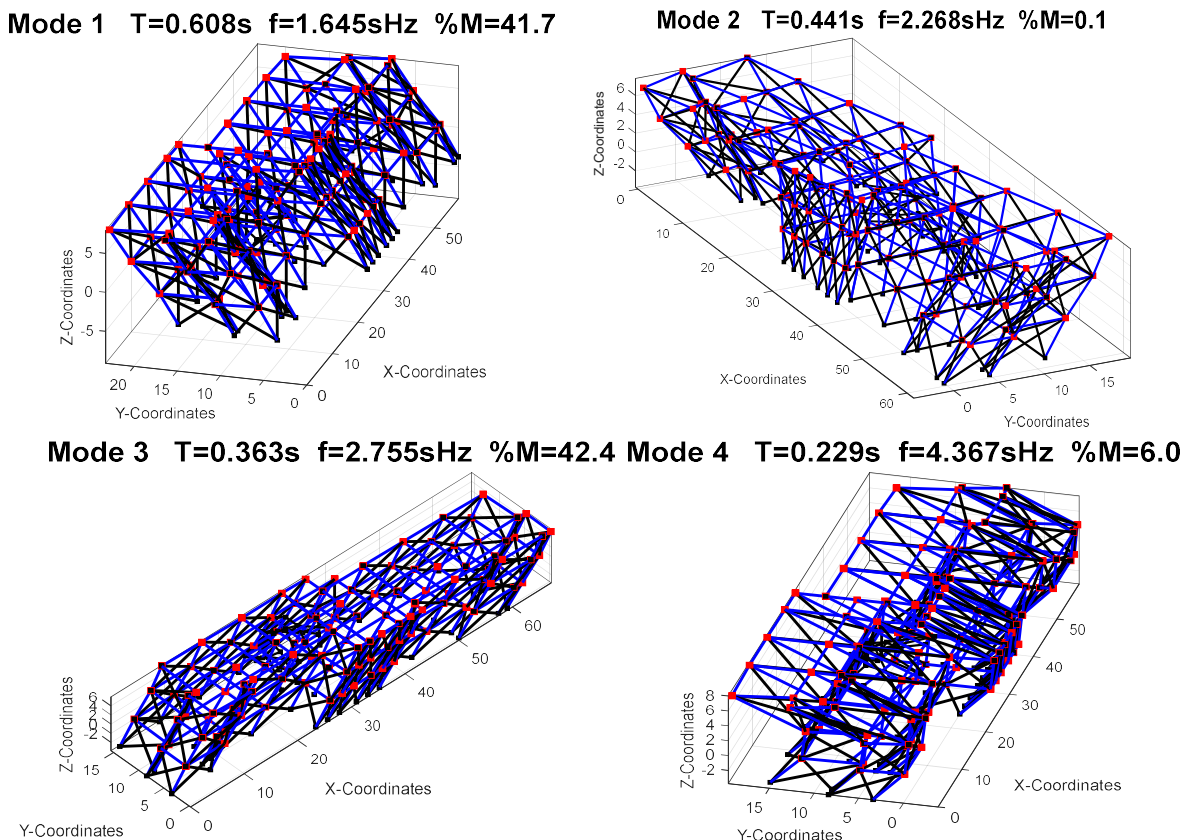


**Figure 3.6. Shape mode of the first four periods of the school building.**

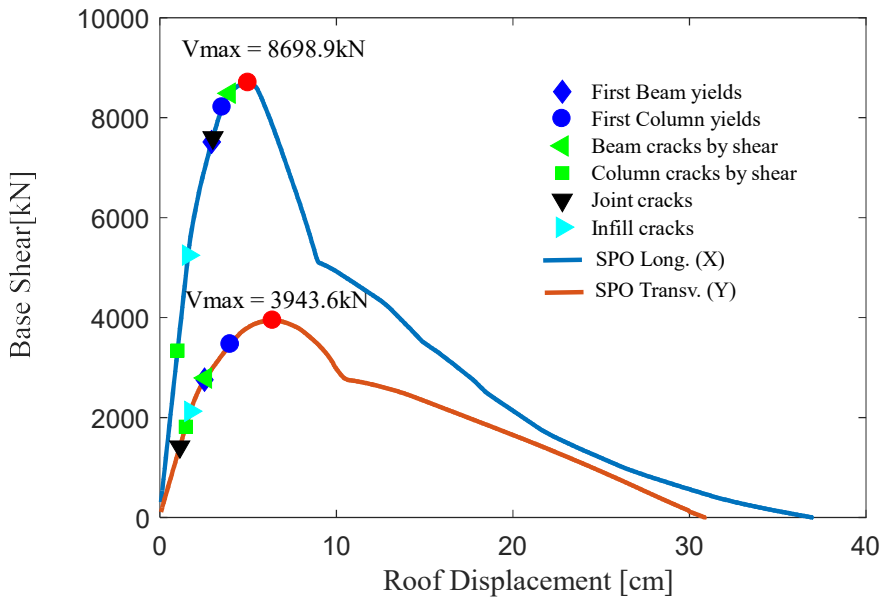
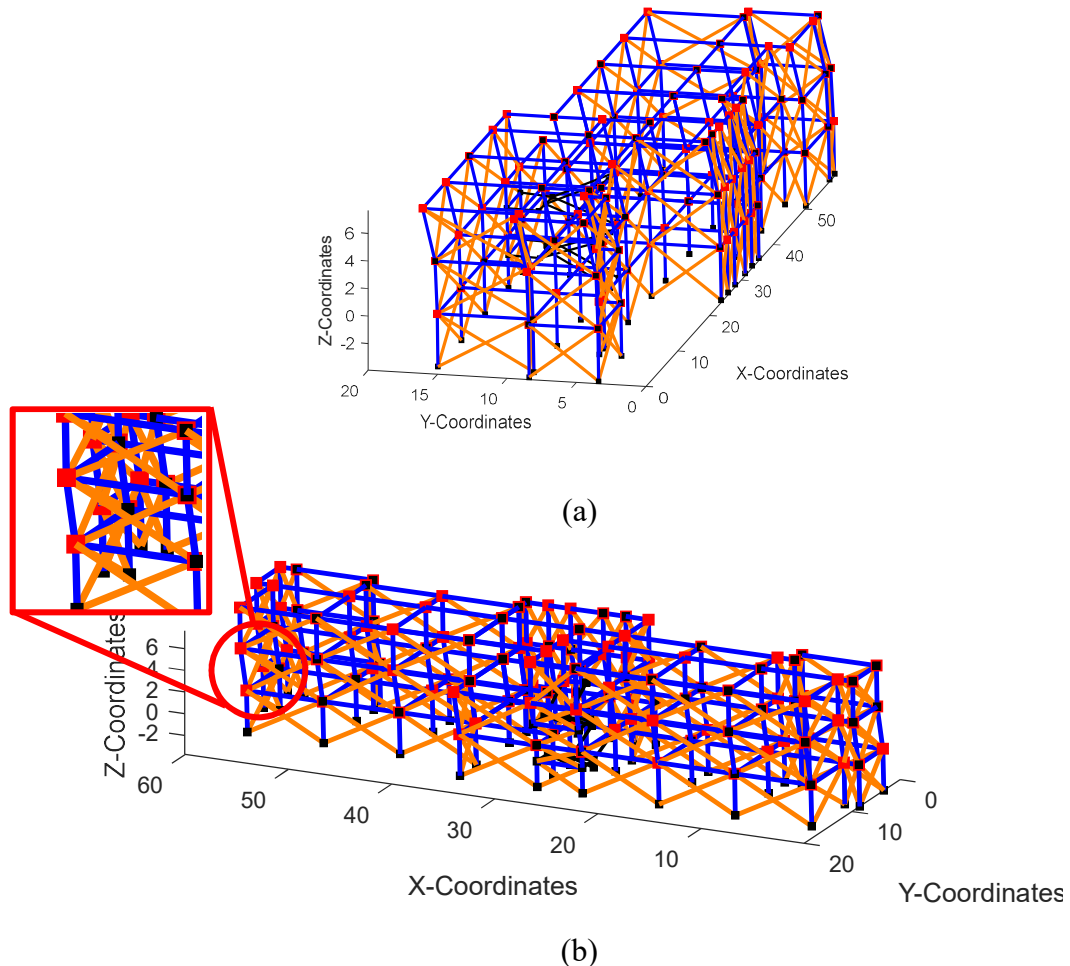


Figure 3.7. SPO curve for both directions of the school building.

Notably, the response of the structure is initially quite stiff due to the presence of the masonry infills. It is then followed by a significant loss in its strength capacity before gradually losing its strength and stiffness with increasing roof displacement. This part is controlled by a gradual loss of strength of the RC members while in the infills the loss of strength is more abrupt. This is a quite typical behaviour for RC frame with infills since they provide a significant increase in the initial capacity, but lose their significance with increased deformation due to the low level of drift typically required to fail an infill panel with respect to the drift required for a RC frame element to reach its ultimate limit state. The deformed shape of the structure at the end of the pushover is also worth commenting on since the mechanism is slightly different in either direction, as illustrated in Figure 3.8. In the longitudinal direction, SPO Long. (X), which corresponds to the direction along the longer side of the structure, a soft-storey forms in the first floor, whereas a soft-storey forms at the second storey in the transverse direction, SPO Transv. (Y). This is somewhat surprising at first, as soft-storey mechanisms at the ground floor are generally the anticipated mechanism in structures without any seismic provisions. Upon further inspection, however, the relative strength of the column members in the upper storeys with respect to the beams shows how the columns in the upper storeys are relatively weak with respect to the beams (possess a strong beam-weak column strength hierarchy) since these were designed for gravity loading only. In summary, the pushover curve gives an idea of the strength capacity of the building and its general behaviour; the building has a higher shear capacity in the longitudinal direction whereas the transverse direction is about 45% of the longitudinal, also presenting a higher deformability capacity in its longest side.



**Figure 3.8.** Weak-Storeys mechanism after performing SPO, (a) mechanism in the second floor in Y, (b) mechanism in the first floor in X.

### 3.7 Evaluation of Structural Performance

To evaluate the seismic structural performance of the school building with respect to a specified site hazard, the non-linear static analysis method commonly referred as the N2 Method [Fajfar, 2000], was applied.

#### 3.7.1 Selection of Elastic Response Spectra

The N2 method works based on using a smoothed code-defined spectrum intended to be representative of a uniform hazard spectrum (UHS). Figure 3.9 displays the interface of the software REASSESS V 2.0 [Iervolino *et al.*, 2015] for getting the UHS. Typically, the elastic spectrum equations specified in Eurocode 8, or similar, can be utilised. However, since site hazard analysis and ground motion selection for a specific site location in Italy was adopted, and will be discussed in Chapter 5, care was needed here when defining the UHS to maintain consistency between the models adopted. That is, that the smoothed spectrum utilised here is consistent with the hazard model and selected ground motions used later in this study. Therefore, it was decided to fit a smoothed elastic response spectrum conditioned to the return period ( $T_r$ ) for each limit state considered in the multi-strip incremental dynamic analyses (45, 75, 712 and 1463 years), as described in Chapter 4. To do this, the elastic response spectrum

was first determined from a UHS involving the return period for the limit states to assess using the software REASSESS V2.0. The seismic model adopted in the assessment was developed for Italy by Meletti *et al.* [2008] and the magnitude rates taken from DPC-ING-Branch 921 of the logic tree considering a soil type C (Eurocode 8 classification). The seismic hazard site for getting the UHS was selected as Cassino in Italy, which represents a high seismicity location. More information about this selected site is provided in Chapter 5.

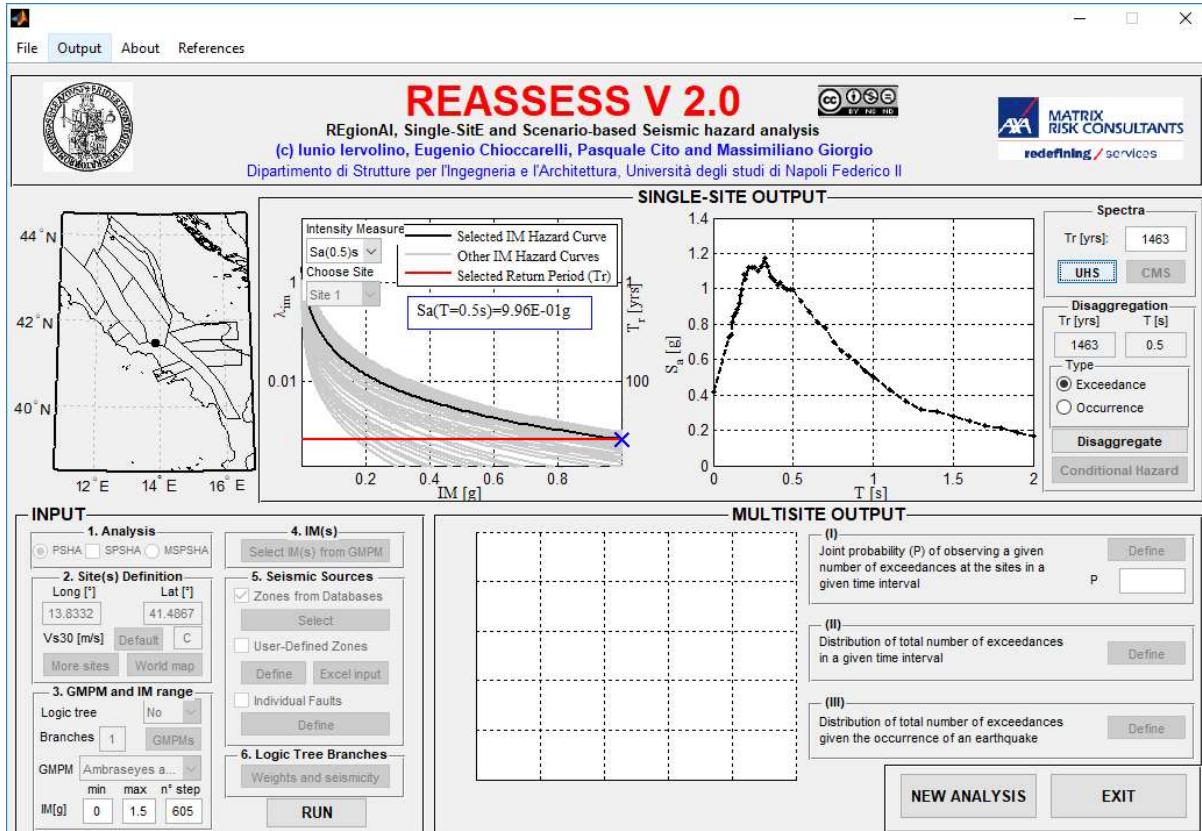


Figure 3.9. Scheme of the software REASSESS V 2.0 for obtaining a UHS.

Once the UHS was defined for each return period considered, a fitting process to keep the format of the N2 method outlined in Eurocode 8 was prepared. The fitting was based on the equations proposed by Eurocode 8 [EN 1998-1:2004, 2004] for building an elastic design spectrum, therefore, the input parameters  $a_g$ ,  $S$ ,  $T_B$ ,  $T_C$ , and  $T_D$  had to be provided, where:

$a_g$  is the design ground acceleration on type A ground;

$T_B$  is the lower limit of the period of the constant spectral acceleration branch;

$T_C$  is the upper limit of the period of the constant spectral acceleration branch;

$T_D$  is the value defining the beginning of the constant displacement response range of the spectrum;

$S$  is the soil factor; and

$a_{max}$  is the maximum spectral acceleration, constant branch, in the elastic design spectrum.

The periods of the different regions were selected as follow:  $T_B$  as the period in which the maximum coordinate descends by 5-6% from the peak spectral value,  $T_C$ , and  $T_D$  as the periods

intersecting the curves of normalised acceleration with normalised velocity and normalised velocity with normalised displacement, respectively, as illustrated in Figure 3.10(b). While Figure 3.10(a) describe the location of the corresponding variables  $a_g$  and  $a_{max}$ . Figure 3.11 displays the fitting for the elastic response spectrum related to  $T_r = 1463$  years. The idealised curve matches quite well the elastic response spectrum demonstrating that the assumptions and procedure used are suitable.

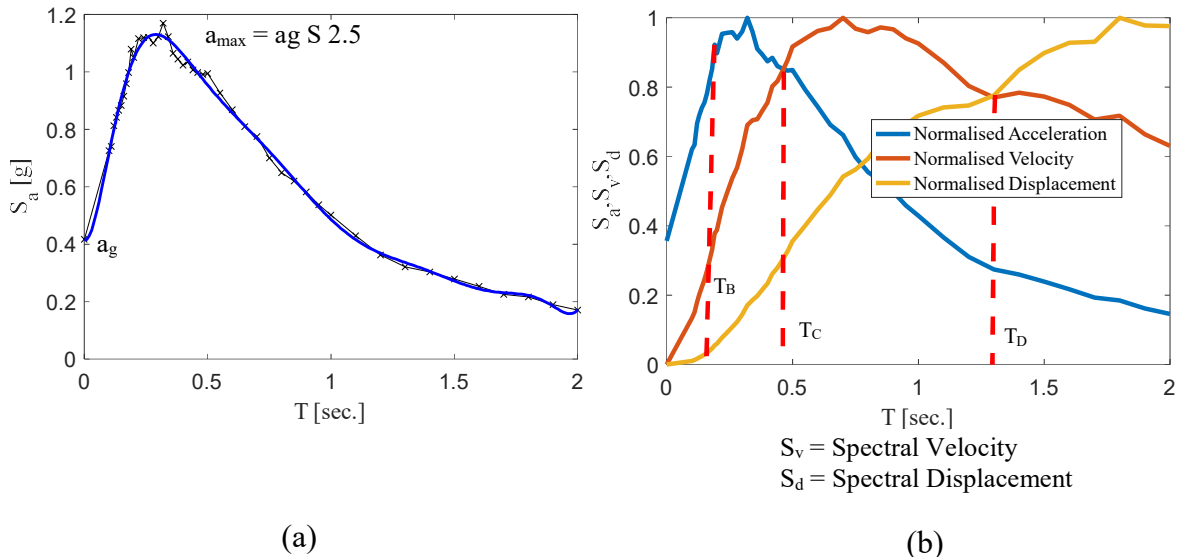


**Figure 3.10. Determination of parameter for fitting the elastic response spectrum for  $T_r = 1463$  years, (a) initial fitting, (b) defining periods according to the different ranges.**

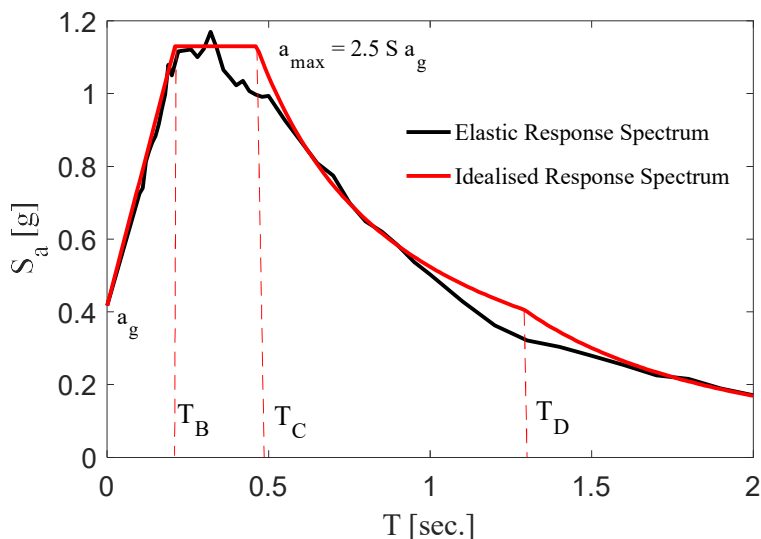


**Figure 3.11. Idealised Elastic Response Spectrum for  $T_r = 1463$  years.**

The goal of using the N2 method was to implement the same methodology and scope as a practitioner engineer would approach an assessment. Therefore, the results of the assessment, especially storey drifts were verified and compared with the requirements for the limit states specified by NTC 2008, previously stated in Chapter 2.

Figure 3.12 displays the idealised elastic response spectra conditioned to the return period for each limit state (return period) used for the seismic assessment, which match quite well with the fitting process used.

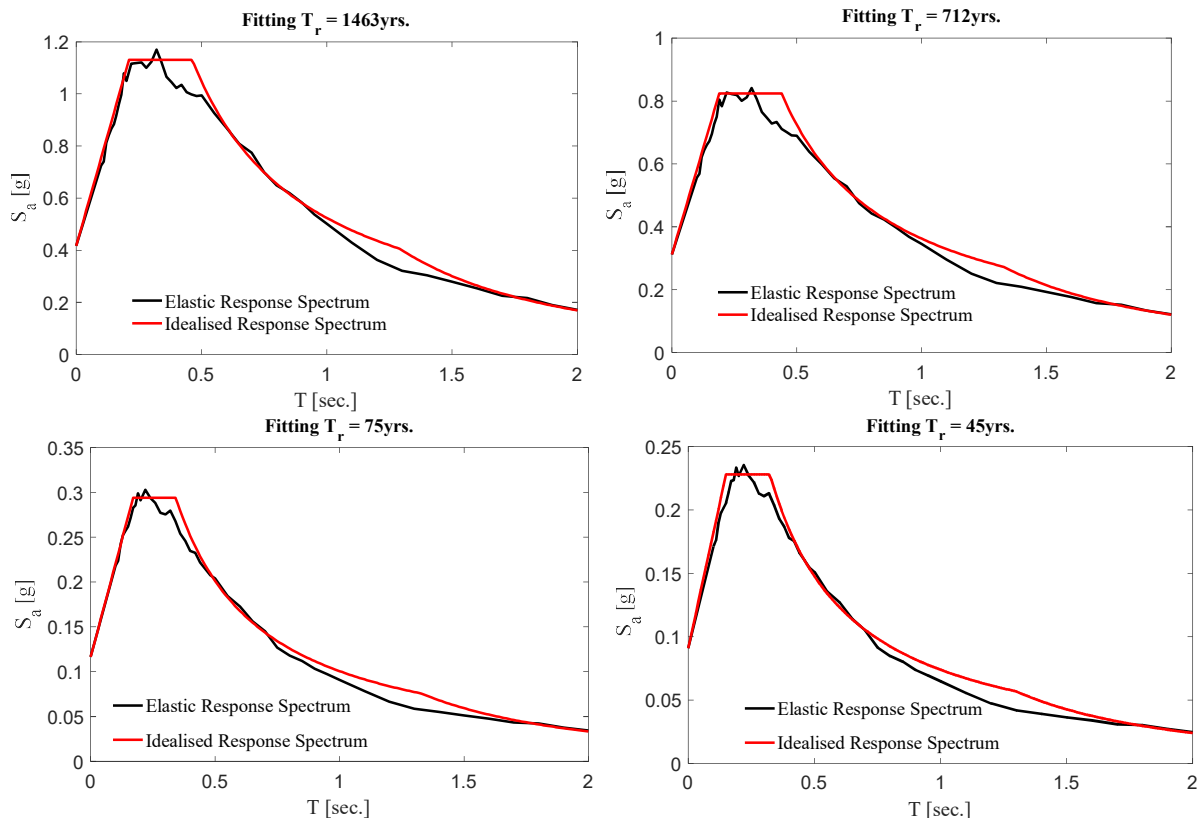


**Figure 3.12. Idealised elastic response spectrum for Cassino, soil type C.**

### 3.7.2 Application of the N2 Method

As part of the N2 method, the strength capacity in both directions was idealised as a single-degree-of-freedom (SDOF) system, as shown in Figure 3.13. The multi-degree-of-freedom (MDOF) system was simplified by using the multi-linear force-displacement relationship described by Dolšek and Fajfar [2004; 2005]. The mass at each floor was determined along with the mode shape to obtain a transformation factor. This transformation factor relates the response of an MDOF system to an equivalent SDOF response. Once the equivalent mass, yielding displacement and strength were obtained, the equivalent period was determined, which is represented by the initial linear portion on the base shear-top displacement plots of Figure 3.13. Then, the idealisation resulted after applying equations described in Dolšek and Fajfar [2004], which takes into account some characteristic points of the original capacity curve in a way that the area of the original curve with the idealised one match. These points consider both strength and deformation in cases where the structure yields, reaches its maximum capacity, and drops about 30-40%. At the latter point a complete failure of the infills in one or more storeys is considered after that only the frame contributes to the resisting system. This equivalent SDOF capacity curve was then used to obtain the target displacement of the structure corresponding to each level of seismic hazard examined, as described below.

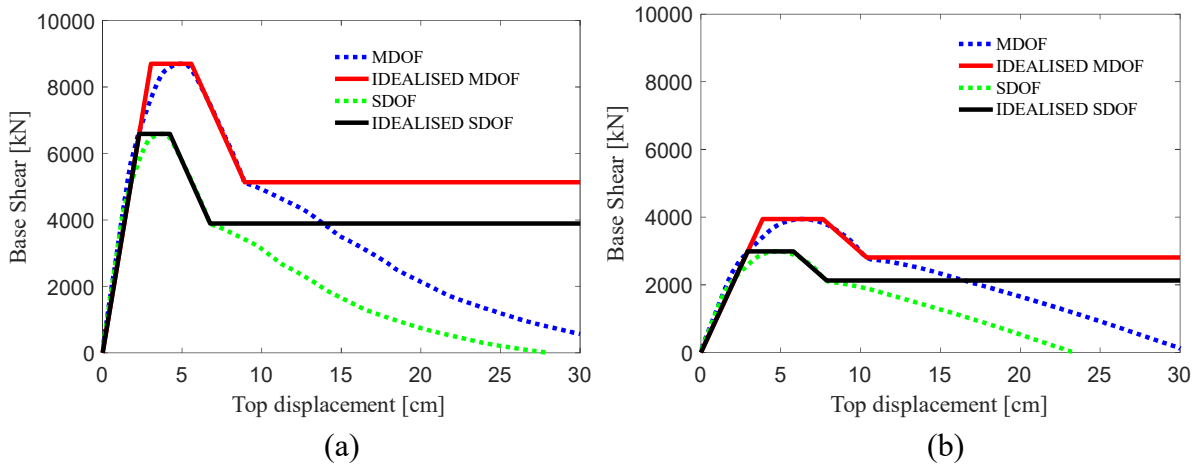


**Figure 3.13. Idealised strength capacity of the school building, (a) SPO in longitudinal-X direction, (b) SPO in transverse-Y direction.**

The intersecting point obtained by extending the equivalent period of the idealised capacity curve of the SDOF to the elastic demand spectrum is displayed on the plots of Figure 3.14 for both orthogonal directions of the building. The target displacement is determined for the different hazard levels to assess. In Appendix A the plots for the other return periods can be found where the same capacity diagram was used, but with different elastic spectra ( $T_r = 712, 75$ , and  $45$  years). Figure 3.14 represents this procedure graphically, but the equations, based on a  $R - \mu - T$  relationship presented by Dolšek and Fajfar [2005] were used, where  $\mu$  refers to ductility and  $R$  to normalised force or reduction factor. To determine the target displacement through these equations, the equivalent period was compared with  $T_c$  as different equation expressions for  $R$  and  $\mu$  are used depending on where the equivalent period is in relation to  $T_c$ . Based on this condition, the ductility ( $\mu$ ) and reduction factor ( $R$ ) were obtained and consequently: the target displacement related to that level of seismic hazard. This target displacement corresponds to the SDOF system, illustrated in Figure 3.14, which was then multiplied by the transformation factor to obtain the target displacement for the actual MDOF system.

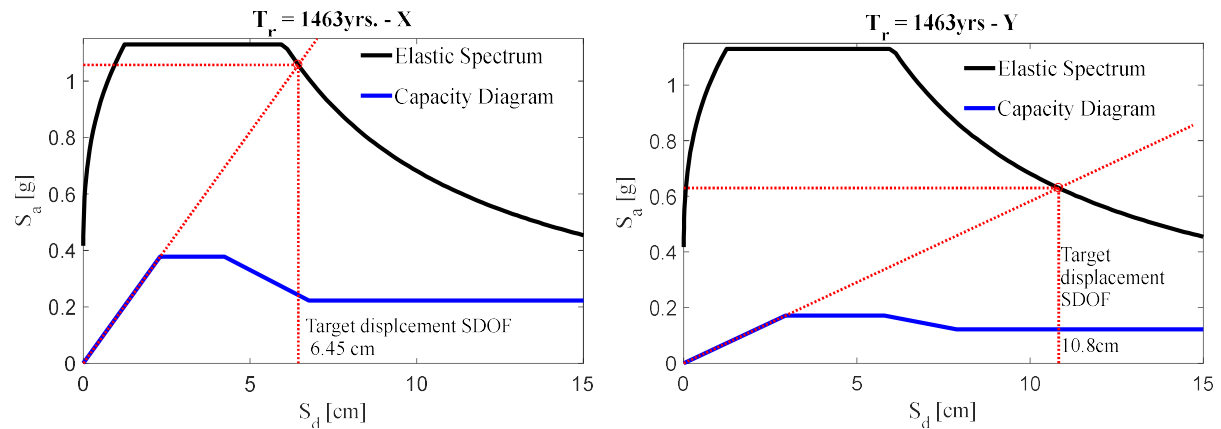


**Figure 3.14. Determination of target displacement for SDOF for the  $T_r = 1463$  years in both directions.**

Table 3-3 details the target displacement of MDOF to be reached by the control node located at the roof of the building through a SPO in both direction as a function of each return period.

**Table 3-3. Target displacements for the seismic assessment of the school building.**

Return Period [years]	Top displacement [mm] Long. (X)	Top displacement [mm] Transv. (Y)
45	12	21
75	16	28
712	62	99
1463	88	143

### 3.7.3 Assessment of Limits States

As presented in Table 2-5, NTC 2008 describes four limit states, each one with different return periods discussed in Chapter 2, which are defined to preserve a desirable behaviour in the structure. Therefore, the maximum storey drift obtained for each return period must be verified to meet the requirement prescribed by the code. In case of the operational (SLD) and damage control (SLO) limit states, the maximum storey drift must be limited to a value of either 0.5% or 1% as detailed in Table 3-4, these values depend on the attachment of internal partitions. This limitation will reduce the damage on internal partitions and others non-structural elements. For the case study building, the limit of 0.5% was used since this type of internal partitions is presented in the school building.

**Table 3-4. Compliance criteria defined in NTC 2008 for the protection of drift sensitive non-structural elements.**

Non-Structural Element Typology	Drift Limit
Internal partitions connected rigidly	0.5%
Internal partitions detailed to not suffer damage due to storey displacement	1%

On the other hand, for the case of life safety (SLV) and collapse prevention (SLC) limit states, the requirement is defined in terms of maintaining a stable, ductile mechanism that avoids soft-storey or weak-storey failure, promoting a ductile mechanism with the appropriate strength hierarchy criteria [O'Reilly, 2018a]. Additionally, this requirement can be evaluated through the strength hierarchy from which a beam-column joint that does not follow a ductile failure sequence may lead to soft-storey mechanism.

### 3.7.4 N2 Method Application Results

The storey drifts profiles for each direction and limit state using the N2 method are presented in Figure 3.15 and Figure 3.16. The assessment for the return periods of 45 and 75 years correspond to the serviceability limit state. The assessment for this limit state has to be verified

according to Table 3-4, which is derived from NTC 2008. The verification is based on limiting the maximum storey drift to 0.5%. This limit is applied to improve the performance of the non-structural elements, especially to reduce damage in internal partitions. For both return periods and directions, the maximum storey drift is lower than the limit, as illustrated in Figure 3.15.

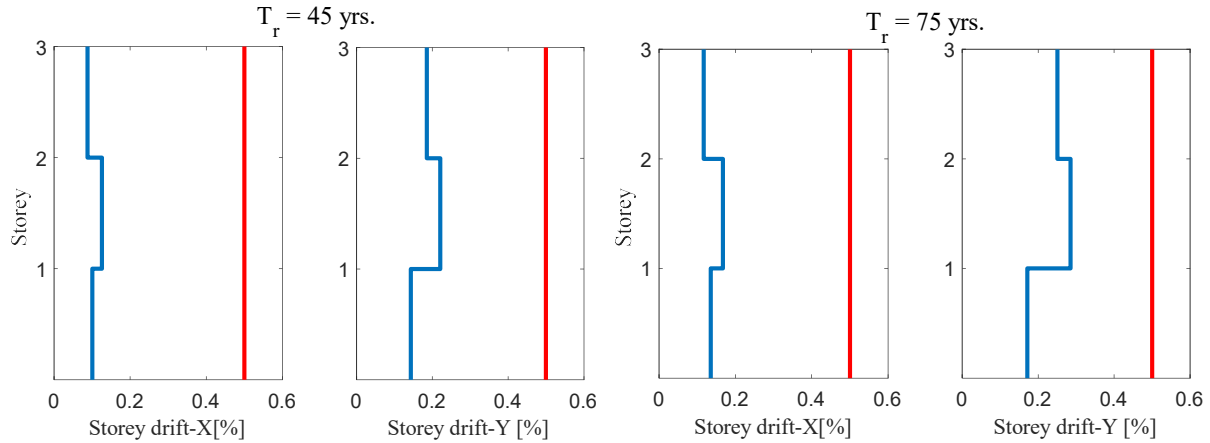


**Figure 3.15. Maximum storey drift of the school building for the serviceability limit states.**

The ultimate limit states are checked for the return period of 712 and 1463 years, as illustrated in Figure 3.16, since the requirement for this limit state is defined in terms of stability, allowing ductile mechanisms. However, for both directions, weak-storey mechanism has formed, this can be visualised through the excessive drifts in case of the second storey for X and third storey for Y. These mechanisms can be better visualised in Figure 3.8(a) and Figure 3.8(b), in which a weak-storey for the top floor in the transverse direction, and another one in the second storey for the longitudinal direction are presented.

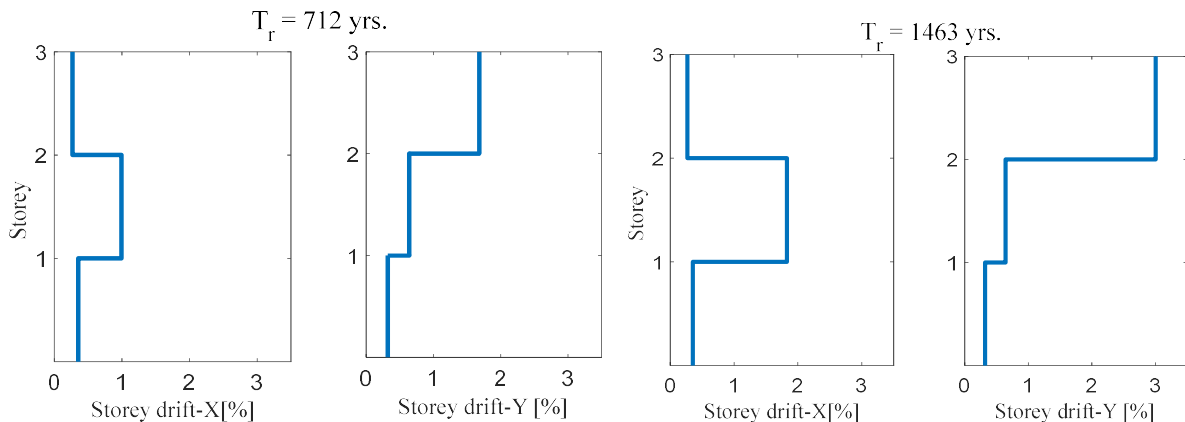


**Figure 3.16. Maximum storey drift of the school building for the ultimate limit states.**

Furthermore, in the following section the results of N2 method will be used to evaluate the strength hierarchy in beam-column joints. This analysis will support the presence of non-ductile mechanism as the ones found in this section, as well as indicate possible local failures. These weak-storeys mechanisms may be related to the fact the framing systems do not comply with the capacity design requirements of modern seismic codes, presenting weak column-strong beam systems. As explained by O'Reilly [2016], columns in this class of non-ductile frame buildings are often weaker than beams, forcing yielding firstly in vertical elements. Additionally, they are vulnerable to collapse if a shear failure in columns develop.

Likewise, the assessment was also evaluated in terms of the number of elements that failed for the target displacement at the period of 1463 years, considered as the most critical case. An element was assigned to fail when there is a drop of about 20% of its maximum capacity, which is consistent with the deformation of an element's ultimate limit state in Eurocode 8 [EN 1998-3:2005], before reaching the target displacement, shown in Figure 3.17. Similarly, the plots in Figure 3.18 show the different types of failures that the structural elements undertook.

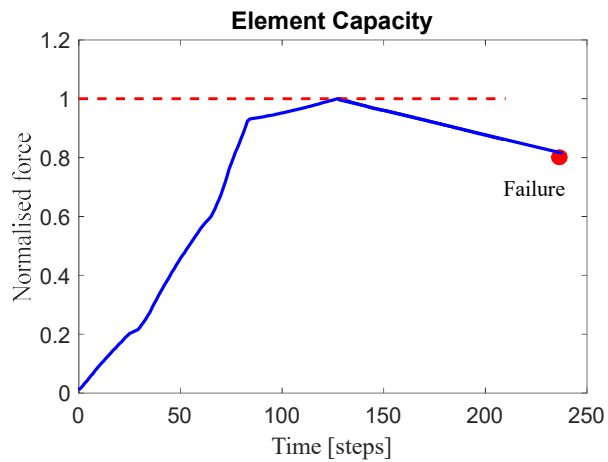
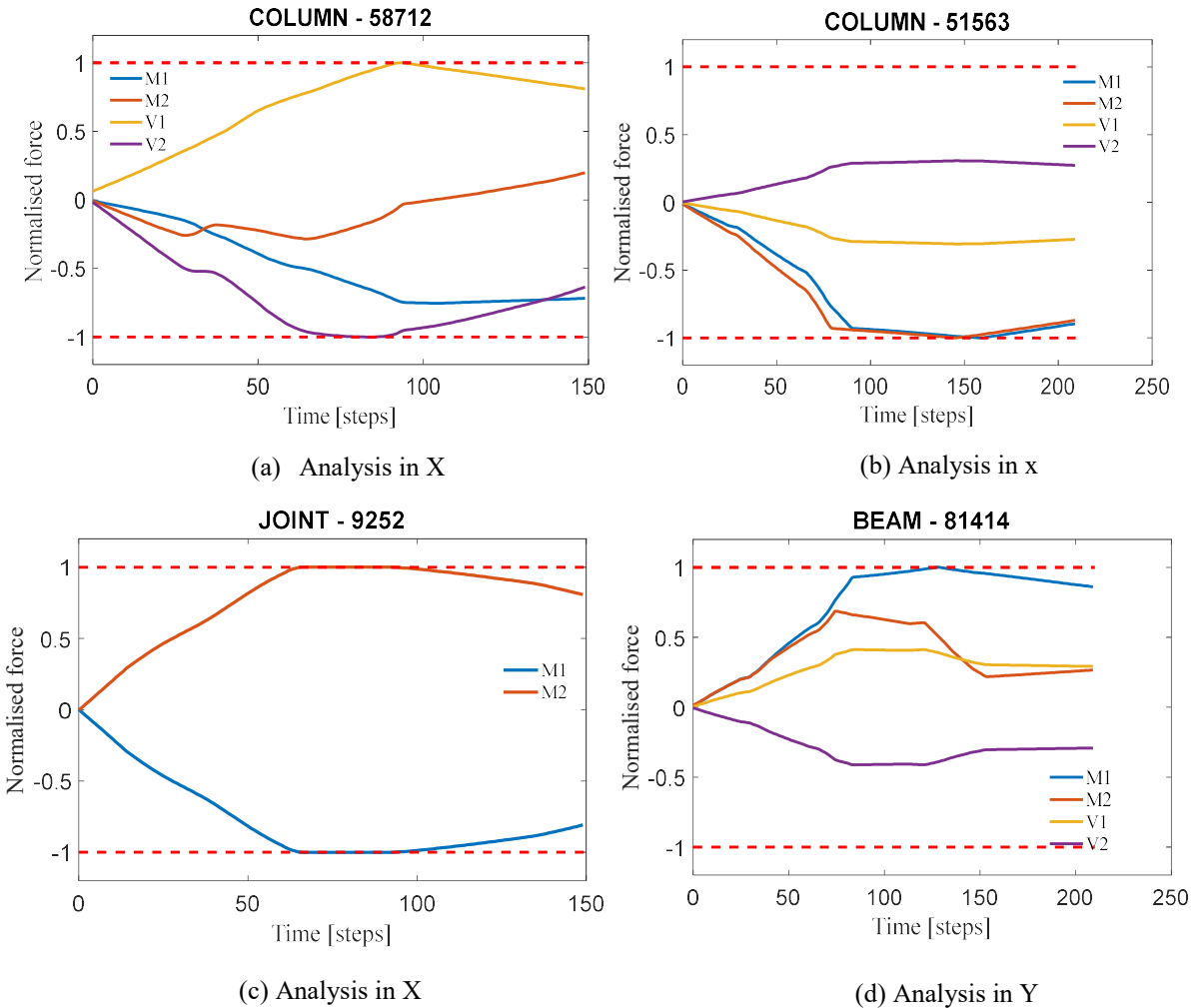


**Figure 3.17. Criteria for defining the failure of an element, after a drop of 20% of its maximum capacity.**



M1 = bending moment at end 1

M2 = bending moment at end 2

V1 = shear force at end 1

V2 = shear force at end 2

**Note:** column 58712 is located in the second storey supporting the staircase; column 51563 correspond to a corner column in the top floor; joint 9252 corresponds to a perimeter joint in the second storey; and beam 81414 corresponds to an exterior beam in the Y direction at the top floor.

**Figure 3.18. Failure of elements for the target displacement of  $T_r = 1463$  years, (a) Column fails at shear, (b) Column fails at flexure, (c) Joint fails at flexure, (d) Beam fails at flexure.**

The results presented in Figure 3.19 shows the type of failure undergone by the structural elements at the hazard level intensity  $T_r = 1463$  years. These results will also be used to compare each of the retrofitting alternatives described in Chapter 4, which will be referred to in later chapters, since one of the targets of the retrofitting is to reduce the level of structural damage.

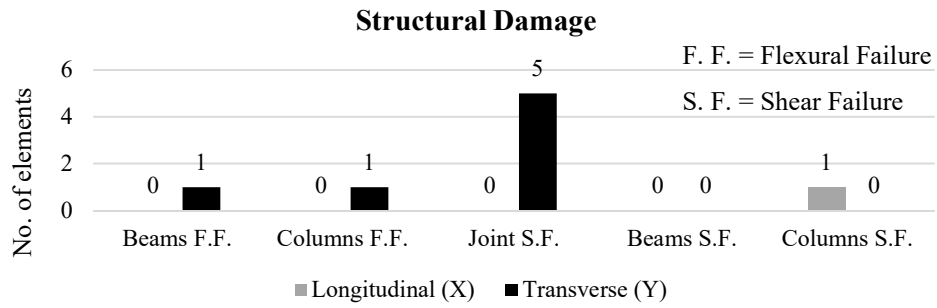


**Figure 3.19. Damage presented in structural elements due to SPO for  $T_r = 1463$  yrs.**

The damage in the elements provides information about the level of damage undergone by the structure for the most critical limit state (1463 years). It can be seen from Figure 3.19 that only failure in structural elements is presented for the transverse direction, being critical in the case of joints (five joints failed). Moreover, this evaluation also specifies the type of failure in each element, from which either ductile failure mode or fragile one as shear failure can be determined. This is the case where shear failure occurred in one column in the longitudinal direction displayed in Figure 3.19. This led to special attention being paid to this element, e in the subsequent retrofitting intervention so that this type of undesirable failure could be mitigated. Additionally, this information was useful since by identifying the weakest element within a beam-column-joint, the strength hierarchy can be verified, meaning that a strength sequence of failure can be defined. These parameters were used to assess the different retrofitting alternatives, which will be discussed in Chapter 4.

### 3.7.5 Hierarchy Assessment

The strength hierarchy criteria, previously described in Section 2.3.4, helped determine which beam-column joints were not meeting the requirement of a beam hinging behaviour, meaning following an appropriate failure sequence defined as beam-column-joint. The criteria for selecting and evaluating specific beam-column joints was based on the damage of the elements that presented either joint failure or failure in surrounding beams and/or columns, as illustrated in Figure 3.20. Additionally, beam-column joints in which no failure occurred were also evaluated, so that a wide range of joints failure typologies were considered.

- beam-column joints evaluated for the strength hierarchy through the N2 method (1463 years) - Transverse direction (Y)
- beam-column joints evaluated for the strength hierarchy through the N2 method (1463 years) - Longitudinal direction (X)

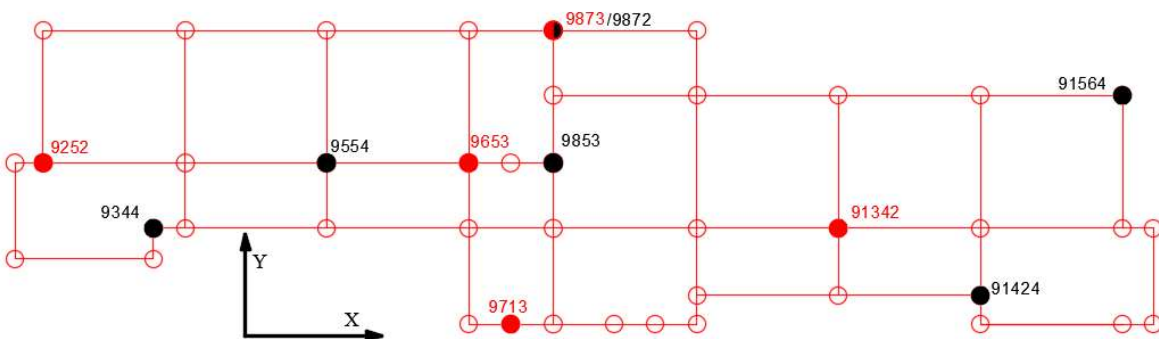
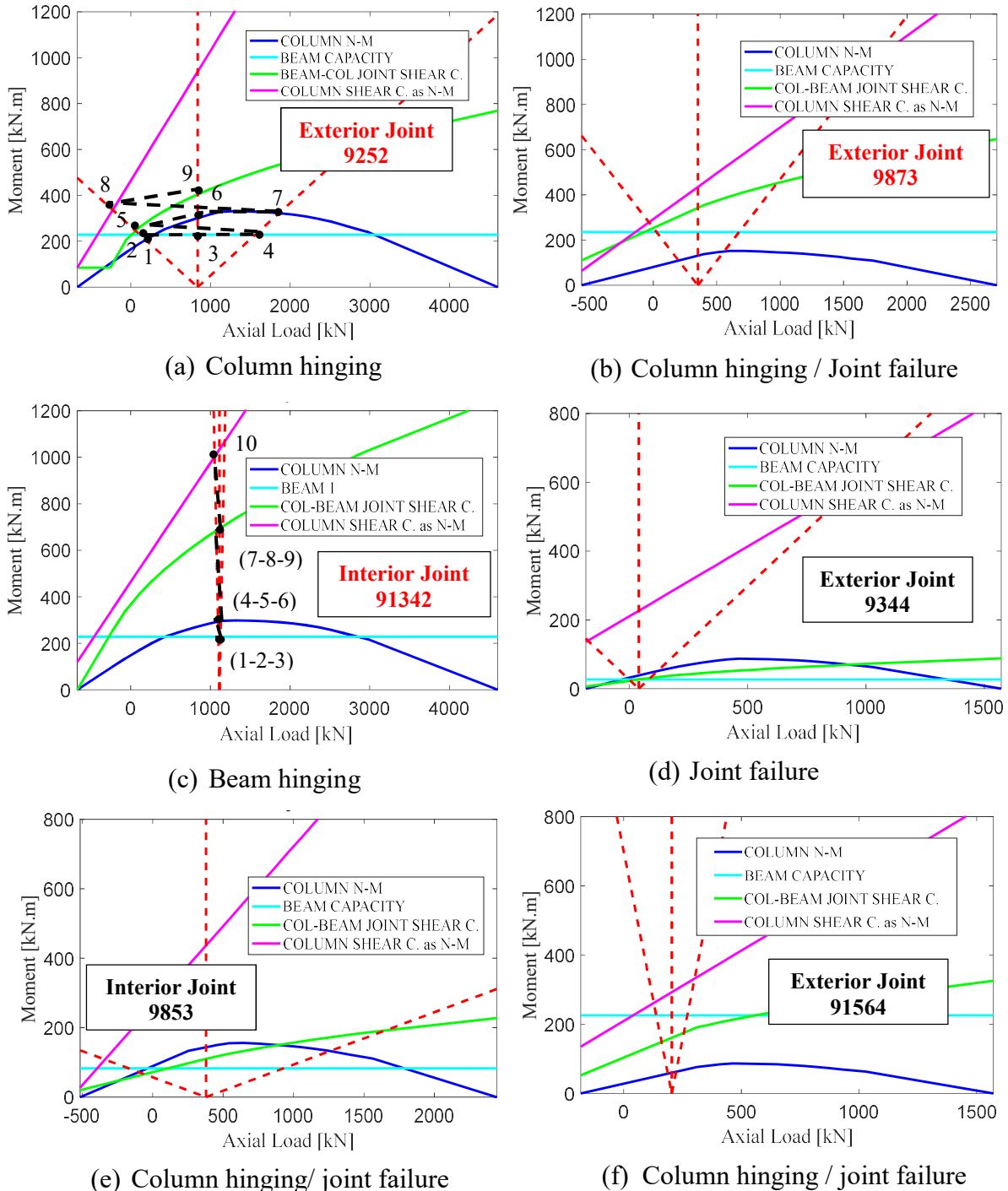


**Figure 3.20. Beam-column joints evaluated according to the strength hierarchy procedure.**

Figure 3.21 displays some beam-column joint strength hierarchy diagrams along with the first elements undergoing failure.



N-M = axial load – bending moment interaction.

**Figure 3.21. Strength hierarchy evaluation of some beam-column joints.**

Figure 3.21(a) displays the failure path undergone by the elements of joint 9252 (see Figure 3.20). In this case, the column is the first element that fails and is denoted by the label (1), followed by the beam (2-3-4), and lastly the joint (5). The failure path continues for the column

(6-7), followed by the first shear failure of column (8), and then again joint flexural failure (9). This progression of damage follow a zig zag pattern due to the reverse loading of the joint during a seismic event represented by the red dotted line. According to the strength hierarchy sequence, the column fails before the beam leading to column hinging. In case of joint 9873, it is noted that the columns capacity is below the beam and joint and, as a result, column hinging is produced, followed by the joint failure. On the other hand, joint 91342 follows a desirable behaviour in terms of failure sequence, as displayed in Figure 3.21(c), since the flexural capacity of the column and joints exceeds the beam capacity for the range of axial load considered. The failure path follows a ductile failure sequence as beam-column-joint and lastly shear failure in the column, as illustrated by the black dotted line. Therefore, no intervention would be required for any of these joint elements since it would be governed by a hinging behaviour in this joint. For joint 9344, only joint failure takes place, but not column failure since the column capacity is slightly above the capacity of the beam. As a result, a desirable strength hierarchy can be achieved by strengthening only the joint. Finally, Figure 3.21 (e) and Figure 3.21(f) show cases in which both columns and joint fail so column and joint strengthening could be necessary. However, the strengthening is more feasible for the case of joint 9853 than joint 91564, since the joint and column capacity for the joint 9853 are closer to that of the beam. This means that joint 91564 will require more material in order to increase the column and joint capacity or even may be closer to the beam capacity but not higher. The strength hierarchy diagram for the other joints shown in Figure 3.20 are presented in Appendix A.

As stated in Chapter 2, the numerical model assumed that failure mechanisms are governed by plastic hinges and that shear failure is not a controlling failure mode. Even though Figure 3.19 indicates that some columns fail at shear, a flexural mechanism is still the controlling case. This last statement was verified by combining the shear strength and flexural strength of columns in terms of their ductility illustrated by Galal and Ghobarah [2004] in Figure 3.22, where the UCSD shear model presented by Priestley [1993] for estimating the shear capacity was used.

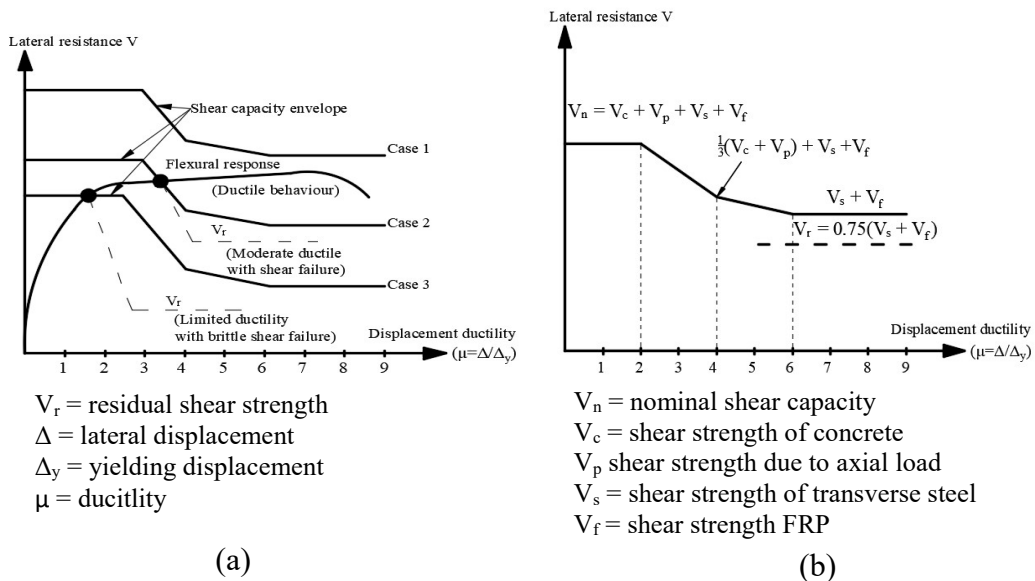


**Figure 3.22. Combined flexural and shear response for columns, (b) shear strength-displacement ductility relationship, [after Galal and Ghobarah, 2004].**

If we apply the above approach to the case study building, the combine shear and flexural strength plots shown in Figure 3.23 are obtained. Two types of behaviour govern the columns: moderate ductile and ductile, since the two plots are either intersecting for a ductility higher than 5 or are not intersecting at all [Galal and Ghobarah, 2004].

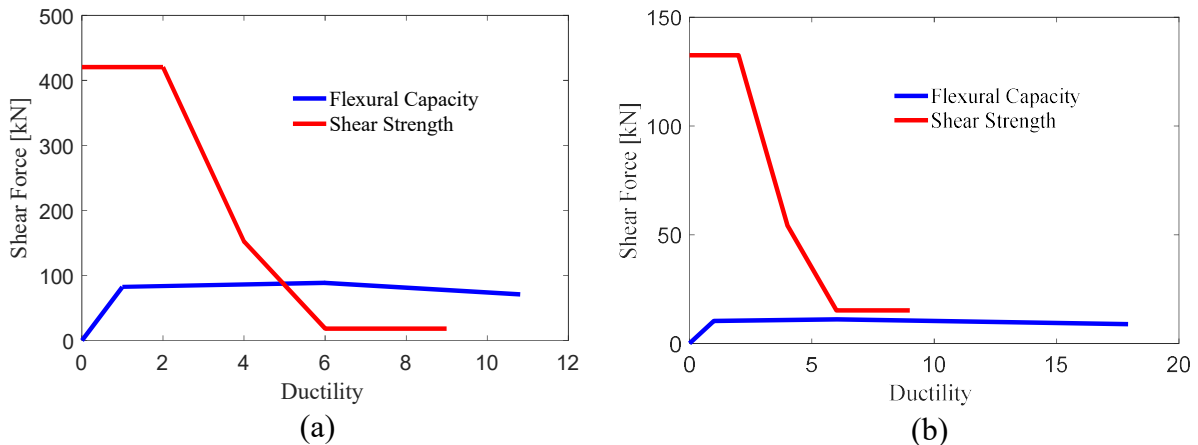


**Figure 3.23.** Combined shear strength and flexural strength to evaluate whether a ductile or shear failure mode controls the behaviour in a column, (a) moderate-ductile behaviour, (b) ductile behaviour.

### 3.8 N2 Analysis on the Bare Frame

In order to highlight the importance of modelling infills walls and show their influence on the overall structural behaviour in assessment, the performance of the bare frame (i.e. the original structure without infills walls) was carried out in the same manner as before so that results can be compared with the original building. Consequently, all the analysis done for assessing the school building in previous sections were recreated for the bare frame, but considering the traditional N2 methods outlined by Eurocode 8 [EN 1998-1:2004, 2004].

It is notable that by removing the infills walls from the numerical model, the structural capacity and properties of the school building are affected substantially. On one hand, Figure 3.24 shows the capacity curves for both principal directions of the building, which were reduced considerably. The initial stiffness is lower than that the original building since the removal of infill makes the structure more flexible. This also affects the maximum capacity because no infills are contributing to the lateral capacity of the structure. Another important difference is that the maximum capacity is developed at a larger top displacement than for the original building. Additionally, the maximum top displacement seems to be the same for both directions, reaching zero force at 26 cm and 28cm for the longitudinal (X) and transverse (Y) directions, respectively. As stiffness is inversely proportional to the period, which indicates that as stiffness decreases, the period lengthens. Table 3-5 indicates the properties for the bare frame in which the periods have increased almost twice from the values presented for the original building [Table 3-2]. More importantly, the first translational mode is now found in the second shape mode unlike the original building which is presented in the first shape mode since its stiffness was modified. Furthermore, the mass participation in the translational mode is lower when compared with the analysis of the original building. Figure 3.25 displays the first four shape

modes for the bare frame which are different from the original building as result of the factors mentioned above.

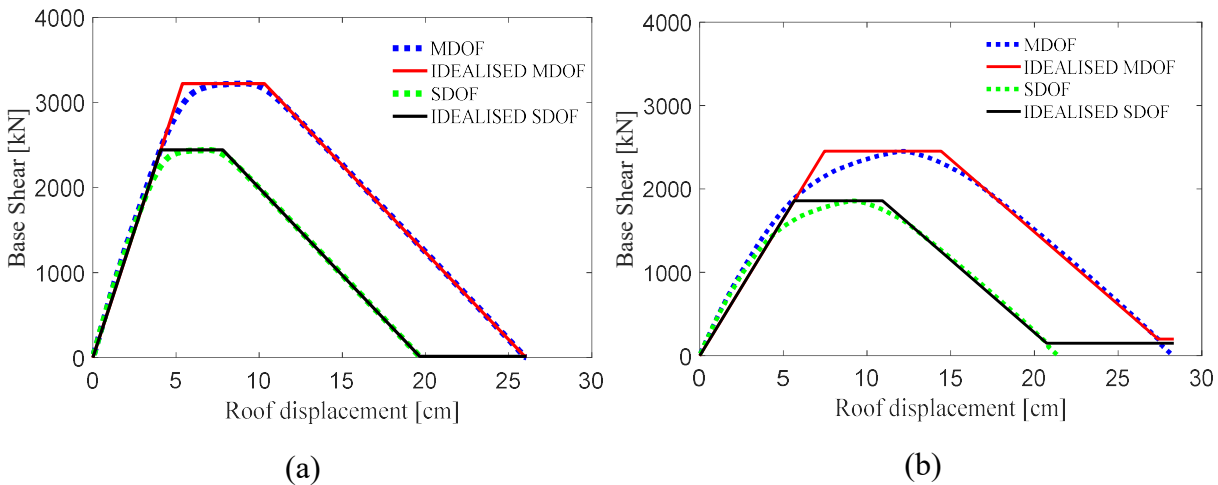


**Figure 3.24. Idealised strength capacity of the bare frame, (a) SPO in longitudinal-X direction, (b) SPO in transverse-Y direction.**

**Table 3-5. Dynamic properties of the bare frame structure (school building modelled without infills).**

Mode	Period [s]	Motion	Participation Mass
1	1.32	Torsional	4.1%
2	1.22	Translational Y	35.5%
3	1.00	Translational X	35.1%
4	0.46	Translational Y	8.1%

The performance assessment of the bare frame was evaluated by applying the target displacement shown in Table 3-6 obtained after applying the N2 method, but considering the variations in the structural analysis for structures without infill, as it is explained in Chapter 2. Figures of the target displacement are displayed in Appendix A.

**Table 3-6. Target displacements for the seismic assessment of the bare frame.**

Return Period	Top displacement [mm]		Top displacement [mm]
	Long. (X)	Transv. (Y)	
45	26		31
75	36		44
712	130		160
1463	190		220

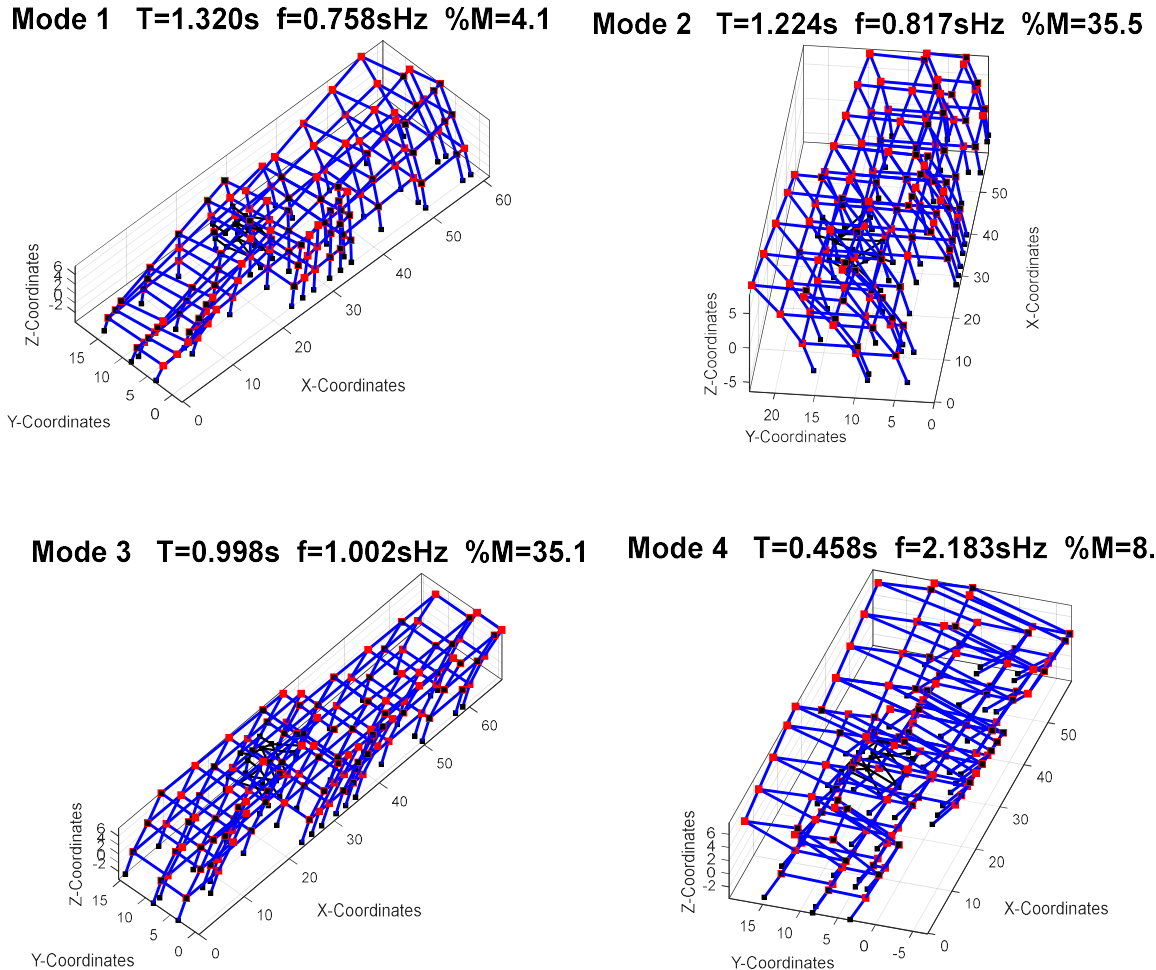


**Figure 3.25. Shape mode of the first four periods for the bare frame.**

The target displacement was expected to be larger than the ones obtained for the original building since the equivalent period is now longer.

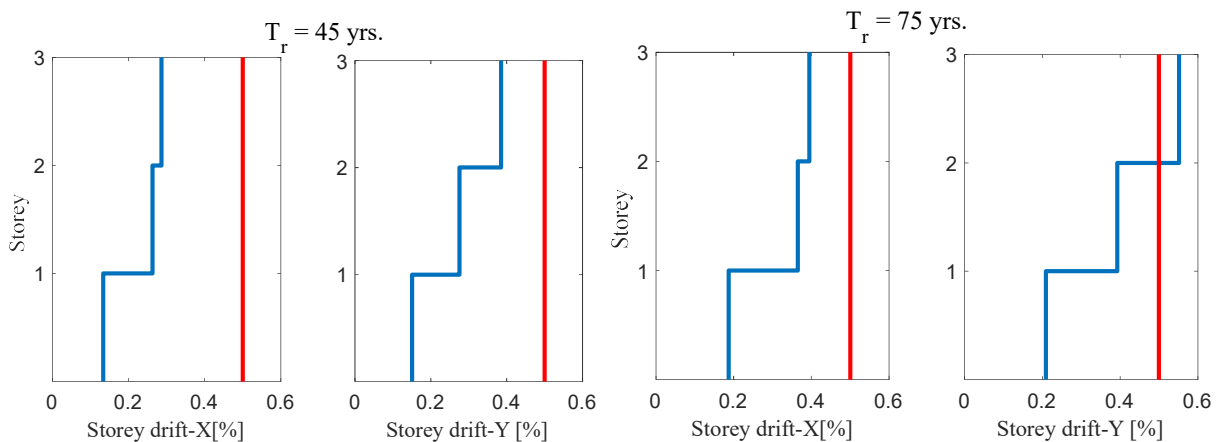


**Figure 3.26. Maximum storey drift of the bare frame for the serviceability limit state.**

For the serviceability limit state, the only case that does not meet the limit drift requirement is for the return period of 75 years in the Y direction, as shown in Figure 3.26. It is worth noting that the maximum drifts are higher compared to those of the original building.

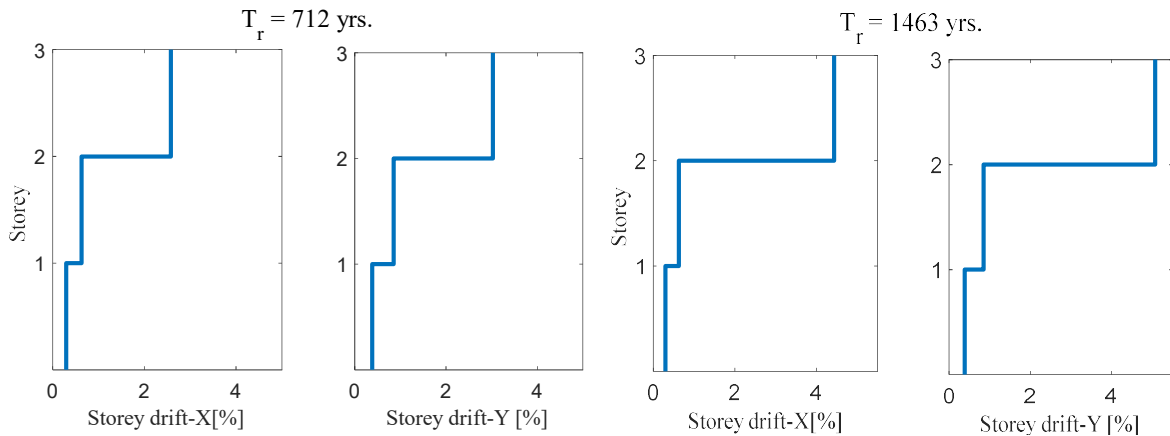


**Figure 3.27. Maximum storey drift of the bare frame for the ultimate limit state.**

In the case of the ultimate limit state, the weak-storey mechanism has moved to the top floor for the analysis in the X direction, while in the Y direction it remains in the same location, as illustrated in Figure 3.27. Weak-storey mechanisms were not avoided and maximum drifts are extremely high compared with the analysis of the original building for that limit state. The new soft-storey mechanisms are shown in Figure 3.28(a) and Figure 3.28.

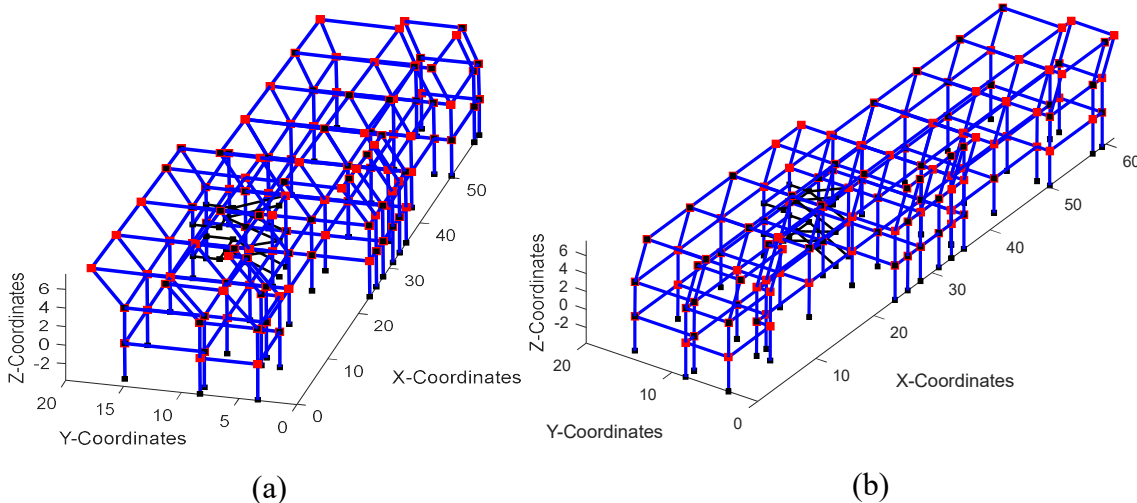


**Figure 3.28. Weak-Stories mechanism after performing SPO for the bare frame, (a) mechanism in the second floor in Y, (b) mechanism in the first floor in X.**

In terms of damage in the various frame elements, there is a considerable increase of failure of joints for the Y direction analysis and in columns for the X direction analysis, as illustrated in Figure 3.29. Since the elements are undergoing higher displacements and therefore, more deformations, removing the infills led to a slight increasing in the number of damaged elements for a given return period.

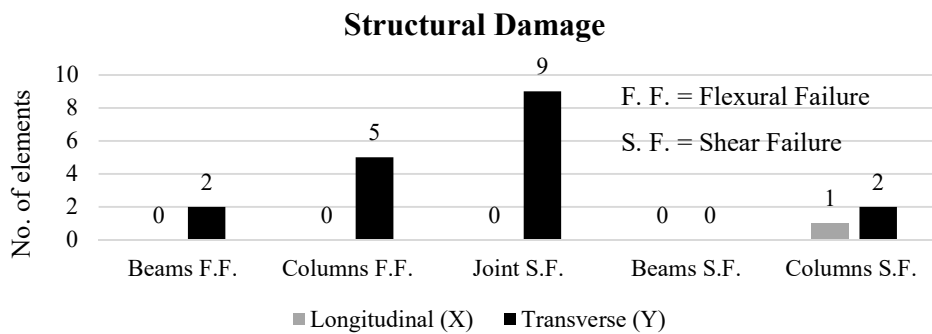


**Figure 3.29. Damage presented in structural elements due to SPO for  $T_r = 1463$  years, bare frame.**

### 3.9 Summary and Discussions

In this chapter, the structural performance of the school building was evaluated using the N2 method, which consisted on carrying out a SPO for different target displacements based on the limit states imposed by NTC 2008 from which hazard levels are defined in terms of return periods. The drifts obtained for these analyses were compared with the limits specified by NTC 2008 for the case of serviceability limit state. In the case of the ultimate limit state, the presence of non-ductile failure mechanisms was checked. However, weak-storeys were present in both direction and these were also verified by applying the strength hierarchy criteria for several beam-column joints. From this, it was found that many joints did not follow a failure sequence that leads to a beam hinging but producing non-ductile failure mechanisms instead.

Furthermore, the assessment performed for the original building was recreated for the case of the bare frame (i.e. without masonry infills). The results of this analysis brought information about the influence of infills on the overall behaviour and structural performance of the case study building. On one hand, the lateral capacity decreased in terms of strength but its deformability was along the same lines as the original building. The drift limits for the serviceability limit state were within the limits except for one analysis in the Y direction. In case of the ultimate limit state weak-storey mechanism also formed. The number of damaged elements was higher than the original building making the behaviour of the bare frame more detrimental.

Moreover, the poor performance of the elements was also verified by the strength hierarchy where the capacity of columns and joints were way below to that of the beams. This results supports the fact of having such an undesirable behaviour since by failing these elements before the beams, no ductile hinging in the beams can be produced, and therefore failure is produced in joints or columns instead. This analysis is vital for proposing a retrofit intervention in which the strength hierarchy is met as a failure sequence of beam-column and joint.

The results of the assessment conducted in this will aid the development of the retrofitting schemes for the school building that are presented and detailed in the following chapters. The retrofit will be based on strengthening actions for the elements lacking adequate capacity as well as on preventing non-ductile mechanisms, since by increasing the elements capacity lead to a desirable failure mechanisms and failure sequence. The performance results are not only

the starting point for the selection and design the retrofitting alternatives but also the final stage in which the most convenient alternative will be selected by comparing the improvement obtained by either scheme.

## 4 IDENTIFICATION OF POTENTIAL RETROFITTING SOLUTIONS

### 4.1 Introduction

This chapter describes the retrofitting interventions proposed for the school building in order to comply with the requirements of NTC 2008, both in terms of structural and non-structural performance. The performance of each retrofitting scheme alternative was evaluated in a similar fashion to the original building presented in Chapter 3, verifying both the serviceability and ultimate limit states. The serviceability limit state was used to evaluate the non-structural elements, as it corresponds to events that are more frequent and the ultimate limit states was utilized for the overall structural response of the building since it is aimed to ensure life safety and collapse prevention during more rare events.

The different alternatives were compared with the result of the assessment of the original building in order to determine the most effective retrofit scheme based on structural behaviour. In the next chapter (Chapter 5), the retrofit of non-structural elements is evaluated via the expected annual loss (EAL), for this reason in this chapter the scheme for retrofitting non-structural elements is only presented and discussed but not evaluated.

### 4.2 Structural Retrofitting

Initially three retrofitting solutions for the school building were examined and involve: A) masonry infill retrofitting via the introduction of a perimeter gap; B) fibre reinforced polymer (FRP) wrapping of columns, joints and beams; and C) wrapping with the addition of diagonal braces in a number of bays in both directions of the building. These three alternatives provide cases in which the period of the structure increases, remains the same, and decreases, respectively. In addition to these alternatives, a fourth (D) strategy was also evaluated, which combines the effect of FRP and a vertical gap placed in the masonry infill panels. For a better organization and comprehension of results, the alternatives were named as follows:

- Retrofit Alternative A: Gap.
- Retrofit Alternative B: FRP.
- Retrofit Alternative C: FRP + Braces.
- Retrofit Alternative D: FRP + Gap.

The infill retrofit, alternative A, consists of detaching infill walls from the surrounding frames through a perimeter gap. This technique aimed to delay the interaction between the infill and surrounding RC frame, meaning that the entire structural response was modified, and converging to the structural behaviour of the bare frame, depending on the gap size. On the other hand, the FRP aimed to ensure the strength hierarchy at each joint, by strengthening columns and joints to make the beams the weaker elements, thus satisfying the strong column-weak beam requirements of NTC 2008 for the case of alternatives B, C, and D. Foreseeing that the FRP does not significantly modify the stiffness of the structure, the hybrid alternative C in which braces are included was also implemented so that any weak-story could be prevented. Finally, alternative D aimed to provide the benefits of alternatives A and B as a retrofitting solution.

#### 4.2.1 Retrofit Alternative A: Gap

The behaviour modelling of the cellular material and gap-frame interaction was done using the procedure described by Tsantilis and Triantafillou [2018], as illustrated Figure 4.3. The gap was assumed to be filled with foamed polyethylene material, displayed in Figure 4.1(a), which can absorb energy due to its high deformability capacity and permit lateral frame movement. The partial isolation is aimed to delay the interaction between the infill wall and the surrounding frame so that damage to the infill can be controlled and reduced. Figure 4.1(b) displays the results of a numerical trial conducted for a single bay frame to illustrate how the lateral capacity is affected by the interaction between the infill and frame for different gap widths.

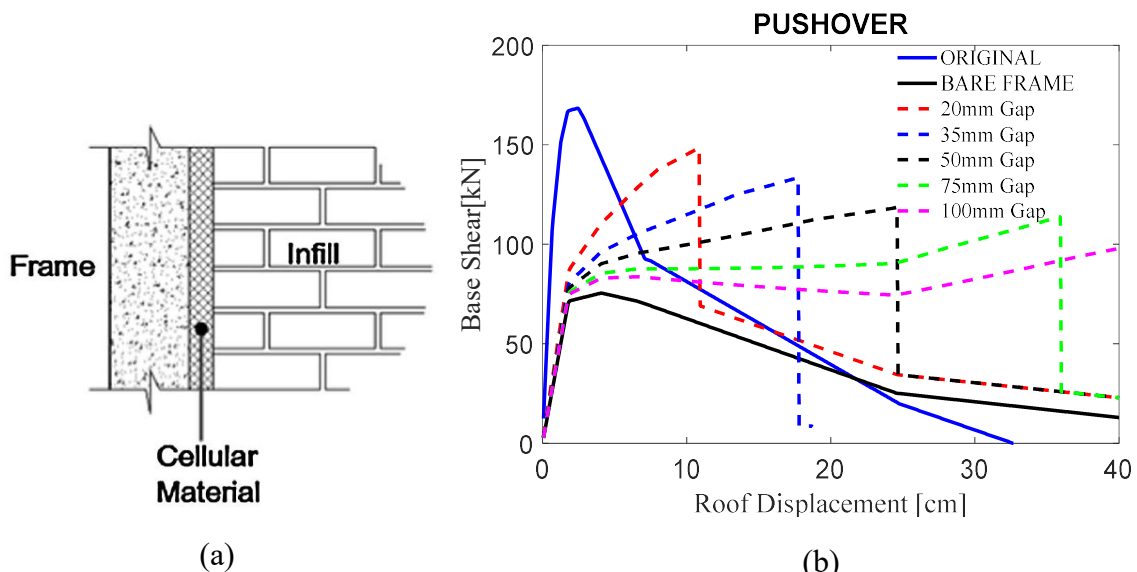


**Figure 4.1. Gap retrofitting, (a) cellular material between the infill and frame, (b) structural response of a single bay for different gap width.**

It can be seen that the wider the gap is, the closer the response of the structure converges to that of the bare frame. This clearly demonstrates the influence of the gap width on the overall response of the frame. Following the recommendation for a gap width between 18-80mm by Charleson [2008], static pushover (SPO) analyses of the building were conducted for three gap widths (20, 50, and 75 mm) and are presented in Figure 4.2 for both directions. Nevertheless, it was decided to use a minimum gap of 20mm since wider gaps led to bigger drifts similar to the

bare frame, and therefore to an unfavourable structural behaviour since this may potentially lead to higher displacements, residual drifts, and damage in the structural elements.

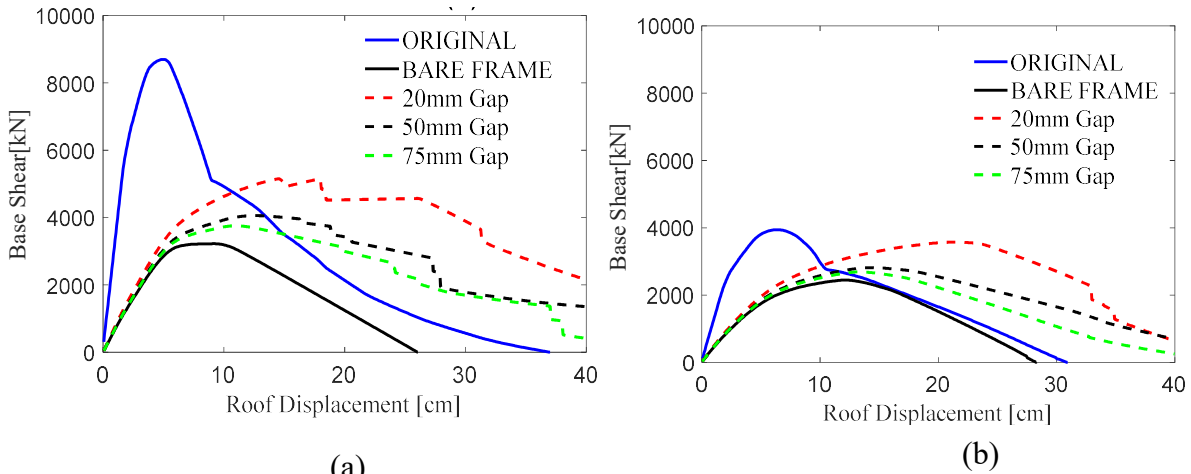


**Figure 4.2. Comparison of the structural response of the school building for different gap width, (a) SPO in the longitudinal-X direction, (b) SPO in the transverse-Y direction.**

The critical deformation at which the infill-frame interaction is activated is approximately equal to the joint thickness divided by the ratio of the infill height to the overall column clear height [Tsantilis and Triantafillou, 2018]. The gap model at the frame-infill interface only consider in-plan behaviour, which was modelled in OpenSees [McKenna *et al.*, 2000] through a zero-length spring element<sup>3</sup>, with the material constitutive law described by the uniaxial ElasticMultiLinear material<sup>4</sup> model illustrated in Figure 4.3. This model was calibrated and verified from uniaxial test results on the foamed polyethylene used in the experimental program by Tsantilis and Triantafillou [2018].

The non-linear load ( $F$ ) and displacement ( $u$ ) of the gap were determined by using the data listed in Table 4-1 and Equations (4.1) and (4.2) provided by Tsantilis and Triantafillou [2018]. Tsantilis and Triantafillou [2018] reported that for fully isolated infills (horizontal and vertical gaps), joints are activated at lateral (storey) displacement approximately equal to four times the joint thickness. On the other hand, for just side isolation (vertical gaps) the joint is activated at lateral displacements approximately equal to the joint thickness. For full isolation, infills can be accommodated as the frame deforms unlike vertical isolation in which the infill is restricted by the frame when this reaches a lateral displacement equal or greater than the joint thickness. For this reason the action of a full isolated infill is activated at a higher lateral displacement.

$$F = \sigma \frac{w_{inf} t_{inf}}{2 \cos \theta_i} \quad (4.1)$$

$$u = \varepsilon \frac{t_{joint}}{\cos \theta_i} \quad (4.2)$$

where:

$\sigma$  = compression stress of foamed material, Table 4-1.

$w_{inf}$  =width of the infill equivalent strut model.

<sup>3</sup> [http://opensees.berkeley.edu/wiki/index.php/ZeroLength\\_Element](http://opensees.berkeley.edu/wiki/index.php/ZeroLength_Element)

<sup>4</sup> [http://opensees.berkeley.edu/wiki/index.php/ElasticMultiLinear\\_Material](http://opensees.berkeley.edu/wiki/index.php/ElasticMultiLinear_Material)

$t_{\text{inf}}$  = thickness of the infill equivalent strut model.

$t_{\text{joint}}$  = thickness of the gap.

$\varepsilon$  = strain of foamed material, Table 4-1.

$\theta_i$  = angle of the infill equivalent strut model.

As seen in Figure 4.3(b) once the gap has been compressed totally (point P5), the full action of the infill is incorporated into the model from point P5 and P6 onward. A slight initial resistance is provided due to the behaviour of the cellular material, which presents relatively small strains from point P1 to P4.

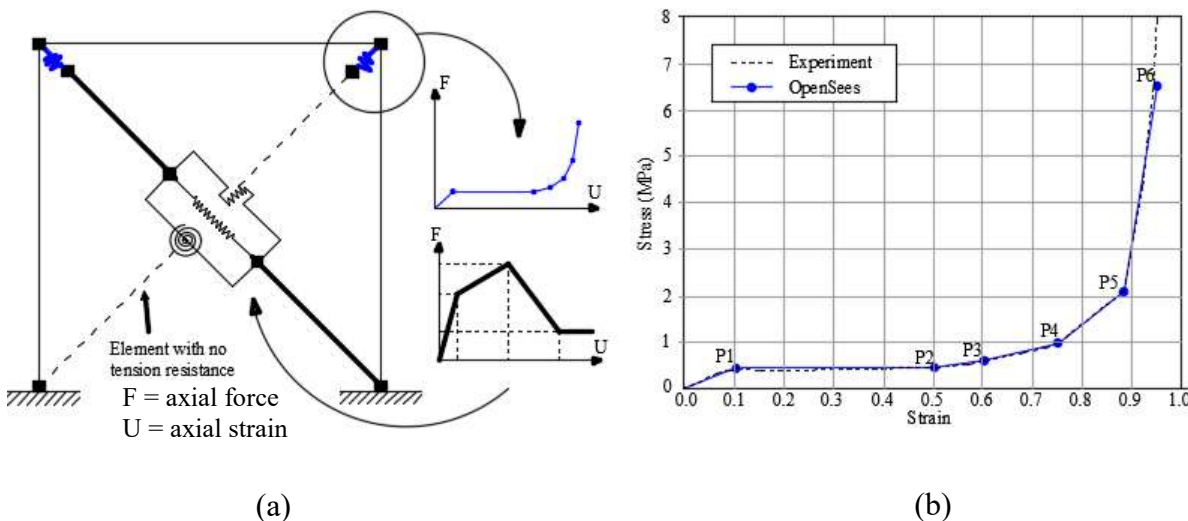


Figure 4.3. Gap modelling, (a) numerical model of gap and infills, (b) model of the stress-strain behaviour of the gap material, [after Tsantilis and Triantafillou, 2018].

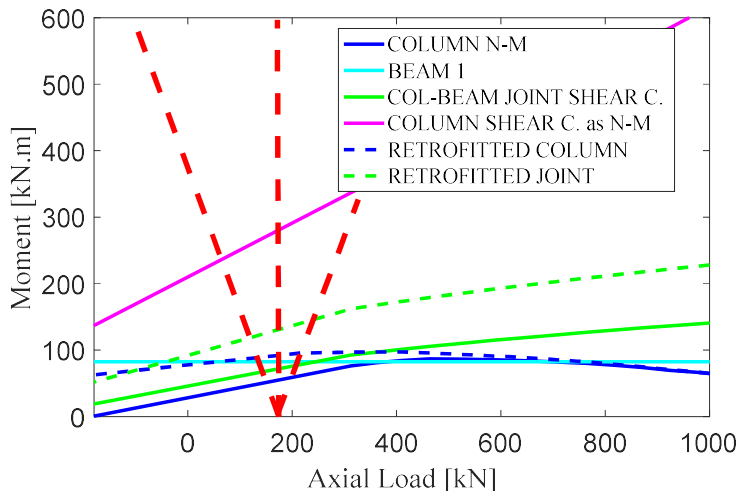
Table 4-1. Definition of material model for the isolation joints [Tsantilis and Triantafillou, 2018].

Point	1	2	3	4	5	6
Stress $\sigma$ (MPa)	0.39	0.44	0.58	0.95	2.11	6.50
Strain (%)	10	50	60	75	88	95

#### 4.2.2 Retrofit Alternative B: FRP

The procedure used to compute the new capacity of the elements strengthened with FRP was presented by EN 1998-3:2005 [2005], and afterwards slightly modified by Triantafillou [2018]. The sizing and amount of FRP were determined to improve the strength hierarchy of the beam-column joint elements for the existing school building, as presented in Chapter 3. To respect and guarantee a ductile failure mechanism, a beam hinging was identified to be the required mechanism controlling the strength hierarchy. Therefore, it was decided to keep the beams as the weakest elements within each beam-column joint zone. Columns and joints were strengthened in a way that the failure sequence after the beam is followed by the columns and lastly for the joints.

Figure 4.4 displays this process. The strengths of column and joint (continuous green and blue lines, respectively) are lower than the beam capacity (continuous cyan line). Consequently, the capacity of the column and joint are increased until they are higher than the capacity of the beam and in this way, a ductile failure sequence is achieved.



N-M = axial load – bending moment interaction.

**Figure 4.4. Strength hierarchy improvement for columns and joints, showing the capacity of the beam, column and joint as a function of the axial load.**

Provided that the weakest element is the beam, the column members were retrofitted for flexural and shear resistance, whereas the beam-column joints were retrofitted for shear capacity alone. In the case of the columns, it was opted to retrofit them with carbon fibre reinforced polymer (CFRP) bars and wrapping as stated in Chapter 3. The CFRP bars were aimed to increase the flexural capacity of columns, whereas, wrapping was aimed not only to improve their confinement capacity but also their shear and deformability capacity. In the case of the joints, continuous strips were placed horizontally and vertically to compensate the lack of shear capacity. Finally, even though the beams present a ductile behaviour and just a few show shear failure, no flexural intervention was required. However, to guarantee a more ductile behaviour and a better chord rotational capacity, confinement at the ends of the beam was assumed, in a length of twice the beam depth. According to the recommendation of EN 1998-1:2004 [2004]. The design parameters were taken from Table 2-6, where in order to optimise flexural strengthening, a high tensile strength and low modulus of elasticity has to be provided. Therefore an ultimate tensile strain of 1.6% and elastic modulus of 215GPa were selected. On the other hand, for confinement strengthening a low strain and high modulus of elasticity has to be used, which is why the values selected were 0.7% for ultimate tensile strain, 350GPa for elastic modulus and 2450 MPa for tensile strength. Additionally, the confinement of rectangular cross sections is achieved by rounding the corners so that stress concentrations can be reduced. For each element a radius of 15mm was adopted. The way in which each element was strengthened with FRP is described in the following text.

(a) Beam Intervention

U-jackets (three-sided) configuration was used for beams, placed at each end in a length of two times its depth [EN 1998-1:2004, 2004]. The shear capacity was

computed using Equation (4.3) and (4.4) which are described in Triantafillou [2018] and the maximum bond length ( $l_{b,\max}$ ) through Equation (4.5) and (4.6) [Triantafillou, 2018]. The confinement and ductility capacity were not calculated, but it was considered three layers of the CFRP material. A gap of 15mm is recommended at the ends for ductility since this allows for unrestraint rotation of the end cross-section as well as to prevent damage of the FRP in compression [Triantafillou, 2018].

$$\sigma_{\text{fed}} = f_{\text{fbd}} \left[ 1 - \left( 1 - \frac{2}{\pi} \right) \frac{l_{b,\max} \sin \alpha}{d_f} \right] \quad (4.3)$$

$$V_{Rd,f} = 2t_f d_f \sigma_{\text{fed}} \cot \theta \quad (4.4)$$

$$l_{b,\max} = 0.6 \sqrt{\frac{E_f t_f}{\sqrt{f_{\text{ctm}} k_b}}} \quad [\text{mm}] \quad (4.5)$$

$$k_b = \sqrt{\frac{1.5 \left( 2 - \frac{b_f}{b_w} \right)}{1 + \frac{b_f}{100}}} \geq 1 \quad (4.6)$$

where:

$\sigma_{\text{fed}}$  = design value of mean stress in the FRP crossing the shear crack.

$d_f$  = height of FRP crossed by the shear crack (mm).

$t_f$  = FRP strip thickness (mm).

$\alpha$  = angle of FRP strips.

$\theta$  = angle of shear cracks.

$E_f$  = elastic modulus of FRP (MPa).

$f_{\text{ctm}}$  = mean tensile strength of concrete (MPa).

$b_f$  = width of FRP strip (mm).

$b_w$  = member width (mm).

In Figure 4.5, a possible scheme for the strengthening configuration in the beams is illustrated.

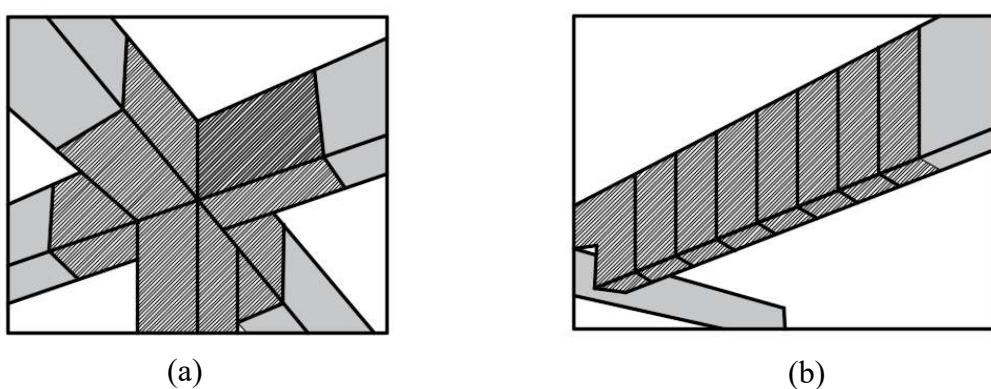


**Figure 4.5. CFRP U-jackets configuration, (a) Scheme for beams connecting internal joints, (b) CFRP scheme for beam ends, [after Triantafillou, 2018].**

To avoid strip debonding of anchorage, the configuration illustrated in Figure 4.6(a) can be adopted. For the coming sections the general term FRP, in this study, refers to CFRP, carbon fiber reinforced polymer.

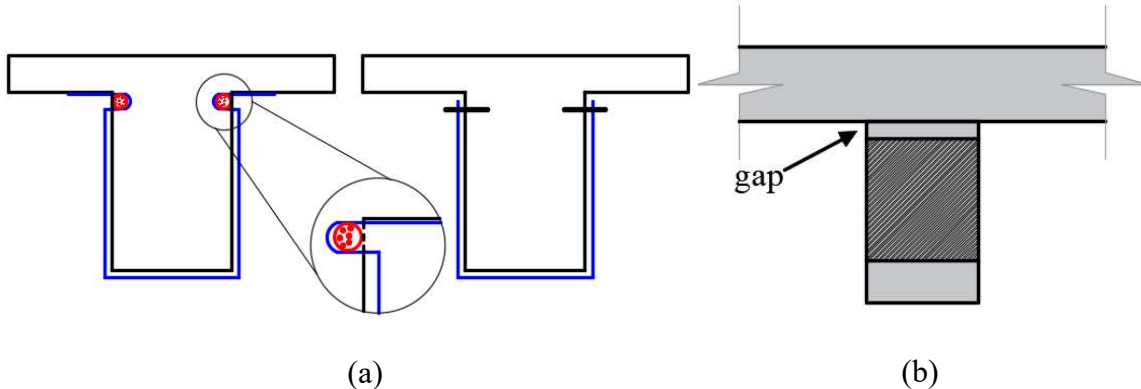


**Figure 4.6. (a) FRP anchorage scheme for beams, (b) FRP wrapping scheme at the end of columns, [after Triantafillou, 2018].**

#### (b) Joint Intervention

The increase of shear capacity for corner beam-column joints was done following the procedure described by Del Vecchio *et al.* [2015] and therefore, equations stated here refer to this work. The equivalent FRP area was obtained with Equations (4.7) and (4.8) assuming continuous strips in the horizontal and vertical direction of the joint as shown in Figure 4.7. The magnification of the principal tensile stress due to FRP contribution was computed, through Equations (4.9) and (4.10). Finally, the total tensile stress, Equation (4.11), was obtained and the moment capacity of the joint recalculated.

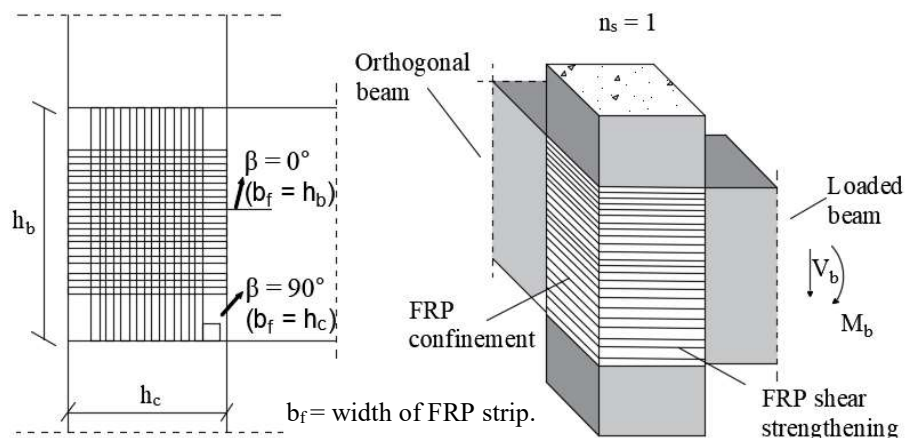


**Figure 4.7. FRP strips assumptions for design, [after Del Vecchio *et al.*, 2015].**

In case of internal joints, externally bonded L-shape FRP laminates were assumed since it has been demonstrated that they provide a better behaviour and give more strength to internal joints [Yu *et al.*, 2015]. Figure 4.8 displays some potential external bonded L-shape configurations used in the design procedure, Akguzel and

Pampanin, [2012] also proposed some equations based on strain compatibility that lead to the computation of the additional tensile strength provided by the FRP.

$$A_{f,eq} = n_l n_s t_f h_b \sin \theta, \text{ for } \beta = 0^\circ \quad (4.7)$$

$$A_{f,eq} = n_l n_s t_f h_c \cos \theta, \text{ for } \beta = 90^\circ \quad (4.8)$$

$$\varepsilon_{f,e} = 31.6 C_{ID} C_{MA} \left( \frac{f'_c}{A_{f,eq} E_f} \right)^{0.6}, C_{ID} = 1.0, C_{MA} = 1.0 \quad (4.9)$$

$$p_{t,f} = \frac{A_{f,eq} E_f \varepsilon_{f,e}}{b_c h_c \sin \theta} \quad (4.10)$$

$$p_{t,tot} = p_{t,c} + p_{t,f} \quad (4.11)$$

where:

$n_l$  = number of FRP layers.

$n_s$  = number of joint panels sides strengthened in shear with FRP systems in the plane of the load.

$h_b$  = beam height.

$h_c$  = column height.

$\beta$  = angle of strips.

$f'_c$  = compressive strength of concrete.

$p_{t,c}$  = concrete contribution of joint panel principal tensile stress.

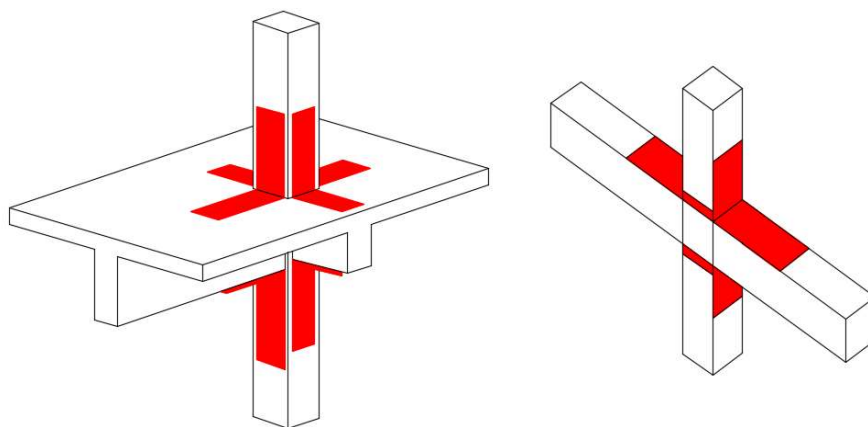


**Figure 4.8. Flange strips scheme for retrofitting internal joints, [after Yu et al., 2015] and [after Maher et al., 2012].**

The numerical modelling of the new capacity of joint was also done in OpenSees in the same way as for the existing building, but by increasing the flexural capacity in the hysteresis model as shown through the red line in Figure 4.9. Pampanin [2017] presented results of tests developed on the retrofitting of exterior and internal joints for a frame where the capacity of the joints increased about 15-20%, similar results were found by Parvin et al. [2005].

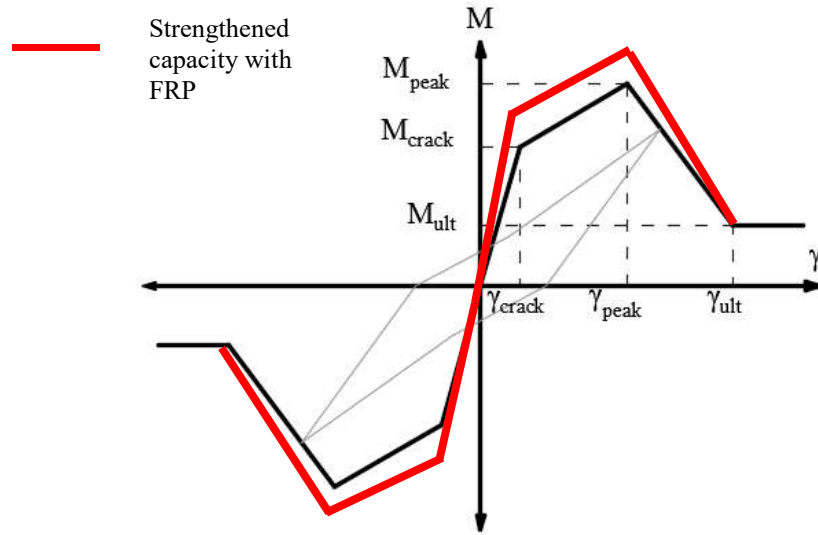


**Figure 4.9. Modelling of retrofitted beam-column joint with FRP.**

(c) Column Intervention

The confinement of columns increases their axial, shear strength and deformation capacity, delay buckling and prevent lap-splice failure. However, only the first two aspects were considered since no apparent rebar buckling or lap-splice failure were reported in Chapter 3. The shear capacity was computed through Equations (4.12) to (4.15) and then (4.4) [Triantafillou, 2018], the confinement strength by Equations (4.16) and (4.17) assuming a bilinear confinement model [Triantafillou, 2018].

$$0 \leq \frac{R}{b_w} \leq 0.5 \quad (4.12)$$

$$\eta_R = 0.2 + 1.6 \frac{R}{b_w} \quad (4.13)$$

$$f_{fu,W}(R) = f_{fbd} + \langle \eta_R f_{fd} - f_{fbd} \rangle \quad (4.14)$$

$$\sigma_{fed} = f_{fbd} \left[ 1 - \left( 1 - \frac{2}{\pi} \right) \frac{l_{b,max} \sin \alpha}{2d_f} \right] + \frac{1}{2} \left[ f_{fu,W}(R) - f_{fbd} \right] \left[ 1 - \frac{l_{b,max} \sin \alpha}{d_f} \right] \quad (4.15)$$

$$\frac{f_{ccd}}{f_{cd}} = 1 + k_1 \left( \frac{\sigma_{lud}}{f_{cd}} \right)^m \quad (4.16)$$

$$\varepsilon_{ccu} = \varepsilon_{cu} + k_2 \left( \frac{\sigma_{lud}}{f_{cd}} \right)^n \quad (4.17)$$

where:

R = radius at the corner of the cross section.

b<sub>w</sub> = member width.

f<sub>fu,W</sub>(R) = tensile strength of closed jackets.

σ<sub>lud</sub> = confining stress.

f<sub>ccd</sub> = strength of confined concrete.

f<sub>cd</sub> = compression strength of concrete.

ε<sub>cu</sub> = ultimate compression strain.

$\varepsilon_{ccu}$  = ultimate confined strain.

Typical values for the empirical constants recommended by Triantafillou [2018] are  $k_1=2.10$ ,  $m=1.0$ ,  $k_2 = 0.02$  or  $0.04$  for carbon or glass fibres, respectively, and  $n=1.0$ . Similarly, a gap of 15mm is recommended at the ends of the column for ductility as shown in Figure 4.6(b). The flexural strengthening was done through an iterative process using the diagram of the interaction of the column in order to obtain the amount of FRP needed as illustrated in Figure 4.10, where the contribution of FRP was only considered in tension. As the amount of FRP increases the combined behaviour of a column (flexure-compression) becomes linear as shown in Figure 4.10.

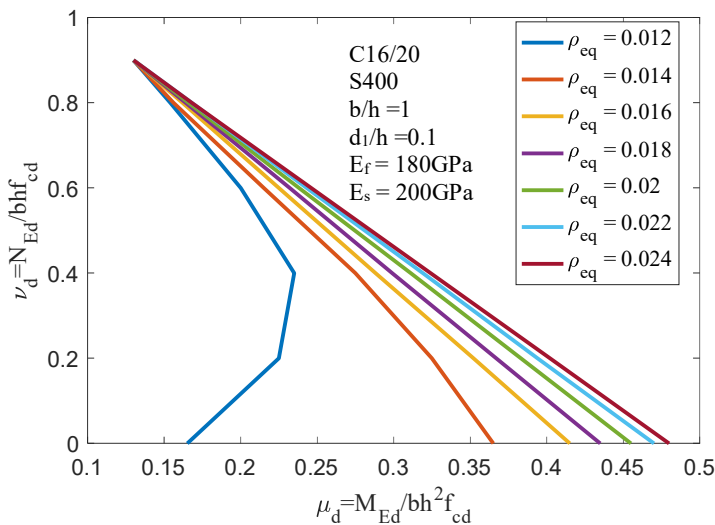


Figure 4.10. Interaction diagram for a RC column retrofitted with FRP, [after Triantafillou, 2018].

The equivalent geometric ratio of steel and FRP reinforcement is defined as:

$$\rho_{eq} = \frac{A_{s,tot}}{b_w d} + \frac{A_{f,tot}}{b_w d} \frac{E_f}{E_s} \quad (4.18)$$

where:

$N_{Ed}$  = total axial force.

$M_{Ed}$  = total bending moment.

$f_{cd}$  = compression strength of concrete.

$A_{s,tot}$  = total area of steel reinforcement.

$A_{f,tot}$  = total area of FRP.

$E_f$  = modulus of elasticity of FRP

$E_s$  = modulus of elasticity of steel.

$b_w d$  = width and depth of section.

It was assumed that FRP debonding is prevented through proper anchorage inside slabs or joints. The modelling of the new column capacity in OpenSees was done in the same way as in the existing building, but by increasing the flexural capacity in the hysteresis model as shown via the red line in Figure 4.11. This plot is similar to Figure 2.12 presented in Chapter 2, where the strength and ductility capacity is increased in this case. The curvature at yielding remains the same since at this level

the steel reinforcement starts yielding, but the force required to produce yielding is higher. Even though there is a slight increase in the stiffness of the elements, this is not reflected in the overall stiffness of the structure since FRP is not modifying the cross sections of the elements.

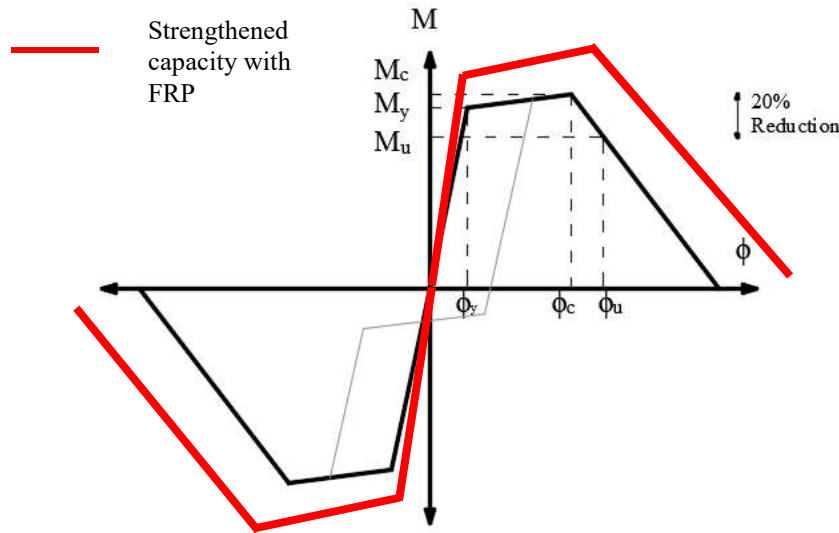


**Figure 4.11.. Modelling of retrofitted beam-column elements with FRP.**

Additionally, it was verified that the strength of the column provides a ductile behaviour by applying the criteria stated by Galal and Ghobarah [2004], previously evaluated in Chapter 3. In fact, the additional shear strength, contribution of FRP is incorporated into the shear capacity of the columns in the expression presented by Priestley [1993] for estimating the shear capacity by Galal and Ghobarah [2004]. As discussed in Chapter 3, a moderate-ductile and ductile behaviour govern the columns, but after incorporating FRP wrapping, a ductile behaviour controls as illustrated in Figure 4.12.

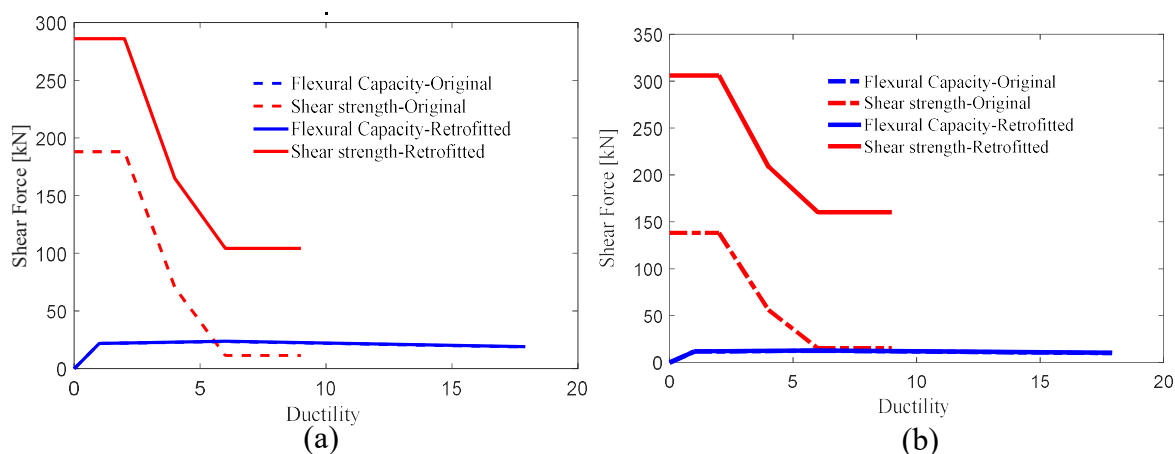


**Figure 4.12. Combined shear strength and flexural strength after wrapping columns with FRP, (a) previous moderate-ductile behaviour, post-retrofit ductile behaviour, (b) ductile behaviour.**

A possible scheme of column retrofitting is shown in the following Figure 4.13.

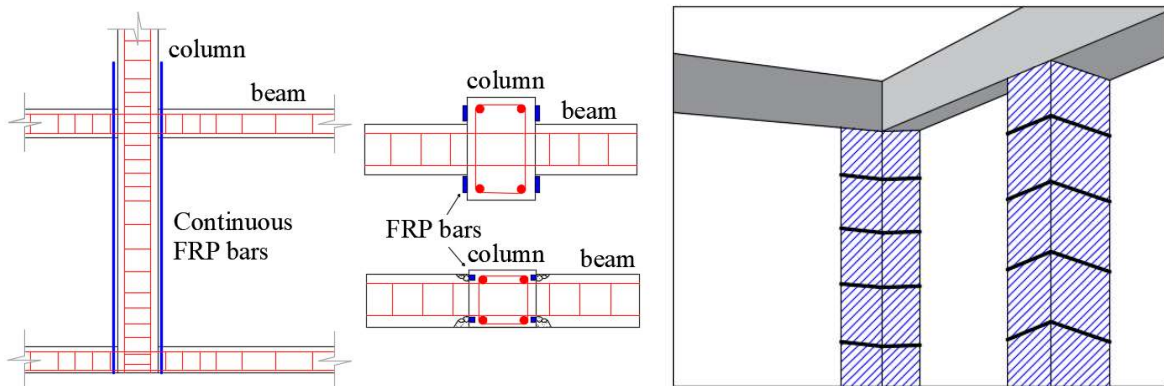
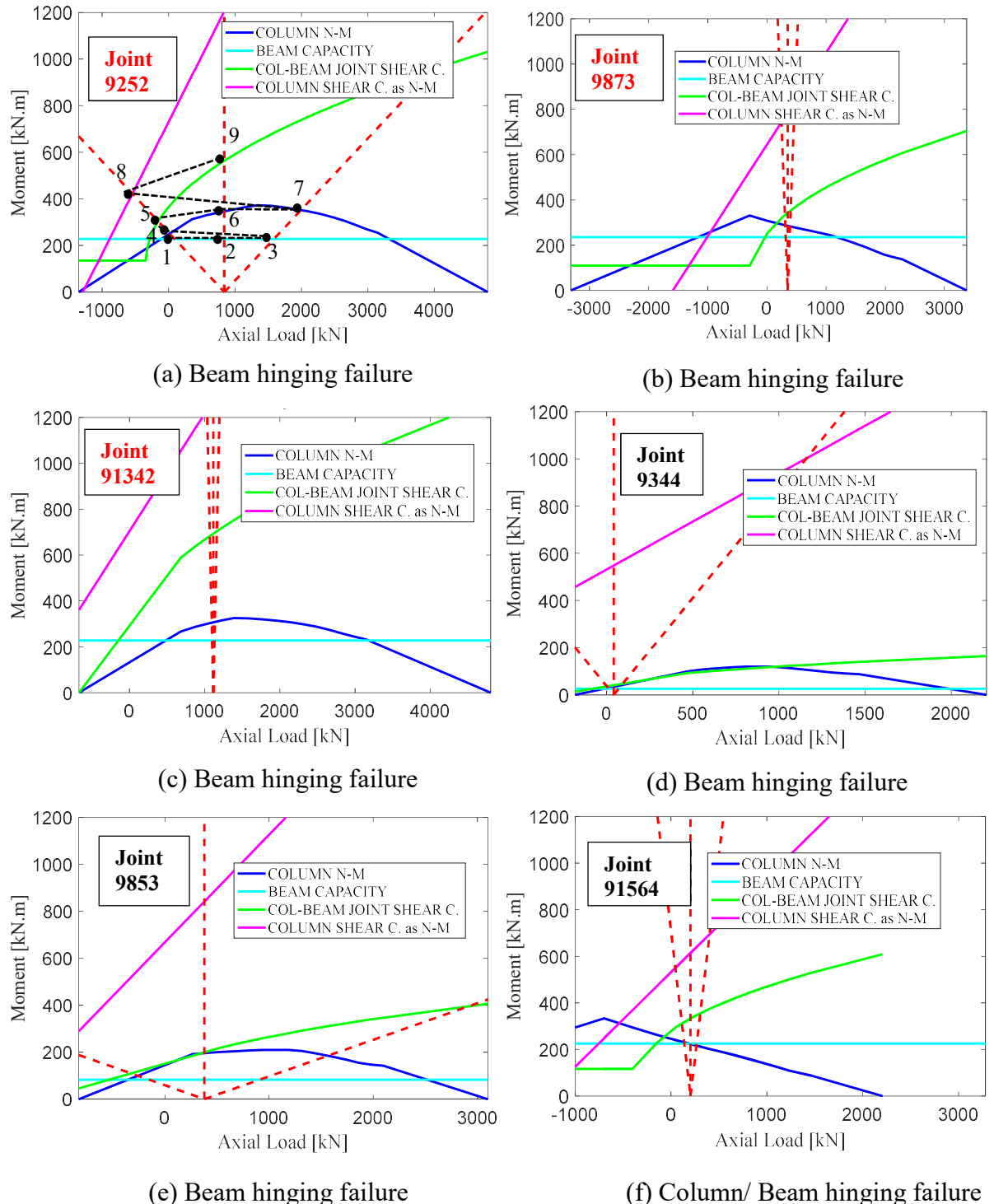


**Figure 4.13. FRP scheme for retrofitting columns, [after Triantafillou, 2018].**

Figure 4.14 displays the strength hierarchy for the strengthened columns and joints for some beam-column joints presented in Chapter 3. The black segmented line in Figure 4.14(a) shows the failure sequence as beam-column-joint since the first element that fails is the beam (1-2-3), then follows by the column(4) and lastly by the joint (5). This sequence leads to a ductile failure mechanisms required in seismic design. It is important to mention that during an earthquake the joint undergoes unloading first and then is loaded again. This effect is illustrated with the two red dotted lines in Figure 4.14(a) and for this reason the sequence of failure, represented by the black dotted line, follows a zig zag path indicating loading, unloading and reloading of the joint.



N-M = axial load – bending moment interaction.

**Figure 4.14. Strength hierarchy evaluation after retrofitting the elements with FRP with their failure mechanisms.**

Even though a ductile failure sequence is provided, there are some beam-column joints such as node 91564 (exterior joint in the top floor), illustrated in Figure 4.14(f), in which the strength of the column could not be increased higher than the capacity of the beam, since the required amount of FRP was impractical. In any case, the strength is close to that of the beam and the

strength of the joint is much higher than these two and therefore a column/beam hinge will be expected to occur in this joint. As will be shown in the following sections, the level of damage to these elements was reduced considerably despite the hierarchy criteria not having been improved for every single beam-column joint.

#### 4.2.3 *Retrofit Alternative C: FRP + Braces*

As previously mentioned in Chapter 2, the addition of FRP to the structure does not modify its stiffness. Furthermore, it was found that the structure has weak storeys in both direction due to the lack of lateral stiffness. With this in mind, a hybrid retrofitting intervention was implemented by adding steel braces in some bays at the floors presenting weak-storey mechanisms.

As illustrated in Figure 4.15, two braces were modelled in OpenSees. The braces were assumed connected in the middle so that the unbraced length is reduced. To consider not only different capacities, for tension and compression, but also strain on the braces, global buckling was modelled using the recommendation of Lignos *et al.* [2012]. An initial camber proportional to the unbraced length was considered, to induce in and out-plane buckling and recreate a realistic behaviour under earthquakes loads. It was found adequate to induce a camber of 0.75% in the plane of the brace, while 0.05% for out of the plane. To avoid having two cambers on the same brace, it was decided to model buckling only in the inferior braces, as shown in Figure 4.15. It was found that this does not modify the overall response of the structure. Following the procedure described by Uriz and Mahin [2008], the braces were modelled including rigid elements to account for the geometry of the connection, which connects braces and columns, and gusset plates to consider the out-of-the plane failure. The rigid elements were modeled as elasticBeamColumn elements<sup>5</sup>, gusset plates as a zero-length spring element, and braces as forceBeamColumn elements<sup>6</sup>. The material considered was Giuffré-Menegotto-Pinto Model with isotropic strain hardening, termed Steel02<sup>7</sup> in OpenSees. Each brace was discretised with six elements, which were divided into three integration points to consider the effects of the non-linearity. The out-of-the plane rotation that could be generated for the gusset plates, was modelled as pin connection, with a relatively low out-of-the plane rotational stiffness.

---

<sup>5</sup> [http://opensees.berkeley.edu/wiki/index.php/Elastic\\_Beam\\_Column\\_Element](http://opensees.berkeley.edu/wiki/index.php/Elastic_Beam_Column_Element)

<sup>6</sup> [http://opensees.berkeley.edu/wiki/index.php/Force-Based\\_Beam-Column\\_Element](http://opensees.berkeley.edu/wiki/index.php/Force-Based_Beam-Column_Element)

<sup>7</sup> [http://opensees.berkeley.edu/wiki/index.php/Steel02\\_Material -- Giuffr%C3%A9-Menegotto-Pinto\\_Model\\_with\\_Isotropic\\_Strain\\_Hardening](http://opensees.berkeley.edu/wiki/index.php/Steel02_Material -- Giuffr%C3%A9-Menegotto-Pinto_Model_with_Isotropic_Strain_Hardening)

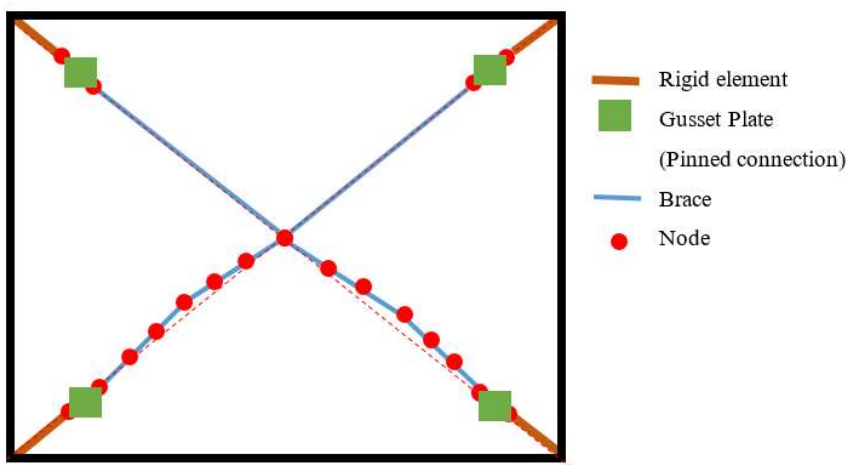


**Figure 4.15. Modelling of steel braces**

The sizing of braces was selected as follows:

First, to guarantee an adequate stiffness distribution on each storey and also to determine which storeys are lacking lateral stiffness, a proportional stiffness distribution along the height of the building as an inverted triangle was assumed. Figure 4.16 displays the proportions of the total lateral stiffness in each floor.

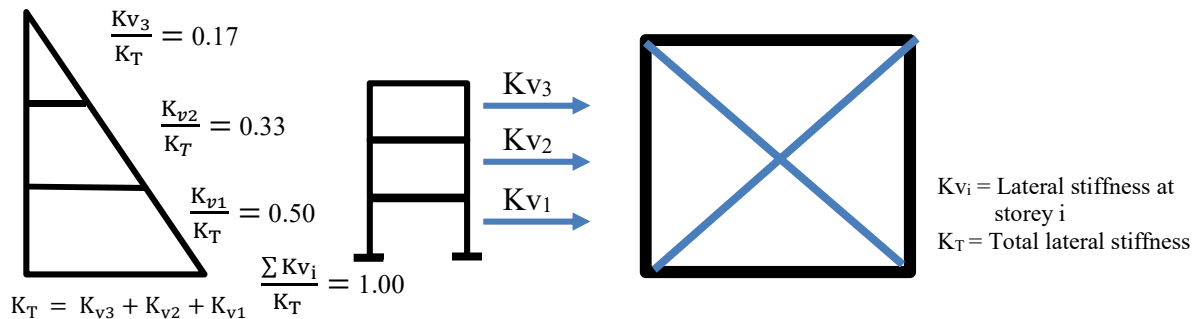


**Figure 4.16. Target stiffness of each storey.**

The fraction of stiffness at each storey is obtained through Equation (4.19) and then compared with the values presented in Figure 4.16, these values are represented in the last column of Table 4-2. The values of the column “storey lateral stiffness” ( $Kv_1$ ,  $Kv_2$  and  $Kv_3$ ) presented in Table 4-2 were determined by using Equations (4.20), (4.21), and (4.22); the lateral displacement ( $u$ ) and shear at each floor ( $V_s$ ) were taken from the SPO analysis by adding the shear in columns and also the contribution of infills. The stiffness fractions that are distant from the values indicated in Figure 4.16 will need intervention in other words, braces will be placed in those storeys.

$$\frac{K_{vi}}{K_T} = \%K_i \quad (4.19)$$

$$V_{s3} = K_{v3}(u_3 - u_2) \quad (4.20)$$

$$V_{s2} = K_{v2}(u_2 - u_1) + K_{v3}(u_2 - u_3) \quad (4.21)$$

$$V_{s1} = K_{v1}(u_1) + K_{v2}(u_1 - u_2) \quad (4.22)$$

where:

$V_{si}$  = total shear at storey i.

$u_i$  = lateral displacement at storey i.

Table 4-2 details the proportional stiffness distribution in the linear range of the structure. The linear range was defined as the initial part of the SPO, at a relative small roof displacement. It can be seen that the stiffness in the second storey is quite low compared with the target value of 0.33. Consequently, additional stiffness has to be incorporated in this storey, which is confirmed by the analysis done in Section 3.7.4 that showed that a soft-storey was formed here.

**Table 4-2. Distribution of shear strength and stiffness in the longitudinal direction in the linear range ( $T_r = 1463$  yrs.).**

Storey	Storey Shear [kN]		Storey Relative Displacement [m]		Storey Stiffness [kN/m]		Fraction of Stiffness	
	3	544.8	$V_{s3}$	0.0062	$u_3 - u_2$	87871	$K_{v3}$	0.22 %K <sub>3</sub>
2	926.6	$V_{s2}$	0.0138	$u_2 - u_1$	106623	$K_{v2}$	0.26	%K <sub>2</sub>
1	1058.7	$V_{s1}$	0.0093	$u_1$	213473	$K_{v1}$	0.53	%K <sub>1</sub>
					407967	$K_T$	1.00	

In the same way, the distribution of lateral stiffness was evaluated in the non-linear range, which was defined as the final point in the SPO for a target displacement related to the hazard level of  $T_r = 1463$  yrs. previously presented in Chapter 3. Table 4-3 indicates that the lateral stiffness in the second storey needs to be increased in order to have a triangular distribution along the height of the building.

**Table 4-3. Distribution of shear strength and stiffness in the longitudinal direction in the non-linear range ( $T_r = 1463$  yrs.).**

Storey	Storey Shear [kN]		Storey Relative Displacement [m]		Storey Stiffness [kN/m]		Fraction of Stiffness	
	3	5112.6	$V_{s3}$	0.008	$u_3 - u_2$	389075	$K_{v3}$	0.27 %K <sub>3</sub>
2	5226.3	$V_{s2}$	0.068	$u_2 - u_1$	122631	$K_{v2}$	0.085	%K <sub>2</sub>
1	5928.8	$V_{s1}$	0.012	$u_1$	929592	$K_{v1}$	0.64	%K <sub>1</sub>
					1441298	$K_T$	1.00	

Table 4-4 presents the analysis for the Y direction in the linear range, from which is indicated that braces are needed in the second storey due to its very low fraction.

**Table 4-4. Distribution of shear strength and stiffness in the transverse direction in the linear range ( $T_r = 1463$  yrs.).**

Storey	Storey Shear [kN]	V <sub>s3</sub>	Storey Relative Displacement [m]		Storey Stiffness [kN/m]	Fraction of Stiffness	
			0.002	u <sub>3</sub> – u <sub>2</sub>		K <sub>v3</sub>	0.51 %K <sub>3</sub>
3	231	V <sub>s3</sub>	0.002	u <sub>3</sub> – u <sub>2</sub>	115500	K <sub>v3</sub>	0.51 %K <sub>3</sub>
2	330	V <sub>s2</sub>	0.0057	u <sub>2</sub> – u <sub>1</sub>	17368	K <sub>v2</sub>	0.087 %K <sub>2</sub>
1	430	V <sub>s1</sub>	0.0083	u <sub>1</sub>	91566	K <sub>v1</sub>	0.41 %K <sub>1</sub>
					224434	K <sub>T</sub>	1.00

In the case of the non-linear range, Table 4-5 indicates that braces are needed in the third storey to increase the lateral stiffness in the Y direction. The results of this analysis corroborate the presence of a soft-storey mechanism already shown in Section 3.7.4.

**Table 4-5. Distribution of shear strength and stiffness in the transverse direction in the non-linear range ( $T_r = 1463$  yrs.).**

Storey	Storey Shear [kN]	V <sub>s3</sub>	Storey Relative Displacement [m]		Storey Stiffness [kN/m]	Fraction of Stiffness	
			0.06	u <sub>3</sub> – u <sub>2</sub>		K <sub>v3</sub>	0.06 %K <sub>3</sub>
3	2085	V <sub>s3</sub>	0.06	u <sub>3</sub> – u <sub>2</sub>	34750	K <sub>v3</sub>	0.06 %K <sub>3</sub>
2	2071	V <sub>s2</sub>	0.0204	u <sub>2</sub> – u <sub>1</sub>	203725	K <sub>v2</sub>	0.328 %K <sub>2</sub>
1	3279	V <sub>s1</sub>	0.014	u <sub>1</sub>	382143	K <sub>v1</sub>	0.62 %K <sub>1</sub>
					620618	K <sub>T</sub>	1.00

After determining the storeys that need intervention, a static analysis was performed following the procedure described by Eurocode 8 [EN 1998-1:2004, 2004]. A lateral load representing the demand for the hazard level of 1463 years was determined in both direction and then distributed to each storey as illustrated in Figure 4.17. The demand was obtained from the idealised elastic spectrum of 1463 years for both translational periods (0.61 and 0.36 , Table 4-7). It was assumed that for the hazard level only the braces in tension will contribute to the lateral resisting system since braces in compression may be buckled at such hazard level. Once the lateral force was distributed in each storey a static analysis was carried out in order to obtain the axial force (N<sub>b</sub>) in the brace, then with Equation (4.23) the area of the braces was estimated.

$$A_b = \frac{N_b}{F_{yst}}, N_b = \text{axial force in the brace.} \quad (4.23)$$

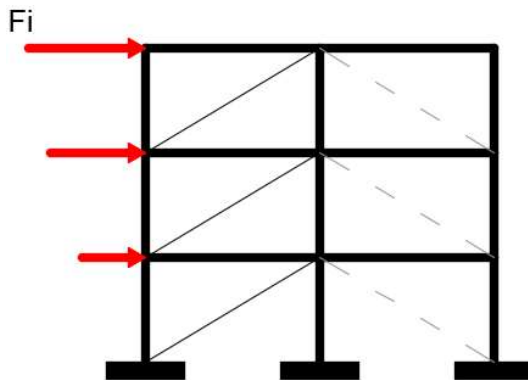


**Figure 4.17. Distribution of lateral load along the height of the building.**

Figure 4.18 illustrates the braces configuration for each direction of the building, this configuration was based on providing a less invasive intervention. Therefore, braces will be placed parallel to the infill masonry.

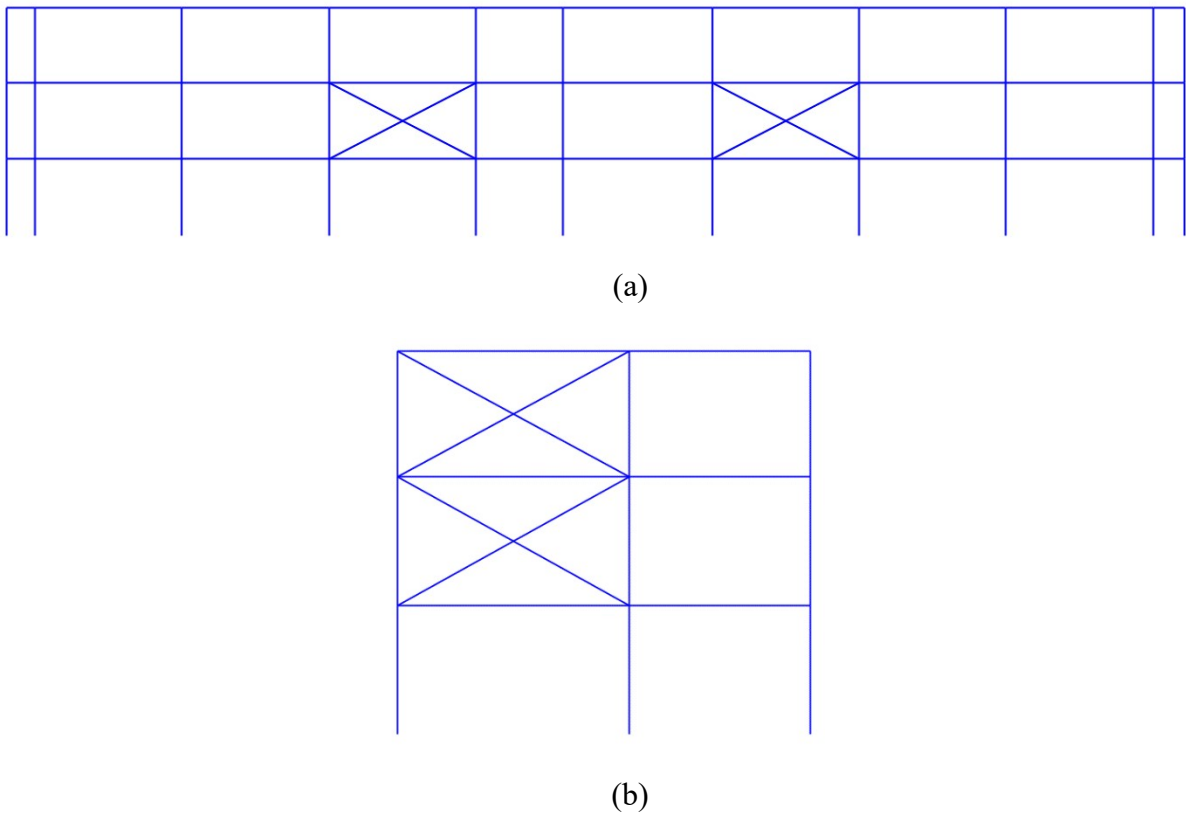


**Figure 4.18. Braces configuration along the height of the building, (a) The longitudinal-X direction, (b) The transverse-Y direction.**

The outcomes of this analysis indicated that the brace area required in the longitudinal direction was  $0.0017\text{m}^2$  and in the transverse direction  $0.0013\text{m}^2$ . In the end, it was decided to use hollow pipe sections with a yielding strength ( $F_{y\text{st}}$ ) of  $245\text{MPa}$ . The corresponding brace sections were defined as a ratio between exterior diameter/thickness given in mm. Therefore, in case of the

longitudinal direction a hollow pipe section of 140/5 ( $A=0.0021 \text{ m}^2$ ) will be placed and for the transverse direction a hollow pipe section 102/4.5 mm ( $A=0.0014 \text{ m}^2$ ).

#### 4.2.4 Retrofit Alternative D: FRP + Gap

This alternative was based on the combined effect on the two previous alternatives. Therefore, the modelling and criteria used for this scheme was the same as FRP and FRP plus braces.

### 4.3 Non-Structural Retrofitting

This section summarises a set of non-structural retrofit solutions taken from FEMA E-74 [FEMA E-74, 2012], which provides techniques to reduce the risk of non-structural damage during earthquakes. In addition to improving their seismic performance, the retrofitting of non-structural elements is also aimed to reduce the direct loss as it has been shown by Calvi *et al.* [2014; 2016], among others, to contribute significantly. Therefore, the most prudent solution is to reduce the vulnerability of such elements.

As stated in Chapter 2, the retrofitting of non-structural elements can be done separately from the structure and their improvement is reflected in the loss estimation presented in Chapter 5 by using the improved fragility functions. The fragility functions, illustrated in Figure 4.19 for a suspended ceiling, indicate the probability of incurring damage as a function of a demand. These functions are defined by quantity, vulnerability, and distribution of damageable components and contents for one or multiple damage states.

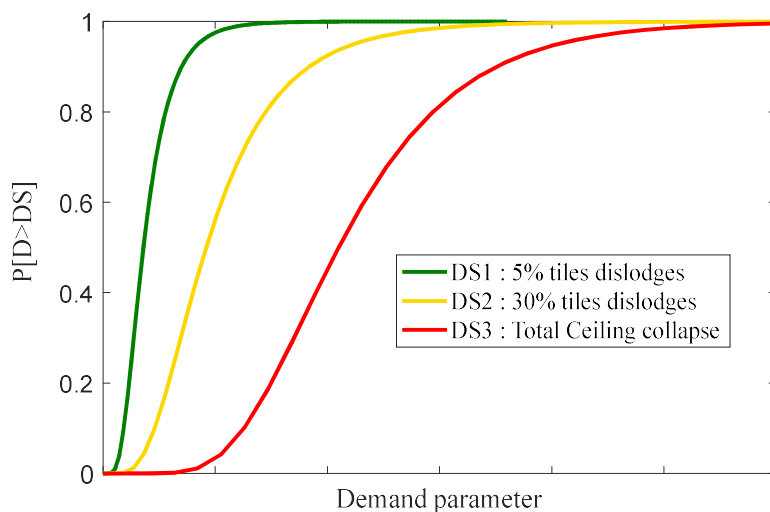


Figure 4.19. Illustration of a fragility function for a suspended ceiling, C3032.001b: PACT library.

#### 4.3.1 Drift-Sensitive Components

These elements are directly vulnerable to building deformation; when the building deforms, the columns or walls deform causing any windows or partitions rigidly attached to the structure displace also. However, brittle material like glass, gypsum partitions and masonry infill or veneer cannot tolerate any significant deformation and crack when the gaps are overtaken and the building structure pushes directly on the brittle elements. This leads them to dislodge and fall from their original location, possibly injuring occupants passing underneath. Peak storey drift, PSD (%) is the demand parameter typically used for these type of non-structural elements.

#### ***4.3.2 Acceleration-Sensitive Components***

These elements are sensitive to the inertial force produced by earthquake motions in the structure, the acceleration is severe if the location of the component is higher than the base (floor base where they are attached or placed), where excitations are amplified, thus the forces experienced above the base can be much time larger, these inertial forces may cause them to slide, swing, rock, strike other objects, or overturn. The shaking can also cause damage to internal components of equipment without any visible damage or movement from its original location. Peak floor acceleration, PFA (g) is the demand parameter for this type of components, the same total quantity is assumed in both directions, meaning that they can be damaged by the demands from either direction and not only to one.

#### ***4.3.3 Velocity-Sensitive Components***

Velocity generated on each floor can cause overturning, or sliding of some non-structural elements such as bookshelves, possibly injuring occupants or blocking evacuation egress paths. Peak floor velocity, PFV (m/s) is the demand parameter used for these elements.

#### ***4.3.4 Improved Fragility Functions***

Table 4-6 describes the retrofitting strategies to be undertaken to improve the seismic performance of the non-structural elements. A building performance model was developed in the software PACT [FEMA P58-3, 2012] and for considering the retrofit of non-structural elements, the model was modified based on the type of non-structural element detailing assumed, which also included modifying the damageable inventory and rerunning the improved non-structural inventory. These results will be discussed later in Chapter 5.

A comparison is shown in Appendix B between the original and improved non-structural fragility curves as well as a visual and better description of the retrofitting strategy to be undertaken for each non-structural element.

**Table 4-6. Table of improved fragility function for non-structural elements.**

<b>Element</b>	<b>Demand Parameter</b>	<b>Type of Detail</b>	<b>Retrofitting Strategy</b>
Infill walls	Drift [%]	ER (Engineering Required)	Steel angles. Detach walls from frame with a gap of cellular material 20mm, [FEMA E 74, page 6-64, Figure 6.3.2.1-7].
Internal partitions	Drift [%]	ER	Steel angles. Detach walls from frame with a gap of cellular material 20mm, [FEMA E 74 page 6-64, Figure 6.3.2.1-7].
Doors	Drift [%]	NE (Non-engineered)	Isolation of the supporting frame with plastic material or something of similar.
Windows	Drift [%]	PR (Prescriptive)	Isolation of the supporting frame with plastic material or something of similar.
Desks	Drift [%]	PR	Seismic fastener and security restraints (anchored to wall or floor).
Chairs	Drift [%]	NE	
Ceiling Systems	PFA [g]	PR, NE	Lateral bracing (vertical truss, with diagonal wire braces). Angles connected on two sides with a wall, [FEMA E 74, page 6-104, Figure 6.3.4.1-9].
Fancoils	PFA [g]	NE, ER	Bracing and/or fasteners.
Lights	PFA [g]	PR, NE	Hangers and braces (splay wire), [FEMA E 74, page 6-423, Figure 6.4.9.1-8].
Piping-Water Distribution	PFA [g]	ER	Transverse and longitudinal bracing (pipe clamp, riser clamp, welded lug). Supplemental damping system, [FEMA E 74, page 6-242, Figure 6.4.3.1-4].
Piping-Heating Distribution	PFA [g]	ER	Transverse and longitudinal bracing (pipe clamp, riser clamp, welded lug). Supplemental damping system, [FEMA E 74, page 6-242, Figure 6.4.3.1-4].
Bookcases	PFV [m/s]	ER, NE	Bracing and anchorage (to structural walls or structural studs), [FEMA E 74, page 6-504, Figure 6.5.2.1-4].
Mobile Blackboard	PFA [g]	NE	Seismic fastener and security restraints (anchored at wall or floor). Electronic equipment on wall mount brackets, [FEMA E 74, page 6-484, Figure 6.5.1.1-4].
Electronic Blackboard	PFA [g]	ER	Brackets installation (installed in structural elements). Electronic equipment on wall mount brackets, [FEMA E 74, page 6-364, Figure 6.4.7.1-10].
Computer and Printers	PFA [g]	NE	Use of predrilled holes and wall anchorage. Anchored or tethered, [FEMA E 74, page 6-536, Figure 6.5.3.3-3].
Projector	PFA [g]	NE	Brackets installation (installed in structural elements), [FEMA E 74, page 6-540, Figure 6.5.3.4-4].
Switchboards	PFA [g]	NE	Welded brackets or predrilled hole (in walls or base), [FEMA E 74, page 6-415, Figure 6.4.8.2-3].

## 4.4 Evaluation of Retrofitting Solutions

The results of each retrofit alternative are presented in the same way as in Chapter 3.

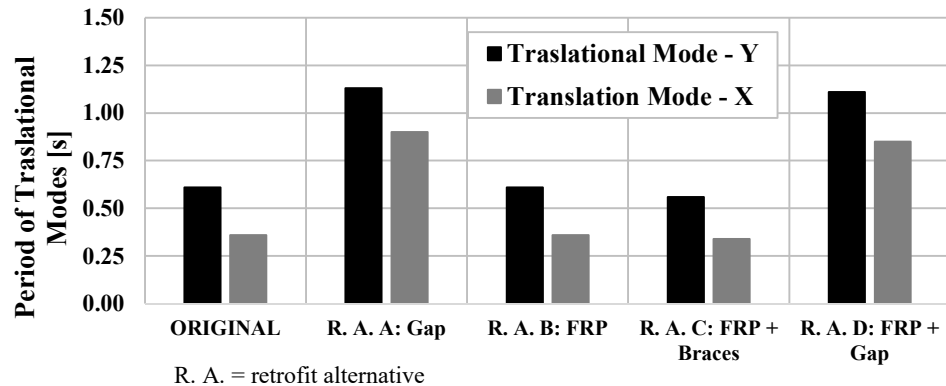
### 4.4.1 Modal Properties

Table 4-7 displays the natural period, motion, and mass contribution for the first four shape mode of each retrofitting strategy.

**Table 4-7. Comparison of dynamic properties among all the retrofitting alternatives.**

<b>Alternative A: Gap</b>			
<b>Mode</b>	<b>Period [s]</b>	<b>Motion</b>	<b>Mass Contribution</b>
1	1.13	Translational Y	38.0%
2	1.11	Torsional	1.5%
3	0.90	Translational X	36.4%
4	0.43	Translational Y	8.8%
<b>Alternative B: FRP</b>			
<b>Mode</b>	<b>Period [s]</b>	<b>Motion</b>	<b>Mass Contribution</b>
1	0.61	Translational Y	41.7%
2	0.44	Torsional	0.0%
3	0.36	Translational X	42.8%
4	0.23	Translational Y	5.9%
<b>Alternative C: FRP + Braces</b>			
<b>Mode</b>	<b>Period [s]</b>	<b>Motion</b>	<b>Mass Contribution</b>
1	0.56	Translational Y	43.2%
2	0.40	Torsional	0.2%
3	0.34	Translational X	43.7%
4	0.21	Translational Y	5.3%
<b>Alternative D: FRP + Gap</b>			
<b>Mode</b>	<b>Period [s]</b>	<b>Motion</b>	<b>Mass Contribution</b>
1	1.11	Translational Y	40.6%
2	1.09	Torsional	0.0%
3	0.85	Translational X	38.7%
4	0.40	Translational Y	7.4%

As mentioned before, each of these alternatives provide cases in which the period of the structure increases, remains unchanged or decreases, as reflected in the comparison provided in Figure 4.20.



**Figure 4.20.** Translational period comparison among models.

#### 4.4.2 Pushover Analyses

As predicted, the static pushover response of the structure shown in Figure 4.21 of the retrofit alternative A with the 20mm gap tends towards that of the bare frame since it presents the same initial behaviour, especially in terms of initial stiffness. Nevertheless, with increasing roof displacement, the capacity lies between the capacity of the original structure and bare frame for both curves in the longitudinal-X and transverse-Y directions. The portion in which the maximum capacity is developed maintains a wider roof displacement range than the original structure, as well as reaching higher deformation capacity. This effect is produced due to the remaining capacity in the infills. The gap delays the interaction between the infills and surrounding frame, thereby providing a reserve strength and deformation capacity that comes from the infills, allowing the structure to undergo higher displacements.

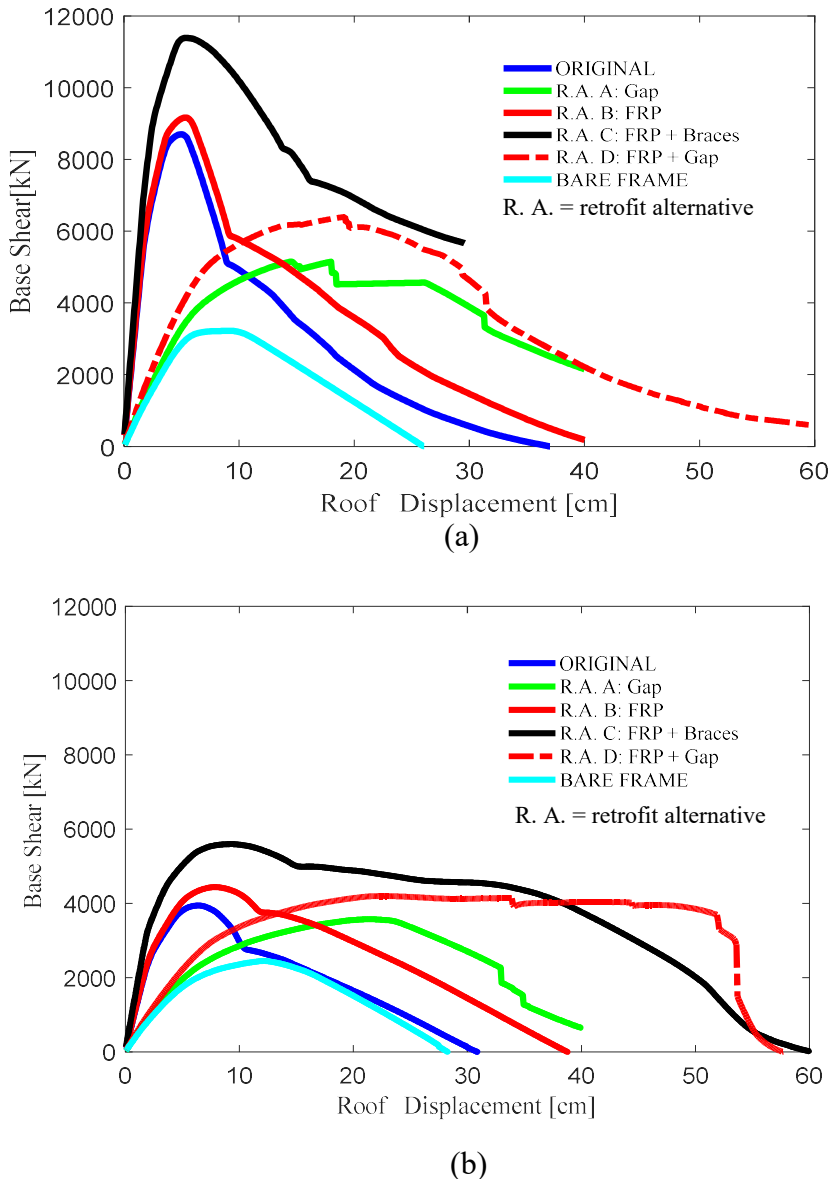


**Figure 4.21. Comparison of capacities for the different models, (a) SPO in longitudinal direction, (b) SPO in transverse direction.**

In the case of the retrofit alternative B, the behaviour is quite similar to that of the original structure. It can be seen from Figure 4.21(a) and Figure 4.21 (b) that the stiffness has not changed, but the shear capacity slightly increases as well as the deformation capacity. Even after the capacity has dropped by approximately 40%, the remaining capacity in the structure is higher compared to the original building since the elements that have not failed contribute with a remaining capacity due to the contribution of the FRP reserve strength.

The retrofit alternative D has a capacity that also lies between the original structure and the bare frame. Additionally, it presents not only a higher shear capacity but also a higher deformability range than that of alternative A with the just gap. Both the gap and FRP allowed the structure to undergo larger displacements, giving the structure a more ductile behaviour even though the weak-storey mechanism has not been completely mitigated. It is also shown how the FRP substantially increases the capacity of the bare frame, which indicates that a weak-storey

mechanism may be restricting the structure to develop a higher capacity. Besides, it is important to highlight the shape of the pushover curve in the case of the Y direction in Figure 4.21(b), due to the sudden drop after 50cm of roof displacement. This sudden drop is related to the increased deformation capacity in the columns provided by the FRP plus a reduction effect on the rigidity of each floor due to the presence of an infill gap. As result, the floor deformability increases substantially but drops quickly after past a roof displacement of 50cm.

Lastly, the retrofit alternative C increased both shear and deformability capacity proving the effectiveness of the FRP on increasing the structure capacity once the weak-storey mechanism is prevented. Although the analysis did not converge for roof displacements larger than 30cm in the X direction, this did not affect any subsequent non-linear time history analyses or another types of analysis since the collapse criterion of the structure was defined for a roof displacement lower than 25cm. Furthermore, for the analysis in the X direction shown in Figure 4.21(a), the initial stiffness is slightly higher due to the contribution of braces and the shape of the pushover curve is slightly different since brace buckling initiated at a roof displacement of 4.4cm, which is when the structure is beginning to enter the non-linear range. As buckling continues, the contribution of the braces to the lateral capacity reduces progressively. When a roof displacement of 14 cm is reached, all braces have failed even though fracture was not modelled directly but implicitly. At such level of deformations, the braces are not contributing more to the lateral resisting mechanism. At this point all braces have an extensive camber. Similarly, in Figure 4.21(b) the behaviour of alternative C is linear until the braces begin buckling, which occurs for a roof displacement of 2.9cm. Thereafter when a roof displacement of 15cm is reached, fracture of the braces takes place since no contribution of braces to the lateral resisting system is provided.

#### **4.4.3 Limit States Assessment**

The performance assessment presented in Section 3.7.3 was repeated and evaluated for each of the retrofitting alternatives using the criteria outlined in NTC 2008.

The storey drifts for the serviceability limit state assessment (return period of 45 and 75 years) are illustrated in Figure 4.22 and are lower than the limit of 0.5% defined by NTC 2008, except for the alternative A with the gap for the return period of 75 years in the transversal direction. Therefore, this alternative cannot be considered as a satisfactory structural retrofit case, but can be used to examine the effect of isolating the infills wall on the overall structural response. Moreover, alternative C (FRP plus gap) exhibits larger drifts than the original building since the gap modifies their behaviour, which tends to be similar to the bare frame, but with storey drifts larger than the original structure. The presence of the FRP rarely affected the storey drift since there was little improvement for the return period of 75 years in the transverse direction. When the braces are added, an improvement is achieved but then again for both return periods in the transversal Y direction, a weak-storey occurs in the first floor, although the storey drift in the second floor has been reduced considerably. However, even though this mechanism has formed, storey drifts are within the prescribed limit, therefore, these alternatives seem practical for the serviceability limit state.

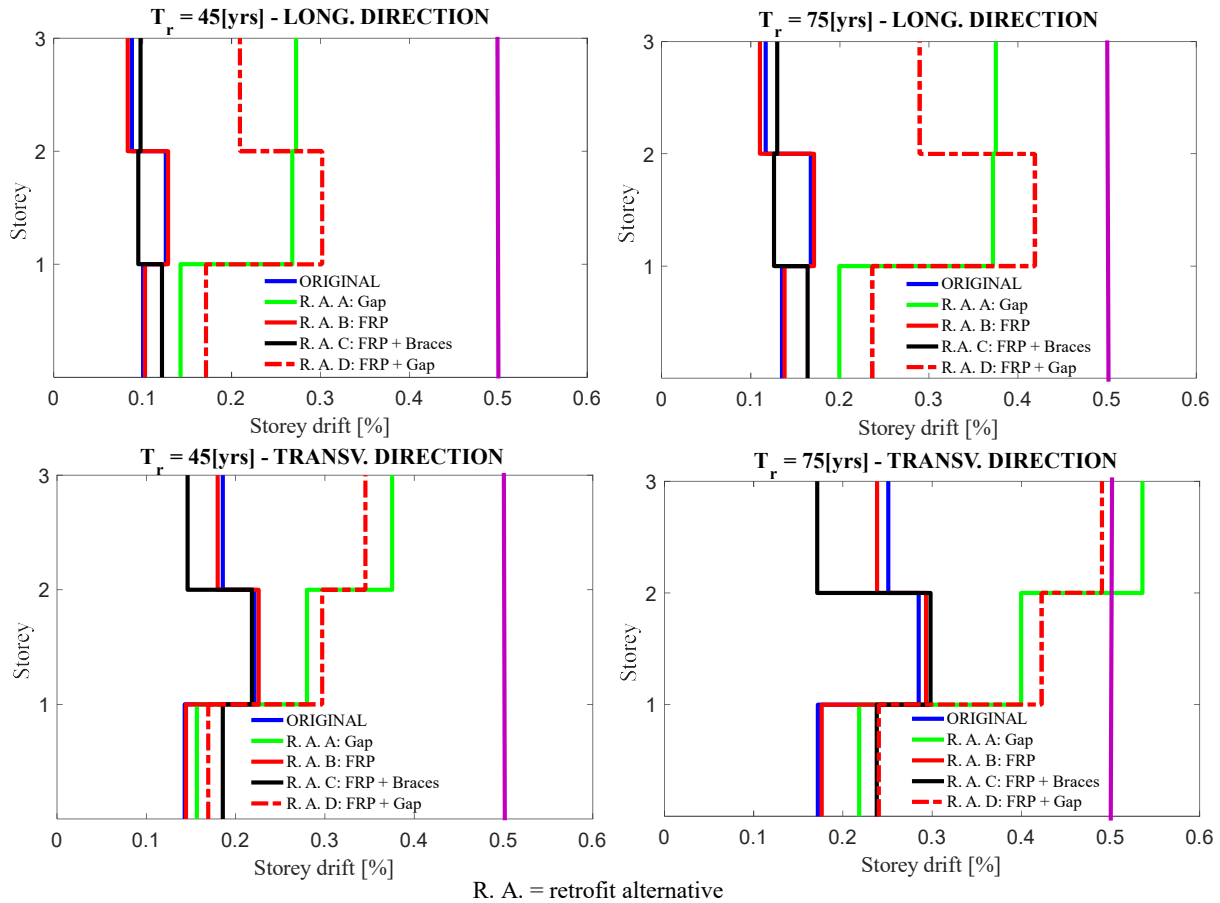


**Figure 4.22. Comparison of maximum drifts for the different alternatives for the serviceability limit state.**

Special attention was paid to the assessment of the ultimate limit state, illustrated in Figure 4.23, especially for the return period of 1463 years, for which a ductile mechanism has to be guaranteed. Again alternative A with a perimeter gap presents no improvement since drifts are not reduced, but rather increased by approximately 20%. In contrast, retrofit B with FRP shows an improvement in both directions but in the longitudinal X direction, this improvement seems to be not great enough to avoid a weak-storey in the first floor despite the FRP providing a more ductile behaviour. Fortunately, the solution with FRP plus braces (alternative C) solved this problem; the drifts are reduced and the non-ductile mechanism is improved (i.e. weak-storey mechanisms are mitigated). As mentioned earlier, by preventing the weak-storey mechanism the capacity in the structure can be developed further, which enhances the structural behaviour both in term of strength and ductility. In terms of drift improvement, alternative D of FRP plus gap is not a good option since the problem of weak-storey magnified. In other words, drifts in each storey were increased.

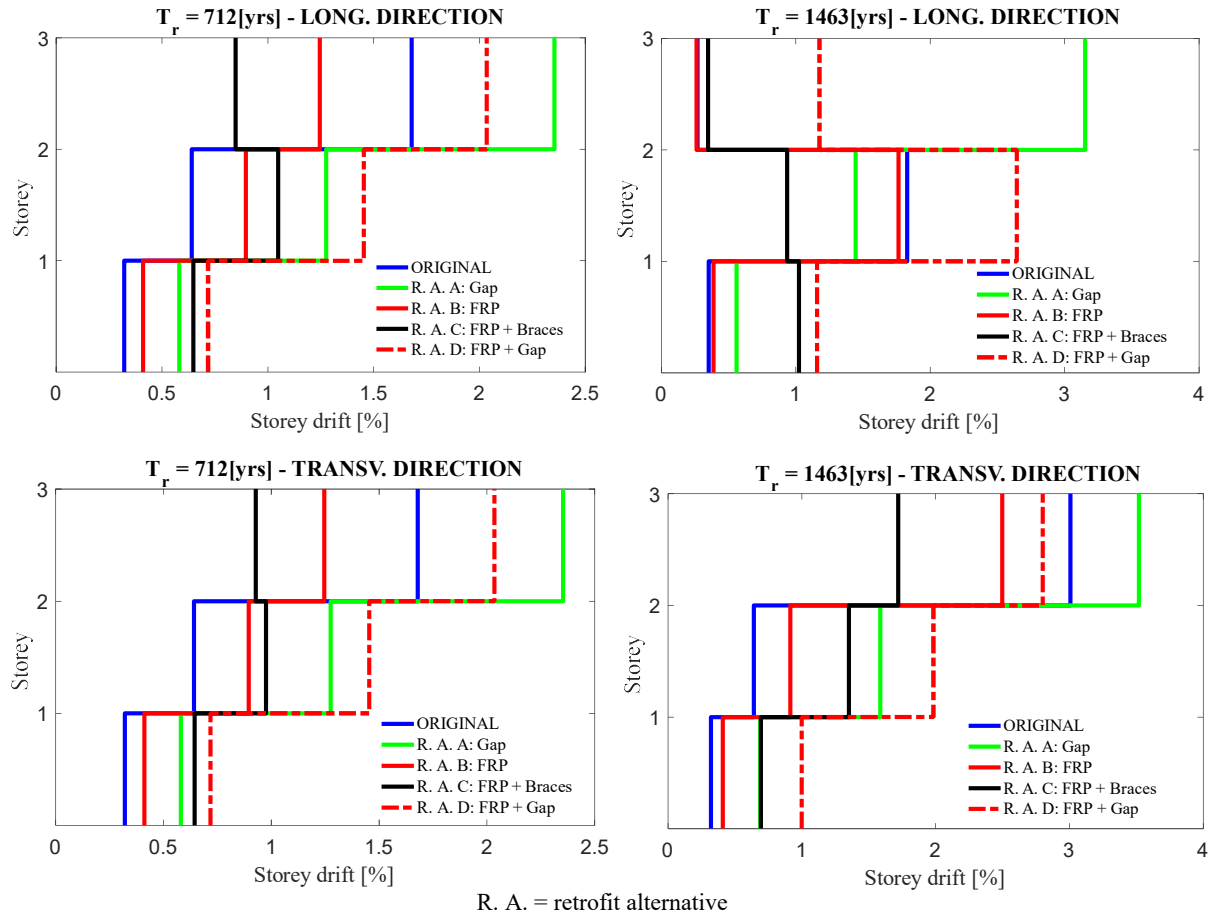


**Figure 4.23. Comparison of maximum drifts for the different alternatives for the ultimate limit state.**

Other criteria to evaluate the performance of each retrofitting alternative was based on the reduction of structural damage achieved, as presented in Section 3.7.4. Figure 4.24 and Figure 4.25 compare the improvement obtained for each alternative. It is clear that alternative A does not reduce the damage in the structural elements. In fact, it remains the same or even increase for the case of columns and beams. On the other hand, the other three alternatives work perfectly at mitigating the damage in these elements for the demand level used ( $T_r = 1463$  years), especially for joints, which have to maintain theirs structural integrity to avoid an undesirable failure.

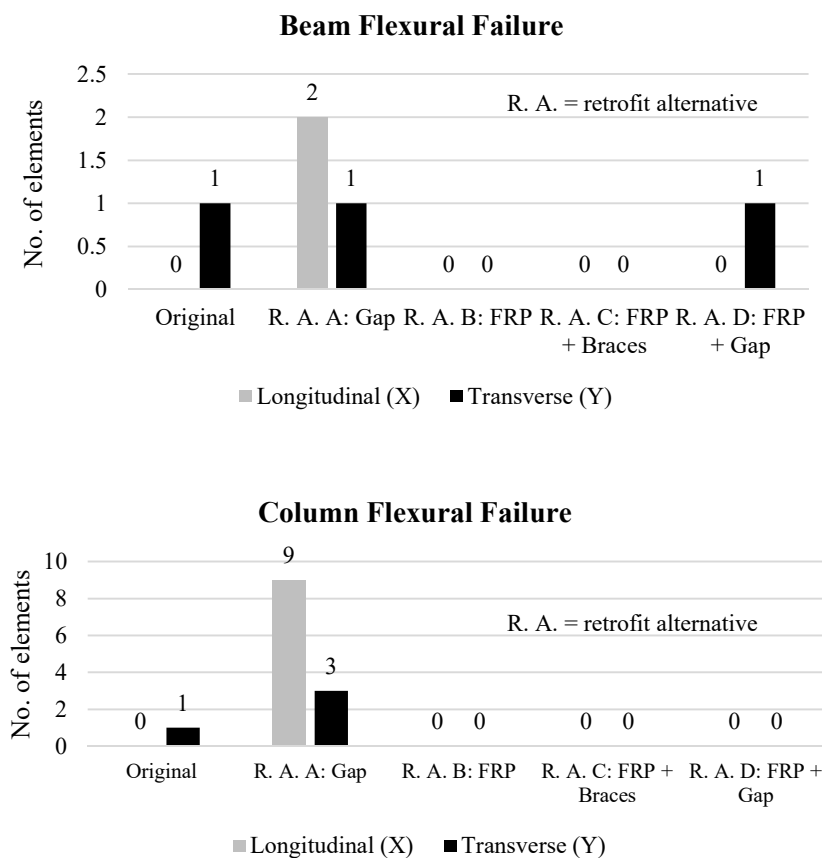


**Figure 4.24. Comparison of structural damage due to flexural failure.**

The reduction on the level of damage achieved by the other alternatives is related to the use of FRP, which allows more deformability without losing strength or degradation of the element integrity and also provides a higher strength to the structural elements, accomplishing a failure sequence that meets hierarchy sequence for a ductile behaviour.

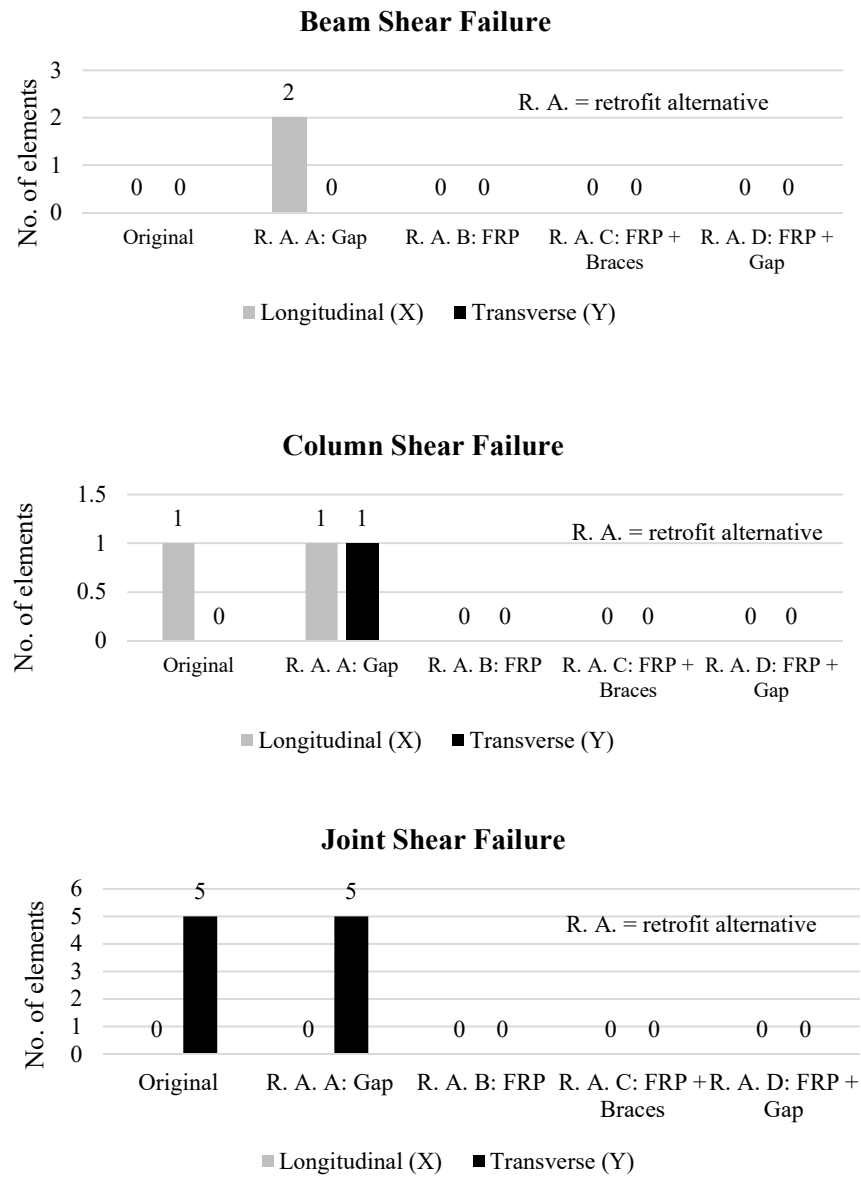


Figure 4.25. Comparison of structural damage due to shear failure.

#### 4.5 Summary and Discussions

Four retrofitting alternatives were presented in order to improve the seismic performance of the school building. These alternatives were named as retrofit alternative A: Gap; B: FRP; C: FRP + Braces; and D: FRP + Gap. The improvement achieved for each alternative was evaluated in terms of having an adequate strength hierarchy, which means failure sequence of beam-column-joint to guarantee a beam hinging behaviour, avoiding soft-storey or weak-storey mechanisms, reducing the damage undergone by the structural elements, and limiting the maximum storey drift to values indicated by NTC 2008 to control damage in non-structural elements and guarantee life-safety under collapse.

On one hand, implementing alternative A is not a practical solution since no evident improvement in terms of the structural performance was achieved as a weak-storey mechanism

was not prevented, damage undergone by elements was the same or even worse. Even though the strength and deformability capacity was higher compared with the bare frame, the requirements for limiting storey drifts were not met.

In case of alternative B, the strength and deformability capacity were enhanced which limit and reduce the damage on the structural elements, but weak-storey mechanisms were not avoided, although the strength hierarchy was adjusted to a more ductile mechanism, not the desired one due to practical restrictions on the implementation of the retrofit. Similarly, alternative D improved the structural behaviour in terms of strength and deformability capacity since the damage of the elements was also controlled and reduced, but then again the even though the drifts are within the limit the weak-storey mechanism were still present.

Lastly, alternative C seemed to be the most effective one since it maintains the integrity of the structural behaviour, weak-storey were prevented which reduces the maximum drifts for all the limit states assessed. Additionally, this alternative substantially increased the lateral capacity of the school building as well as its deformability capacity. Similarly, the strength hierarchy followed a satisfactory beam hinging behaviour, which was reflected by the reduction of damage undergone by the elements, being almost zero for the most critical limit state.

The type of analysis used for the seismic assessment in each alternative, N2 method, proved its effectiveness for designing a retrofit able to improve the structural performance of the school building. Doing this type of analysis leads a practising engineer to a retrofit solution without performing any NRHA beforehand. In the end, this procedure provides a practical way of assessing a structure and proposing a retrofit configuration that improve the structural performance.

While the actual structural performance of the building and its retrofit solutions may be deemed adequate, its overall performance may be investigated further to examine the economic vulnerability in terms of the direct economic losses due to the cost of repairs required following a seismic event, as well as to evaluate the vulnerability of collapse. These approaches are covered in Chapter 5, not only for assessing the original building but also for each of the retrofit alternatives presented in this chapter.

## 5 ASSESSMENT OF RETROFITTING SCHEMES

### 5.1 Introduction

In previous chapters, non-linear static analysis was used not only to evaluate the structural performance of a school building but also to propose some structural retrofit schemes to improve its performance. However, if other parameters or aspects need to be verified, more elaborated assessment methods ought to be implemented. The target of this chapter is to illustrate the progression of damage through a multiple stripe analysis (MSA) in order to properly evaluate the performance of each structural model in terms of collapse vulnerability and the expected annual loss (EAL). With this in mind, each model was subjected to a number of ground motion (GM) intensity measure levels so that the assessment may include the loss estimation of the building over a specified period (generally corresponding to the useful lifetime of the building, which is usually assumed to be 50 years) considering all earthquakes that could occur in that period. Therefore, GMs were properly selected according to the chosen site hazard for each intensity measure level (IML). The results of these analyses are reflected in the collapse fragility curve for the building in its original configuration and also for each of the proposed retrofit alternatives. In addition to the collapse evaluation, the monetary loss as a function of the repair cost for each alternative was discussed and compared among all the retrofit schemes. In the end, the most convenient retrofit alternative in terms of the EAL and collapse vulnerability improvement was selected.

### 5.2 Site Hazard and Ground Motion Selection

As stated in Chapter 3, the site location for evaluating the hazard was Cassino, Lazio (41.494 latitude, 13.838 longitude). From the topographic point of view, the site can be considered as flat, while for what concerns to the local soil conditions, soil type C has been assumed using the classification proposed by Eurocode 8 [EN 1998-1:2004 2004]. This was identified using available geotechnical reports about the local soil condition provided during in-situ surveying.

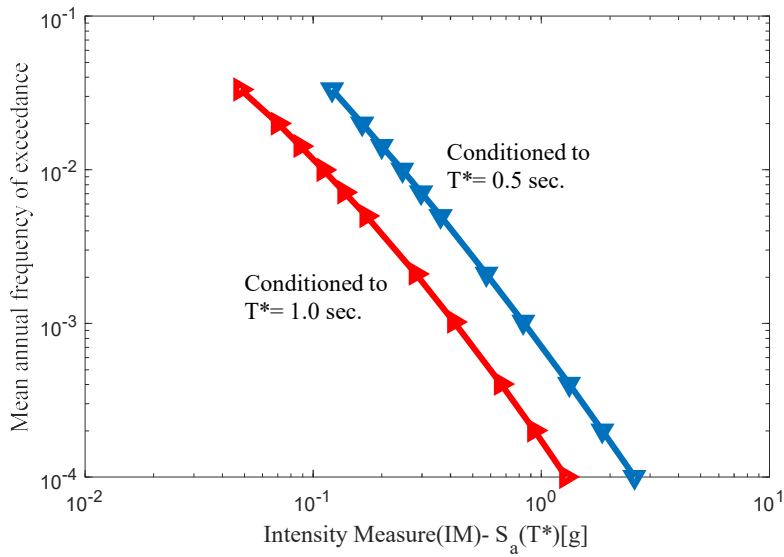
The seismic assessment involved a total of 20 pairs of ground motion records at 11 return periods for a soil type C. The set of GMs was selected in correspondence with the available hazard disaggregation at the conditioning period,  $T^*$ . The conditioning period,  $T^*$ , was taken as the mean value between the periods of the two first translational shape modes. Torsional modes were not considered since their limited participation mass has little influence on their dynamics response in comparison to the translational modes. The seismic hazard calculations and the derivation of the conditional mean spectra were performed using the REASSESS

software [Iervolino *et al.*, 2015]. To evaluate the response of the structure at increasing IML, each GM was selected to maintain consistency with the actual seismic hazard of the given location.

Figure 5.1 illustrates the mean annual frequency of exceedance (MAFE) at a conditioning period of  $T^*=0.5\text{s}$  and  $T^*=1.0\text{s}$  for the site. Moreover, the hazard disaggregation information required for GM selection was available at  $T^*$  equal to 0.50s and 1.0s, which was suitable since some models have a mean period close to 0.5s and the others to 1.0s as shown in Table 5-1.

**Table 5-1. Conditional periods for different structural models.**

<b>ORIGINAL</b>			
<b>Mode</b>	<b>Period [s]</b>	<b>Mean Period [s]</b>	<b>Conditional Period [s]</b>
1	0.61	0.49	0.5
3	0.36		
<b>BARE FRAME</b>			
<b>Mode</b>	<b>Period [s]</b>	<b>Mean Period [s]</b>	<b>Conditional Period [s]</b>
2	1.22	1.11	1.00
3	1.00		
<b>Alternative A: Gap</b>			
<b>Mode</b>	<b>Period [s]</b>	<b>Mean Period [s]</b>	<b>Conditional Period [s]</b>
1	1.13	1.02	1.00
3	0.90		
<b>Alternative B: FRP</b>			
<b>Mode</b>	<b>Period [s]</b>	<b>Mean Period [s]</b>	<b>Conditional Period [s]</b>
1	0.61	0.49	0.5
3	0.36		
<b>Alternative C: FRP + Braces</b>			
<b>Mode</b>	<b>Period [s]</b>	<b>Mean Period [s]</b>	<b>Conditional Period [s]</b>
1	0.56	0.45	0.5
3	0.34		
<b>Alternative D: FRP + Gap</b>			
<b>Mode</b>	<b>Period [s]</b>	<b>Mean Period [s]</b>	<b>Conditional Period [s]</b>
1	1.11	0.98	1.00
3	0.85		



$S_a(T^*)$  = spectral acceleration at a conditioning period  
 $g$  = gravity

**Figure 5.1. Illustration of the hazard curve for the site Cassino.**

A series of non-linear response history analysis (NRHA) were conducted using the GMs to evaluate the response of the structure at increasing IML. GMs are not scaled to different levels of intensity as in an incremental dynamic analysis (IDA), but are individually selected at each IML to maintain consistency with the seismic hazard of the given site location. Baker and Cornell [2006] have stated that this procedure is more suitable for single building assessment. The GMs were taken from PEER NGA-West database [Ancheta *et al.*, 2013], where the selection criteria considered the spectral acceleration as the maximum between the two as-recorded components pairs, which is consistent with the GM prediction equation by Ambraseys *et al.* [1996] employed here for the hazard calculations. A maximum scaling factor of four was imposed to achieve spectral compatibility, with the exception of the 4975 and 9975 year return periods where scale factors up to a value of eight were considered. Ground motions at such high return periods were required in order to assess the collapse fragility of the building in a hazard consistent manner that would require no adjustment to the median collapse intensity or dispersion in order to account for the effects of spectral shape [Baker and Cornell, 2006].

### 5.3 Non-linear Response History Analysis (NRHA)

Following the selection of the GMs at different conditioning periods for multiple intensity levels, NRHAs were conducted using the different numerical models presented in Chapters 3 and 4. In order to assess the collapse vulnerability of each model, as discussed in the next section, MSA results were processed during each GM. At each limit-step of each analyses the current maximum peak storey drift (PSD) was verified. If the current maximum PSD exceeded a prescribed maximum storey drift capacity, which was chosen as 5% [O'Reilly *et al.*, 2018b], the NRHA was terminated at that point and marked as a collapsed case. This avoids cases where a structural model has accumulated excessive drift and has essentially collapsed, but the software (OpenSees) continues the analysis for the GM record. Therefore, only the non-collapse cases were processed and evaluated through the median values of the maximum PSD, peak

floor velocity (PFV), and peak floor acceleration (PFA) at any location in the building. Figure 5.2 to Figure 5.5 show some of the NRHA results for the frames in terms of the median value of the maximum PSD and PFA for non-collapsed cases, where intensities up to a probability of collapse lower than 50% are illustrated.

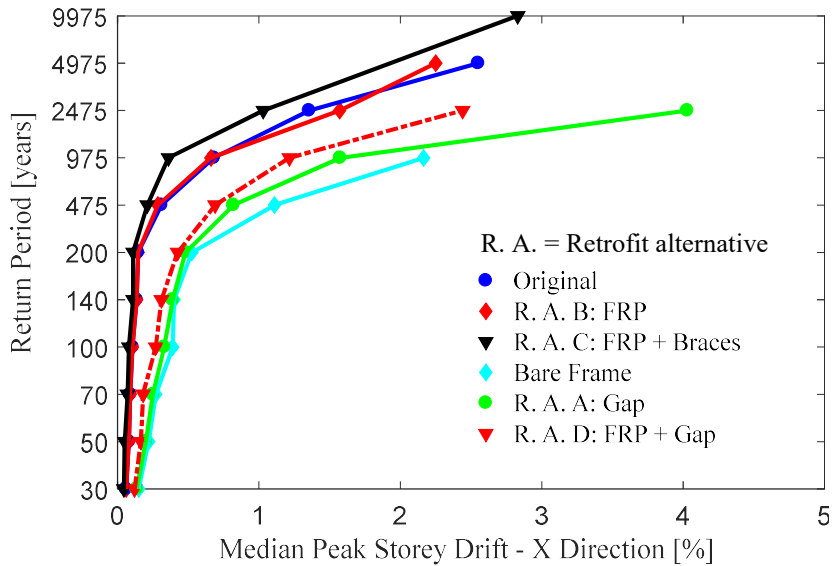


**Figure 5.2. Median of the maximum values over the height for peak storey drift in X (longitudinal) direction, conditioned on no collapse.**

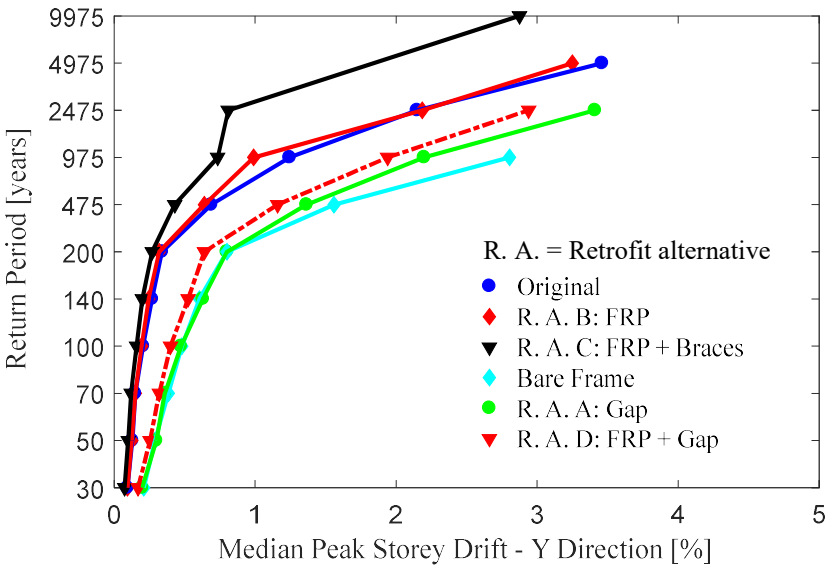
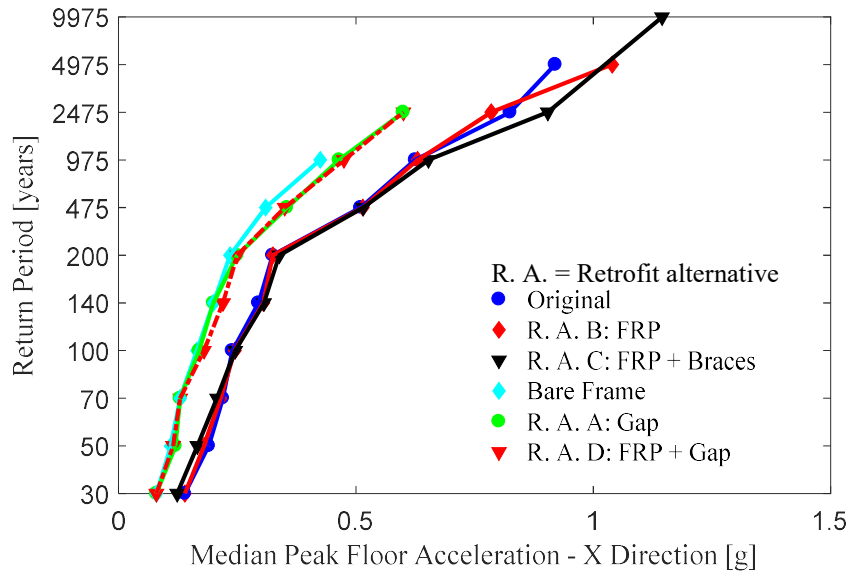


**Figure 5.3. Median of the maximum values over the height for peak storey drift in Y (transverse) direction, conditioned on no collapse.**

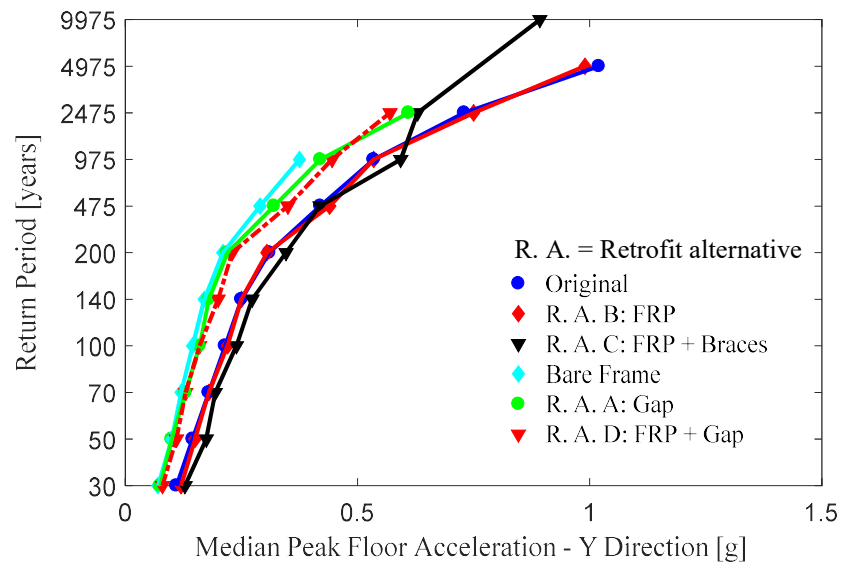
The analysis of the bare frame is also included in Figure 5.2 to Figure 5.5 to highlight the similarities between this model and the retrofit alternative A that consists of providing a perimeter gap to the masonry infills, especially for low return periods ( $\leq 140$  years) in which PSDs in both directions are similar. However, for higher intensities, alternative A exhibits lower PSDs since the infill has been engaged more in the structural response. Infills provide additional stiffness and strength to the structure and therefore reduce lateral displacements and consequently storey drifts. It can be said that for higher intensities, PSDs tend to reduce slightly

towards the values of the original building. Likewise, the original model and retrofit alternative B show the same PSDs at lower intensities since the addition of FRP does not significantly modify the section stiffness of the elements, but only their strength and ductility. In other words, there is no apparent change in stiffness and therefore the PSDs are not altered for lower return periods although there is a slight difference at higher intensities. However, when the gap and/or braces are added for alternatives D and C, the PSDs are increased and reduced, respectively. On one hand, the gap reduces the lateral stiffness of the frames, making the system more flexible, unlike the original building. On the other hand, the braces are reducing storey drifts considerably in both directions since weak-storey mechanisms that were controlling PSDs are being mitigated by this strategy. In fact, this alternative is the only one with median values for higher return periods since it is more resilient to collapse, meaning that this retrofit is able to withstand higher intensities unlike the other models.

In the case of PFAs, the behaviour displayed in Figure 5.4 and Figure 5.5 was expected, especially for alternative C since by adding the braces, the stiffness was increased causing also an increase in the PFAs. In contrast, alternative A accounts for the lowest PFAs due to its low lateral stiffness because of the gap addition. Again, the PFAs exhibited by alternative B remains unchanged in comparison with the original model since no significant modification in its properties was made when examining the pushover curves presented in Figure 4.21. Additionally, it is important to highlight how the braces placed in the transverse direction buckled before the ones in the longitudinal direction. This can be seen in Figure 5.5 for the return period of 2475 years where accelerations decrease since the braces have buckled early in the records and subsequently resulted in a reduced maximum PFAs due to the reduced stiffness. Once the braces were buckled, their contribution to the lateral stiffness was too low and the resisting system relays only on RC elements. Despite the fact that the analyses were conducted for two groups of NRHA due to the conditioning periods, PFAs presented by the structural models were not that far from each other, especially for low IML, ( $\leq 475$  years). This may be related to the fact that the structural retrofit was design based on drift limits and therefore an improvement in terms of PSDs is being reflected through a wider range, whereas there is not apparent variation of PFAs.



**Figure 5.4.** Median of the maximum values over the height for peak floor acceleration in X (longitudinal) direction, conditioned on no collapse.



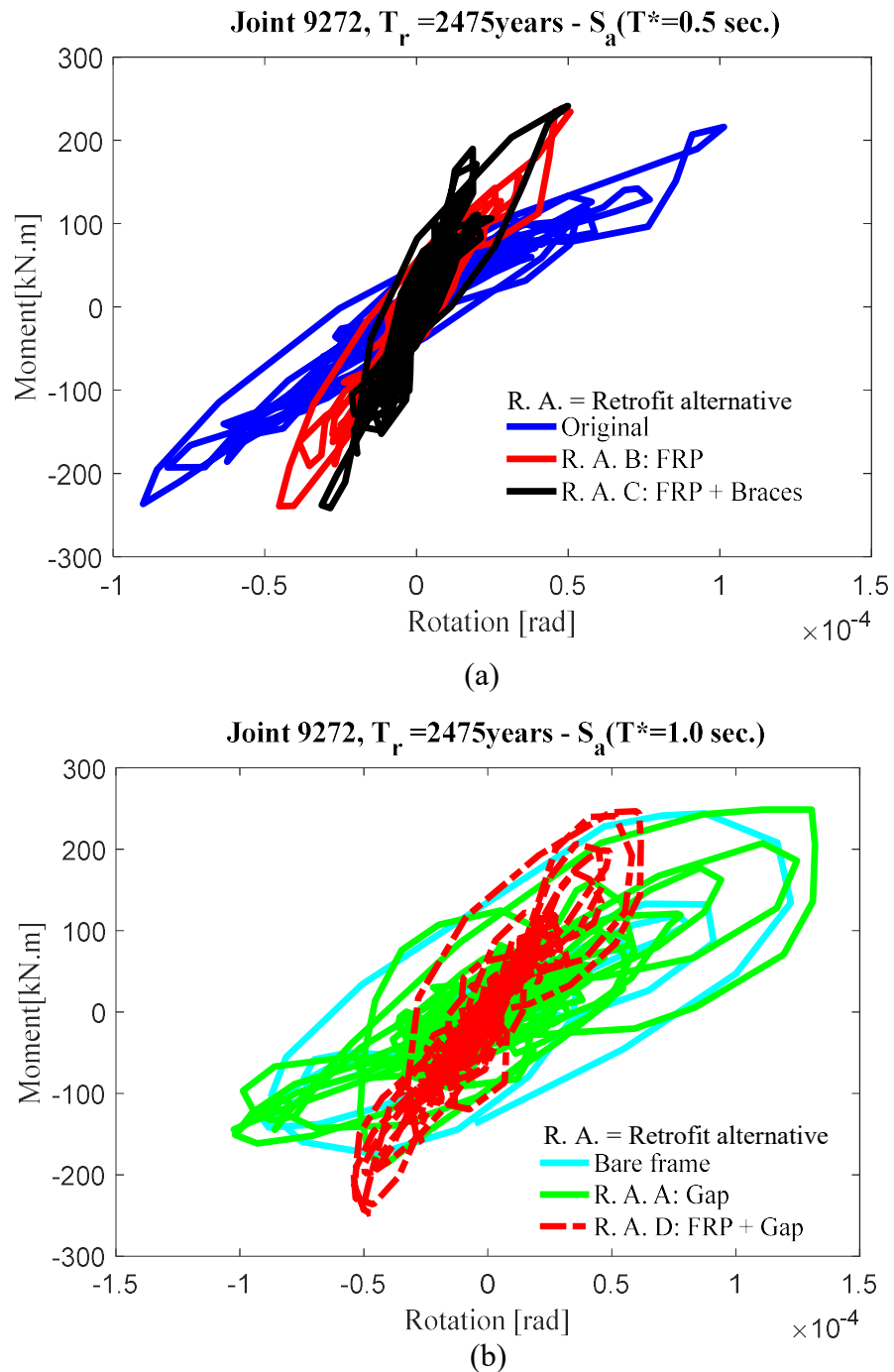
**Figure 5.5.** Median of the maximum values over the height for peak floor acceleration in Y (transversal) direction, conditioned on no collapse.

Figure 5.6, 5.7, and Figure 5.8 display hysteresis curves of some structural elements for a medium-high hazard intensity ( $T_r = 2475$  years), corresponding to record 9 from the ensemble set of 20 ground motions. Figure 5.6 shows the hysteresis (moment-rotation) behaviour of a joint element. From Figure 5.6(a), it can be seen that alternatives with the FRP increase the strength capacity of the joint (diagonal cracking), providing a more elastic behaviour. Even though alternative B and C reached the same moment capacity, alternative C limited the rotation demands on the joint due to the addition of the braces. The braces restrict the lateral displacement undergone by the frame and therefore deformations on the structural element. On the other hand, Figure 5.6(b) shows higher rotations since these models either develop a more flexible behaviour in the case of the bare frame and alternative A, or have a higher ductility in the case of alternative D. The hysteresis curves in the bare frame and alternative A have the

same behaviour since at this intensity, that particular joint underwent a considerable amount of damage. On the other hand, alternative D demonstrates that by increasing the capacity of the joint by introducing the FRP, the strength capacity can be increased, allowing a more elastic behaviour and delaying cracks opening, which translate in lower damage in the joint. Although the gap was also incorporated into this alternative, the joint did not undergo higher rotations. This may be related to a new load redistribution since failure presented in some structural elements may be avoided or delayed in comparison with the original model.

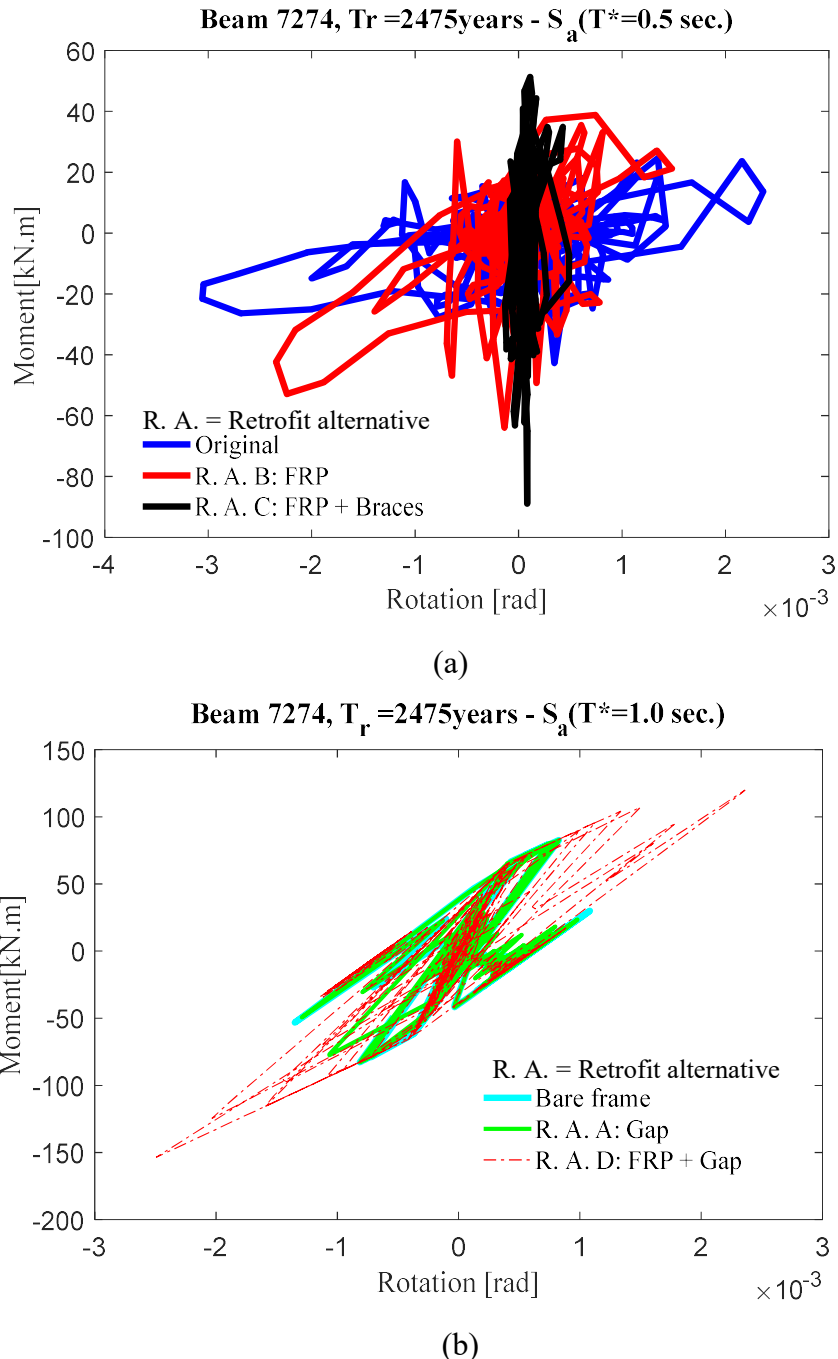
The hysteresis (moment-rotation) behaviour of the end of a beam is illustrated in Figure 5.7. The response falls in the linear range as the hysteresis curve is almost elastic for that intensity level. However, it can be noticed the improvement achieved by each alternative in terms of strength and deformation capacity. Alternative B and C increased the moment capacities considerably but then again alternative C accounts for a better performance, almost doubling the moment capacity compared to that of the original building. Similarly, alternative D enhanced the behaviour of the beam by not only increasing its flexural strength but also its rotational capacity. Again, the bare frame and alternative A present the same hysteresis curve indicating that for that level of intensity and for that specific beam, the load distribution is the same.

Finally, Figure 5.8 presents the hysteresis (moment-rotation) behaviour of the end of a column. The improvement obtained by alternative B and C is identical, but alternative C reaches a slightly higher strength and deformation capacity due to the properties of the FRP and contribution of the braces. Once again, the effectiveness of the FRP on increasing the strength of the elements and their deformation capacity is observed. On the other hand, the response of the same column presented a different behaviour for alternative A. The gap has produced higher deformations, which can be translated into a higher energy absorption, whereas, the bare frame maintains an elastic behaviour. Furthermore, alternative D has increased the capacity of the column allowing a linear behaviour and therefore less plastic deformation.



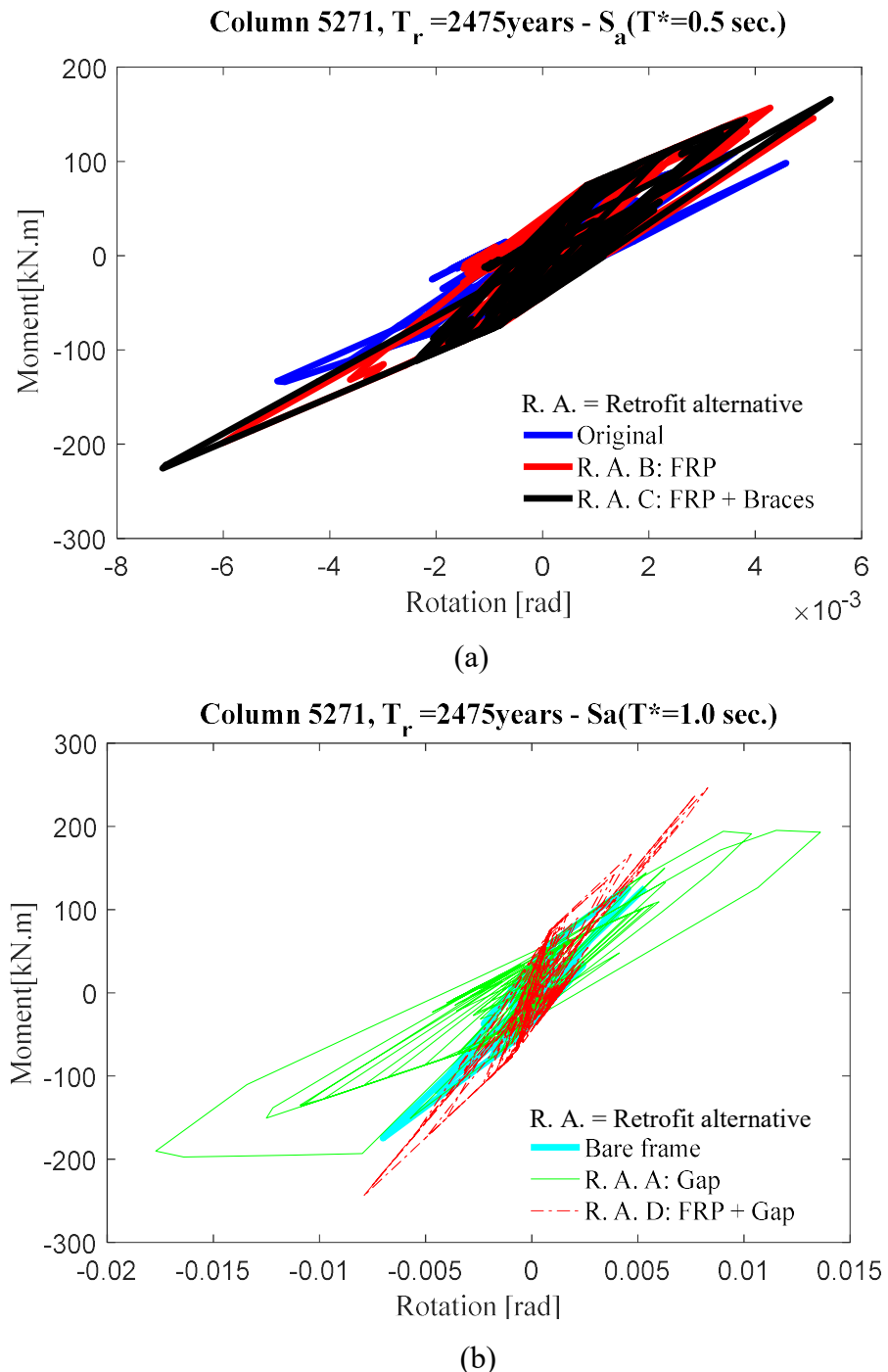
Note: Joint 9272 corresponds to a corner joint located in the first storey.

**Figure 5.6. Time history response of joint 9272 in terms of Moment-rotational capacity, (a) Hysteresis behaviour conditioned to  $T^* = 0.5$  sec., (b) Hysteresis behaviour conditioned to  $T^* = 1.0$  sec.**



Note: Beam 7274 corresponds to an exterior beam in the X direction located in the top storey.

**Figure 5.7. Time history response of beam 7274 in terms of Moment-rotational capacity, (a) Hysteresis behaviour conditioned to  $T^*=0.5 \text{ sec.}$ , (b) Hysteresis behaviour conditioned to  $T^*=1.0 \text{ sec.}$**



Note: Column 5271 to a corner column located in the first storey.

**Figure 5.8. Time history response of column 5271 in terms of Moment-rotational capacity, (a) Hysteresis behaviour conditioned to  $T^*=0.5$  sec., (b) Hysteresis behaviour conditioned to  $T^*=1.0$  sec.**

## 5.4 Evaluation of Retrofitting Techniques

### 5.4.1 Collapse Assessment

This assessment only considers complete collapse cases, which are based on the collapse criterion explained in Section 5.3. From MSA results. The ratio between the numbers of ground motion records causing collapse and the total number of fully converged ground motions in the ensemble was used to describe the probability of collapse of the structure for several intensity levels. By using the maximum likelihood method, whose application to fitting fragility functions to truncated data sets has been described in Baker [2015], a collapse fragility function was established. This method assumes a lognormal distribution for the collapse fragility and by trialling a value of median collapse intensity and dispersion, compares the likelihood of the actual data retrieved from MSA to the trial combination of median and dispersion to fit the distribution and iterate until the best match is found. Figure 5.9 shows the collapse probability data and the fitted lognormal collapse fragilities functions for each retrofit alternative and Table 5-2 provides the median and dispersion values. It is important to note that the dispersion in the collapse fragility functions described here account for record-to-record variability only and do not incorporate the adjustment proposed by O'Reilly and Sullivan [2018b] to account for modelling uncertainty.

Figure 5.9 illustrates how the collapse risk is reduced when the structure is strengthened, thereby quantifying the effectiveness of each retrofit alternative on improving the seismic behaviour of the school building. The collapse fragility functions for each retrofit alternative are shifted to the right from the original building and bare frame, meaning that the building requires a higher level of seismic intensity to reach a same probability of collapse. This is also shown by the higher median values presented in Table 5-2. Furthermore, it is important to highlight that the non-structural elements do not have any impact on the collapse fragility of the building, since they were not explicitly modelled, except for the gap retrofit of the exterior infill walls (alternative A).

**Table 5-2. Median collapse intensity and dispersion for each model.**

Model	Median	Dispersion
Original	1.93g	0.28
Alternative B: FRP	2.25g	0.25
Alternative C: FRP + Braces	2.54g	0.24
Bare Frame	0.54g	0.16
Alternative A: Gap	0.69g	0.22
Alternative D: FRP + Gap	0.81g	0.29

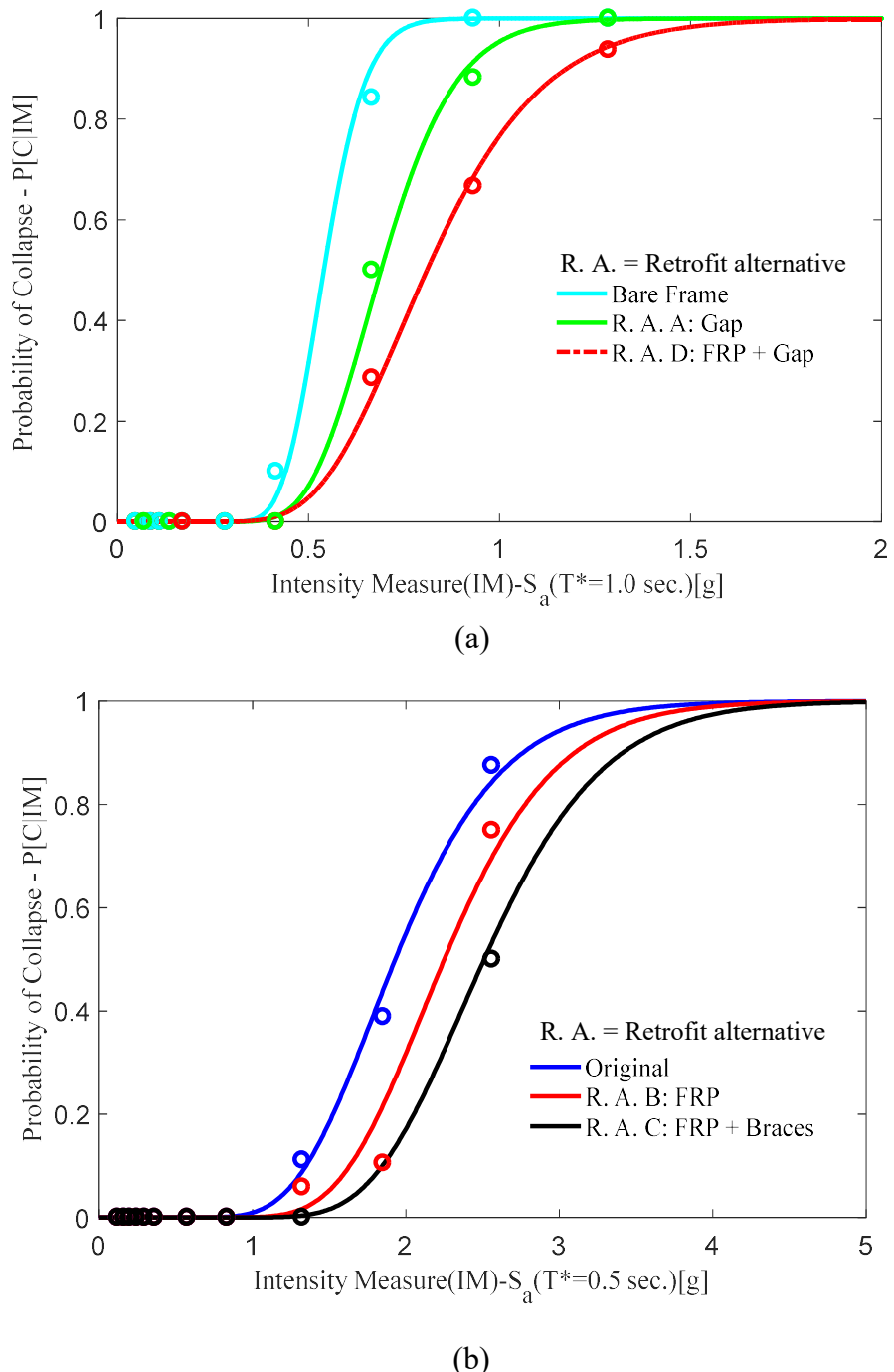


**Figure 5.9. Fitting of the collapse fragility function for different conditioning periods, (a) Fragility curve conditioned to  $T^*=0.5$  sec., (b) Fragility curve conditioned to  $T^*=1.0$  sec.**

No direct comparison among all the models can be done as they are conditioned to either  $S_a$  ( $T^*=0.5$ ) or  $S_a$  ( $T^*=1.00$ ), but they can be compared in terms of collapse margin ratio (CMR), which has been outlined in FEMA P695 [2009]. As explained by O'Reilly [2016], the evaluation of the collapse criteria outlined in FEMA P695 [2009] for ensuring collapse prevention is done through the CMR. For the school building, this CMR was taken as the ratio between the median collapse intensity  $P[C] = 50\%$  to the intensity level corresponding to the maximum considered earthquake (MCE), for  $T_r = 1463$  years. Table 5-3 presents these results and demonstrates that all the models, even the bare frame, have a collapse margin ratio higher

than unity, indicating probabilities of collapse less than 50%. These ratios range from 1.08 to 2.46, with the bare frame exhibiting the lowest value and alternative C exhibiting the highest margin against collapse, indicating the efficacy of this retrofit in reducing the vulnerability of collapse.

As previously noted, the results of the NRHA do not account for the modelling uncertainty and only consider record-to-record variability in the building response. O'Reilly and Sullivan [2018b] proposed a simple way to account for modelling uncertainty in collapse assessment of old RC frames in Italy. This approach considers a reduction factor for the median collapse intensity (0.99). Additionally, the effects of modelling uncertainty was incorporated through a Square Root of the Sum of the Squares (SRSS) combination with the record-to-record variability to represent the overall dispersion in the demand parameters and the model dispersion, described by Equation (5.1) and (5.2) if the two sources are assumed to be uncorrelated.

$$\beta_{D,\theta} = \sqrt{\beta_{DR,\theta}^2 + \beta_{DU,\theta}^2} \quad (5.1)$$

$$\beta_{D,a} = \sqrt{\beta_{DR,a}^2 + \beta_{DU,a}^2} \quad (5.2)$$

Where:

$\beta_{D,\theta}$  = total dispersion in peak storey drift demand.

$\beta_{DR,\theta}$  = record-to-record variability in peak storey drift demand.

$\beta_{DU,\theta}$  = modelling uncertainty in peak storey drift demand.

$\beta_{D,a}$  = total dispersion in peak floor acceleration demand.

$\beta_{DR,a}$  = record-to-record variability in peak floor acceleration demand.

$\beta_{DU,a}$  = modelling uncertainty in peak floor acceleration demand.

The use of an SRSS combination of the two sources of uncertainty gave a good representation, albeit slightly conservative, of the overall dispersion in the two demands. Table 5-5 the values of dispersion for record-to-record variability, modelling uncertainty used in the assessment, as well as the reduction factor for the median collapse intensity. The dispersion due to record-to-record variability was obtained through the fitting process of a lognormal distribution, whereas O'Reilly and Sullivan [2018b] proposed values for modelling uncertainty, which range from 0.1 to 0.5. Figure 5.10 displays the collapse fragility functions considering the model uncertainty and also evaluates the compliance criteria outline in FEMA P695 [2009], which requires that the probability of collapse at the MCE level be less than 10%. This MCE level is defined as the 2475-years return period event in FEMA guidelines, but in NTC 2008, it is specified as 1463 years for the life safety limit state when considering school structure with nominal life of 50 years. For this reason, the hazard level corresponding to 1463 years was adopted here and are 1.02g for the original model and 0.502g for the bare frame. These values are presented in Figure 5.10 from which all models have a probability of collapse lower than 10% at the life safety intensity level, except for the case of the bare frame whose probability is higher than 10%. This approach differs from CMR since it accounts for the model uncertainty (dispersion) whereas CMR is insensitive of dispersion; in other words, CMR is not affected by the model uncertainty.

As seen in Figure 5.10, alternatives B,C, and D present a low probability of collapse for the hazard level of  $T_r = 1463$  years, which highlights the effectiveness of these structural retrofits on improving the structural behaviour and decreasing the vulnerability to collapse.

**Table 5-3. Collapse margin ratio to evaluate the collapse safety.**

<b>Model</b>	<b>Collapse Margin Ratio (CMR)</b>
Original	1.89
Alternative B: FRP	2.21
Alternative C: FRP + Braces	2.46
Bare Frame	1.08
Alternative A: Gap	1.37
Alternative D: FRP + Gap	1.61

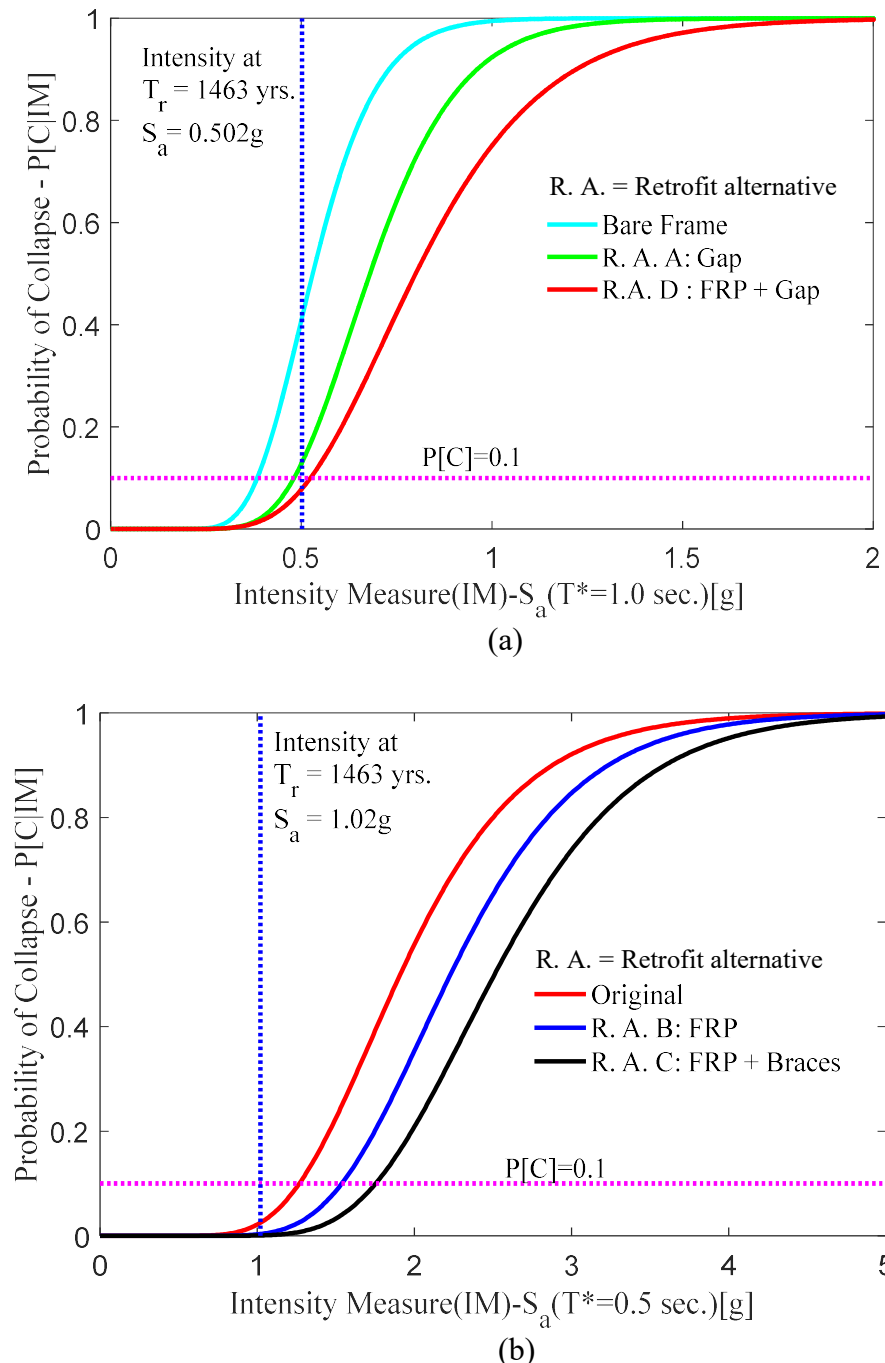


**Figure 5.10. Evaluation of collapse criteria for each model,** (a) Fragility curve conditioned to  $T^*=0.5$  sec., (b) Fragility curve conditioned to  $T^*=1.0$  sec.

Figure 5.11 presents the mean annual frequency of collapse (MAFC), which was determined by integrating the individual collapse fragility function, Figure 5.10, with the assumed mean hazard curve for the Cassino site (see Figure 5.1). Dolšek *et al.* [2017] stated that typical values of MAFC from studies around the world lies in the range of  $10^{-5}$  to  $10^{-4}$ . MAFC for the original building exceeds slightly the limit of  $10^{-4}$ . The retrofit alternatives B and C proved to be effective for improving MAFC placing it within this range. Despite that alternative A and D have a MAFC higher than the original building, there is a reduction if they are compared with the bare frame since these models were conditioned to  $S_a (T^*=1.0\text{s})$ .

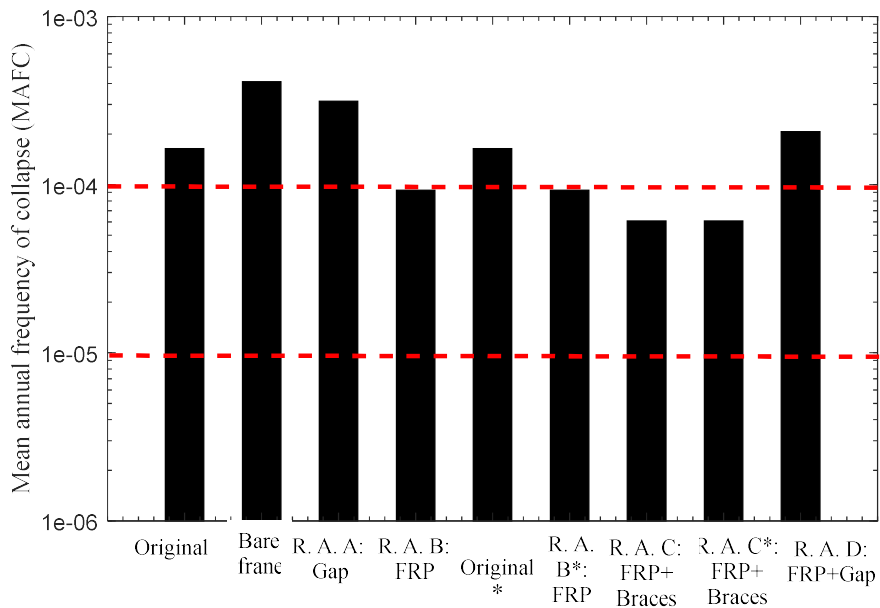


**Figure 5.11. Mean annual frequency of collapse**

#### 5.4.2 Loss Estimation

While the collapse vulnerability for the school building may be deemed satisfactory, the overall performance may be investigated further to examine its economic vulnerability defined in terms of direct economic losses due to the cost of repairs required following a seismic event. The retrofitting measures were targeted to improve the performance of both the structural and non-structural elements and to illustrate: how both are contributing to the expected loss, and how by improving their seismic behaviour the overall performance is improved. This was highlighted by the impact that the different retrofit strategies had on the expected annual loss (EAL), which is defined as the integral of the vulnerability function with the mean hazard curve. The vulnerability function describes the expected monetary loss undergone by the structure for different IMLs. Therefore, the overall effectiveness of the retrofit alternatives could be evaluated in terms of expected loss rather than relying on code defined storey drift limits to ensure satisfactory performance. Additionally, the direct monetary losses in the building were examined through the detailed consideration of the damageable elements in the building. Conducting the loss estimation required an inventory of the damageable elements along with associated damage and repair cost functions. This inventory, presented in Table 3-1, was compiled here from the available structural information from an actual visit to the school building [O'Reilly and Perrone, 2016]. The repair cost functions adopted here were provided with the aid of an Italian engineering firm [Moratti and Studio Calvi, 2017]. The costs were ensured to be representative the different required repair measures in Italy and the fragility functions.

The loss estimation was conducted with the software PACT [FEMA P58-3, 2012] that utilizes the PEER PBEE methodology described in Chapter 2. The input values came from structural analysis results recorded at the centre of mass (COM), at each level of the structure that includes the peak storey drift (PSD), peak floor velocity (PFV), and peak floor acceleration (PFA). For

example, the drift at the COM was used as a representative demand parameter for the damage induced in the drift sensitive components at all locations in the floor plan. This is the default approach used in the software PACT which requests a single drift in both principal directions of the structure, to which the various drift sensitive components are assigned. This assumption was made to simplify the loss estimation, although it is noted that using COMs demands in torsionally sensitive buildings can result in an underestimation of the EAL, as demonstrated by O'Reilly *et al.*, [2017a]. However, since the purpose of the loss estimation conducted here is to illustrate the relative difference in performance of the different retrofitting schemes, this simplification is not anticipated to influence the conclusions of this study. Furthermore, a non-directional conversion factor equal to 1.2 was considered to account for the amplification of the orthogonal effect of PFA, recommended by O'Reilly and Sullivan [2018b].

The replacement cost was computed considering the mean price of reconstruction following the Emilia Romagna earthquake in Central Italy in 2012 that described a replacement cost, demolition and removal cost of €1805.75/m<sup>2</sup> and €95.50/m<sup>2</sup>, respectively. The loss threshold was taken as 60% of the replacement cost during the loss estimation analysis that indicates a point at which it would be more practical to replace the building rather than repair it. Figure 5.12 illustrates the overall improvement achieved in terms of the vulnerability curve of the building which has been reduced by each retrofit alternative. The curves have been shifted slightly to the right, meaning that the intensity required to induce a given level of expected loss in the structure has increased or in other words, the performance has improved.

Nevertheless, the bare frame tends to accumulate more losses in drift sensitive elements as this model undergoes higher storey drifts. As illustrated by Taghavi and Miranda [2003], drift sensitive elements may account for 53% of the total repair cost of non-structural elements. The disaggregation of expected losses is very useful for deciding how to improve the overall performance of the building.

It was found that alternative B and C presented the same losses for hazard levels corresponding to return periods lower than 200 years since at such low intensities, the non-structural elements are contributing to losses more than the structural elements. Meaning that little structural damage occurred for such low intensities. It is important to highlight that these alternatives only considered structural retrofitting. On the other hand, for intensities higher than 975 years the models presented higher deformation and therefore damage was quite substantial in both structural and non-structural elements, contributing both to the expected loss. In the case of intensities ranging from 200 to 975 years, the improvement with alternative C can be observed, since the FRP delays the damage of structural elements and the braces reduce the storey drifts, translating into a reduction in the expected economic losses. Moreover, alternative D accounts for the best improvement due to the combined effect of the FRP and gap, plus the retrofit of non-structural elements, bringing satisfactory results in terms of loss reduction. It is clear that the FRP improved the structural behaviour of the elements and the gap prevented premature failure not only to infill walls but also to other non-structural elements related to infill failure.

Incidentally, for the three higher return periods, the expected loss ratio for the original building and retrofit alternatives falls above the loss threshold value, meaning that GMs at these return periods would be expected to result in demolition of the school building due to excessive

damage. However, once the non-structural elements are also retrofitted, which are presented for the models labelled with an asterisk (\*) in Figure 5.12, the area under the vulnerability curve decreases and the intensity related to 2475 years falls under the threshold value. The target to incorporate the analyses Original(\*), R. A. B\*, and R. A. C\* as illustrated in Figure 5.12, which include retrofit of non-structural elements, was to illustrate how the expected loss is reduced by improving such elements, evidently the monetary improvement is substantial since the losses have been reduced considerably. This supports what Calvi *et al.* [2014, 2016], among other, stated about the benefit of improving the seismic behaviour of non-structural elements to reduce monetary losses. Even though all the alternatives have improved the monetary losses, R. A. C\* achieved the highest reduction for intensities lower than 2475 years, demonstrating the efficacy of this retrofit as long as the retrofit of non-structural elements is incorporated.

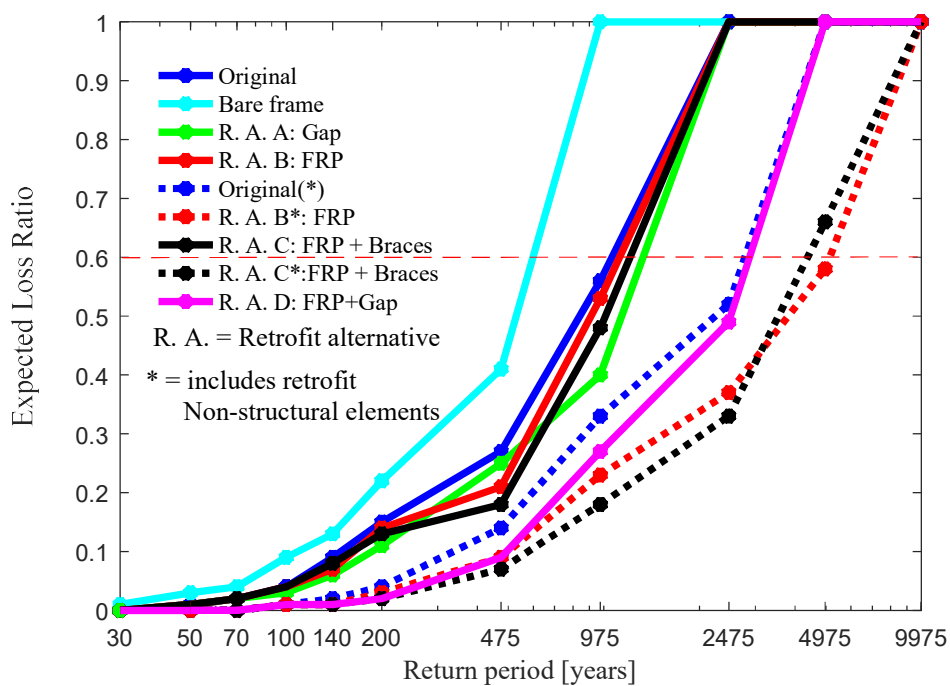


**Figure 5.12. Vulnerability curves comparison.**

Table 5-4 presents the fragility functions used in the assessment of the original building as well as for evaluating the performance of the retrofit alternatives (shown in the column of improved fragility functions), which are illustrated in Appendix B and C.

**Table 5-4. List of the element fragility curves used for the loss estimation of the school building.**

<b>Damagable Elements</b>	<b>Demand Parameter</b>	<b>Fragility and Repair Cost Functions</b>	<b>Improved Fragility Functions</b>
<b>Structural Elements</b>			
Non-Ductile Columns	Drift [%]	Cardone [2016] - DWC (lapped)	FEMA P58-3[2012] : B1041.001a
Exterior Beam-Column Joints	Drift [%]	Cardone [2016] - EWJs (end hooks)	FEMA P58-3[2012] : B1041.001a
Interior Beam-Column Joint	Drift [%]	Cardone [2016] - IWC	FEMA P58-3[2012] : B1041.001a
Exterior Masonry Infill	Drift [%]	Cardone & Perrone [2015] - EIW	Shifted 0.005 (drift that activates the gap)
Stairs	Drift [%]	FEMA P58-3 [2012] - C2011.011b	FEMA P58-3[2012] : C2011.011a
<b>Non-Structural Elements</b>			
Infill walls	Drift [%]	Sassun <i>et al.</i> [2015]	Shifted 0.005 (drift that activates the gap)
Internal Partition	Drift [%]	Sassun <i>et al.</i> [2015]	Shifted 0.005 (drift that activates the gap)
Doors	Drift [%]	Cardone & Perrone [2015] - IP_d	Shifted 0.005 (drift that activates the gap)
Windows	Drift [%]	Cardone & Perrone [2015] - EIW_w	Shifted 0.005 (drift that activates the gap)
Desks	Drift [%]	Sassun <i>et al.</i> [2015]	Shifted 0.005 (drift that activates the gap)
Chairs	Drift [%]	Sassun <i>et al.</i> [2015]	Shifted 0.005 (drift that activates the gap)
Ceiling Systems	PFA [g]	FEMA P58-3 [2012] : C3032.001b	FEMA P58-3[2012] : C3032.003b
Fancoils	PFA [g]	FEMA P58-3 [2012] : E2022.020	FEMA P58-3[2012] : D3041.102b
Lights	PFA [g]	FEMA P58-3 [2012] : C3034.001	FEMA P58-3[2012] : C3034.002
Piping-Water Distribution	PFA [g]	FEMA P58-3 [2012] : D2022.011a	FEMA P58-3[2012] : D2022.011b
Piping-Heating Distribution	PFA [g]	FEMA P58-3 [2012] : D2022.011a	FEMA P58-3[2012] : D2022.011b
Bookcases	PFV [m/s]	FEMA P58-3 [2012] : E2022.104a	FEMA P58-3[2012] : E2022.104b
Mobile Blackboards	PFA [g]	FEMA P58-3 [2012] : E2022.020	FEMA P58-3[2012] : E2022.021
Electronic Blackboard	PFA [g]	FEMA P58-3 [2012] : E2022.020	FEMA P58-3[2012] : E2022.021
Computers and Printers	PFA [g]	FEMA P58-3 [2012] : E2022.023	FEMA P58-3[2012] : E2022.022
Projector	PFA [g]	FEMA P58-3 [2012] : C3034.001	FEMA P58-3[2012] : C3034.002
Switchboards	PFA [g]	FEMA P58-3 [2012] : D3067.011	FEMA P58-3[2012] : D3067.013b

As mentioned earlier, the EAL was obtained by integrating the individual vulnerability functions, as illustrated in Figure 5.12, with the mean hazard curve for the Cassino site, shown in Figure 5.1. This integration is illustrated as a ratio to the replacement cost in Figure 5.13 for each model. It is clear that the bare frame model has the less effective behaviour in terms of the EAL since this model presented the highest storey drifts and also for higher intensities more collapse cases were developed. On the other hand, alternative C\* accounts for an excellent improvement since the EAL is the lowest among all models, indicating the efficacy of this alternative on reducing monetary losses.

The EAL for the original school building was found to be 0.31% of the replacement cost, being close to the range of 0.5% - 1.5% presented by Calvi *et al.* [2014] for the assessment of RC moment resisting frames. Likewise, Cardone [2017] illustrated that the EAL for different configurations of RC buildings, typically residential buildings built in Italy before the 70s, ranged between 0.1% and 1.89% of the total replacement cost. Therefore, the EAL obtained for the original school building is along the same lines as values obtained in other studies. Similarly, the EAL computed for all the retrofit alternatives presented by O'Reilly and Sullivan [2018a] falls between 0.2% - 1.3% for four gravity load designed RC frames of various numbers of storeys. Alternatives B and C achieved a slight reduction in the EAL, which were compared as ratios of EAL, being 0.94 and 0.97 times of that the original building, respectively. On the other hand, alternative D presented a higher improvement, achieving an EAL of 0.39 times of that the original model. Moreover, alternative A worsened the EAL if it is compared with the original building, but when it is compared with the bare frame the EAL is 0.95 times of that the bare frame. There were cases, such as the one reported by O'Reilly and Sullivan [2018a], in which some retrofit alternatives for RC building, RC jacketing and RC wall, worsened the performance in terms of the EAL since PFA increased and more distributed damage throughout the height of the structure was developed. Therefore, it is not surprising that alternative A achieved a higher EAL. In fact, this alternative by itself cannot be considered as a retrofit intervention aimed to improve the EAL or the structural performance.

Finally, when the non-structural retrofit (\*) was also incorporated into the models, the EAL was reduced considerably reaching ratios between 0.35 to 0.48 times of the original building, demonstrating the importance that non-structural elements have on the EAL improvement and reduction. This approach allowed to evaluate the performance of the school building in terms of the EAL rather than structural performance as presented in Chapter 3 and 4. Therefore, the retrofit alternatives can be considered to have a satisfactory performance as long as the retrofit of non-structural elements is included. Table 5-6 summarizes the values of EAL and MAFC, as well as presents the expected losses for all the assessed model for each level of intensity.

Additionally, residual drifts were also incorporated in the assessment to consider the situation where excessive residual drift leads to demolition. Ramirez and Miranda [2009] proposed median and dispersion values for the drift fragility curve of RC building, which were 1.5% and 0.3, as indicated in Table 5-5.

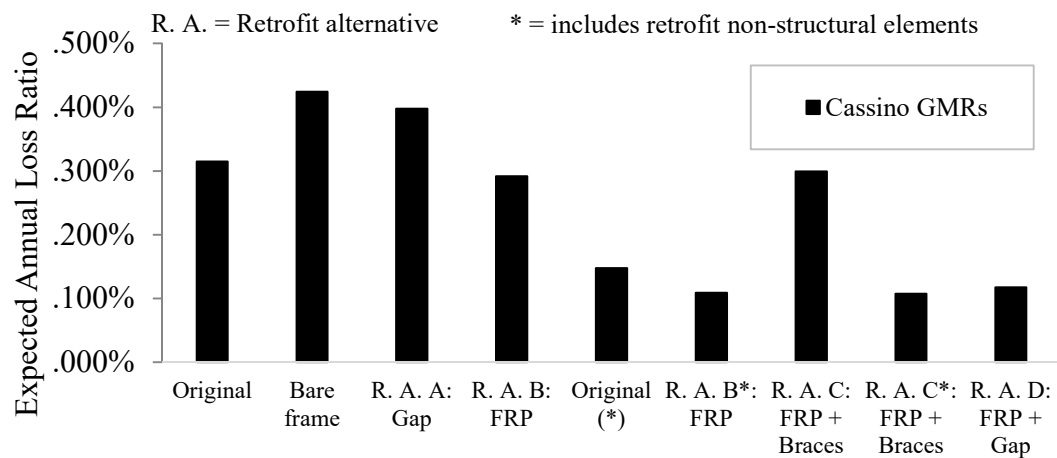


**Figure 5.13. EAL ratio of the replacement cost.**

**Table 5-5. Inputs values for performing the loss estimation assessment.**

Site Model	Cassino								
	Original	Bare frame	R. A. A: Gap	R. A. B: FRP	Original (*)	R. A. B*: FRP	R. A. C: FRP + Braces	R. A. C*: FRP + Braces	R. A. D: FRP + Gap
<i>General Input</i>									
T* for ground motions [s]	0.5	1.0	1.0	0.5	0.5	0.5	0.5	0.5	1.0
No. of storeys	3	3	3	3	3	3	3	3	3
Floor Area (m <sup>2</sup> )	689.1	689.1	689.1	689.1	689.1	689.1	689.1	689.1	689.1
Total replacement cost (€)	€ 3,929,94	€ 3,929,94	€ 3,929,94	€ 3,929,94	€ 3,929,94	€ 3,929,94	€ 3,929,94	€ 3,929,94	€ 3,929,94
Core and shell replacement cost	€ 3,929,94	€ 3,929,94	€ 3,929,94	€ 3,929,94	€ 3,929,94	€ 3,929,94	€ 3,929,94	€ 3,929,94	€ 3,929,94
Total loss threshold	0.6	0.6	0.6	0.6	0.6	0.6	0.6	0.6	0.6
<i>Collapse</i>									
Median Intensity from MSA [g]	1.93	0.54	0.69	2.25	1.93	2.25	2.54	2.54	0.81
Dispersion (Record-to-Record)	0.28	0.2	0.22	0.25	0.28	0.25	0.24	0.24	0.29
Dispersion (Modelling Uncertainty)	0.15	0.15	0.15	0.15	0.15	0.15	0.15	0.15	0.15
Median Intensity Reduction Factor	0.99	0.99	0.99	0.99	0.99	0.99	0.99	0.99	0.99
Input Median Intensity [g]	<b>1.91</b>	<b>0.53</b>	<b>0.68</b>	<b>2.23</b>	<b>1.91</b>	<b>2.23</b>	<b>2.51</b>	<b>2.51</b>	<b>0.80</b>
Input Dispersion	<b>0.32</b>	<b>0.25</b>	<b>0.27</b>	<b>0.29</b>	<b>0.32</b>	<b>0.29</b>	<b>0.28</b>	<b>0.28</b>	<b>0.33</b>
<i>Residual Drift</i>									
Median story drift ratio [%]	1.5	1.5	1.5	1.5	1.5	1.5	1.5	1.5	1.5
Dispersion	0.30	0.30	0.30	0.30	0.30	0.30	0.30	0.30	0.30
No. of Realizations	200	200	200	200	200	200	200	200	200
Non-directional conversion factor	1.2	1.2	1.2	1.2	1.2	1.2	1.2	1.2	1.2
Modelling Uncertainty (Demand)	0.15-0.6	0.15-0.6	0.15-0.6	0.15-0.6	0.15-0.6	0.15-0.6	0.15-0.6	0.15-0.6	0.15-0.6

**Table 5-6. Loss estimation results and expected repair cost.**

<b><i>Loss Estimation Results</i></b>									
Model	Original	Bare frame	R. A. A: Gap	R. A. B: FRP	Original (*)	R. A. B*: FRP	R. A. C: FRP + Braces	R. A. C*: FRP + Braces	R. A. D: FRP + Gap
EAL [€]	€ 12,371.3	€ 16,671.6	€ 15,633.3	€ 11,478.5	€ 5,813.8	€ 4,290.1	€ 11,765.0	€ 4,230.6	€ 4,625.6
EAL Ratio [%]	0.31%	0.42%	0.40%	0.29%	0.15%	0.11%	0.30%	0.11%	0.12%
MAFE of Collapse	1.64E-04	4.10E-04	3.13E-04	9.26E-05	1.64E-04	9.26E-05	6.07E-05	6.07E-05	2.07E-04
<b><i>Vulnerability Curve E/Lt IM </i></b>									
Intensity 1 - 30 years	€ 12,444.4	€ 43,000.0	€ 838.1	€ 12,333.3	€ 2,150.0	€ 2,562.5	€ 9,300.0	€ 940.6	€ 387.5
Intensity 2 - 50 years	€ 33,500.0	€ 110,909.1	€ 24,973.7	€ 34,230.8	€ 7,909.1	€ 7,769.2	€ 39,000.0	€ 6,200.0	€ 6,849.3
Intensity 3 - 70 years	€ 76,363.6	€ 175,000.0	€ 77,692.3	€ 79,333.3	€ 16,833.3	€ 16,375.0	€ 77,500.0	€ 12,666.7	€ 9,434.0
Intensity 4 - 100 years	€ 150,000.0	€ 370,000.0	€ 122,941.2	€ 160,000.0	€ 32,400.0	€ 35,800.0	€ 165,000.0	€ 26,071.4	€ 30,000.0
Intensity 5 - 140 years	€ 363,333.3	€ 512,857.1	€ 218,000.0	€ 290,000.0	€ 73,846.2	€ 55,000.0	€ 310,000.0	€ 50,526.3	€ 58,571.4
Intensity 6 - 200 years	€ 607,142.9	€ 883,333.3	€ 430,000.0	€ 565,000.0	€ 162,857.1	€ 130,000.0	€ 520,000.0	€ 85,000.0	€ 95,000.0
Intensity 7 - 475 years	€1,045,000.0	€1,625,000.0	€ 1,001,428.	€ 833,333.3	€ 550,000.0	€ 370,000.0	€ 720,000.0	€ 293,333.3	€ 335,000.0
Intensity 8 - 975 years	€ ,200,000.0	€3,921,935.5	€1,590,000.0	€2,080,000.0	€1,280,000.0	€ 890,000.0	€ 1,886,666.7	€ 720,000.0	€ 1,050,000.0
Intensity 9 - 2475 years	€3,924,152.1	€3,925,000.0	€3,923,464.1	€3,923,548.4	€2,060,000.0	€1,450,000.0	€ 3,924,047.6	€1,286,666.7	€ 1,910,000.0
Intensity 10 - 4975 years	€3,924,949.5	€3,925,000.0	€3,924,736.8	€3,924,818.7	€3,924,117.7	€2,290,000.0	€ 3,925,000.0	€2,605,409.4	€ 3,924,011.9
Intensity 11 - 9975 years	€3,925,000.0	€3,925,000.0	€3,925,000.0	€3,925,000.0	€3,925,000.0	€3,924,535.5	€ 3,925,000.0	€3,924,152.1	€ 3,925,000.0

## 5.5 Summary and Discussions

The performance of the original school building and each of the retrofit alternatives were evaluated in terms of monetary losses and collapse vulnerability. To proceed with the assessment, NRHA was used by collecting a set of ground motions for several return periods. Once the analyses were conducted, the median values of maximum PSD and PFA were evaluated in order to compare all models and conclude on the improvement obtained by each one. It was found that alternative A (Gap) and the bare frame showed the highest PSD but lowest PFA. On the other hand, alternative C (FRP + braces) accounted for the highest PFA but lowest PSD, highlighting the work done by the gap model in allowing higher deformation and by the braces in restricting lateral displacements. Collapse fragility functions were then developed to assess the collapse vulnerability of each retrofit. Fortunately, all the models presented a collapse margin ratio higher than unity, meaning that all the model guarantee the limit state of life safety and collapse prevention. The effectiveness of FRP on improving the structural behaviour was reflected by a lower probability of collapse for the same level of intensities as the original building.

Furthermore, the EALs for all the cases were similar to the values presented by other authors [Calvi *et al.*, 2014; Cardone, 2017; O'Reilly and Sullivan 2018a], supporting the findings of this study. The performance of the school building and the different retrofit alternatives was almost the same, 0.29% to 0.31% of the replacement cost when only structural retrofit was considered. But when the retrofit of non-structural elements was also considered, the EAL could be reduced to 0.11% to 0.15% of the replacement cost, indicating an improvement on the building performance based on an EAL evaluation. It is important to mention that by only retrofitting the structural elements a slightly improvement on the EAL was achieved, but when the retrofit of non-structural elements was included the improvement was quite substantial. This means it is not enough to only focusing on the structural retrofitting but also in the non-structural elements in order to obtain a better improvement in terms of the EAL.

Even though the traditional way of assessing the retrofit solutions for a structure is based on the structural performance, evaluating performance in terms of the EAL allows one to determine how effective these solutions actually are, since rather than just evaluating the structural performance, a monetary point of view is being incorporated into the assessment. For instance, a structural retrofit that achieves a great structural improvement may not be effective in terms of monetary losses since in order to reduce them, it may be increasing the EAL. Therefore, this study has highlighted this important issue by presenting the classification of the retrofit alternatives based on the EAL. Additionally, it has illustrated that is not enough to focus on improving the structural behaviour. Mitigating the vulnerability of non-structural elements is important, so that a satisfactory overall performance can be achieved.

## 6 SUMMARY, CONCLUSIONS AND FUTURE STUDIES

### 6.1 Summary

This study has assessed an existing RC school building to evaluate its seismic performance and propose several retrofitting alternatives aimed at not only improving its structural behaviour, but also at reducing its expected annual loss (EAL) and collapse vulnerability. This assessment followed the guidelines indicated in FEMA P58 and ASCE/SEI 41-17, as well the requirements outlined in NTC 2008.

The initial part of the assessment consisted of quantifying the performance of the existing school building by applying a non-linear static procedure, the N2 method along with approaches specified by a simple lateral mechanism analysis (SLaMA) methodology to replicate what practitioners would typically do in such a scenario. The structural performance was evaluated using the limit states definitions of NTC 2008, which are related to different hazard levels and expected performance of structural and non-structural elements. Smoothed, elastic response spectra were developed from uniform hazard spectra data as a function of return periods in order to obtain target displacements related to those intensities. Afterwards, a static pushover (SPO) analysis was performed so that the maximum storey drifts and failure mechanisms could be evaluated against the requirements of NTC 2008. From the analysis, it was found that the serviceability limit states (SLO and SLD) were met, but some weak-storey mechanisms were present at the ultimate limit states (SLV and SLC). Additionally, a strength hierarchy assessment was carried out to corroborate the presence of non-ductile mechanisms. It was also used to determine the possible local failures within a joint element region that did not follow a failure sequence resulting in beam member hinging. Likewise, this strength hierarchy assessment was used to identify and propose the retrofit alternatives so that the building's structural performance could be improved via the provision of a more stable and ductile failure mechanism.

Four retrofit alternatives were evaluated and denoted as retrofitting alternatives A, B, C, and D. Alternative A consisted of a perimeter gap aimed at isolating the infill walls from the surrounding frames so that their interactions could be delayed. However, this retrofit strategy was not beneficial since little structural improvement was achieved and no reduction of structural damage or storey drift was observed. Alternative B involved the addition of FRP bars and sheet wrapping for columns, and FRP strips in the beam-column joints. This strategy was beneficial for the improvement of the strength hierarchy providing higher capacity to structural

elements and achieving a desirable failure sequence. Nevertheless, this retrofit could not prevent a weak-storey mechanism due to physical limitations of the technique in this case study application. Alternative D combined the effect of the FRP with the perimeter gap, providing an appropriate strength hierarchy and also limiting structural damage, but yet weak-storey mechanisms persisted. Finally, alternative C was a hybrid retrofit, which incorporated steel braces with alternative B. This scheme seemed to be the most effective structural retrofit strategy since weak-storey mechanism were prevented via the introduction of the braces. Furthermore, it provided a safe strength hierarchy sequence and drifts in all the storeys at the assessed return period were reduced with respect to the original building.

Once the structural performance was evaluated, an assessment based on the collapse risk and loss estimation was carried out. All the models presented a collapse margin ratio (CMR) higher than unity, indicating that the collapse performance was not a critical issue requiring specific attention. It is also important to highlight the improvement achieved by the retrofit strategies on reducing the vulnerability to collapse since each retrofitting alternative increased the collapse margin ratio. Furthermore, the retrofit of non-structural elements was not directly conducted, but some strategies were outlined to reduce their seismic risk using the recommendations and methods described by FEMA E -74. Moreover, in terms of loss estimation, all the alternatives presented a reduction in the annualised direct monetary losses associated with repair cost after a seismic event. When only structural retrofits were considered, the EAL exhibited a slight reduction. On the other hand, the EAL was substantially improved when the retrofit of non-structural elements was also incorporated.

## 6.2 Conclusions

The concluding remarks that arose as result of this study are detailed as follows:

- The N2 method provided a very simple and practical way of assessing the structural performance of the existing building and its possible retrofit alternatives. It can be easily implemented, allowing practising engineers with no or little background on performance assessment to utilise it. The application of SPO analysis as function of a target displacement allowed the structural behaviour of the RC school building based on hazard levels to be determined. This simple non-linear static method avoided more sophisticated and time consuming analysis like non-linear response history analysis (NRHA) in order to obtain the structural performance of the building and its retrofitted schemes.
- The strength hierarchy criteria was very useful in providing additional information about local failure modes in the structural elements so that undesirable failure sequence could be controlled and modified. Similarly, it demonstrated to be quite effective for sizing and designing the amount of FRP required in the structural elements so that an appropriate failure sequence could be obtained.
- The existing building met the requirements for drift limitation for the serviceability limit states, which indicated that for more frequent events the non-structural elements would not undergo extensive damage. On the other hand, the structural performance of the

school building for the ultimate limit states was not adequate since weak-storey mechanisms were formed in both directions. Likewise, non-ductile failure sequences were present in some beam-column joints and this strength hierarchy led to local failure modes such as column hinging and joint shear failure prior to the desired mechanism of beam hinging.

- The bare frame model of the existing building highlighted the influence of infills on the overall performance. On one hand, the lateral strength capacity was reduced considerably but its deformation capacity was not significantly modified, at least the maximum deformation was along the same lines as to the original building. Furthermore, a weak-storey mechanism also formed, albeit in a different storey for the longitudinal direction due a reduction on the lateral stiffness. Similarly, increased structural element damage was noted, indicating that the increased flexibility of this model makes it more prone to overestimate the structural damage.
- Even though the perimeter gap, denoted as alternative A, delayed and controlled the damage in the infill walls, no structural improvement was achieved using this retrofit. It was found that weak-storey mechanisms were not mitigated, but moved to different storeys because the strength hierarchy was not modified and therefore no structural upgrading was achieved. Likewise, the damage undergone by elements was the same or worse, in some cases. Despite the strength and deformability capacity being higher compared to that of the bare frame, the requirements for limiting storey drifts were not met for both limit states considered.
- The application of the FRP, denoted as alternative B, proved to be effective in improving the strength and deformation capacity of columns and joints. As a result, a desirable strength hierarchy was achieved, leading to beam hinging before the failure of columns and joints. Similarly, the damage undergone by the structural elements was substantially reduced, presenting no failure cases for the hazard level related corresponding to a return period  $T_r = 1463$  years. However, the FRP could not mitigate the formation of weak-storey mechanisms. Even though the FRP increased the strength of the structural elements considerably, it could not provide enough lateral capacity to the building to avoid the formation of weak-storey mechanisms.
- When combining the FRP and the steel braces, denoted as alternative C, weak-storey mechanisms were mitigated since a better stiffness distribution along the height of the building was provided as well as a higher lateral capacity. This resulted in lower storey drifts and a different load path distribution in the elements, thereby inducing less damage undergone by structural elements.
- When the FRP and the perimeter gap were combined, denoted as alternative D, the same benefits achieved by each retrofit individually were obtained, meaning higher strength capacity, larger deformation capacity and appropriate strength hierarchy. Even though the maximum storey drifts were within the limits, weak-storey mechanisms were not mitigated.

- The collapse risk of the existing school building could be considered as satisfactory. For one thing, the mean annual frequency of collapse (MAFC) of the original building was on the conservative side compared to the limits outlined by Dolšek et al. [2017]. Furthermore, the CMR was higher than unity which indicates that the median level of intensity value is higher than the hazard level of intensity related to collapse prevention. In the case of the gap retrofit, no apparent improvement of the collapse performance was obtained. In fact, the CMR was lower and the MAFC higher than of that the original building. This may be related to the higher flexibility of this model, which led to more collapse cases, especially for higher intensities. On the other hand, the FRP reduced the collapse risk as the additional strength provided by this material generated fewer collapse cases, even for higher intensities, thereby decreasing the MAFC and increasing the CMR. Similar improvement was obtained with the steel braces. In fact, they reduced the collapse risk even more since the braces allowed the structure to withstand higher level of intensities, meaning fewer collapse cases for higher intensities and therefore a better structural performance.
- In terms of monetary losses, the expected annual loss (EAL) of 0.31% for the school building as a ratio of the replacement cost was along the lines with the values presented by other authors [Calvi *et al.*, 2014; Cardone, 2017; O'Reilly and Sullivan 2018a]. The EAL of the bare frame was almost twice the values obtained for the actual building, meaning that more damage and increased losses in the drift sensitive elements would be expected due to the flexibility of this model. In the case of the gap retrofit, the EAL was almost twice the obtained for the original building, but when it was compared to the bare frame a substantial improvement was obtained since the lateral resistance of infill was incorporated to the structure for higher intensities. On the other hand, the structural retrofit based on the FRP and braces achieved a slight reduction on the EAL, which was approximately 0.94 times of that of the original building. For one thing, the FRP did not affect the section properties of the elements so the PSD and PFA were almost the same as the original building, but with fewer collapse cases. In contrast, the braces modified the dynamics response by reducing the PSD and increasing the PFA. Consequently, the reduction of losses due to drift-sensitive elements was overshadowed by the increased losses related to acceleration-sensitive elements.
- Considering the overall performance, alternative A was not practical for the case of the study school building since neither the structural behaviour nor the expected losses were enhanced. Despite that alternative B achieved an EAL reduction, its structural performance was not as satisfactory as alternative C. Similarly, alternative D improved EAL but still the structural integrity of the building was not completely improved. Alternative C can be considered as a satisfactory retrofit scheme since it achieved a better overall performance in terms of improved structural performance and monetary loss reduction.
- During the performance assessment, it was not necessary to consider directly the retrofit of non-structural elements. Non-structural retrofit was incorporated in the loss estimation analysis by using improved fragility curves. In this way, the modelling of

such elements was avoided and their vulnerability was evaluated in terms of demand parameter at which they are sensitive. It is important to mention that by only retrofitting the structural elements, a slight improvement in EAL was achieved. However, when non-structural elements were also retrofitted, the improvement was quite substantial. Improvements in EAL of approximately 0.39 times that of the original building were observed, which implies that focusing only on the structural retrofitting may not be the most effective way to reduce EAL. Paying attention to the non-structural elements is also crucial.

### 6.3 Future Studies

Based on the work presented here, there are some future studies that could be undertaken:

- Further experimentation has to be carried out for some non-structural elements in order to obtain their fragility curves. In the case of the masonry infill walls, it was assumed to shift all the fragility functions by an amount equal to the drift required to active the gap, this was considered practical but yet needs to be verified. Additionally, due to the lack of information on electronic blackboards, the fragility functions of electronic equipment were used instead. Despite that these two fragility curves may be equivalent, if further research is conducted to determine the fragility curves for these non-structural elements, more representative results can be obtained.
- Even though this study did not consider the effect of the vertical components of earthquakes, this issue has to be addressed to determine its effect on the structural and non-structural response. By considering vertical ground motions, the overall performance of the structure may be modified and may compromise the structural integrity. It is known that vertical ground motion contribute to higher axial loads in columns, which may be critical not only for columns but also for other structural elements. Likewise, vertical floor accelerations can potentially increase the damage to some non-structural typologies such as ceiling systems. Furthermore, as highlighted by Tasligedik et al., [2016] the strength hierarchy is altered since the vertical components would increase the axial load and therefore beam-column joints may suffer earlier shear failure. Consequently, the effect of vertical acceleration for evaluating the structural performance, needs further investigation.
- Limited information and bibliography was found for estimating the strength capacity of internal joints after retrofitting them with FRP. Despite there have been many studies addressing the improvement in shear capacity for internal joints using FRP, limited equations are still proposed for estimating that capacity, or at least they are not as detailed and straight forward as the ones presented by Del Vecchio et al., [2015] for exterior or corner joints. Therefore, more equations have to be proposed for a better estimation of shear capacity in internal joints retrofitted with FRP.

## 7 REFERENCES

- Akguzel, U., Pampanin, S. [2012] “Assessment and design procedure for the seismic retrofit of reinforced concrete beam-column joints using FRP composite materials,” *ASCE, J. Compos. Constr.*, Vol. 16, No. 1, pp. 21-34.
- Ambraseys, N. N., Simpson, K. A., Bommer, J. J. [1996] “Prediction of horizontal response spectra in Europe,” *Earthquake Engineering & Structural Dynamics*, Vol. 25, pp. 371–400.
- Ancheta, T. D., Darragh, R. B., Stewart, J. P., Seyhan, E., Silva, W. J., Chiou, B. S. J., Wooddell, K. E., Kottke, A. R., Boore, D. M., Kishida, T., and Donahue, J. L. [2013] “PEER NGA-West2 Database,” PEER Report 2013/03, *Pacific Earthquake Engineering Research Center*, Berkeley, California.
- ASCE/SEI 41-17 [2017] “Seismic Evaluation and Retrofit of Existing Buildings, American Society of Civil Engineers, Structural Engineering Institute”, Reston, Virginia.
- Baker, J. W. [2015] “Efficient Analytical Fragility Function Fitting Using Dynamic Structural Analysis,” *Earthquake Spectra*, Vol. 31, No.1, pp. 579–599.
- Baker, J. W., Cornell, C. A. [2006] “Spectral shape, epsilon and record selection,” *Earthquake Engineering & Structural Dynamics*, Vol. 35, No.9, pp. 1077–1095.
- Borzi B., Ceresa P., Faravelli M., Fiorini E., Onida M. [2013] “Seismic Risk Assessment of Italian School Buildings,” *Computational Methods in Earthquake Engineering. Computational Methods in Applied Sciences*, Vol. 30.
- BS 1881 [1996] Testing concrete. Method for temperature-matched curing of concrete specimens, British Standard.
- Calvi, G. M., Sullivan, T. J., Welch, D. P. [2014] “A seismic performance classification framework to provide increased seismic resilience,” *2nd European Conference on Earthquake Engineering and Seismology*, Istanbul, Turkey.
- Calvi, P.M., Moratti, M., Filiatrault, A. [2016] “Studio della Risposta di Elementi Non Strutturali di edifice scolastici soggetti ad eventi sismici/ Role and Importance of Non-Structural Elements in the Seismic Vulnerability of School Buildings,” (in Italian), *Progettazione Sismica*, Vol. 6, No. 3, pp. 9-29, DOI: 10.7414/PS.6.3.9-29 – <http://dx.medra.org/10.7414/PS.6.3.9-29>

- Cardone, D., Perrone, G., [2015] “Developing fragility curves and loss functions for masonry infill walls,” *Earthquakes and Structures*, Vol. 9, No. 1, pp. 257-279.
- Cardone, D. [2016] “Fragility curves and loss functions for RC structural components with smooth rebars,” *Earthquakes and Structures*, Vol. 10, No. 5, pp. 1181-1212
- Cardone, D., Gesualdi, G., Perrone, G., [2017] “Cost-benefit analysis of alternative retrofit strategies for RC frame buildings,” *Journal of Earthquake Engineering*, DOI: 10.1080/13632469.2017.1323041.
- Chakravorthy A., [2017] “When schools shake: Keeping students and teacher safe during earthquakes,” << <https://www.earthmagazine.org> >>.
- Charleson, A., [2008] Seismic Design for Architects, Architectural Press, Oxford, UK.
- Cornell, C. A., Krawinkler, H. [2000] “Progress and Challenges in Seismic Performance Assessment,” *PEER Center News* 3(2): 1-2, URL <http://peer.berkeley.edu/news/2000spring/index.html>.
- Crisafulli, F. J., Carr, A. J., Park, R. [2000] “Analytical Modelling of Infilled Frame Structures – A General Review,” *Bulletin of the New Zealand Society for Earthquake Engineering*, Vol. 33, No.1, pp. 30–47.
- De Angelis, A., Pecce, M., [2015] “Seismic nonstructural vulnerability assessment in school buildings,” *Nat Hazards*, Vol. 79, pp. 1333-1358.
- Del Vecchio, C., Di Ludovico, M., Prota, A., Manfredi, G., [2015] “Analytical model and design approach for FRP strengthening of non-conforming RC corner beam-column joints,” *Engineering Structures*, Vol. 87, pp. 8-20.
- Del Zoppo, M., Di Ludovico, M., Balsamo, A., Prota, A. Manfredi, G., [2017] “FRP for seismic strengthening of shear controlled RC columns: experience from earthquakes and experimental analysis,” *Composites Part B*, Vol. 129, pp. 47-57.
- Dipartimento Protezione Civile [2009] “Linee Guida per La Riduzione Della Vulnerabilità Sismica Di Elementi Non Strutturali Arredi E Impianti.”
- DM 14.01.2008 [2008] Approvazione delle nuove norme tecniche per le costruzioni. GU 04.02.2008 n29.
- D.M. LL. PP. [1972]. Norme tecniche alle quali devono uniformarsi le costruzioni in conglomerato cementizio, normale e precompresso, ed a struttura metallica. G.U. n. 190 del 22/7/1972.Roma, Italy. (in Italian).
- Dolšek, M., Fajfar, P., [2004] “Inelastic spectra for infilled reinforced concrete frames,” *Earthquake Engng Struct. Dyn*, Vol. 33, pp. 1395-1416.
- Dolšek, M., Fajfar, P., [2005] “Simplified non-linear seismic analysis of infilled reinforced concrete frames,” *Earthquake Engng Struct. Dyn*, Vol. 34, pp. 49-66.

## References

---

- Dolšek M., Lazar S., N., Žižmond, J. [2017] “IM-based and EDP-based decision models for the verification of the seismic collapse safety of buildings,” *Earthquake Engng Struct. Dyn*, Vol. 46, pp.2665–2682.
- El-Betar, S. A., [2015] “Seismic performance of existing R.C. framed buildings,” *HBRC Journal*, Vol. 13, pp. 171-180.
- Elnashai, A. S., Pinho, R. [1998] “Repair and retrofitting of RC walls using selective techniques,” *Journal of Earthquake Engineering*, Vol. 2, No. 4, pp. 525-568.
- EN 1998-1:2004. [2004] Eurocode 8: Design of Structures for Earthquake Resistance - Part 1: General Rules, Seismic Actions and Rules for Buildings, Brussels, Belgium.
- EN 1998-3:2005. [2005] Eurocode 8: Design of Structures for Earthquake Resistance - Part 3: Assessment and Retrofit of Buildings, Brussels, Belgium.
- Fajfar, P., M. EERI, [2000] “A nonlinear analysis method for performance based seismic design,” *Earthquake Spectra*, Vol. 16, No. 3, pp. 573-592.
- FEMA E-74 [2012] Reducing the Risk of Nonstructural Earthquake Damage – A Practical Guide, Washington, DC.
- FEMA P58-2. [2012] Seismic Performance Assessment of Buildings: Volume 2 - Implementation Guide (P-582), Washington, DC.
- FEMA P58-3. [2012] Seismic Performance Assessment of Buildings Volume 3—Performance Assessment Calculation Tool (PACT) Version 2.9.65 (FEMA P-58-3.1), Washington, DC.
- FEMA P695. [2009] Quantification of Building Seismic Performance Factors, Washington, DC, USA.
- FEMA P58-1. [2012] Seismic Performance Assessment of Buildings: Volume 1 - Methodology (P-58-1), Washington, DC.
- Fiore, A., Mezzina, M., Porco, F., Raffaele, D., Uva, G. [2012] “Seismic safety assessment of school building in Puglia (Italy): overview and cases studies,” *15<sup>th</sup> World Conference on Earthquake Engineering*, Lisbon, Portugal.
- Galal, K., Ghobarah A. [2004] “Shear capacity of retrofitted rectangular RC short columns,” *13<sup>th</sup> World Conference on Earthquake Engineering*, Vancouver, B.C., Canada.
- Gara, F., Regni, M., Carbonari, S., Balducci, A., Dezi, L., [2017] “Dynacmis behaviour of a ratrofitted school building subjected to the after-schock sequence of the 2016 Central Italy Earthquake,” *Procedia Engineering*, Vol. 199, pp. 2084-2089.
- GEOHAZARDS INTERNATIONAL. [January21, 2018]. *Safeguarding Schools*. Retrieved from <<<http://www.geohaz.org>>>
- Hak, S., Morandi, P., Magenes, G., Sullivan, T. J. [2012] “Damage Control for Clay Masonry Infills in the Design of RC Frame Structures,” *Journal of Earthquake Engineering*, Vol. 16, No. sup1, pp.1–35.

- Iervolino, I., Chioccarelli, E., Cito, P. [2015] “REASSESS V1.0: A computationally efficient software for probabilistic seismic hazard analysis,” *COMPDYN 2015 - 5th ECCOMAS Thematic Conference on Computational Methods in Structural Dynamics and Earthquake Engineering*, Crete Island, Greece.
- Jones, G. [2016] “L’Aquila is grim reminder of struggle facing Italy’s quake-hit towns,” Reuters, <<http://www.reuters.com/article/us-italy-quake-reconstruction-idUSKCN1130AO>> (Sep.28, 2016).
- Kadid, A., Yahiaoui, D. [2011] “Seismic assessment of braced RC frames”, *Procedia Engineering*; Vol. 14, pp. 2899-2905.
- Kohrangi, M., Bazzurro, P., Vamvatsikos, D. [2016] “Vector and Scalar IMs in Structural Response Estimation: Part II – Building Demand Assessment,” *Earthquake Spectra*, Vol. 32, No.3, pp. 1525–1543.
- Kyriakides, N., [2016] “Derivation of fragility curves for RC frames retrofitted with RC infill walls based on full-scale,” *VII European Congress on Computational Methods in Applied Sciences and Engineering*, Crete Island, Greece.
- Liel, A. B., Deierlein, G. G. [2013] “Cost-benefit evaluation of seismic risk mitigation alternatives for older concrete frame buildings”, *Earthquake Spectra*, Vol. 29, N0. 4, pp. 1391-1411.
- Lignos, D. G., Karamanci E., Martin G. [2012] “A Steel database for modelling post-buckling behavior and fracture of concentrically braced frames under earthquakes,” *15<sup>th</sup> World Conference on Earthquake Engineering*, Lisbon, Portugal.
- Maheri, M. R., Zarandi, S., Niroomandi, A. [2012] “Seismic performance of RC frames retrofitted by FRP at joints”, *15<sup>th</sup> World Conference on Earthquake Engineering*, Lisbon, Portugal.
- Massumi, A., Tasnimi, A. A. [2008] “Strengthening of low ductile reinforced concrete frames using stell X-bracings with different details”, *the 14<sup>th</sup> World Conference on Earthquake Engineering*, Beijing, China.
- Moratti, M., Studio Calvi [2017] Personal Communication.
- McKenna, F., Fenves, G., Filippou, F. C., Mazzoni, S. [2000] “Open System for Earthquake Engineering Simulation (OpenSees),”<[http://opensees.berkeley.edu/wiki/index.php/Main\\_Page](http://opensees.berkeley.edu/wiki/index.php/Main_Page)>.
- Mwafy, A. M., Elkholy, S. [2012] “Comparative vulnerability assessment of retrofit techniques for pre-code RC structures,” *15<sup>th</sup> World Conference on Earthquake Engineering*, Lisbon, Portugal.
- NTC. [2008] Norme Tecniche Per Le Costruzioni, Rome, Italy.
- NZSEE. [2016] “Assessment and improvement of structural performance of building in earthquakes”, New Zealand.

- Oliveto, G., Marletta, M., [2005] “Seismic retrofitting of reinforced concrete buildings using traditional and innovative techniques,” *ISET Journal of Earthquake Technology*, Vol. 42, No. 2-3, pp. 21-46.
- OPCM 20.03.2003 n3274 [2003] Primi elementi in materia di criteri generali per la classificazione sismica del territorio nazionale e di normative tecniche per le costruzioni in zona sismica. GU 08.05.2003 n105.
- O'Reilly, G. J., [2016] “Performance-Based Seismic Assessment and Retrofit of Existing RC Frame Buildings in Italy,” PhD thesis, IUSS Pavia, Italy.
- O'Reilly, G. J., Sullivan, T. J., Filiatrault, A., [2017a] “Implications of more refined damage estimation approach in the assessment of RC frames,” *16<sup>th</sup> World Conference on Earthquake*, Santiago, Chile.
- O'Reilly, G., Perrone, D., Fox, M., Monteiro, R., Filiatrault, A., Lanese, I., Pavese, A. [2017b] “System Identification and Structural Modelling Implications of Italian School Buildings.” DOI:10.1007/978-3-319-5477-0\_37.
- O'Reilly, G. J., Sullivan, T. J. [2018a] “Probabilistic seismic assessment and retrofit considerations for Italian RC frame buildings,” *Bulletin of Earthquake Engineering*, Vol. 16, No.3, pp. 1447–1485 DOI: 10.1007/s10518-017-0257-9.
- O'Reilly, G. J., and Sullivan, T. J. [2018b] “Modelling Techniques for the Seismic Assessment of the Existing Italian RC Frame Structures,” *Journal of Earthquake Engineering*, pp. 1–35 DOI: 10.1080/13632469.2017.1360224.
- O'Reilly, G. J., Perrone, D., Fox, M., Monteiro, R., Filiatrault, A. [2018a] “Seismic Assessment and Loss Estimation of Existing School building in Italy,” *Engineering Structures*, Vol. 168, pp. 142–162 DOI: 10.1016/j.engstruct.2018.04.056.
- O'Reilly, G. J., Sullivan, T. J., and Monteiro, R. [2018b] “On the seismic assessment and retrofit of infilled RC frames structures,” *16th European Conference on Earthquake Engineering*, Thessaloniki, Greece
- O'Reilly, G., Perrone, D. [2016] Personal Communication
- Pampanin, S., [2017] “Performance-based seismic retrofit strategies and solutions for existing R.C. buildings,” *Class Notes*, Scuola Universitaria Superiore IUSS Pavia, Italy.
- Park, R. [1996] “A static force-based procedure for the seismic assessment of existing reinforced concrete moment resisting frames”, *Bulletin of the New Zealand National Society for Earthquake Engineering*, Vol. 30, No. 3.
- Parvin, A., Altay, S., Yalcin, C., Kaya, O., Karpuz, E., [2005] “Retrofit of shear deficient reinforced concrete beam-column joints,” *SMARR 2015 – Third Conference on Smart Monitoring, Assessment and Rehabilitation of Civil Structures*.

- Prevention Web. [2017] "Prevention Web - Serving the information needs of the disaster reduction community," <<http://www.preventionweb.net/countries/ita/data/>> (Sept. 18, 2017).
- Preti, M., Bolis, V., Stavridis, A., [2016] "Design of masonry infill walls with sliding joints for earthquake structural damage control," *Individual study*, University of Brescia, Italy.
- Priestley, M.J.N., Calvi, G.M. [1991] "Towards a capacity-driven assessment procedure for reinforced concrete frames", *Earthquake Spectra*, Vol. 7, No. 3, pp. 413–37.
- Priestley, M. J. N., Seible, F., Verma, R., and Xiao, Y. [1993] "Seismic Shear Strength of Reinforced Concrete Columns," Report SSRP-93/06, San Diego, CA, USA.
- Priestley, M.J.N. [1996] "Displacement-based seismic assessment of existing reinforced concrete buildings", *Bulletin of NZSEE*, Vol. 29, No. 4.
- Porter, K. A. [2003] "An overview of PEER's performance-based earthquake engineering methodology. In: Proceedings of 9th international conference on applications of probability and statistics in engineering", San Francisco, CAGoogle Scholar.
- Regio Decreto. [1939] Norme per la l'esecuzione delle opere conglomerato cementizio semplice od armato - 2229/39, Rome, Italy.
- Salvatore, W., Caprilli, S., Barberi, V. [2009] "Rapporto dei Danni Provocati dall'Evento Sismico del 6 Aprile sugli Edifici Scolastici del Centro Storico dell'Aquila," Pisa, Italy.
- Sassun, K., Sullivan, T. J., Morandi, P., Cardone, D., [2015] "Characterizing the in-plane seismic performance of infill masonry," *Bulletin of the New Zealand Society for Earthquake Engineering*, Vol. 49, No. 1, pp. 100-116.
- SEAOC. [1995] Vision 2000: Performance-based seismic engineering of buildings, Sacramento, California.
- Sollazzo, A., Sgobbo, C. [2011] Le norme ufficiali italiane sul cemento armato e il loro sviluppo durante il XX secolo (in Italian). In: Sicurezza e conservazione delle prime costruzioni in calcestruzzo armato, a cura di Mezzina, M., Uva G., Greco, R. CittàStudi Edizioni, Torino, Italy.
- Sousa L., Monteiro, R., [2016] "Seismic retrofit options for non-structural building partition walls: impact on loss estimation and cost-benefit analysis," *Individual study*, Scuola Universitaria Superiore IUSS Pavia, Italy.
- Ramirez, C. M., Miranda E. [2009] "Building Specific Loss Estimation Methods & Tools for Simplified Performance Based Earthquake Engineering". Blume Rep No 171 2009.
- Taghavi, S., Miranda, E. [2003] "Response Assessment of Nonstructural Building Elements," *PEER Report* 2003/05, Berkeley, California.

- Tasligerdik A. S., Akguzel, U., Kam, W. Y., Pampanin, S., [2016] “Strength hierarchy at reinforced concrete beam-column joints and global capacity,” *Journal of Earthquake Engineering*, Vol. 00, pp. 1-34.
- Triantafillou T. C., [2018] “Advanced materials and seismic retrofit technologies,” *Class Notes*, University of Patras, Greece.
- Tsantilis, A. V., Triantafillou T. C., [2018] “Innovative seismic isolation of masonry infills using cellular materials at the interface with the surrounding RC frames”, *Engineering Structures*, Vol. 155, pp. 279-297.
- Uriz, P., Mahin, S. A., [2008] “Toward earthquake-resistant design of concentrically braced steel-frame structures,” *PEER Report 2008/08*, Berkeley, California.
- U.S. Department of Commerce National Oceanic and Atmospheric Administration, “*EARTHQUAKE DAMAGE TO SCHOOLS*”, National Geophysical Data Center, Boulder, Colorado 80303, USA.
- Verderame, G. M., Iervolino, I., Ricci, P. [2009] Report on the Damage on Buildings Following the Seismic Event of 6th of April 2009 Time 1:32 - L’Aquila M=5.8.
- Verderame, G. M., Polese, M., Mariniello, C., Manfredi, G. [2010] “A simulated design procedure for the assessment of seismic capacity of existing reinforced concrete buildings,” *Advances in Engineering Software*, Vol. 41, No.2, pp. 323–335.
- Wilson C. A., Boehler P. [2016, August 24]. *Italy’s History of Deadly Earthquakes*. The New York Times. URL <https://www.nytimes.com/interactive/2016/08/24/world/europe/italy-earthquakes-history.html>
- Yu, J., Shang, X., Lu, Z. [2015] “Efficiency of externally bonded L-shaped FRP laminates in strengthening reinforced-concrete interior beam-column joints,” *ASCE, J. Compos. Constr.*, 04015064.

## **APPENDIX A (PERFORMANCE ASSESSMENT)**

This appendix presents some figures of the performance assessment results described in Chapter 3 and 4.

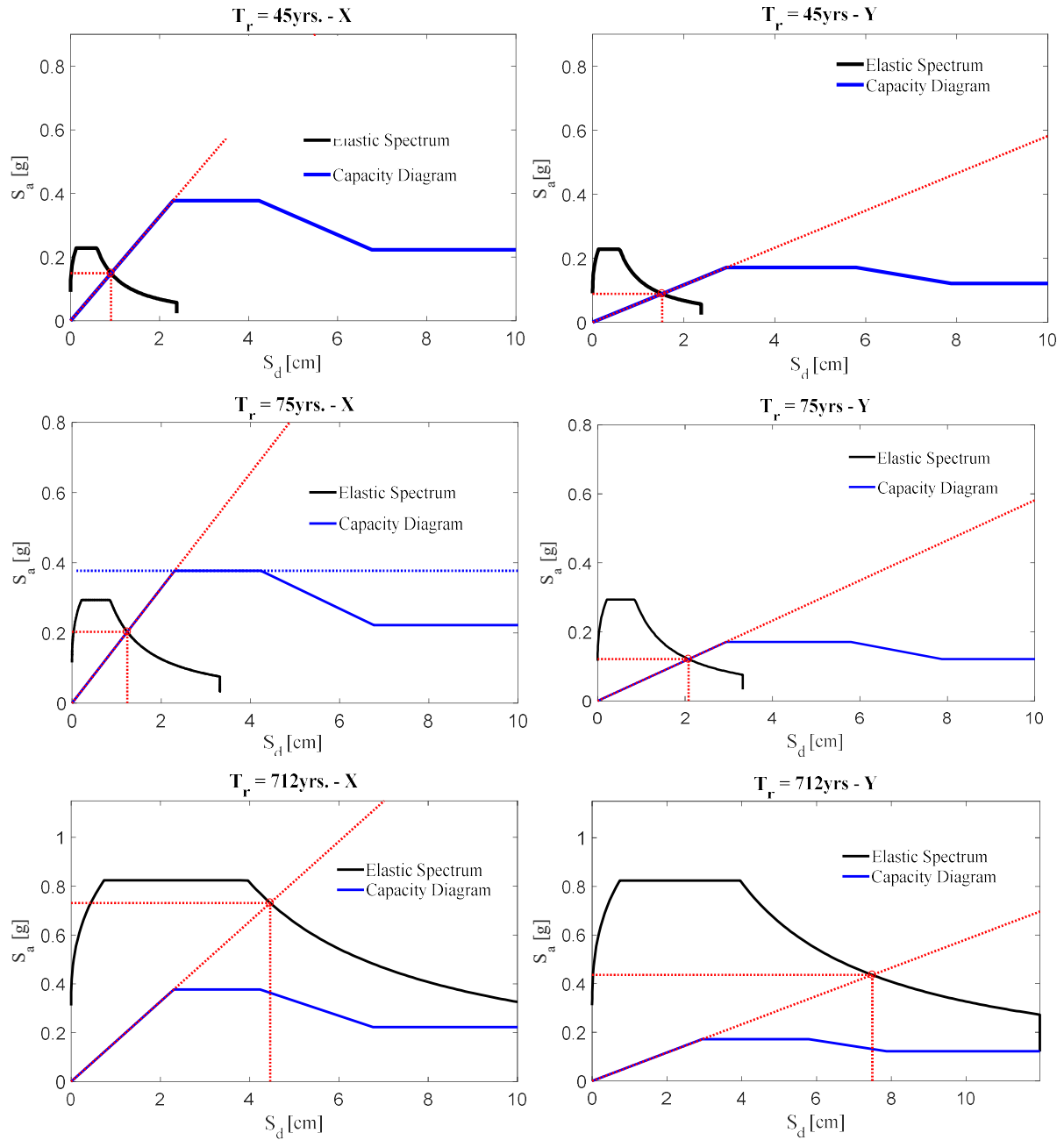


**Figure A. 1. Determination of target displacement for SDOF in both directions, original building.**

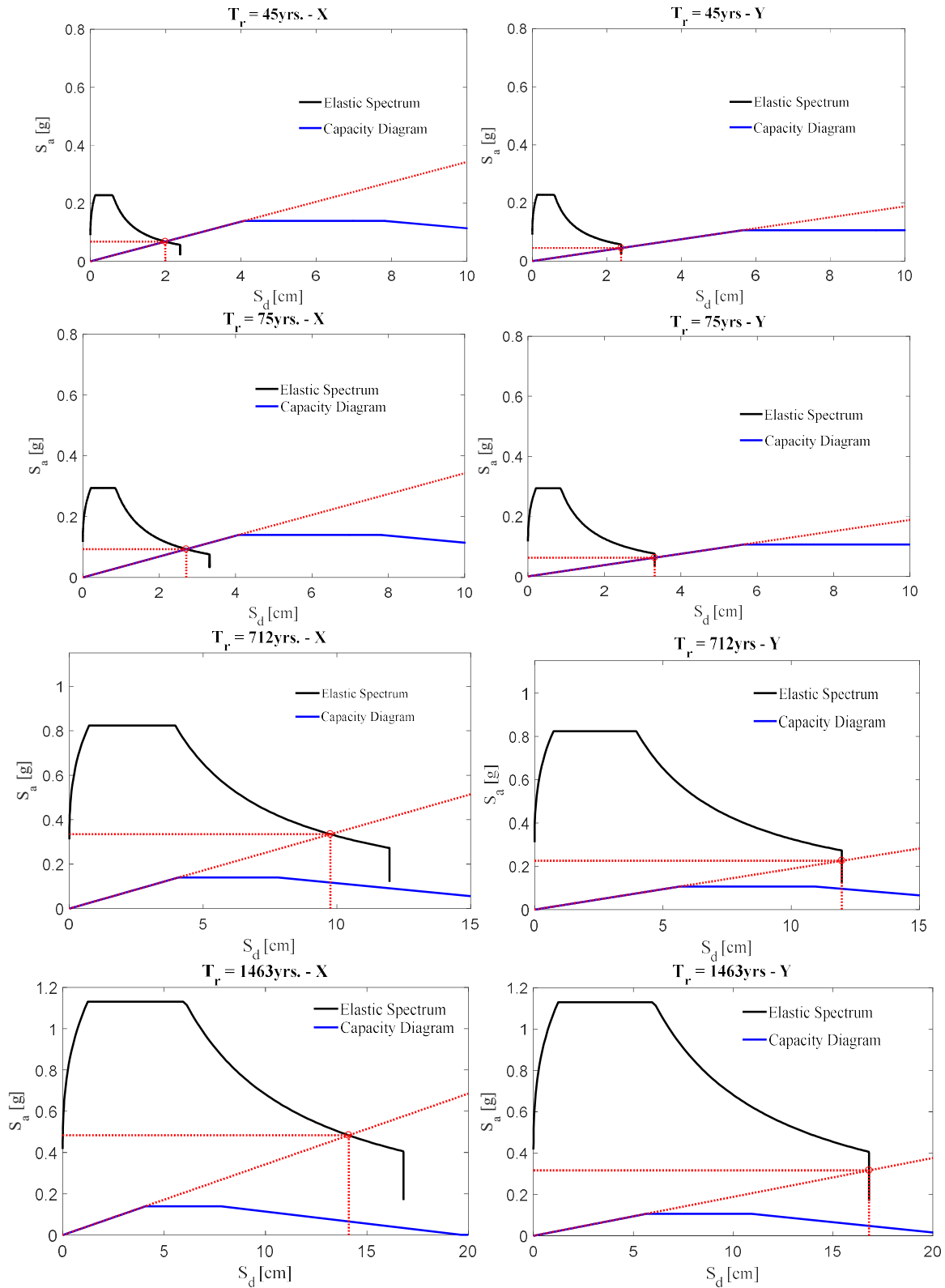


**Figure A. 2. Determination of target displacement for SDOF in both directions, bare frame.**

### Strength hierarchy of original school building

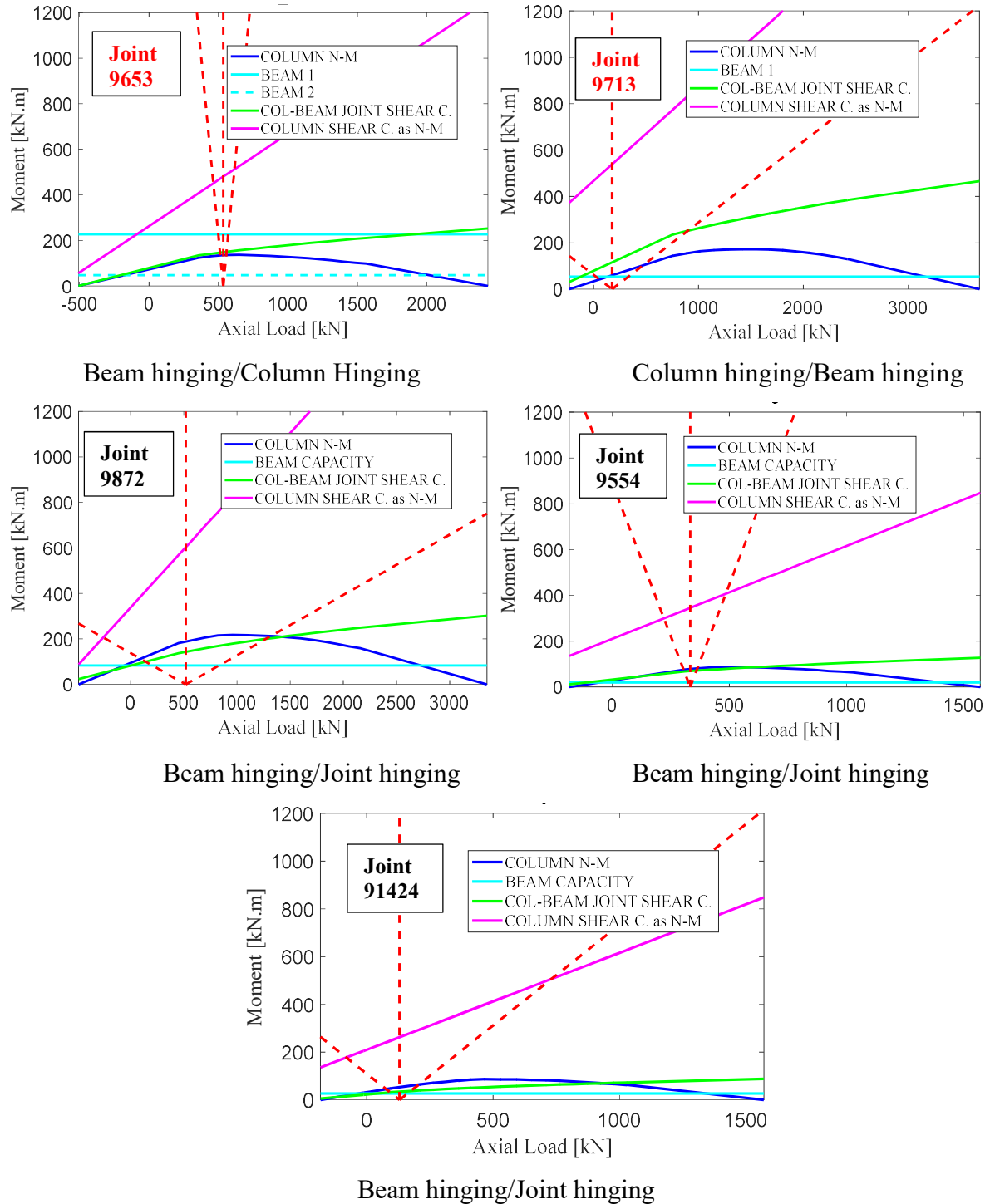


**Figure A. 3. Strength hierarchy evaluation of some beam-column joints**

### Strength hierarchy after strengthening intervention

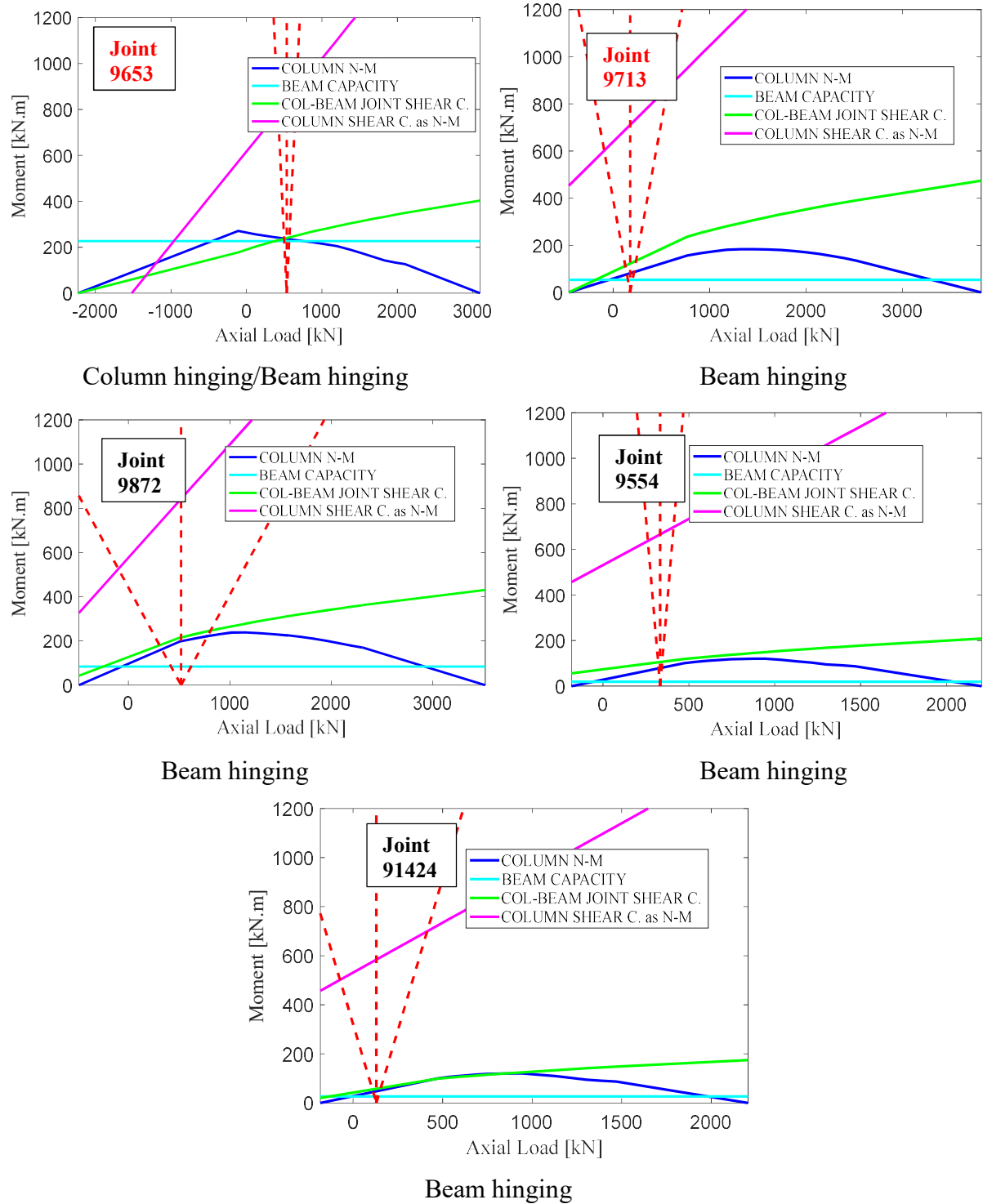


**Figure A. 4. Strength hierarchy evaluation after retrofitting the elements with FRP.**

## APPENDIX B (NON-STRUCTURAL ELEMENTS RETROFIT)

This appendix provides a detailed information about the strategies for retrofitting non-structural elements, the proposed strategies are based on FEMA P58-2[2012] and FEMA E-74[2012].

### Infill walls

The main procedure consists on detaching the infills walls from the surrounding columns providing a gap generally of 20mm. The gap is filled with cellular material (Figure B. 1).

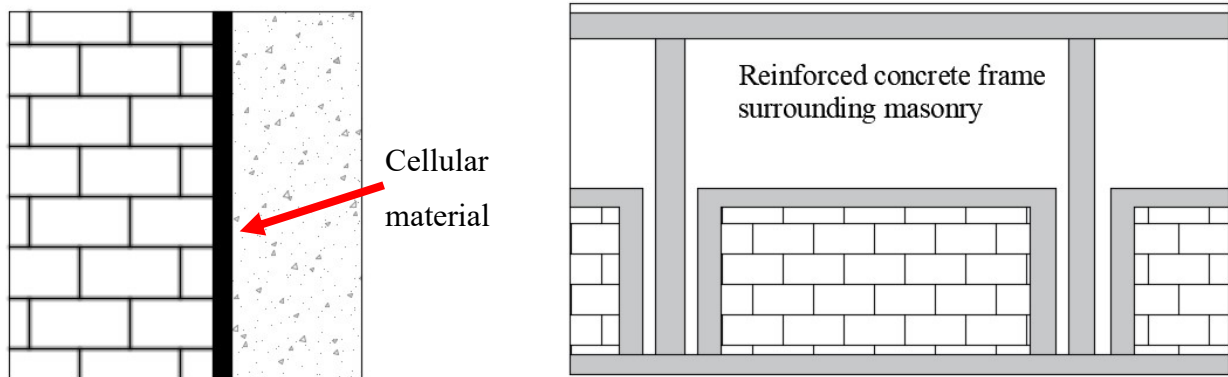


**Figure B. 1. Gap scheme, [FEMA 3-74, 2012].**

The out-of-plane stability is improved by means of steel angles or plates, which must be placed in a continuous or intermittent way on both sides of the infill panels. These steel plates are attached to the beam or slab. In case of additional loading, restraints strength has to be checked.

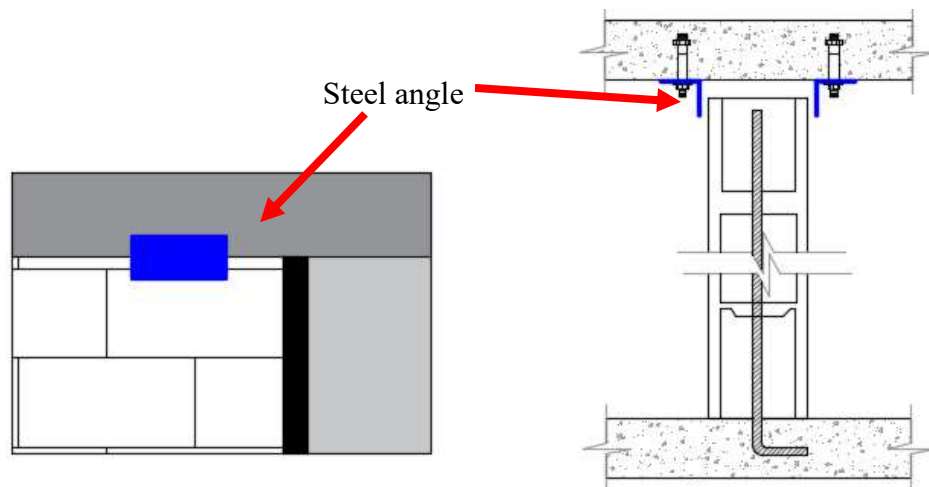


**Figure B. 2. Illustration on how to prevent out-of-plane failure in infill walls, [after FEMA 3-74, 2012].**

The fragility functions of the retrofitted configuration was obtained by shifting the original fragility functions included in the PACT library by 0.5% in terms of drift (drift required to activate the 20mm gap).

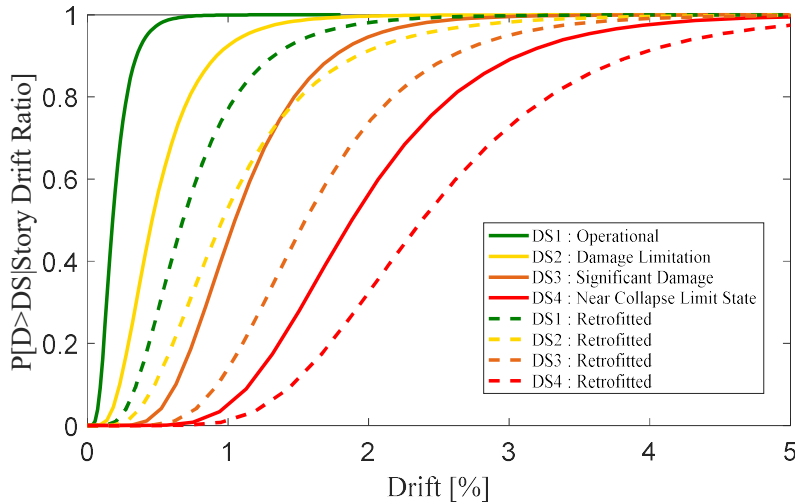


Figure B.3. Fragility functions for infill walls.

Table B-1. Description of damage states for infill walls.

Damage Stage	Original [C1011.200a]	Retrofitted [C1011.200b]
DS1 : Operational	The infill is considered slightly damaged.	
DS2 : Damage Limitation	The infill is damaged, but can be effectively and economically repaired.	
DS3 : Significant Damage	The infill is severely damaged and reparability is economically questionable, however, lives are not threatened.	
DS4 : Near Collapse	The infill is close to collapse.	

## Internal partitions

The retrofitting strategy is the same as infill walls.

## Doors

The improvement of door can be achieved by isolating the supporting frame with plastic material or similar. As for the infill panels, the fragility function of the retrofitted configuration was obtained by shifting the original fragility function included in the PACT library by 0.5% in terms of drift (drift required to activate the 20mm gap).

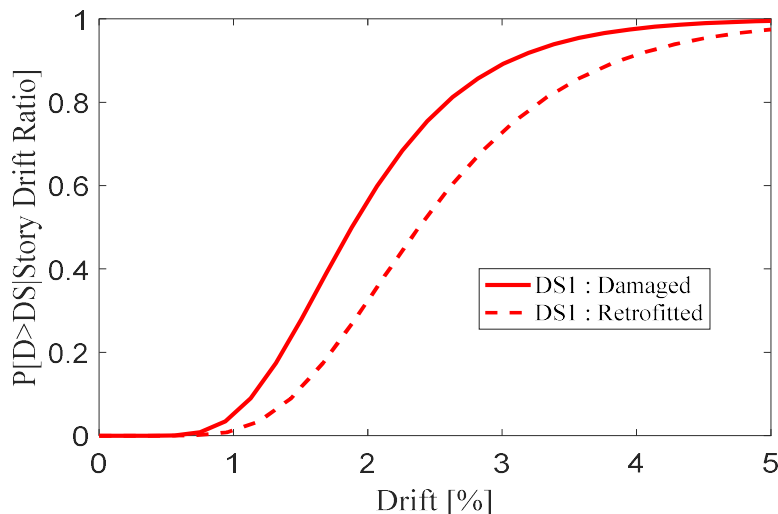


**Figure B. 4. Fragility functions for doors.**

**Table B-2. Description of damage states for Doors.**

Damage Stage	Original [C1011.300a]	Retrofitted [C1011.300b]
DS1 : Damaged	The damage to the door is linked to the collapse of the internal partitions.	

## Windows

The retrofitting strategy is the same as the one implemented for doors.

## Desks

Seismic fasteners and security restraints (anchored at wall or floor) can improve the seismic behavior of desks. The fragility function was improved by shifting the original fragility function included in the PACT library by 0.5% in terms of drift (drift required to activate the 20mm gap).

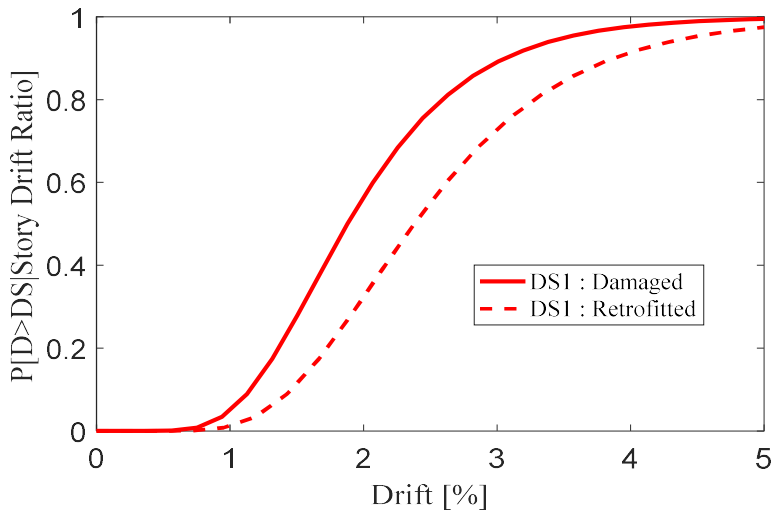


**Figure B. 5. Fragility functions for desks.**

**Table B-3. Description of damage states for desks.**

Damage Stage	Original [C1011.500a]	Retrofitted [C1011.500b]
DS1 : Damaged	The damage to the desk is linked to the collapse of the internal partitions	

## Chairs

The fragility function was improved by shifting the original fragility function included in the PACT library by 0.5% in terms of drift (drift required to activate the 20mm gap).

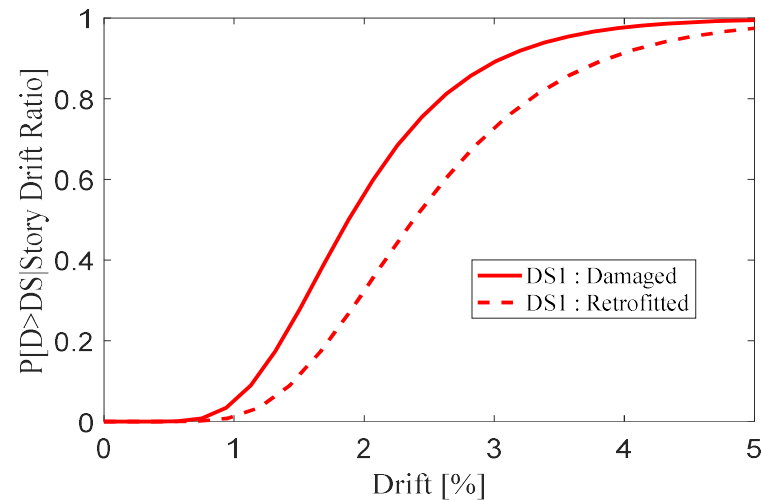


**Figure B. 6. Fragility functions for chairs.**

**Table B-4. Description of damage states for chairs**

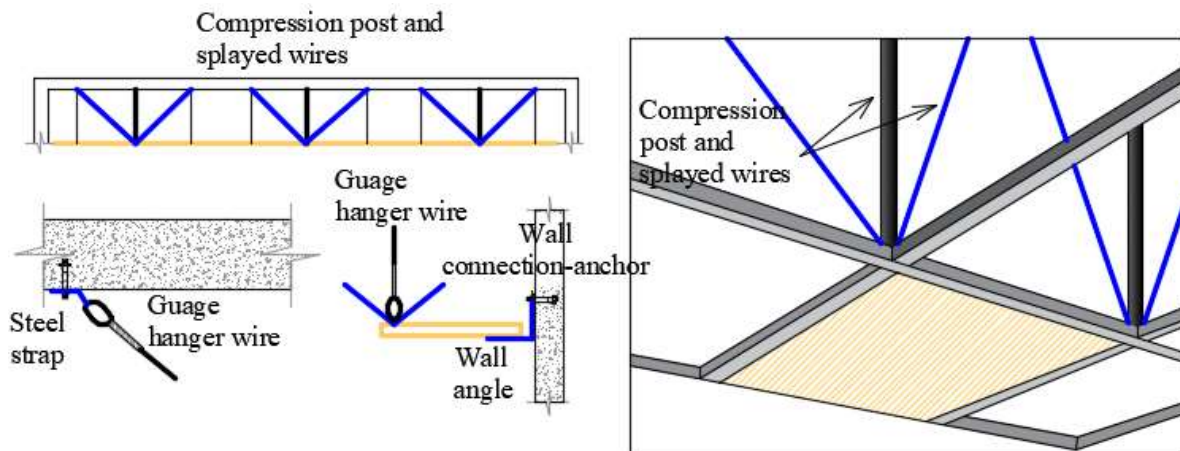
<b>Damage Stage</b>	<b>Original [C1011.600a]</b>	<b>Retrofitted [C1011.600b]</b>
DS1 : Damaged	The damage to the chairs is linked to the collapse of the internal partitions	

### Ceiling systems

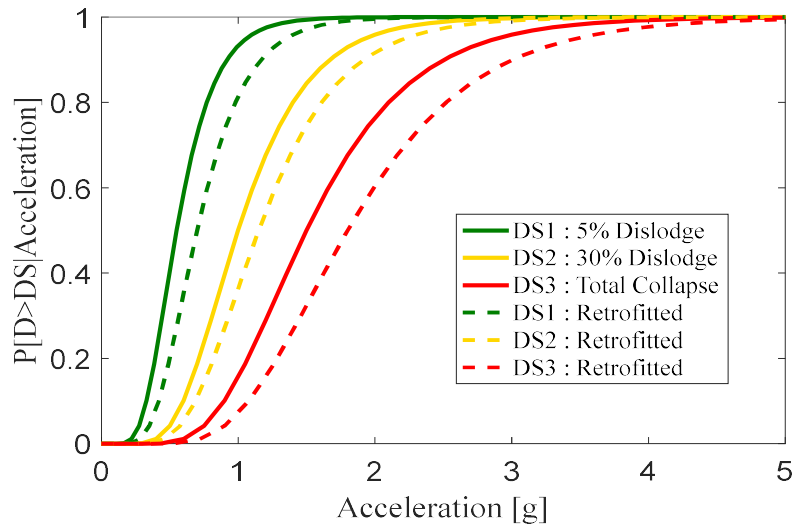
The retrofit of ceiling systems is obtained by placing lateral bracing (vertical truss, with diagonal wire braces). The ceiling system should be fixed to the surrounding walls only on two perpendicular sides.

FEMA E-74 allows  $\frac{3}{4}$ " of slip on the opposite sides as well as periodic bracing assemblies in ceilings larger than 1000 sqft, a minimum size (2") for the closure angle, and a seismic separation of joints for ceilings with a seismic category D, E, and F larger than 2500 sqft. It can also be provided a restrained system with connection to the perimeter wall and with or without riding assemblies , it has to be specified the aforementioned parameter and also of the lateral bracing assemblies (2" minimum perimeter closure angles, minimum edge clearances, etc. ) for all areas greater than 1000 psf.

Typical bracing consist of vertical posts and diagonally splayed wire braces. For example, in California the ceiling systems installed in schools need bracing assemblies at a spacing not more than 12 feet in each direction; essential services buildings require bracing assemblies at a spacing of not more than 8 ft. by 12 ft. on center. Ceilings heavier than 4 psf, or those with a plenum larger than a certain threshold, may require engineering.

**Figure B. 7. Retrofitting schemes for ceiling systems, [after FEMA 3-74, 2012].**

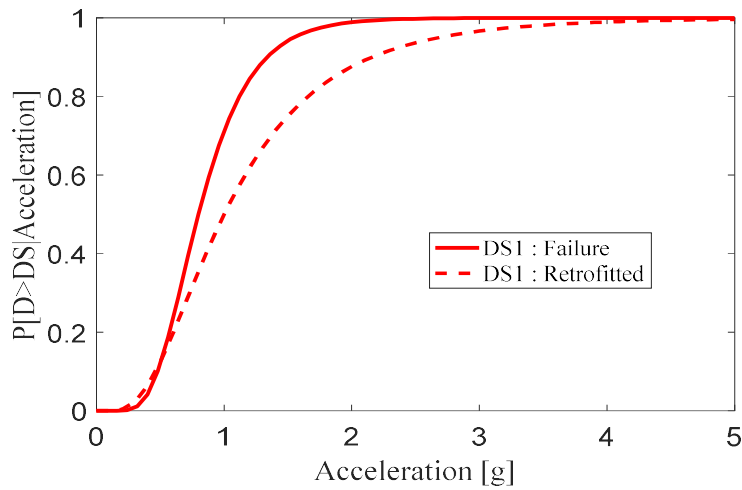
The improved fragility functions were obtained from the PACT library.

**Figure B.8. Fragility functions for ceiling systems.****Table B-5. Description of damage states for ceiling systems.**

Damage Stage	Original [E1011.130a]	Retrofitted [E1011.130b]
DS1 : 5% dislodge	5% of tiles dislodge and fall	
DS2 : 30% dislodge	30% of tiles dislodge and fall	
DS3 : Total collapse	Total ceiling collapse	

## Fancoils

The seismic performance of Fancoils can be enhanced by placing bracing and/or fasteners. The improved fragility function we obtained from the PACT library.

**Figure B. 9. Fragility functions for fancoils.****Table B-6. Description of damage states for fancoils.**

<b>Damage Stage</b>	<b>Original [E1011.100a]</b>	<b>Retrofitted [E1011.100b]</b>
DS1 : Failure	Falls, does not function	Damaged, inoperative but anchorage is OK.

## Lights

Lighting systems are retrofitted through hangers and braces (splay wires). In the case of acoustic tile ceilings, safety wires or independent vertical supports for each light fixture are required. Additionally, positive attachment from the light fixtures to the ceiling grid also helps to improve its seismic behaviour. Bracing for the ceiling grid is also adequate to resist the lateral loading. For existing construction where the ceiling grid is not adequately braced or not strong enough to provide lateral restraint for the lighting, splay wire bracing at each corner of the fixture can be used to provide horizontal restraint. Such bracing would also help prevent swinging lights from damaging the surrounding ceiling. Pendant fixtures in suspended ceilings must be supported directly from the structure above by no less than #9 gauge wire or an approved alternate support. The ceiling suspension system shall not provide any direct support and rigid conduit. This is not permitted for the attachment of fixtures. A bracing assembly, is required where the pendant hanger penetrates the ceiling.

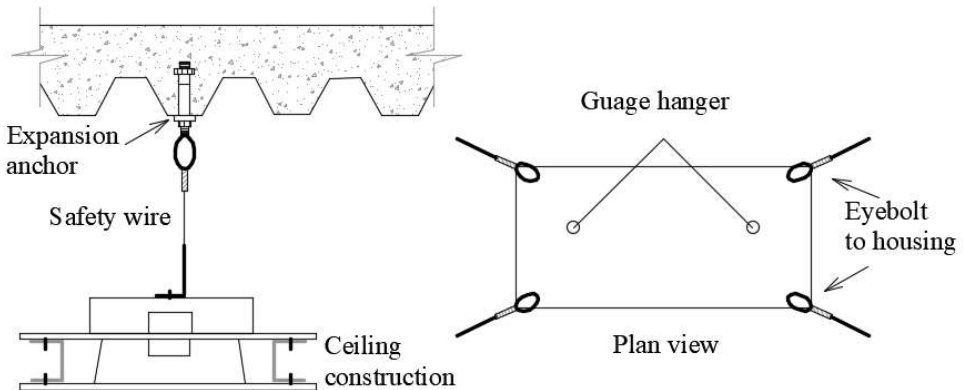


**Figure B. 10. Retrofitting schemes for light systems, [after FEMA 3-74, 2012]. .**

The improved fragility function was obtained from the PACT library.

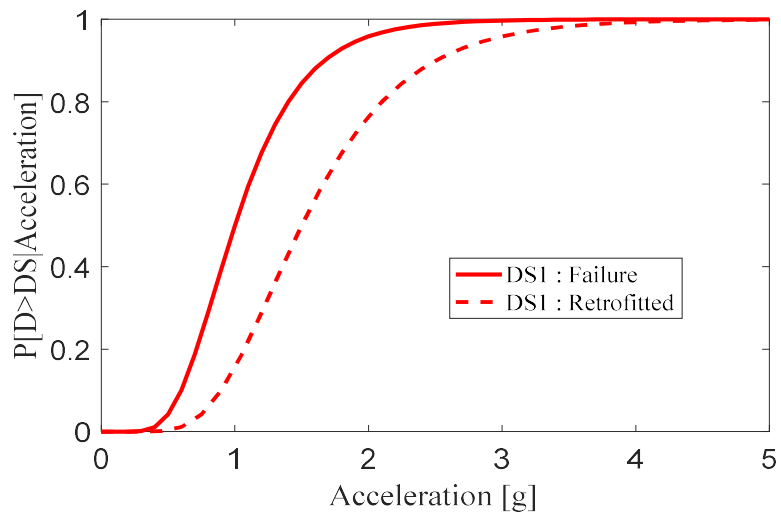


**Figure B. 11. Fragility functions for lights.**

**Table B-7. Description of damage states for lights**

<b>Damage Stage</b>	<b>Original [E1011.200a]</b>	<b>Retrofitted [E1011.200b]</b>
DS1 : Failure	Disassembly of rod system at connections with horizontal light fixture, low cycle fatigue failure of the threaded rod, pull-out of rods from ceiling assembly.	

## Piping-Water Distribution

Implementing transverse and longitudinal bracing assemblies (pipe clamp, riser clamp, and welded lug) help to improve the seismic behaviour of piping systems. Additionally, supplemental damping system can be placed to reduce the acceleration acting on the pipes. The retrofitting intervention needs both transverse and longitudinal braces, the spacing of pipe bracing is related to the level of seismicity, location in a building, size of the pipe, type of pipe, and strength of connections to the structure. Longitudinal pipe bracing requires the use of a pipe clamp, riser clamp, welded lug or device that provides positive attachment to mounted. Flexible connections are often required at fixed equipment or where piping crosses an expansion joint or seismic separation.

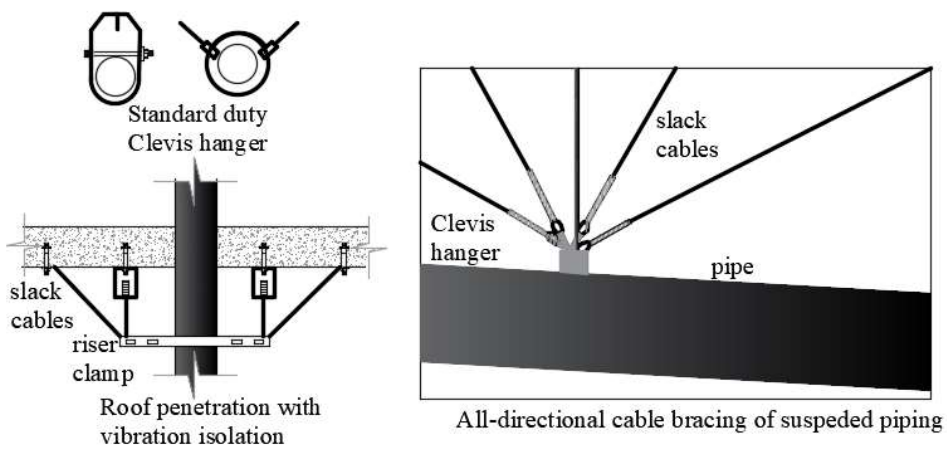


**Figure B. 12. Retrofitting schemes for piping systems, [after FEMA 3-74, 2012].**

The improved fragility functions were obtained from the PACT library.

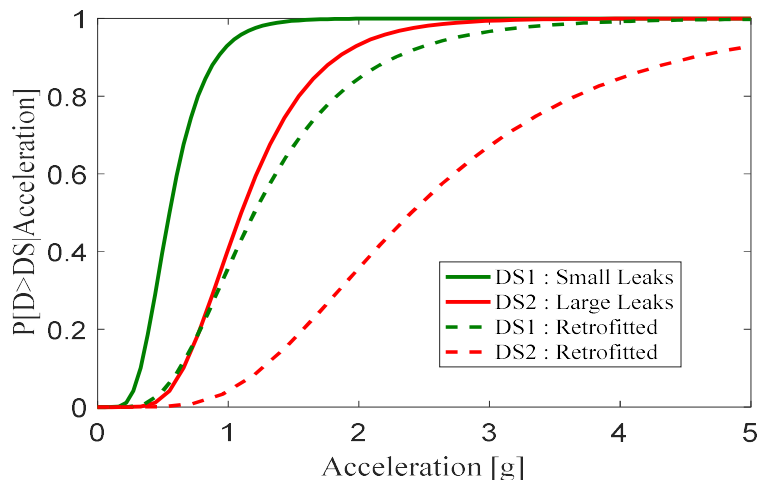


**Figure B. 13. Fragility functions for piping-water distribution.**

**Table B-8. Description of damage states for piping-water distribution**

<b>Damage Stage</b>	<b>Original [E1011.300a]</b>	<b>Retrofitted [E1011.300b]</b>
DS1 : Small leaks	Small Leakage at joints - 1 leak per 1000 feet of pipe.	Isolated support failure w/o leakage - 0.5 supports fail per 1000 feet of pipe (assuming supports every 20 feet).
DS2 : Large leaks	Large Leakage w/ major repair - 1 leak per 1000 feet of pipe.	Multiple supports failure and 60 feet of pipe fail per 1000 feet of pipe (assuming supports every 20 feet).

## Piping-Heating Distribution

The retrofitting approach is the same as the one described for piping-water distribution.

### Bookcases

The seismic performance of bookcases can be improved by bracing and anchorage (to structural walls or structural studs). Bracing and anchorage should be designed considering the weight of the unit and weight of shelved contents, the anchor can be done to an adjacent stud wall, concrete or masonry wall.

Shelving should not be located adjacent to doors or exits if their failure would block the exit. Any connections to stud walls must engage the structural studs. Stud walls, partitions and unreinforced or lightly reinforced heavy partitions may not have adequate lateral capacity to support multiple bookshelves. The bracing or anchorage of walls and partitions to the structure above must also be checked for adequacy considering the seismic loads imposed by all anchored items. It is preferable to locate the screws or clip angles on the inside of the unit bracing, the unit should be strong enough to receive the attached ties and bracing strengthening. Steel shelving may require additional cross bracing. Wood shelving units could be strengthened with the addition of corner brackets or hardware to tie the top, back and sides more securely together. Other alternative could be to anchor the shelving units to the floor, tie freestanding back-to-back units together to create a larger base.

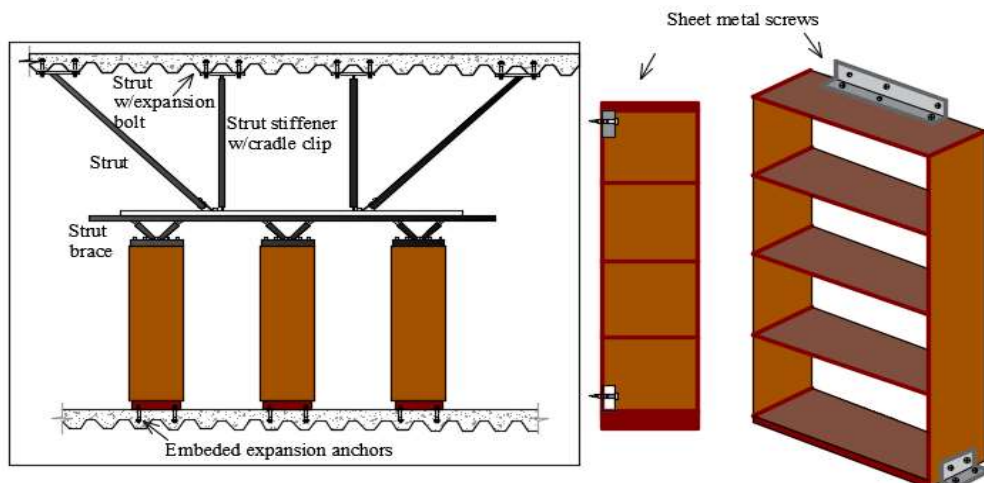


**Figure B. 14. Retrofitting schemes for bookshelves, [after FEMA 3-74, 2012].**

The improved fragility function was obtained from the PACT library. The parameter used to evaluate the performance of the retrofitted bookcases has been modified with respect to the original configuration. Originally, bookcases were considered as velocity sensitive, while they become acceleration sensitive when are fastened or anchored to the floor or to the wall.

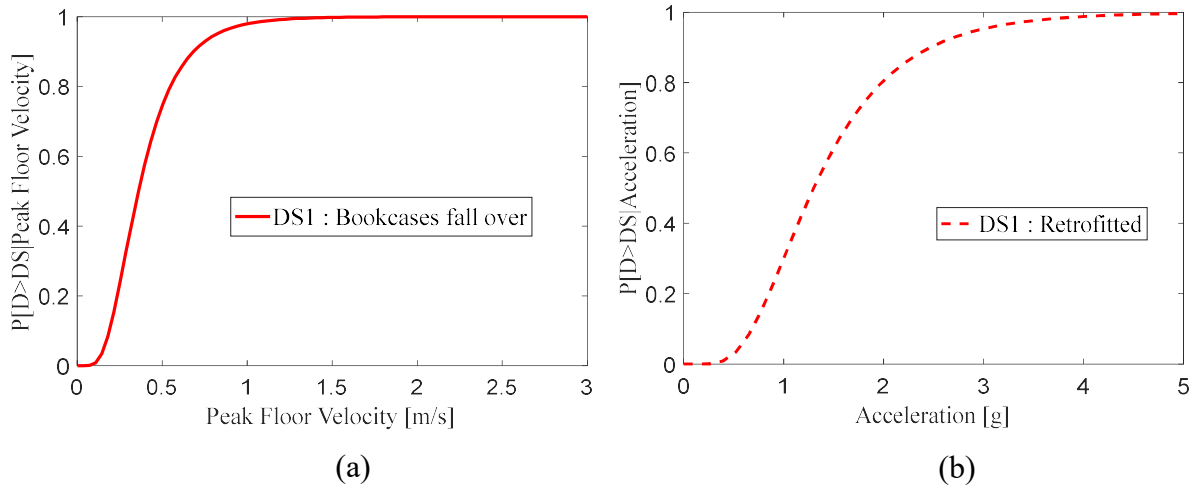


**Figure B. 15. Fragility functions for bookcases, (a) Original, (b) Retrofitted.**

**Table B-9. Description of damage states for bookcases**

Damage Stage	Original [D1011.100a]	Retrofitted [D1011.100b]
DS1 : Bookcase falls over	Book case falls over and contents are scattered.	Book case falls over and contents are scattered. Likely damage to bookcase.

### Mobile Blackboards

The retrofitting of mobile blackboards was done through seismic fasteners and security restraints (anchored at wall or floor), anchorage can be done to both to the floor or to the wall. Because specific data about this typology of non-structural element is not available, the fragility function of electronic equipment mounted on wall brackets was selected.

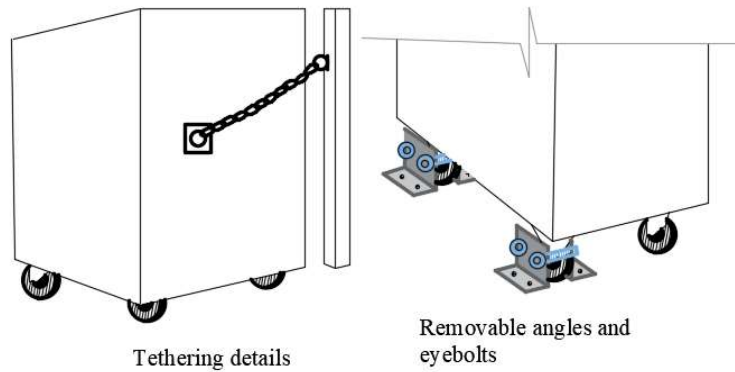


**Figure B. 16. Retrofitting schemes mobile boards, [after FEMA 3-74, 2012].**

The improved fragility function was obtained from the PACT library.

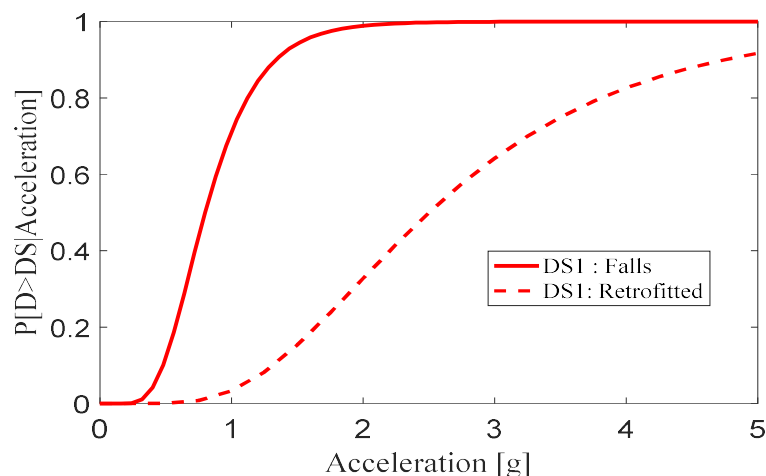


**Figure B. 17. Fragility functions for mobile blackboards.**

**Table B-10. Description of damage states for mobile blackboard**

<b>Damage Stage</b>	<b>Original [E1011.600a]</b>	<b>Retrofitted [E1011.600b]</b>
DS1 : Falls	Falls, does not function	

## Electronic Blackboards

Electronic blackboard are enhanced by brackets installation (installed in structural elements), brackets will not provide seismic protection unless properly installed. The lag bolts, screws, or expansion bolts can be installed directly into structural elements such as studs, concrete or masonry wall, or ceiling joists having adequate capacity to support the additional loading. Because specific experimental studies are not available, the fragility function selected for this element corresponds to electronic equipment on wall mount brackets.

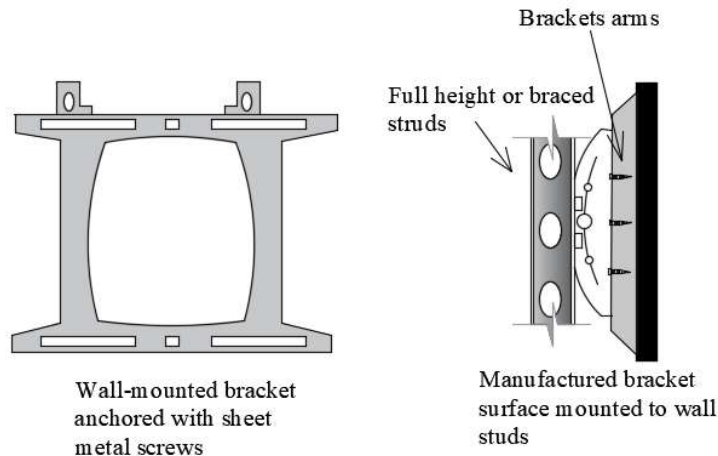


**Figure B. 18. Retrofitting schemes electronic blackboards, [after FEMA 3-74, 2012].**

The improved fragility function was obtained from the PACT library.

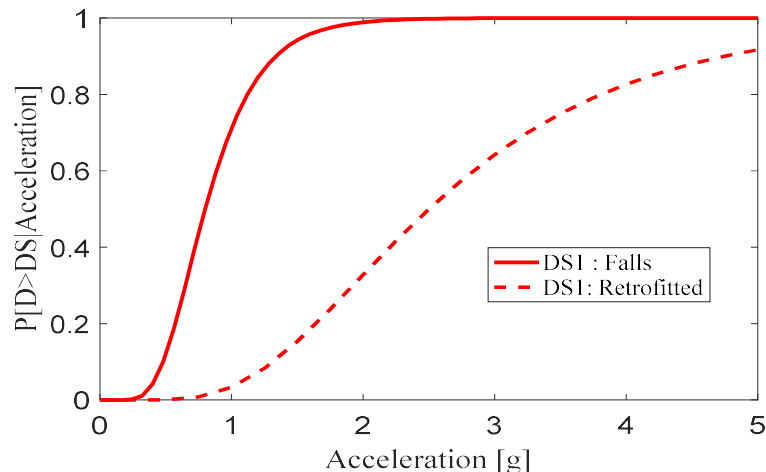


**Figure B. 19. Fragility functions for electronic blackboards.**

**Table B-11. Description of damage states for electronic blackboard**

Damage Stage	Original [E1011.700a]	Retrofitted [E1011.700b]
DS1 : Falls	Failure	Falls, does not function.

### Computers and Printers

Use of predrilled holes, wall anchorage, and/or tethered improve the seismic performance of computers and printers. For one thing, predrilled holes can be anchored to the floor or to the

wall. If they are anchored to a partition wall, it has to be verified that the wall along with the wall anchorage to the structure above are adequate to resist the imposed loads. Cables and wiring should be installed with sufficient slack to allow sufficient seismic deformations. A backup and recovery plan should be developed for all electronic data including offsite backup to a location not likely to be affected by the same earthquake. The supporting desks, tables or carts should also be anchored or tethered if movement could cause additional damage. Alternatively, cables and cords should be installed with sufficient slack to allow for some movement.

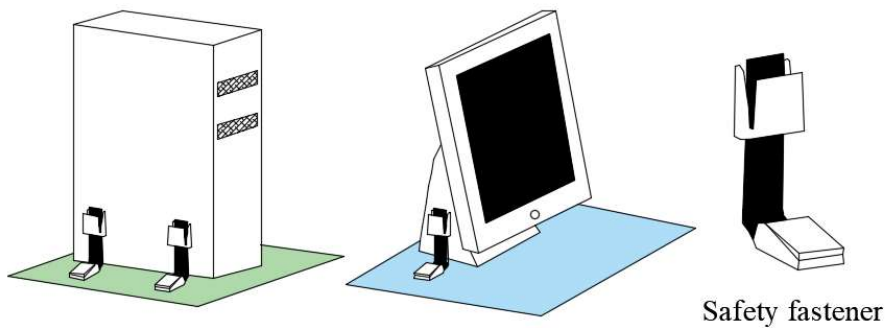


**Figure B. 20. Retrofitting schemes computers and printers, [after FEMA 3-74, 2012].**

The improved fragility function was obtained from the PACT library.

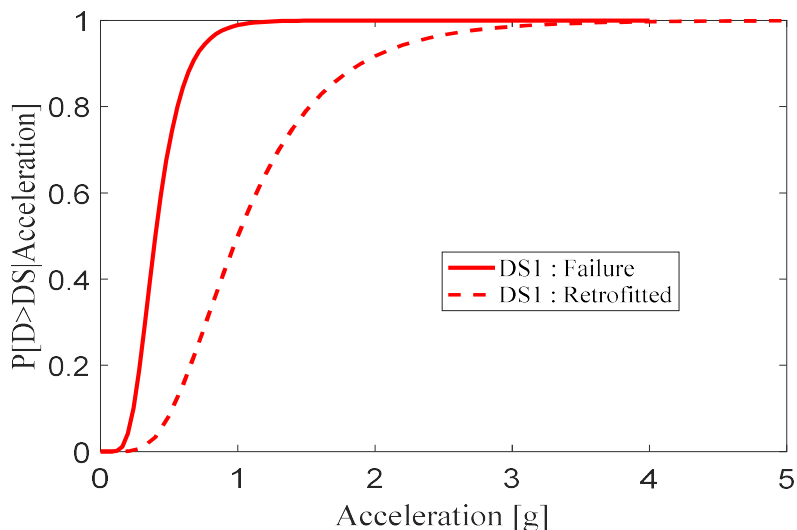


**Figure B. 21. Fragility functions for computers and printers.**

**Table B-12. Description of damage states for computer and printers**

Damage Stage	Original [E1011.800a]	Retrofitted [E1011.800b]
DS1 : Failure	fails	Falls, does not function.

## Projectors

Brackets installation (installed in structural elements) can improve the performance of projectors. The improved fragility function was obtained from the PACT library.

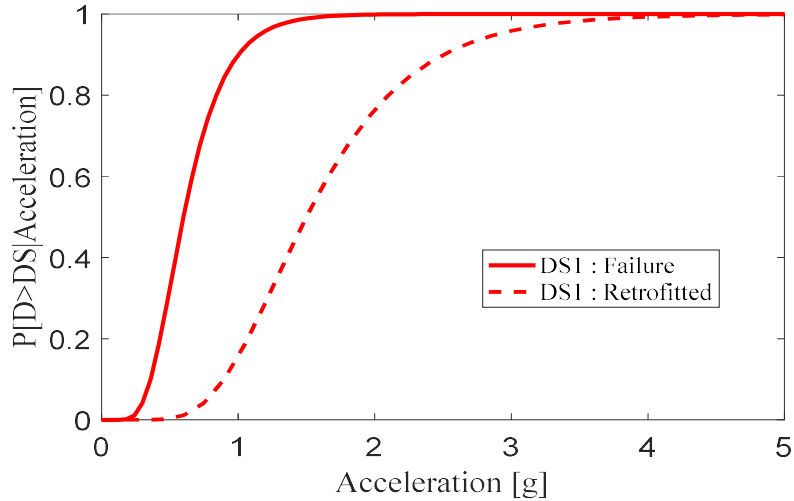


**Figure B. 22. Fragility functions for projectors.**

**Table B-13. Description of damage states for projectors.**

Damage Stage	Original [E1011.900a]	Retrofitted [E1011.900b]
DS1 : Failure	Disassembly of rod system at connections with horizontal light fixture, low cycle fatigue failure of the threaded rod, pull out of rods from ceiling assembly.	

## Switchboards

Switchboards are retrofitted with welded brackets or predrilled hole (in walls or base). Seismic anchorage provisions have to be provided by the manufacturer. Flexible connections between the equipment and raceways, bus ducts, or conduits that are braced to the level above will limit damage due to story drift.

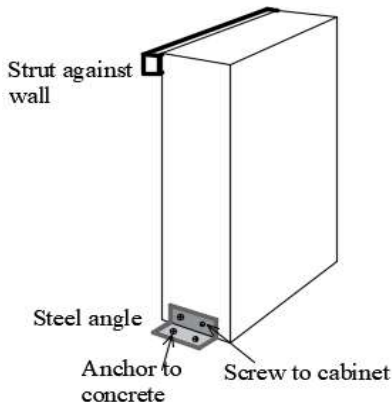


**Figure B. 23. Retrofitting schemes for switchboards, [after FEMA 3-74, 2012].**

The improved fragility function was obtained from the PACT library.

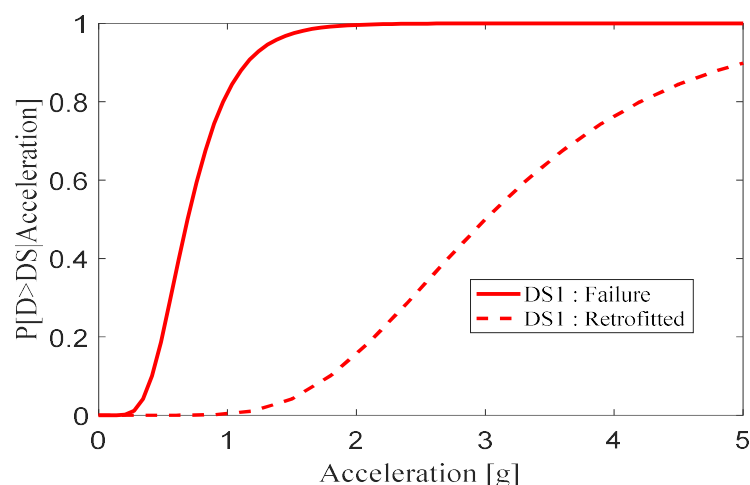


**Figure B. 24. Fragility functions for switchboards.**

**Table B-14. Description of damage states for switchboards**

Damage Stage	Original [E1011.110a]	Retrofitted [E1011.110b]
DS1 : Failure	Damaged, inoperative.	Damaged, inoperative but anchorage is OK.

## APPENDIX C (STRUCTURAL ELEMENTS)

This appendix illustrates the fragility functions of structural elements, based on FEMA P58-2[2012], FEMA P58-3[2012] PACT library and Cardone and Perrone [2015].

### Exterior Beam-Column Joints (End-Hooks)

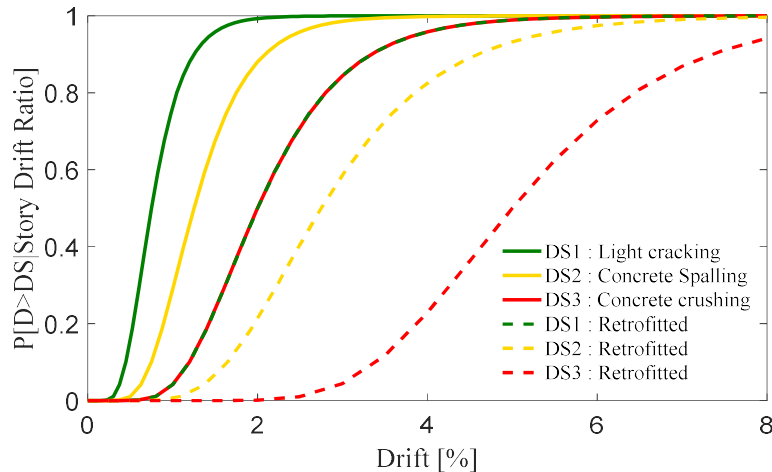
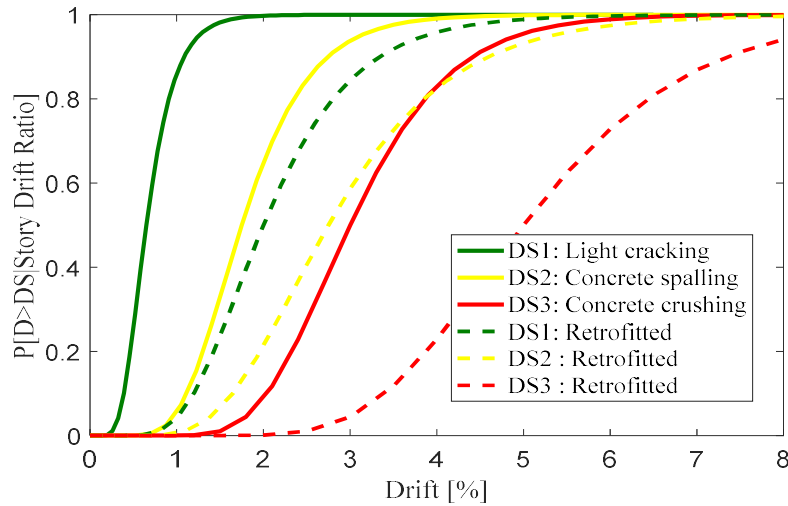


**Figure C. 1. Fragility functions for exterior beam-column joints, Cardone [2016], PACT library.**

**Table C-1. Description of damage states for exterior beam-column joints.**

Damage Stage	Original [A1011.101a]	Retrofitted [B1041.001a]
DS1 : Light cracking	Residual crack width <1-1.5 mm or less likely column-joint interfaces, and possible first inclined joint cracks. A second crack on beam is also expected at a distance equal to half beam height, due to yielding of beam rebars.	Beams or joints exhibit residual crack widths > 0.06 in. No significant spalling. No fracture or buckling of reinforcing.
DS2 : Concrete spalling	Existing cracks, at beam-joint interface, widen ( $3 \text{ mm} < \text{residual crack width} < 5 \text{ mm}$ ). Further cracks at a distance of the order of $3/4$ the beam height may develop. Spalling of cover concrete is expected in the joint, involving an area of the order of 10% the area of the joint panel.	Beams or joints exhibit residual crack widths > 0.06 in. Spalling of cover concrete exposes beam and joint transverse reinforcement but not longitudinal reinforcement. No fracture or buckling of reinforcing.
DS3 : Concrete crushing	Damage tends to concentrate in the joint, through the appearance of interconnected cracks, progressive spalling of cover concrete and activation of a concrete wedge expulsion collapse mechanism. Spalling of concrete is expected to involve an area of the order of 30% the joint panel. Buckling of column	Beams or joints exhibit residual crack widths > 0.06 in. Spalling of cover concrete exposes a significant length of beam longitudinal reinforcement. Crushing of core concrete may occur. Fracture or buckling of reinf. requiring replacement may occur.

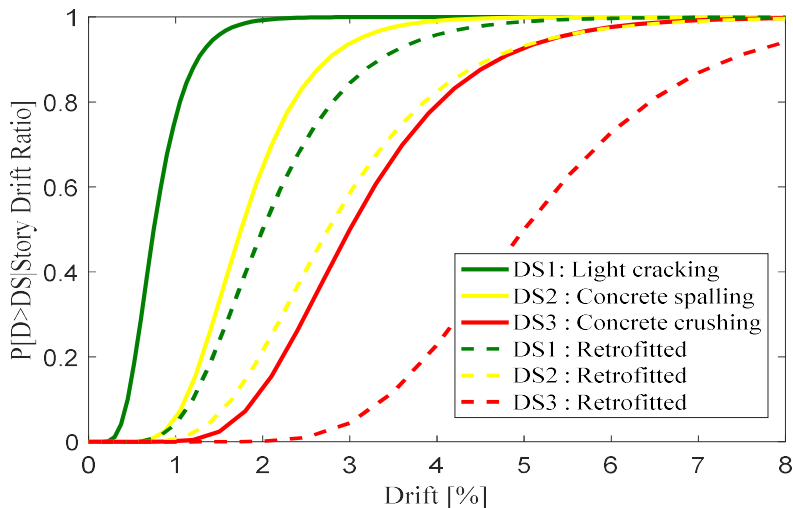
### Interior Beam-Column Joints (Weak Columns)



**Figure C. 2. Fragility functions for interior beam-column joints, Cardone [2016], PACT library.**

**Table C-2. Description of damage states for interior beam-column joints.**

Damage Stage	Original [A1011.104a]	Retrofitted [B1041.001a]
DS1 : Light cracking	The crack pattern is similar to that described above for IWB, with the only difference that it involves columns instead of beams.	Beams or joints exhibit residual crack widths > 0.06 in. No significant spalling. No fracture or buckling of reinforcing.
DS2 : Concrete spalling	The damage pattern is similar to that described above for IWB, with the only difference that it involves columns instead of beams.	Beams or joints exhibit residual crack widths > 0.06 in. Spalling of cover concrete exposes beam and joint transverse reinforcement but not longitudinal reinforcement. No fracture or buckling of reinforcing.
DS3 : Concrete crushing	The damage pattern is similar to that described above for IWB, with the only difference that it involves columns instead of beams. In addition, possible buckling of longitudinal rebars is expected.	Beams or joints exhibit residual crack widths > 0.06 in. Spalling of cover concrete exposes a significant length of beam longitudinal reinforcement. Crushing of core concrete may occur. Fracture or buckling of reinf. requiring replacement may occur.

**Ductile Weak Columns (Lapped)****Figure C.3. Fragility functions for ductile columns, Cardone [2016], PACT library.****Table C-3. Description of damage states for columns.**

<b>Damage Stage</b>	<b>Original [A1011.110a]</b>	<b>Retrofitted [B1041.001a]</b>
DS1 : Light cracking	Yielding of column rebars, light opening (<1-1.5 mm) of concrete cracks at the base of the column. In presence of lap-spliced bars, further cracks may develop up to at a distance of the order of half the column depth	Columns exhibit residual crack widths > 0.06 in. No significant spalling. No fracture or buckling of reinforcing.
DS2 : Concrete spalling	The existing crack at the base of the column widen (3 mm < residual crack width < 5 mm), according to the fixed-end rotation mechanism. Additional column cracks are possible up to a distance of the order of the column height. Spalling of cover concrete is expected at the base of the column, near the section corners, for a length of the order of 10% the column depth.	Columns exhibit residual crack widths > 0.06 in. Spalling of cover concrete exposes columns transverse reinforcement but not longitudinal reinforcement. No fracture or buckling of reinforcing.
DS3 : Concrete crushing	Loss of strength due to extensive spalling of cover concrete is expected, along the whole section perimeter, for a length equal to the column depth. Crushing of concrete core in the section corners is likely to occur. Concrete cracking may extend further, involving a column length (from the base of the column) twice the column height. Buckling of longitudinal rebars may also occur.	Columns exhibit residual crack widths > 0.06 in. Spalling of cover concrete exposes a significant length of columns longitudinal reinforcement. Crushing of core concrete may occur. Fracture or buckling of reinf. requiring replacement may occur.

### Exterior Masonry Infills (with Windows)

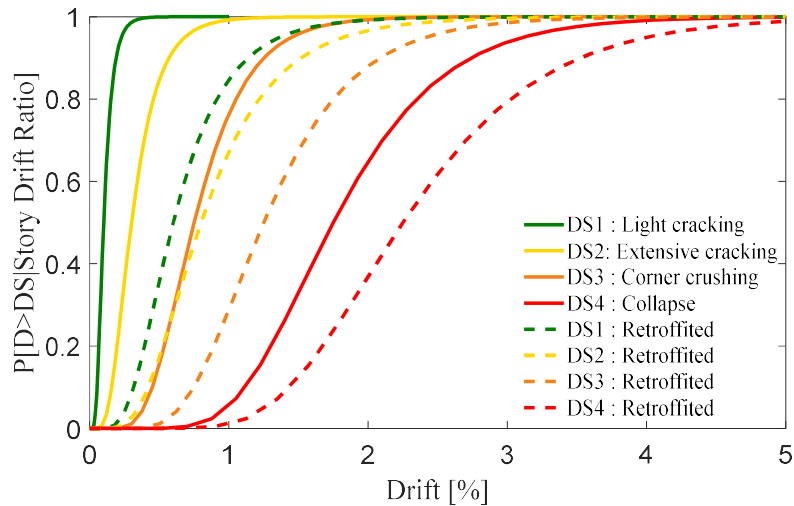


**Figure C. 4. Fragility functions for exterior masonry infills, Cardone and Perrone [2015], PACT library.**

**Table C-4. Description of damage states for exterior masonry infills.**

Damage Stage	Original [A1011.121a]	Retrofitted [A1011.121b]
DS1 : Light cracking	Damage results in detachment of the masonry panel from the RC frame, at the intrados of the top beam and along the upper half-height of the columns. Light diagonal cracking of the infill (1-2 cracks with width <1 mm) in both directions may also occur.	
DS2 : Extensive cracking		Cracks developed at DS1 widen (1 mm < width < 2 mm). In addition, new diagonal cracks are expected to form in both directions (25-35% of the panel area is assumed to be affected by cracks at DS2). Possible failure of some brick units, located on the upper corners and top edge of the infill (corresponding to 10% of the panel area),
DS3 : Corner crushing		Detachment of large plaster area and significant sliding in the mortar joints are expected to occur. In addition, crushing and spalling of brick units are more widespread on the panel (30% of the panel area is assumed to be affected by crushing/spalling of bricks). The wall is not repairable at reasonable costs (it is more convenient to demolish and reconstruct the entire wall). Frames (if any) are not damaged and can be retrieved and re-installed.
DS4 : Collapse		Corresponds to the in-plane or out-of-plane (whichever occurs first) global collapse of the wall. Frames (if any) are damaged and cannot be retrieved and used again.

## Stairs

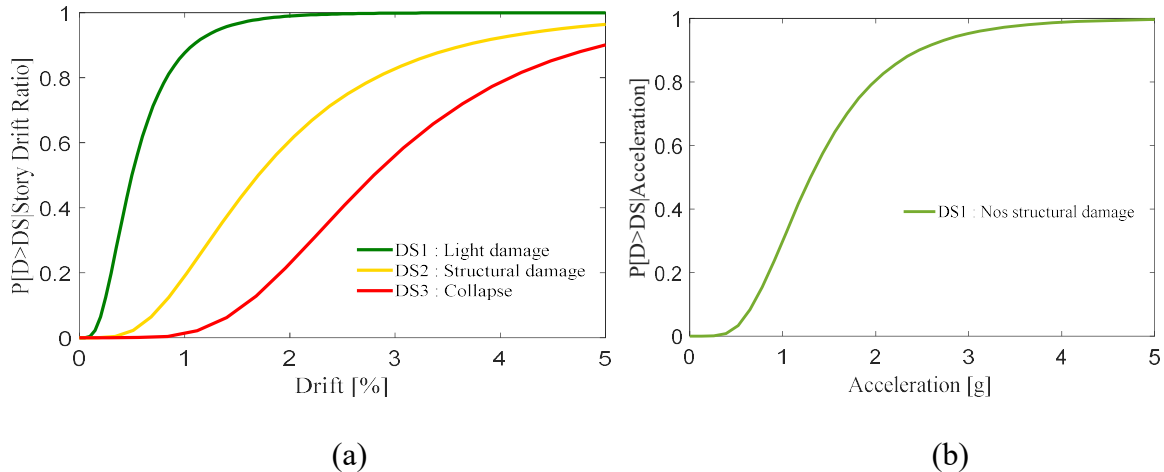


**Figure C. 5. Fragility functions for stairs, PACT library, (a) Original, (b) Retrofitted.**

**Table C-5. Description of damage states for stairs.**

Damage Stage	Original [A1011.110a]	Retrofitted [B1041.001a]
DS1 : Light damage	Non structural damage, local concrete cracking, localized concrete spalling, localized rebar yielding.	Non structural damage, local concrete cracking, localized concrete spalling, localized rebar yielding.
DS2 : Structural collapse	Structural damage but live load capacity remains intact. Extensive concrete cracking, concrete crushing, buckling of rebar.	-
DS3 : Collapse	Loss of live load capacity. Extensive concrete crushing, connection failure.	-